Centre Européen de Recherche et de Formation Avancée en Calcul Scientifique
European Center for Research and Advanced Training in Scientific Computing

CERFACS
Scientifi c Activity Report
Jan. 2004 – Dec. 2005

CERFACS
42, Avenue Gaspard Coriolis, 31057 Toulouse Cedex 1, FRANCE.
Tel. : 33 (0) 561 19 31 31 – Fax : 33 (0) 561 19 30 30
secretar@cerfacs.fr – http://www.cerfacs.fr

Table des matières

Table des figures

3 Electromagnetism Team 85

Foreword

Welcome to the 2004-2005 issue of the CERFACS Scientific Activity Report.

Before turning to more scientific issues it is worth recalling that two main events took place during the period. Firstly, on January 1^{st}, 2004, SNECMA (to be transformed later on into SAFRAN) became the 5^{th} CERFACS shareholder. This brought new support to a number of CERFACS' research activities, among which turbulent combustion is certainly at the forefront. Secondly, on June 30^{th}, 2004, we organized a seminar between shareholder's representatives, members of the Scientific Council and leaders of our research teams to look at CERFACS priorities and possible new research topics. This fruitful seminar led to some reorganization, with on the one hand much more importance given to data assimilation, and on the other hand the establishment of a research team dealing with the environmental impacts of aviation. This new organization reflects somehow in the following pages.

Now, what have been the major scientific achievements of these past two years ? Reading through the report will hopefully provide the reader with very many answers to this question, but let me just select a few results for each team as an appetizer :

Parallel Algorithms

Many tools were successfully developed by the team :

- the Krylov suite of public domain packages (CG, GMRES, FGMRES) was downloaded more than 3,000 times up to 2005, showing the great worldwide interest in such tools,
- improved spectral preconditioners allowed the time necessary for simulating the COBRA problem arising in electromagnetic propagation to be reduced by a factor of 3 ;
- a fast parallel out-of-core solver has been developed, of special use for solving least-squares problems arising in gravity field computation, which requires only half of the computer memory compared with the Scalapack package ;
- the "Open MP/MPI" paradigm has been used on SMP's to efficiently parallelize the MOCAGE code used for atmospheric chemistry simulation.

As a way to better disseminate these and other results, as well as encouraging work on new issues, another session of the "Sparse Days" meeting was organized at CERFACS on June 2^{nd} and 3^{rd}, 2004. On a greater scale the team organized the 2^{nd} international workshop on "Combinatorial Scientific Computing" (CSC05) on June 21^{st} to 23^{rd}, 2005, with large European and overseas participation.

Computational Fluid Dynamics

With all the earlier NSMB functionalities being implemented within elsA, this latter code, developed cooperatively with ONERA, was deployed within AIRBUS at the beginning of 2004, with approximately 100 users.

elsA has then allowed CERFACS scientists to :

- capture the transonic buffet phenomenon : in collaboration with ONERA, the DES (Detached Eddy Simulation) technique led to results showing that, in contrast to the URANS approach, DES is able to catch the physics at the right angle of attack ;

– develop, evaluate and validate the unsteady Navier-Stokes simulations with mesh deformation to capture the flutter phenomenon : in collaboration with AIRBUS, effective and accurate prediction of this phenomenon have been achieved for the overall flight domain, in good agreement with the experimental data.

Additional CFD activities have been concerned with applied simulations of ventilation in aircraft painting halls and of air-conditioning efficiency within buildings with large glass panels.

Simulation methods for turbulent combustion kept progressing at a very rapid pace. Let us just mention a few highlights in this field :

– a detailed comparison was organized between the AVBP CERFACS code and the CDP Stanford code, both for the cold, and later on, hot cases, which confirmed the excellent capacities of AVBP ;
– the capacities of the AVBP LES tools have been combined with the power of IBM eServer Blue Gene to run on a high-resolution mesh, in order to compute ignition and flame propagation in the combustor of an helicopter turbo shaft engine from Turbomeca. In this computation, all fuel injectors (18) and dilution jets (108) are included and a full ignition sequence starting from two igniters has been computed ;
– high-resolution LES of turbulent flows in Diesel intake pipes of piston engines have also been successfully performed on an IBM Blue Gene eServer ;
– in such simulations linear speedups of 4,078 were measured up to 4,096 processors on configurations of 40 million cells. As a result, the AVBP code is more than ever recognized as the main French code for unsteady combustion and is deployed by many national and international groups, as well as in industrial laboratories.

Computational Electromagnetism

Among the main developments which occurred over the period one should mention :

– the use of domain decomposition techniques, which have been applied to stealth technology by coupling integral equations with an asymptotic approach : this resulted in a factor 5 reduction of the computing time, without loss of accurary ;
– the coupling of finite-element and fast multipole methods, which has then been successfully implemented to compute the effects of a satellite on the radiation of its geometrically complex antenna ;
– the improvement of the code to take advantage of various symmetries of the simulated objects, which can be made out of both metal and dielectrics.

Climate Modelling, Data Assimilation, Oceanography, Atmospheric Chemistry and Couplers

Occurrence of extreme events has been explored, the question being : what is the link between the large-scale environment, as defined by weather regimes, and the occurrence of extreme events :

– in the case of European heat waves, such as the one which occurred in 2003, it was shown by simulation that changes of the warm regime occurrence for the 3 summer months occured in response to tropical Atlantic forcing ;
– on the contrary, weather regimes did not appear to be the determining factor regarding the occurrence of extreme precipitation.

In the field of data assimilation, new preconditioners (spectral, deflation-based, BFGS) have been developed to improve overall convergence of the minimization. A hybrid 3D-Var/4D-Var algorithm has also been developed in which the cheaper 3D-Var is used to provide a good initial "guess" for 4D-Var, leading to results very close to those obtained with the much more expensive 4D-Var method.

Data assimilation methods have also been applied to atmospheric chemistry problems. Using the PALM software and the MOCAGE model, data assimilation led to a significantly better agreement with independent data, and to an improvement of both the polar ozone depletion timing and the equatorial ozone field.

As another very promising application of data assimilation, a 3D-Var scheme is now being implemented for the estimation of neutron activity within electricity-producing nuclear reactors. The so-called MANARA

system, which is indeed intended to improve the estimation of the 3D neutron flux, is presently developed and improved to account for multi-variate assimilation.
The MERCATOR group successfully participated in :

– the improvement of the operational Atlantic ocean model at $1/15^{th}$ degree resolution, by developing a multivariate optimal interpolation scheme and including, in addition to assimilation of sea-level anomalies, assimilation of sea-surface temperature and of vertical profiles of temperature and salinity ;
– the implementation of the new global ocean forecasting system at $1/4°$, which just went into operational on October 14^{th}, 2005.

Numerical simulation of aircraft exhaust dispersion in the atmosphere has been achieved through a semi-Lagrangian scheme for two-phase flow. Starting from initial conditions with an exhaust jet loaded with water vapour and soot particles, interactions taking place within the wake vortex led to ice nucleation around the soot particles and ice crystals formation, in good agreement with available observations.
Couplers were actively developed over the period, with :

– OASIS4 being chosen for the EU FP'6 GEMS project and staying at the heart of the PRISM initiative for earth-system modelling ;
– PALM being improved with accounting for dynamic object size and being applied to new fields like hydrology, ecosystem modelling, code coupling, ...

Technology Transfer

The so-called N'S'^{3} solution, for collaborative working for the extended enterprise benefited from many new functionalities like the automatic hyperlink and the launch of a 3D data base directly out of the powerpoint document.

Computing resources

A new computer (Cray XD1) was installed in 2005, multiplying by 6 the internal number-crunching capacity. The storage capacity was also increased by a factor of 10 over the period.

CERFACS scientific production is still increasing :

– the number of high-standard publications, i.e. in internationally-refereed journals, is 77 for the period, showing an increase as compared to past years when the mean rate of publications was closer to 30 per year ;
– CERFACS' researchers have produced yearly more than 230 technical reports, book chapters, and papers in conference proceedings ;
– they are active in training new researchers, with 17 Ph. D. theses being awarded over the period.
– they have also very actively developed applied research, with more than 60 grants per year being held over the period, approximately 15 of them coming from the European Commission through its various programmes or from other international bodies, and the rest, of the order of 45-50, being awarded by national funding agencies and/or industrial partners ;
– let us also finally mention that CERFACS wide-interest seminars have attracted high-level and well-known external scientists (see below).

During 2004 and 2005, the mean number of (full-time equivalent) people working at CERFACS has been 92.15 (see Tables ii to viii), with a global annual budget varying between 6.3 and 6.4 M€.

I sincerely hope that you will have some time to read through the detailed activity reports of the teams, and that you will find there enough interest to pursue your collaboration with us, or to initiate some new ones.

Enjoy your reading.

Jean-Claude ANDRÉ
CERFACS Director

CERFACS Structure

As a "Société Civile" CERFACS is governed by two bodies. Firstly, the "Conseil de Gérance", composed of only 5 managers (in French, "Gérants") nominated by the 5 shareholders (see table i), follows quite closely the CERFACS activities and the financial aspects. It met 8 times during the period (2 April 2004, 16 June 2004, 15 September 2004, 16 December 2004, 27 April 2005, 24 June 2005, 16 September 2005 and 21 December 2005). Secondly the Board of Governors (in French "Assemblée des Associés"), composed of representatives of CERFACS shareholders and of 3 invited personalities, including the Chairman of the Scientific Council. It met 4 times during the period (27 January 2004, 30 September 2004, 27 January 2005 and 5 October 2005).

CERFACS Scientific Council met for the eighth and ninth times, on 21 January 2005 and 16 December 2005, under the chairmanship of Prof. Jean-François MINSTER.

The general organization of CERFACS is depicted in the CERFACS chart, where the two support groups (Administration and Computing) are shown together with the research teams.

CENTRE NATIONAL D'ÉTUDES SPATIALES (CNES)	26 %
ÉLECTRICITÉ DE FRANCE	26 %
MÉTÉO-FRANCE	26 %
EUROPEAN AERONAUTIC DEFENCE AND SPACE COMPANY (EADS)	11 %
SAFRAN	11%

Table i : Société Civile Shareholders

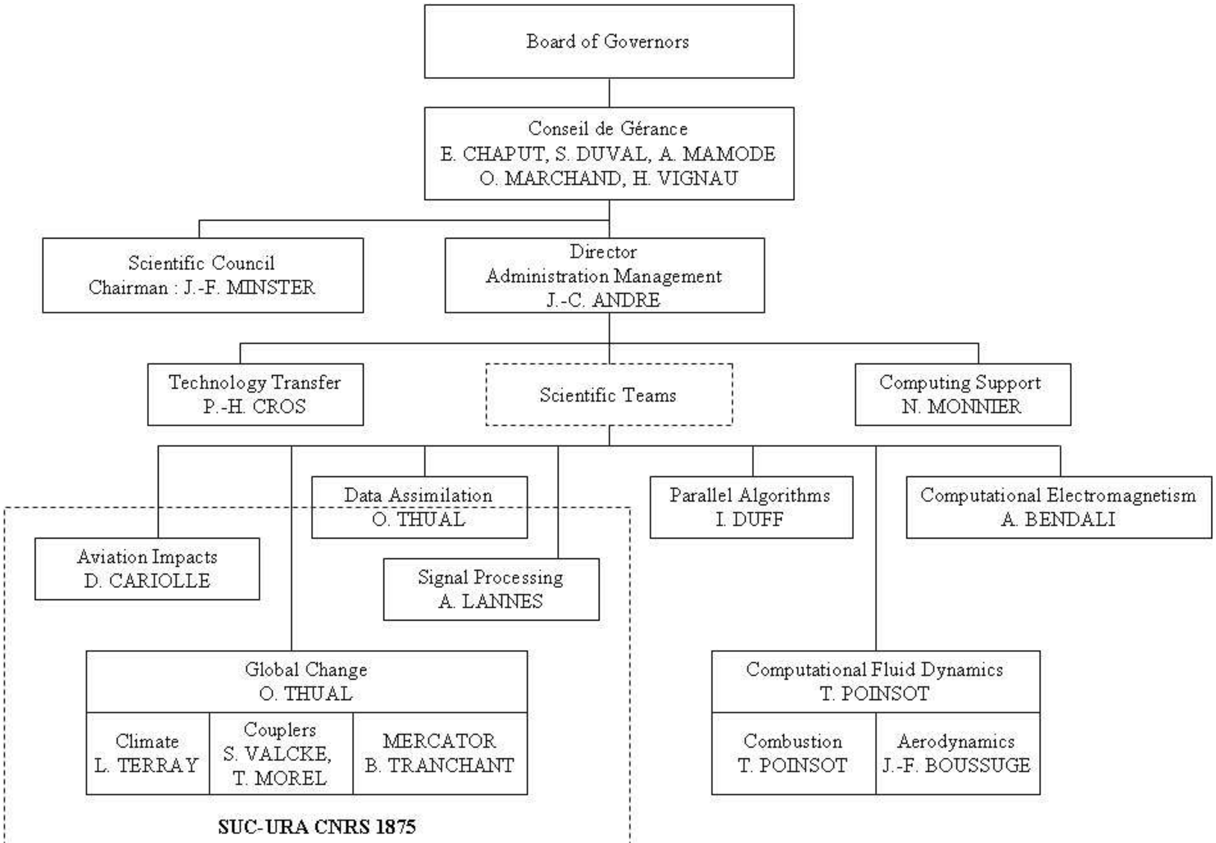

CERFACS chart as of Dec. 31, 2005

CERFACS Staff

NAME	POSITION	PERIOD
DUFF	Project Leader	1988/11
CHATELIN	Group leader	1988/09
GIRAUD	Senior	1993/10-2005/08
GRATTON	Senior	2002/07
VAN GIJZEN	Senior	2002/02-2004/10
BASTIN	Post Doc	2005/01
CARPENTIERI	Post Doc	2003/01-2004/12
HULSEMANN	Post Doc	2005/04-2005/11
LOGHIN	Post Doc	2002/10-2004/10
VASSEUR	Post Doc	2005/10
AHMADNASAB	Ph.D student	2003/08
BABOULIN	Ph.D student	2003/09
HAIDAR	Ph.D student	2005/03
MARTIN	Ph.D student	2001/10-2005/09
MOUFFE	Ph.D student	2005/10
RIYAVONG	Ph.D student	2002/07-2004/12
SLAVOVA	Ph.D student	2005/03
PRALET	Ph.D student	2002/09-2004/10
HAMERLING	Engineer	2004/02-2005/07
BOUALAOUI	Student	2004/06-2004/07
DELMAS	Student	2005/06-2005/09
DHOUIB	Student	2004/06-2004/07
DUBOIS	Student	2004/06-2004/07
FORCINAL	Student	2004/06-2004/07
FRIEDMANN	Student	2005/02-2005/07
KOUTCHOUGALI	Student	2004/06-2004/07
MOCH	Student	2005/06-2005/07
MORTAJI	Student	2004/06-2004/07
OBERDORFF	Student	2004/04-2004/07
ZIRCHER	Student	2005/02-2005/06
AMESTOY	Engineer	2005/12
HAMERLING	Engineer	2004/02-2005/07
LE BERRE	Engineer	2005/06

TAB. ii – List of members of the PARALLEL ALGORITHMS project.

NAME	POSITION	PERIOD
POINSOT	Project Leader	1992/09
CHEVALIER	Senior	1999/11
CUENOT	Senior	1996/10
JOUHAUD	Senior	2001/10
GICQUEL	Senior	2004/02
MONTAGNAC	Senior	2000/11
PAOLI	Senior	2004/07
PUIGT	Senior	2005/12
BARTON	Post Doc	2002/09-2004/08
BEER	Post Doc	2004/06-2005/05
BOIN	Post Doc	2004/12-2005/11
CELIC	Post Doc	2003/09-2005/03
HANSS	Post Doc	2003/04-2005/03
MOET	Post Doc	2003/04-2004/11
VAROQUIE	Post Doc	2003/01-2004/12
VERMOREL	Post Doc	2005/11
ALBOUZE	Ph.D student	2005/10
ARTAL	Ph.D student	2002/11-2005/10
AUFFRAY	Ph.D student	2003/10
BENOIT	Ph.D student	2001/10-2005/03
BOILEAU	Ph.D student	2003/10
BOUDIER	Ph.D student	2004/10
COLIN	Ph.D student	2004/12
DAUPTAIN	Ph.D student	2002/10
DELBOVE	Ph.D student	2001/10
DEVESA	Ph.D student	2003/10
DUCHAINE	Ph.D student Student	2004/10 2004/02-2004/08
GARCIA	Ph.D student Engineer	2005/10 2004/03-2005/08
GIAUQUE	Ph.D student	2003/09
LACAZE	Ph.D student	2005/11
LAMARQUE	Ph.D student Student	2004/10 2004/02-2004/08
LAVEDRINE	Ph.D student Student	2004/10 2004/03-2004/08
MARTIN	Ph.D student	2002/05-2005/04
MENDEZ	Ph.D student Student	2004/10 2004/02-2004/09
MOSSA	Ph.D student	2001/10-2005/03
NYBELEN	Ph.D student Student	2004/11 2004/04-2004/09
PASCAUD	Ph.D student	2002/10
PORTA	Ph.D student	2004/04
PRIERE	Ph.D student	2001/10-2004/12
RIBER	Ph.D student	2003/10
ROUX	Ph.D student	2003/10

TAB. iii – List of members of the COMPUTATIONAL FLUID DYNAMICS project (1/2).

SCHMITT	Ph.D student Student	2005/10 2005/03-2005/09
SELLE	Ph.D student	2000/09-2004/04
SENGISSEN	Ph.D student	2002/10
SENSIAU	Ph.D student	2005/03
STAFFELBACH	Ph.D student	2002/10
THOBOIS	Ph.D student	2002/10
TOUSSAINT	Ph.D student	2002/10-2005/09
TRUFFIN	Ph.D student	2001/09-2005/01
BOUSSUGE	Research Engineer	2002/02
CHAMPAGNEUX	Research Engineer	1997/11-2005/05
SOMMERER	Research Engineer	2002/04
BLANC	Research Engineer Student	2005/10 2005/02-2005/08
DENEVE	Engineer	2003/03-2004/08
LOERCHER	Engineer	2004/01-2004/06
MARGERIT	Engineer	2003/10-2005/01
NEGULESCU	Engineer	2005/01-2005/11
SAUDREAU	Engineer	2004/04-2005/04
SCHMITT	Engineer Ph.D student	2005/04-2005/09 2002/03-2005/03
TOURNIER	Engineer	2005/04
JAEGLE	Student	2005/04-2005/09
LABEYRIE	Student	2004/02-2004/08
MARTINEZ	Student	2005/02-2005/08
ROUX	Student	2005/03-2005/09
SICOT	Student	2005/09
WILLEMSE	Student	2004/09-2005/03
BAILLY	Visitor	2004/03-2004/03
BREAR	Visitor	2005/09
MULLER	Visitor	1997/11/
NICOUD	Visitor	2001/10
RIZZI	Visitor	1987/10
SAGAUT	Visitor	2003/12
SCHONFELD	Visitor	2001/01

List of members of the COMPUTATIONAL FLUID DYNAMICS project (2/2).

NAME	POSITION	PERIOD
THUAL	Project Leader	1991/09
ROGEL	Senior	1998/10
TERRAY	Senior	1992/10
WEAVER	Senior	1999/11
MASSART	Senior Post Doc	2004/12 2002/12-2004/11
SANCHEZ	Post Doc Post Doc	2005/05 2004/01-2004/12
BOE	Ph.D student Student	2004/10 2004/02-2004/06
CAMINADE	Ph.D student	2003/10
CIBOT	Ph.D student	2001/09-2004/08
DAGET	Ph.D student Engineer	2005/05 2003/11-2005/04
MINVIELLE	Ph.D student Student	2005/09 2005/02-2005/06
NAJAC	Ph.D student	2005/10
BUIS	Research Engineer	2003/01-2005/10
DECLAT	Research Engineer	2001/08-2004/09
MAISONNAVE	Research Engineer	2000/12
MOREL	Research Engineer	2000/03
VALCKE	Research Engineer	1997/02
BARRIQUAND	Engineer	2003/12-2005/05
BOURRIQUET	Engineer	2005/11
EPITALON	Engineer Engineer	2005/09 2004/10-2005/05
GHATTAS	Engineer	2005/02
MAYNARD	Engineer	2003/12 -2004/03
RICCI	Engineer	2004/01 - 2004/05
RODRIGUEZ	Engineer Student	2005/09 2005/02-2005/06
AGUIR	Student	2005/02-2005/07
ANDREZ	Student	2004/06-2004/09
BENOIT	Student	2005/02-2005/06
GIBERT	Student	2004/03-2004/08
LEFORT	Student	2004/05-2004/06
MASSART	Student	2005/05-2005/06
MINATOUY	Student	2005/02-2005/03
PELISSIER	Student	2004/06-2004/07
RAPAPORT	Student	2004/02-2004/07
STELLA	Student	2005/02-2005/08
UBELMANN	Student	2005/02-2005/06
GACON	Visitor	2003/04
CASSOU	CNRS	2002/11
LORANT	CNRS	2004/09

TAB. iv – List of members of the CLIMATE MODELLING & GLOBAL CHANGE project.

NAME	POSITION	PERIOD
FLEURY	Senior	2001/03-2004/04
TRANCHANT	Senior	2001/07
GARRIC	Senior Post Doc	2005/03 2003/03-2005/02
LELLOUCHE	Senior	2002/10
REMY	Senior	2003/12
SIEFRIDT	Senior	1998/01-2004/08
DREVILLON	Post Doc	2004/06
BOURDALLE-BADIE	Research Engineer	2001/01
DERVAL	Research Engineer	2003/07
DRILLET	Research Engineer	1999/03
LABORIE	Engineer	2005/08

TAB. v – List of members of the MERCATOR group.

NAME	POSITION	PERIOD
BENDALI	Project Leader	1996/01
FARES	Senior	1992/06
MILLOT	Senior	1995/11
BARTOLI	Senior	2003/02-2004/12
PERNET	Post Doc	2005/03
BALIN	Ph.D.student	2002/03-2005/09
ZERBIB	Ph.D.student	2002/10
CLESSE	Student	2005/06-2005/08
DARBAS	Student	2004/06-2004/09
MAKHLOUF	Student	2004/03-2004/07
WADEL	Student	2005/07-2005/08
WOJAC	Student	2005/06-2005/08
COLLINO	Visitor	1994/04

TAB. vi – List of members of the COMPUTATIONAL ELECTROMAGNETISM project.

NAME	POSITION	PERIOD
CARIOLLE	Project Leader	2003/08
PAOLI	Senior	2004/07
PAUGAM	Ph.D Student	2005/01
PIACENTINI	Engineer Engineer	2005/11 2005/02-2005/07
LARRIGAUDERE	Student	2004/02-2004/06

TAB. vii – List of members of the ENVIRONMENTAL IMPACT OF AVIATION project.

NAME	POSITION	PERIOD
LANNES	Project Leader	1994/01
PICARD	Ph.D student	2001/10-2004/11
ANTERRIEU	CNRS	1993/07-2004/11

TAB. viii – List of members of the SIGNAL & IMAGE PROCESSING project.

NAME	POSITION	PERIOD
CROS	Project leader	1997/04
JONVILLE	Engineer	2000/10
MILHAC	Engineer	2004/01
MOINAT	Engineer	2000/03-2004/08

TAB. ix – List of members of the TECHNOLOGY TRANSFER group.

NAME	POSITION	PERIOD
MONNIER	Project Leader	1996/12
D'AST	Engineer	1996/10
LAPORTE	Engineer	1988/04
DEJEAN	Technician	1990/11
FLEURY	Technician	1999/10
BARRAS	Student	2004/06-2004/08
BELHAJI	Student	2004/06-2004/09
FEYTEL	Student	2004/06-2004/08
LAFFORGUE	Student	2004/04-2004/06
POMES	Student	2005/04-2005/06

TAB. x – List of members of the COMPUTER SUPPORT group.

CERFACS Wide-Interest Seminars

Dominikus Noll (Université Paul Sabatier) : *New strategies in robust feedback control design.* (Feb. 4, 2004)

Laurent Dumas (Université Paris VI) :*Méthodes d'optimisation hybride appliquées à des problèmes industriels.* (Feb. 17, 2004)

Andy Wathen (Oxford University, UK) : *Computational models for patterning on a growing butterfly.* (March 18, 2004)

Sean C. Garrick (University of Minnesota, USA) : *The effects of turbulence on nanoparticle growth.* (March 22, 2004)

Kyle D. Squires (Arizona State University, USA) : *Wall-layer modeling for high-Reynolds number prediction using large eddy simulation.* (April 21, 2004)

Sébastien Masson (Kanagawa, Japan) : *Barrier layer in the Indian ocean in a 200 year simulation of the SINTEX-Frontier, CGCM (and other additional results).* (May 4, 2004)

Gene H. Golub (Stanford University, USA) : *Adaptive methods for updating/downdating page ranks.* (June 3, 2004)

Richard C. J. Sommerville (University of California, USA) : *Evaluating new cloud-radiation and hydrologic cycle parameterizations.* (June 17, 2004)

Frédéric Nataf (Ecole Polytechnique, Paris) : *Optimized interface conditions in domain decomposition methods in the case of extreme contrasts in the coefficients.* (Sep. 23, 2004)

Philippe Toint (University of Namur, Belgium) : *A glimpse into daily travel patterns.* (Nov. 4, 2004)

James Orr (CEA) : *Acidification de l'océan au 21ème siècle.* (Feb. 7, 2005)

Robert A. van de Gejin (University of Texas, USA) : *Towards the final generation of dense linear algebra libraries.* (March 7, 2005)

Bruno Koobus (Université de Montpellier II) : *LES, VMS-LES et LNS pour la simulation d'écoulements compressibles en maillages non structurés : application à des écoulements tourbillonnaires autour d'obstacles.* (April 8, 2005)

Jose M. Laginha M. Palma (CesA, Portugal) : *Wind flow predictions over forested and deforested complex terrain for wind energy applications.* (May 3, 2005)

Simon Mason (Columbia University, USA) : *Identifying and predicting the effects of climate variability on malaria incidence in Botswana : an application of the DEMETER project.* (June 17, 2005)

Charles Meneveau (Johns Hopkins University, USA) : *Issues and case studies for experimental validation of LES in incompressible.* (June 20, 2005)

Magdi Shoucri (Institut de Recherche d'Hydro-Québec, Canada) : *The application of a fractional steps method for the numerical solution of the shallow water equations.* (June 23, 2005)

Marc Garbey (University of Houston, USA) : *A few challenging problems in computational sciences.* (June 28, 2005)

Frank Hulsemann (CERFACS) : *Pushing geometric multigrid to its limits.* (Sep. 20, 2005)

Andre Kaufmann (Siemens VDO Regensburg, Germany) : *One dimensional IC engine simulation : from acoustics to heat release.* (Sep. 29, 2005)

Jean-François Royer & Fabrice Chauvin (Météo-France, CNRM) : *Impact du réchauffement climatique sur les ouragans.* (Dec. 13, 2005)

1

Parallel Algorithms Project

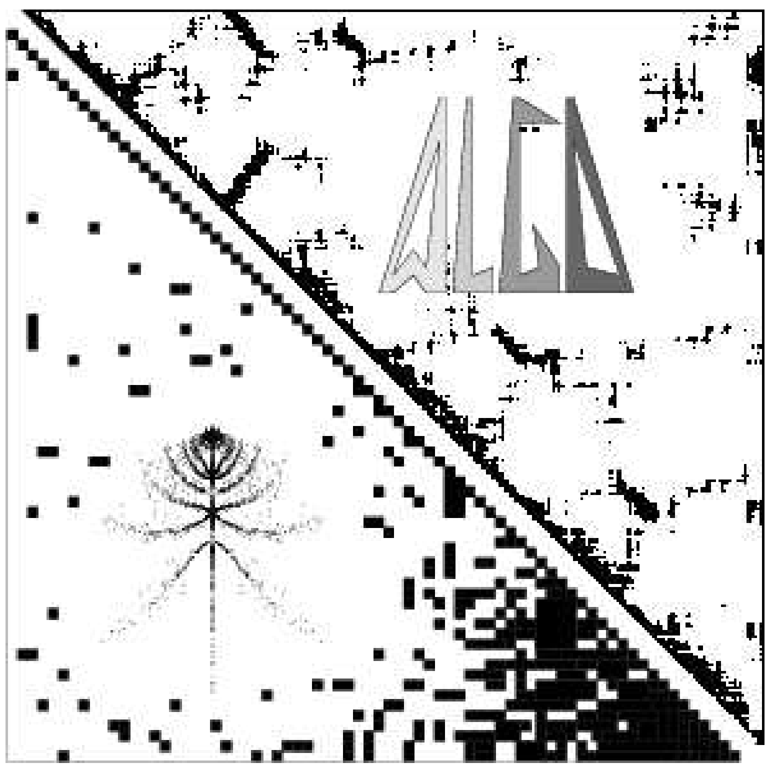

1 Introduction

1.1 Introduction

The research programme conducted by the Parallel Algorithms Project combines the excitement of basic research discoveries with their use in the solution of large-scale problems in science and engineering in academic research, commerce, and industry. We are concerned both with underlying mathematical and computational science research, the development of new techniques and algorithms, and their implementation on a range of high performance computing platforms.

The description of our activities is presented in several subsections, but this is only to give a structure to the report rather than to indicate any compartmentalization in the work of the Project. Indeed one of the strengths of the Parallel Algorithms Project is that members of the Team work very much in consultation with each other so that there is considerable overlap and cross-fertilization between the areas demarcated in the subsequent pages. This cross-fertilization extends to formal and informal collaboration with other teams at CERFACS, the shareholders of CERFACS, and research groups and end users elsewhere. In fact, it is very interesting to me how much the research directions of the Project are increasingly influenced by problems from the partners.

Members of the Team very much play their full part in the wider academic and research community. They are involved in Programme Committees for major conferences, are editors and referees for frontline journals, and are involved in research and evaluation committees. These activities both help CERFACS to contribute to the scientific life of France, Europe and the world while at the same time maintaining the visibility of CERFACS within these communities. Some measure of the visibility of the Parallel Algorithms Project can be found from the statistics of accesses to the CERFACS Web pages where a major part of all the hits for CERFACS projects are on the Algo web pages.

Our main approach in the direct solution of sparse equations continues to be the multifrontal technique originally pioneered at Harwell in the early 1980s. During this last period we have further developed the MUMPS package in conjunction with our colleagues at ENSEEIHT and INRIA-Lyon. The release currently being distributed is Version 4.6. Some research work that will most likely have an impact on future releases is discussed in the following sections. The code continues to be downloaded on a daily basis by researchers throughout the world. The complex version has been accessed extensively and used in many applications, particularly in electromagnetics.

Most of the work discussed in Section 3 is concerned with the direct factorization of symmetric indefinite and general sparse matrices. Considerable work has been done to understand and develop robust approaches to the case of symmetric indefinite matrices and some of the research work discussed later has been incorporated in `MUMPS`. Other work concerns the scheduling of the multifrontal factorization in a distributed memory environment and has a very significant impact on the performance of our parallel code. Some of the work on direct solvers has been supported by the bi-lateral Aurora grant that we have with Norway. Other research on examining the out-of-core parallel solution for one or many right-hand sides is still in its infancy but will hopefully also result in future improvements to `MUMPS`. We also report on the

ACI-GRID Project with ENSEEIHT and others on developing a Grid based expert site for sparse matrices called GRID-Tlse. The project ended in November 2005 and was a great opportunity to develop fruitful collaborations between researchers from different areas ranging from numerical analysis to middleware software. It has enabled some of the partners, namely CERFACS, ENS-Lyon and ENSEEIHT-IRIT, to continue some research in the framework of LEGO, a recently funded ANR project.

Although iterative methods remove many of the bottlenecks of direct approaches, particularly regarding memory, it is now well established that they can only be used in the solution of really challenging problems if the system is preconditioned to create a new system more amenable to the iterative solver. During this last period, we have continued our work on developing such preconditioners, including two-level schemes that effectively and explicitly remove error components in a subspace spanned by eigenvectors corresponding to small eigenvalues of the already preconditioned system. The use of such a two-level spectral scheme has proved very powerful in the solution of very large problems in electromagnetics, including the industry standard COBRA test problem. The notion of two-level schemes has also been implemented within a two level multigrid scheme for solving general unsymmetric problems and an examination comparing various ways of using spectral information has been conducted. Much of the work has been to extend these techniques so that they can be applied to a wide range of problems in different application areas. The work on inner-outer iterations, pioneered by the Team some years ago, has been developed further and extended both computationally and theoretically. The work on matrix partitioning schemes has been developed to provide an efficient block Jacobi preconditioner for use with standard iterative methods such as GMRES. It shows an expected good performance on parallel computers. Since the GMRES and FGMRES routines that are available on our web pages are high on the “google” list, are widely used, and have been downloaded over 5000 times, a future project might involve developing this preconditioner so that it can be used with these packages.

The main area of interest for the Qualitative Computing Group concerns a deep understanding of the influence of finite-precision computation on complex scientific numerical applications. Of particular concern are a deeper understanding of the role of nonlinearities and singularities in the context of floating-point arithmetic. A major tool in this work continues to be the use of homotopic deviations, a technique pioneered at CERFACS by the Qualitative Computing Group. An application of this work gives a theoretical basis to the sometimes unexpected good behaviour of Krylov type methods.

A major focus of our work on nonlinear systems and optimization has been in joint work with the PALM Project and the Climate Modelling Group on data assimilation. This area is becoming one of the main interdisciplinary focus points at CERFACS. We are particularly involved in a study of solution techniques for linear least-squares computations that lie at the heart of data assimilation algorithms, and we have investigated several aspects of this including appropriate condition numbers for this problem and the relationship of the 4D-Var algorithm and Gauss-Newton iterations. We are also developing software for solving large dense linear least-squares systems that is competitive with ScaLAPACK routines from the point of view of efficiency but requires about half the storage. Better techniques for the storage are also being explored. This work has led CERFACS to be included in a list of major contributors to the ScaLAPACK/LAPACK project. A new initiative in our optimization work is the innovative combination of multilevel schemes with trust region methods for optimization problems including those arising in the solution of partial differential equations. This work is being done jointly with our colleagues in Belgium and we have recently recruited a PhD student to do a co-tutelle thesis on this topic in conjunction with the University of Namur.

The Parallel Algorithms Project is heavily involved in the Advanced Training aspects of CERFACS’ mission. We ran internal training courses for new recruits to all Projects at CERFACS to give them a basic understanding of high performance computing and numerical libraries. This course was open to the shareholders of CERFACS. We are involved in training through the “stagiaire” system and feel that this is extremely useful to young scientists and engineers in both their training and their career choice. It can also help us to focus our research efforts and thus can benefit the work of the Team. A win-win situation. In this reporting period, we had five stagiaires : Remi Delmas from INSA, Olivier Friedmann and Christophe Oberdorf from ENSEEIHT, and Xavier Moch from ENS Lyon, and Eline Jonkers from Delft University in the Netherlands. Members of the Team have assisted in many lecture courses at other centres, including ENSICA, INPT, Toulouse 1 and INSA. Stéphane Pralet completed his PhD thesis on “Constrained orderings and scheduling for parallel sparse linear algebra" in September, 2004. I am delighted to record that the thesis was of such a high standard that Stéphane was awarded a Prix Léopold Escande by INPT. This is even more commendable when we consider that the thesis was completed in just over two years. Emeric Martin completed his PhD thesis on “Spectral two-level preconditioners for sequences of linear systems" in July 2005. It also gives us considerable pleasure to record that Serge Gratton successfully defended his HDR thesis on “Fast and Robust Solvers in Scientific Computing Applications in Geosciences” in December 2005.

Our list of visitors is a veritable who’s who of numerical analysts, including many distinguished scientists from Europe and the United States. We have included a list of the visitors at the end of this introduction. Six of our visitors stayed for a reasonably long period. These were : Abdellatif El Ghazi (eigenvalue problems), Gary Howell (matrix factorizations), Nancy Nichols (data assimilation), Marielba Rojas (optimization), Philippe Toint (optimization), and Jean Tshimanga (optimization and climate modelling). As always, it was a pleasure to welcome Gene Golub from Stanford who is a great source of inspiration especially to our younger students. In addition to inviting our visitors to give seminars, some of which are of general interest to other teams, we also run a series of “internal seminars” that are primarily for Team members to learn about each other’s work and are also a good forum for young researchers to hone their presentational skills. Frank Hülsemann took over the responsibility for running the CERFACS wide interest seminars from Martin van Gijzen in 2005 and they both ran a very active and energetic programme in support of these more general seminars.

We continue to have a “Sparse Days at CERFACS” meeting in June each year. In 2005, our normal annual formula was replaced by the Second International Workshop on Combinatorial Scientific Computing. This meeting, which we hosted in the main Météo Conference Centre, was co-sponsored by CERFACS, INRIA, IRIT, Région Midi-Pyrénées and SIAM, and was a great success. We attracted over 80 participants over half from outside France and half again from outside Europe. A number of distinguished scientists who came to this meeting also visited CERFACS and met members of the Team.

I am very pleased to record that, over the reporting period, we have continued our involvement in joint research projects with shareholders and with other teams at CERFACS.

We have a project with EADS on preconditioning techniques in electromagnetics. We have continued our joint effort with the CERFACS electromagnetics project on the solution of discretized Maxwell equations using the boundary element method in the framework of a DGA/Dassault contract. This has been an occasion for us to use techniques developed for perfect conductors in the more general context of impedance, and to run experiments with the GMRES-DR algorithm in this context.

We are represented in the CCT of CNES on orbitography and have developed a strong collaboration with them in the parallel distributed generation of normal equations and their subsequent Choleski factorization for applications in geodesy and computational electromagnetics.

We have had detailed discussions with EDF on parallel linear solvers and on embedded iterations for multi-phase flow. One of our postdocs, Frank Hülsemann, did such an excellent job in studying the use of a direct sparse solver within CODE ASTER, in particular comparing their in-house multifrontal code with `MUMPS`, that he was offered and accepted employment with EDF towards the end 2005. I am pleased that Xavier

Vasseur and Serge Gratton were able steer this project through its final stages and Xavier is now looking at null-space computations that are of great interest to EDF.
Our work on the optimization and linear algebraic aspects of data assimilation has been of great interest to and the subject of some discussions with the Climate Modelling and Global Change Group and Météo France. We now have a strong and growing collaboration with the Climate Modelling Team on aspects of data assimilation, and continue to co-host Jean Tshimanga a researcher from Belgium who is doing a PhD at Namur with Annick Sartenaer. In the context of this work, we have also hosted visits from Amos Lawless from the UK MET Office and from Nancy Nichols of the University of Reading who works partly in numerical analysis and partly with the meteorology department. We have also hosted, supervised, and worked with Hervé Le Berre, who was working on the parallelization of the Mocage code in the framework of a contract between CERFACS and Météo France.
We help the other Projects at CERFACS at all levels from the “over-a-coffee” consultancy to more major collaborations. These include advice on the elsA code of CFD and many aspects of numerical algorithms with Global Change. We are involved in close collaborations over linear solvers in electromagnetic codes with the EMC team. We have also interacted with the CSG group on issues concerning new computer chips and technologies.

As a postscript, I should record my thanks to my three seniors, Luc Giraud, Serge Gratton, and Martin Van Gijzen, for doing all the hard work to ensure the smooth running of the Team. Sadly Martin left us towards the end of 2004 to take up a post on the faculty at the university of Delft in his native Netherlands. It was with very mixed emotions that we learned that Luc had accepted a professorship at INPT. I say “mixed” because, on the one hand, we really will miss his energy and ability as deputy Project Leader in charge of the day to day running of the Team. On the other hand, we are delighted for him that he has such a prestigious post and also that he is not moving far from us so we can continue to welcome him as a senior visitor, thus strengthening even more our strong links with ENSEEIHT-IRIT. It is now Serge who has to bear the many responsibilities of the day-to-day management. I am very pleased to say that he does so in an excellent fashion and is well supported in his efforts by our enthusiastic and talented postdocs.

Iain S. Duff.

2 Dense and Sparse Matrix Computations

2.1 Hybrid scheduling for the parallel solution of linear systems

P. R. Amestoy : ENSEEIHT, *France* ; **A. Guermouche** : INRIA, *France* ; **J-Y. L'Excellent** : INRIA, *France* ; **S. Pralet** : CERFACS, *France*

We consider the problem of designing a dynamic scheduling strategy that takes into account both workload and memory information in the context of a parallel multifrontal factorization. The originality of our approach is that we base our estimations (work and memory) on a static optimistic scenario during the analysis phase. This scenario is then used during the factorization phase to constrain the dynamic decisions. The task scheduler has been redesigned to take into account these new features. Moreover, the performance has been improved because the new constraints allow the new scheduler to make optimal decisions that were forbidden or too dangerous in unconstrained formulations. Performance analysis in [1] show that the memory estimation becomes much closer to the memory effectively used and that, even in a constrained memory environment, we decrease the factorization time with respect to the initial approach. The algorithms will be integrated into the next release of `MUMPS`.

[1] P. R. Amestoy, A. Guermouche, J.-Y. L'Excellent, and S. Pralet, (2004), Hybrid scheduling for the parallel solution of linear systems, Research report RR-5404, INRIA. Also available as LIP report RR2004-53 and as an ENSEEIHT-IRIT technical report.

2.2 Symmetric weighted matching and application to indefinite multifrontal solvers

I. S. Duff : CERFACS, *France and* RUTHERFORD APPLETON LABORATORY, *England* ; **S. Pralet** : CERFACS, *France*

We study techniques for scaling and choosing pivots when using multifrontal methods in the LDL^T factorization of symmetric indefinite matrices where L is a lower triangular matrix and D is a block diagonal matrix with 1×1 and 2×2 blocks.

Our main contribution is to define a new method for scaling and a way of using an approximation to a symmetric weighted matching to predefine 1×1 and 2×2 pivots prior to the ordering and analysis phase. We also present new classes of orderings called “(relaxed) constrained orderings" that select pivots during the symbolic Gaussian elimination using two graphs : the first one contains information about the structure of the reduced matrix and the second one gives information about the numerical values.

We perform experiments with our symmetric preprocessing in [ALG47] and we validate our heuristics with a symmetric multifrontal code `MA57` [2] on real test problems in [ALG48, ALG28]. Our test sets include both augmented matrices and general indefinite matrices.

[2] I. S. Duff, (2002), MA57 - A new code for the solution of sparse symmetric defi nite and indefi nite systems, technical report RAL-TR-2002-024, Rutherford Appleton Laboratory.

2.3 Unsymmetric orderings using a constrained Markowitz scheme

P. R. Amestoy : ENSEEIHT, *France* ; **X. S. Li** : LAWRENCE BERKELEY NATIONAL LAB *Berkeley, CA* ; **S. Pralet** : CERFACS, *France*

We consider the LU factorization of unsymmetric sparse matrices using a three-phase approach (analysis, factorization and triangular solution). Usually the analysis phase first determines a set of potentially good pivots and then orders this set of pivots to decrease the fill-in in the factors. We present in [ALG32] a preprocessing algorithm that simultaneously achieves the objectives of selecting numerically good pivots and preserving the sparsity. We describe the algorithmic properties and difficulties in implementation. By mixing the two objectives we show that we can reduce the amount of fill in the factors and can reduce the number of numerical problems during factorization. On a set of large unsymmetric real problems, we obtain average gains of 14% in the factorization time, 12% in the size of the LU factors, and 21% in the number of operations performed in the factorization phase. Full details of our implementation are available in [ALG28].

2.4 Pivoting strategies for sparse symmetric indefinite systems

I.S. Duff : CERFACS, *France* ; **S. Pralet** : ENSEEIHT, *France*

We consider the direct solution of sparse symmetric indefinite matrices. We develop new pivoting strategies that combine numerical and static pivoting. Then an iterative refinement process uses our approximate factorization to compute a solution. We show that our pivoting strategies are numerically robust, that few steps of iterative refinement are required and that the factorization is significantly faster because of this static/numerical combination. Furthermore, we propose original approaches that are designed for parallel distributed factorization. A key point of our parallel implementation is the cheap and reliable estimation of the growth factor. This estimation is based on an approximation of the off-diagonal entries and does not require any supplementary messages.

2.5 Solving sparse linear systems in an out-of-core environment

P. Amestoy : ENSEEIHT, *France* ; **I.S. Duff** : CERFACS, *France* ; **T. Slavova** : CERFACS, *France*

In collaboration with INRIA and ENSEEIHT, we are working with MUMPS (Multifrontal Massively Parallel Solver) to solve large-scale equations using direct methods. The aim of our research is to design an out-of-core implementation of the solution phase efficient at reducing memory usage and computing time for both sequential and parallel environments.

Preliminary results indicate that, in a sequential environment, the out-of-core implementation is competitive with respect to the standard in core implementation. Although reasonable performance can be obtained on a moderate number of processors much work still has to be done to improve the parallel behaviour of the algorithms.

[3] E. Agullo, A. Guermouche, and J.-Y. L'Exellent, (2005), Preliminary Out-of-core Extension of a Parallel Multifrontal Solver, Technical Report, INRIA / LIP. In preparation.

2.6 Integration of the parallel, direct sparse linear solver MUMPS into CODE ASTER

O. Boiteau : EDF DIVISION R&D, *France* ; **F. Hülsemann** : CERFACS, *France* ; **X. Vasseur** : CERFACS, *France*

The long term goal of this collaboration is the integration of the parallel, direct sparse linear solver MUMPS into CODE ASTER, a structural mechanics code developed at EDF. The topic of the short note [4] is the comparison of the linear solver MUMPS with the inbuilt serial multifrontal out-of-core solver of CODE ASTER for two and three dimensional linear problems arising in structural mechanics. It summarizes the background of this study, explains the main steps of this comparison and presents few results.
A more detailed study was performed on a large number of test cases late in 2005. This comparison was done both in terms of run time performance and stability using backward error estimates. It has been found that MUMPS is an attractive alternative to the current multifrontal solver in CODE ASTER as its run time behaviour is more predictable and it offers error diagnostic and iterative refinement features that are currently not available in the inbuilt solver. A technical report on this work will be published early in 2006.

[4] O. Boiteau and F. Hülsemann, (2005), Suivi de la collaboration CERFACS/EDF R&D autour de MUMPS et de Code Aster, Tech. Rep. CR-I23/2005/032, EDF R&D.

2.7 The Grid-TLSE project

P. R. Amestoy : ENSEEIHT-IRIT**,** ***France*** ; **M. Buvry :** ENSEEIHT-IRIT**,** ***France*** ; **M. Daydé :** ENSEEIHT-IRIT**,** ***France*** ; **I. S. Duff** : CERFACS, *France and* RUTHERFORD APPLETON LABORATORY, *England* ; **L. Giraud :** CERFACS**,** ***France*** ; **Ch. Hamerling :** CERFACS**,** ***France*** ; **J.Y. L'Excellent :** INRIA-ENSL**,** ***France*** ; **M. Pantel :** ENSEEIHT-IRIT**,** ***France*** ; **C. Puglisi :** ENSEEIHT-IRIT**,** ***France***

In the context of large sparse calculations, we are involved as one of the leading partners of a ACI-Grid project (funded by the French Ministry of Research from December 2002 until November 2005). This project uses the Grid at several levels. It adds new services to the Grid and use the Grid capabilities to run these services. The principal services are mainly twofold :

– to provide the users with automatic expertise on sparse direct solvers using matrices either from the data base or provided by the user (a natural follow up step will be to extend this to iterative solvers).
– to make available to the scientific community a set of test problems through a data base. The set of examples will grow dynamically as users submit new problems that are integrated within the data set.

Experiments on the Grid-5000 platform have been performed. The results of the project have been presented at various conferences [6, 7, 5]. More information on the project can be found from the URL :

`http ://www.enseeiht.fr/lima/tlse`

[5] E. Caron, F. Desprez, J.-Y. L'Excellent, C. Hamerling, M. Pantel, and C. Puglisi-Amestoy, (2005), *Future Generation Grids*, vol. 2 of CoreGrid Series, Springer Verlag, ch. Use of A Network Enabled Server System for a Sparse Linear Algebra Application.

[6] M. Daydé, The GRID-TLSE Project and the Nation-Wide Grid Experimental Platform GRID'5000. See `http ://vds.cnes.fr/manifestations/grilles2005/welcome.html`.

[7] M. Daydé, A. Hurault, and M. Pantel, (2005), Gridifi cation of Scientifi c Applications Using Software Components : the GRID-TLSE Project as an Illustration, In *Proceedings of CSIT05, Fifth International Conference on Computer Science and Information Technologies, Yerevan, Armenia*, 419–427.

3 Iterative Methods and Preconditioning

3.1 Combining direct and iterative methods for the solution of large systems in different application areas

I. S. Duff : CERFACS, *France and* RUTHERFORD APPLETON LABORATORY, *England*

We first consider the size of problems that can currently be solved by sparse direct methods. We then discuss the limitations of such methods, where current research is going in moving these limitations, and how far we might expect to go with direct solvers in the near future.

This leads us to the conclusion that very large systems, by which we mean three dimensional problems in more than a million degrees of freedom, require the assistance of iterative methods in their solution. However, even the strongest advocates and developers of iterative methods recognize their limitations when solving difficult problems, that is problems that are poorly conditioned and/or very unstructured. It is now universally accepted that sophisticated preconditioners must be used in such instances.

A very standard and sometimes successful class of preconditioners are based on incomplete factorizations or sparse approximate inverses, but we very much want to exploit the powerful software that we have developed for sparse direct methods over a period of more than thirty years. We thus discuss various ways in which a symbiotic relationship can be developed between direct and iterative methods in order to solve problems that would be intractable for one class of methods alone. In these approaches, we will use a direct factorization on a “nearby” problem or on a subproblem.

We then look at examples using this paradigm in four quite different application areas ; the first solves a subproblem and the others a nearby problem using a direct method.

We presented this work [ALG51] at a conference in Delhi in December 2004.

3.2 Parallel preconditioners based on partitioning sparse matrices (I. S. Duff, L. Giraud, S. Riyavong, and M. B. Van Gijzen)

We describe a method for constructing an efficient block diagonal preconditioner for accelerating the iterative solution of general sets of sparse linear equations. Our method uses a hypergraph partitioner on a scaled and sparsified matrix and attempts to ensure that the diagonal blocks are nonsingular and dominant. We illustrate our approach using the partitioner PaToH and the Krylov-based GMRES algorithm. We verify our approach with runs on problems from economic modelling and chemical engineering, traditionally difficult applications for iterative methods. Our approach and the block diagonal preconditioning lends itself to good exploitation of parallelism. This we also demonstrate. We presented the work at the PMAA’04 conference in Marseilles and have submitted it to the Journal Parallel Computing [ALG50].

3.3 Additive and multiplicative two-level spectral preconditioning for general linear systems

B. Carpentieri : CERFACS, *France* ; **L. Giraud** : CERFACS, *France* ; **S. Gratton** : CERFACS, *France*

Multigrid methods are among the fastest techniques for solving linear systems arising from the discretization of partial differential equations. The core of the multigrid algorithms is a two-grid procedure that is applied recursively. A two-grid method can be fully defined by the smoother that is applied on the fine grid, the coarse grid and the grid transfer operators to move between the fine and the coarse grid. With these ingredients both additive and multiplicative procedures can be defined. In this project, we develop preconditioners for general sparse linear systems that exploit ideas from the two-grid methods. They attempt to improve the convergence rate of a prescribed preconditioner M_1 that is viewed as a smoother, the coarse space is spanned by the eigenvectors associated with the smallest eigenvalues of the preconditioned matrix M_1A. We derive both additive and multiplicative variants of the iterated two-level preconditioners for unsymmetric linear systems that can also be adapted for Hermitian positive definite problems. We show that these two-level preconditioners shift the smallest eigenvalues to one and tend to better cluster around one those that M_1 already succeeded to move to the neighbourhood of one. We illustrate the performance of our method through extensive numerical experiments on a set of general linear systems. Finally, we consider two case studies, one from a non-overlapping domain decomposition method in semiconductor device modelling, another one from electromagnetism applications. Results of this study are presented in [ALG38].

3.4 A comparative study of iterative solvers exploiting spectral information for SPD systems

L. Giraud : CERFACS, *France* ; **D. Ruiz** : ENSEEIHT-IRIT, *France* ; **A. Touhami** : ENSEEIHT-IRIT, *France*

When solving the Symmetric Positive Definite (SPD) linear system $Ax = b$ with the conjugate gradient method, the smallest eigenvalues in the matrix A often slow down the convergence. Consequently if the smallest eigenvalues in A could be somehow “removed”, the convergence may be improved. This observation is of importance even when a preconditioner is used, and some extra techniques might be investigated to futher improve the convergence rate of the conjugate gradient on the given preconditioned system. Several techniques have been proposed in the literature that either consist of updating the preconditioner or enforcing the conjugate gradient algorithm to work in the orthogonal complement of an invariant subspace associated with the smallest eigenvalues. Among these approaches we consider first a two-phase algorithm using a deflation-type idea. In a first stage this algorithm computes a partial spectral decomposition simply using matrix-vector products. More precisely it combines Chebyshev iterations with a block Lanczos procedure to accurately compute an orthogonal basis of the invariant subspace associated with the smallest eigenvalues. Then, the solution on this subspace is computed using a projector while the solution in the orthogonal complement is obtained with Chebyshev iterations that benefit from the reduced condition number.

For the sake of comparison, this eigen-information is used in combination with other techniques. In particular we consider the deflated version of conjugate gradients. As representative of techniques exploiting the spectral information to update the preconditioner we consider also the approaches that attempt to shift the smallest eigenvalues close to one where most of the eigenvalues of the preconditioned matrix should be located. In this work, we study these various variants as well as the observed numerical behaviour on a set of model problems from the Matrix Market or arising from the discretization of some 2D heterogeneous

diffusion PDE problems via finite-element techniques. We discuss their numerical efficiency, computational complexity and sensitivity to the accuracy of the eigencalculation.
For more details on this work we refer to [ALG59].

3.5 Convergence in backward error of relaxed GMRES

L. Giraud : CERFACS, *France* ; **S. Gratton** : CERFACS, *France* ; **J. Langou** : UNIVERSITY OF TENNESSEE, *USA*

This work is the follow up of the experimental study presented in [ALG7]. It is based on and extends some theoretical results in [8, 9]. In a backward error framework, we study the convergence of GMRES when the matrix-vector products are performed inaccurately. This inaccuracy is modelled by a perturbation of the original matrix. We prove the convergence of GMRES when the perturbation size is proportional to the inverse of the computed residual norm ; this implies that the accuracy can be relaxed as the method proceeds which gives rise to the terminology relaxed GMRES. As for exact GMRES, we show under proper assumptions that only happy breakdowns can occur. Furthermore, the convergence can be detected using a by-product of the algorithm. We explore the links between relaxed right-preconditioned GMRES and flexible GMRES. In particular this enables us to derive a proof of convergence of FGMRES. Finally we report results on numerical experiments to illustrate the behaviour of the relaxed GMRES monitored by the proposed relaxation strategies.

[8] V. Simoncini and D. B. Szyld, (2003), Theory of Inexact Krylov Subspace Methods and Applications to Scientific Computing, **25**, 454–477.

[9] J. van den Eshof and G. L. G. Sleijpen, (2004), Inexact Krylov subspace methods for linear systems, **26**, 125–153.

3.6 Incremental spectral preconditioners for sequences of linear systems

L. Giraud : CERFACS, *France* ; **S. Gratton** : CERFACS, *France* ; **E. Martin** : CERFACS, *France*

In many scientific applications a set of linear systems with the same coefficient matrix but different right-hand sides have to be solved in sequence. Such a situation exists for instance in the calculation of the radar cross section for electromagnetic calculations or in the calculation of eigenvalues using shift and invert techniques, etc. Efficient methods for tackling this problem attempt to benefit from the previously solved right-hand sides for the solution of the next. This goal can be achieved either by recycling Krylov subspaces (see for instance [14] and references therein) or by building preconditioner updates based on near invariant subspace information (see for instance [10, 11, 12] and references therein). In this work we investigate the use of Krylov linear solvers based on an Arnoldi process, that are variants of GMRES. In particular, because we aim at removing the possible slowdown effect of the smallest eigenvalues, we consider the GMRES-DR solver [13]. The harmonic Ritz vectors computed by this linear solver for a given right-hand side are used to update an incremental spectral low-rank preconditioner [11] that is used for the next right-hand side. We implement several strategies to extract the appropriate spectral information and illustrate their numerical behaviour on some academic problems from the Matrix Market as well as from large computations in industrial electromagnetic applications.
Results of this study are presented in [ALG55, ALG27].

[10] J. Baglama, D. Calvetti, G. H. Golub, and L. Reichel, (1999), Adaptively Preconditioned GMRES Algorithms, *SIAM J. Scientific Computing*, **20(1)**, 243–269.

[11] B. Carpentieri, I. S. Duff, and L. Giraud, (2003), A class of spectral two-level preconditioners, *SIAM J. Scientific Computing*, **25**, 749–765.

[12] J. Erhel, K. Burrage, and B. Pohl, (1996), Restarted GMRES preconditioned by deflation, *J. Comput. Appl. Math.*, **69**, 303–318.

[13] R. B. Morgan, (2002), GMRES with deflated restarting, *SIAM J. Scientific Computing*, **24(1)**, 20–37.

[14] M. L. Parks, E. de Sturler, G. Mackey, D. D. Jhonson, and S. Maiti, (2004), Recycling Krylov subspaces for sequences of linear systems, Technical Report UIUCDCS-R-2004-2421 (CS), University of Illinois at Urbana-Champaign.

3.7 Parallel algebraic preconditioners for the solution of Schur complement systems in 3D

L. Giraud : CERFACS, *France* ; **A. Haidar** : CERFACS, *France* ; **S. Mulligan** : DUBLIN INSTITUTE OF TECHNOLOGY, , *Ireland*

Domain decomposition methods are a natural way to parallelize the numerical solution of elliptic partial differential equations for 2D and 3D problems. In this study we consider the parallel solution of a standard finite element discretisation of 3D elliptic problems. The method used is a preconditioned conjugate-gradient solver following [16, ALG19] on the Schur complement system for the interface unknowns. An additive Schwarz preconditioner is computed which consists of the local assembled Schur complements for each subdomain. These Schur complements are computed using the MUMPS [15] package. We also used a sparsified version of this preconditioner, where elements whose relative magnitudes are below a certain tolerance are dropped ; this typically results in Cholesky factors that retain only about 10% of the original dense factors. The resulting block-preconditioners are compared with an approach that consists in using a sparsified approximation of the complete Schur complement. This latter sparsified Schur complement is factorized in parallel by MUMPS and used as a preconditioner.
The methods were implemented on an IBM SP by assigning each sub-domain to a single process and using MPI for the parallel communication. The numerical results have been obtained for a number of model problems, including problems with variable and discontinuous coefficients [17]. The preliminary results indicate a good parallel scalability of these methods for 3D problems, in that the convergence rate is not seriously degraded as the number of domains increases. Further tests are being carried out, including comparisons with a direct solver and the results will be the subject of a forthcoming report.

[15] P. R. Amestoy, I. S. Duff, J.-Y. L'Excellent, and J. Koster, (2001), A fully asynchronous multifrontal solver using distributed dynamic scheduling, *SIAM J. Matrix Analysis and Applications*, **23**, 15–41.

[16] L. M. Carvalho, L. Giraud, and G. Meurant, (2001), Local preconditioners for two-level non-overlapping domain decomposition methods, *Numerical Linear Algebra with Applications*, **8**, 207–227.

[17] L. Giraud, S. Mulligan, and J. Rioual, (2004), Algebraic preconditioners for the solution of Schur complement systems. SIAM Conference on Parallel Processing for Scientific Computing, talk.

3.8 Parallel Distributed Numerical Simulations in Aeronautic Applications

G. Alléon : EADS CRC, *France* ; **S. Champagneux** : CERFACS, *France* ; **G. Chevalier** : CERFACS, *France* ; **L. Giraud** : CERFACS, *France* ; **G. Sylvand** : EADS CRC, *France*

Numerical simulation plays a key role in industrial design because it reduces the time and the cost to develop new products. Because of international competition, it is important to have a complete chain of simulation tools to perform efficiently some virtual prototyping. In this paper, we describe two components of large aeronautic numerical simulation chains that are extremely consuming of computer resources. The first concerns computational fluid dynamics for aerodynamic studies. The second is used to study

the wave propagation phenomena and concerns acoustics. Because those softwares are used to analyse large and complex case studies in a limited amount of time, they are implemented on parallel distributed computers. We describe the physical problems addressed by these codes and the main characteristics of their implementation. For the sake of re-usability and interoperability, the software is developed using object-oriented technologies. We illustrate their parallel performance on clusters of symmetric multiprocessors. Finally, we discuss some challenges for the future generations of parallel distributed numerical software that will have to enable the simulation of multi-physics phenomena in the context of virtual organizations also known as the extended enterprise.
Results of this study are presented in [ALG30]

3.9 Bounds on the eigenvalue range and on the field of values of non-Hermitian and indefinite finite element matrices

D. Loghin : CERFACS, *France* ; **M. B. van Gijzen** : CERFACS, *France* ; **E. Jonkers** : CERFACS, *France*

In the beginning of the seventies, Fried [18] formulated bounds on the spectrum of assembled Hermitian (semi-)Positive Definite finite-element matrices using the extreme eigenvalues of the element matrices. Since element matrices are small in size relative to the assembled matrix, these eigenvalue bounds are cheap to compute.
We have generalised the bounds proposed by Fried for non-Hermitian and indefinite matrices. In particular, we have derived bounds on the Field of Values, on the spectrum and on the numerical radius for both the standard and the generalised problem.
We have illustrated our bounds with an example from acoustics that involves a complex, non-Hermitian matrix.
As an application, we have used our estimates in the GMRES algorithm for solving linear systems, to derive an upper bound on the number of iterations that is needed to achieve a residual norm that is smaller than a given tolerance.
We presented our results at the ICCAM 2004 conference in Leuven. The report [ALG61] has been submitted for publication in JCAM.

[18] I. Fried, (1973), Bounds on the spectral and maximum norms of the finite element stiffness, flexibility and mass matrices, *Int. J. Solids and Structures*, **9**, 1013–1034.

3.10 Inner-outer iterations

F. Chaitin-Chatelin : CERFACS AND UNIVERSITÉ TOULOUSE 1, *France* ; **N. Megrez** : CERFACS AND UNIVERSITÉ TOULOUSE 1, *France* ; **G. L. G. Sleijpen** : UTRECHT UNIVERSITY, *Netherlands* ; **J. van den Eshof** : UNIVERSITY OF DÜSSELDORF, *Germany* ; **M. B. van Gijzen** : CERFACS, *France*

There are classes of problems for which the matrix-vector product is a time consuming operation because an expensive approximation method is required to compute it to a given accuracy. Obviously, the more accurate the matrix-vector product is approximated, the more expensive or time consuming the overall process becomes. The question of how to control the accuracy of the matrix-vector product if the outer loop is a Krylov method has been extensively investigated at CERFACS [19, ALG7, 20, ALG42]. This work has led to the development of so called *relaxation strategies* in which the accuracy to which the matrix-vector multiplication is computed is reduced when the process comes closer to the solution. These strategies may yield a significant reduction of the computing time while the target accuracy is still achieved. However, they are far from being well understood theoretically and experimentally. On the theoretical side, some progress has been made by using the theory of Homotopic Deviation. We describe below some algorithmic advances which are supported by extensive numerical evidence. The research that we describe has (in part) been carried out in collaboration with the University of Utrecht and was supported through the Van Gogh programme for Dutch-French scientific collaborations.

In [21] we have investigated the possibility of increasing the computational gain that can be obtained by applying a relaxation strategy using a $nested$ Krylov method. The advantage of this approach is that the matrix-vector products in the inner loop only have to be computed to a low accuracy. The accurate matrix-vector products in the outer loop ensure that the target accuracy can be achieved. A revised and improved version of [21] has been accepted for publication in JCAM ([22]).

In the past year we have progressed in two different ways. Firstly we have studied a suitable strategy to control the error in the matrix-vector multiplications in restarted GMRES. Our first observation is that restarted GMRES is a nested method, with full GMRES in the inner loop (in which only a modest residual reduction has to be achieved) and Richardson's method in the outer loop. We have found that there are two different ways to control the errors, and the appropriate way depends on how the residuals are updated. If the residuals are computed recursively a relaxation strategy should be applied. If the residuals are computed directly form the latest iterand, however, a similar strategy as for Newton's method has to be employed, i.e. in the beginning of the process, the matrix-vector products can be performed with low accuracy, while the accuracy has to be increased when the approximate solution comes closer to the true solution. Our results were presented during a mini-symposium on inner-outer iterative methods (organised by M. van Gijzen) at the NAA'04 conference in Rousse, Bulgaria. [ALG63] has been accepted for publication in a volume of Lecture Notes in Computer Science (Springer).

We have also made progress in the theoretical understanding of the relaxation strategies. In [ALG64] we provide insight into why some iterative methods are more sensitive to errors in the matrix-vector product than others. The key observation is that the sensitivity for errors in the matrix-vector product is determined by the conditioning of the basis vectors to which the matrix-vector product is applied. The paper [ALG64] has been accepted for publication in the proceedings of the Third International Workshop on Numerical Analysis and Lattice QC.

As part of the partnership between EDF and CERFACS, consulting work was carried out with N. Megrez, a visiting post-doc from UT1 (Ceremath), in which we have analysed a nested algorithm for multi-phase flow calculations. One of the main difficulties in the present formulations is that special precautions have to be taken to preserve positive volume fractions. In this work we have suggested alternative formulations of the current algorithm for which we can derive a time-step such that positive volume fractions are always preserved.

[19] A. Bouras and V. Frayssé, (2000), A relaxation strategy for inexact matrix-vector products for Krylov methods, Technical Report TR/PA/00/15. Submitted to SIAM Journal in Matrix Analysis and Applications.

[20] A. Bouras, V. Frayssé, and L. Giraud, (2000), A relaxation strategy for inner-outer linear solvers in domain decomposition methods, Technical Report TR/PA/00/17.

[21] J. van den Eshof, G. L. G. Sleijpen, and M. B. van Gijzen, (2003), Relaxation strategies for nested Krylov methods., Technical Report TR/PA/03/27.

[22] J. van den Eshof, G. L. G. Sleijpen, and M. B. van Gijzen, (2005), Relaxation strategies for nested Krylov methods, **117**, 347–365.

3.11 Rounding error analysis of the classical Gram-Schmidt orthogonalization process

L. Giraud : CERFACS, *France* ; **J. Langou** : UNIVERSITY OF TENNESSEE, *U.S.A.* ; **Miroslav Rozložník** : ACADEMY OF SCIENCES OF THE CZECH REPUBLIC, *Czech Republic* ; **J. van den Eshof** : HEINRICH-HEINE-UNIVERSITÄT, *Germany*

In many applications it is important to compute an orthonormal basis $Q = (q_1, \ldots, q_n)$ of $span(A)$ such that $A = QR$, where R is upper triangular matrix of order n. In this work we focus on the Classical Gram-Schmidt (CGS) orthogonalization process. Due to roundoff errors the set of vectors Q produced by this method can be far from orthogonal and sometimes the orthogonality can even be completely absent. In this work we provide two results on the numerical behaviour of the classical Gram-Schmidt algorithm that enable us to predict the level of orthogonality (*the quality*) obtained after the orthogonalization. Up to now there was no bound available for the loss of orthogonality of vectors computed by the CGS process. In the first part of the work, we derive a new bound for the loss of orthogonality in the CGS process. Provided that the matrix A^TA is numerically nonsingular, we show that the loss orthogonality of the vectors computed by the CGS algorithm can be bounded by a term proportional to the square of the condition number, i.e. $\kappa^2(A)$, times the unit roundoff. We illustrate through an numerical experiment that this bound is indeed tight.

In some other applications it may be important to produce a set of basis vectors for which the orthogonality is close to the machine precision. In this case the orthogonality of the vectors computed by a Gram-Schmidt process can be improved by reorthogonalization, where the orthogonalization step is iterated twice. In the second part of this work we analyse the CGS algorithm with reorthogonalization, where each orthogonalization step is performed exactly twice The main result of this section is a proof of the fact that, assuming full rank of the matrix A, two iterations are sufficient to guarantee that the level of orthogonality of the computed vectors is close to the unit roundoff level.

These results are important from a theoretical point of view ; they fill the last gaps in the understanding of the Classical Gram-Schmidt algorithm. From a computational point of view, these results are very useful ; they enable us to choose the fastest algorithm depending on the level of orthogonality needed by the application on a given computing platform.

For more details on this work we refer to [ALG58, ALG18, ALG17].

3.12 On the parallel solution of large industrial wave propagation problems

L. Giraud : CERFACS, *France* ; **J. Langou** : UNIVERSITY OF TENNESSEE, *U.S.A.* ; **G. Sylvand** : EADS-CCR, *France*

The use of Fast Multipole Methods (FMM) combined with embedded Krylov solvers preconditioned by a sparse approximate inverse is investigated for the solution of large linear systems arising in industrial acoustic and electromagnetic simulations. We use a boundary elements integral equation method to solve the Helmholtz and the Maxwell equations in the frequency domain. The resulting linear systems are solved by iterative solvers using FMM to accelerate the matrix-vector products. The simulation code is developed in a distributed memory environment using message passing and it has out-of-core capabilities to handle very large calculations. When the calculation involves one incident wave, one linear system has to be solved. In this situation, embedded solvers can be combined with an approximate inverse preconditioner to design extremely robust algorithms. For radar cross section calculations, several linear systems have to be solved. They involve the same coefficient matrix but different right-hand sides. In this case, we propose a block variant of the single right-hand side scheme. The efficiency, robustness and parallel scalability of our approach are illustrated on a set of large academic and industrial test problems. For more details on this work we refer to [ALG57].

4 Qualitative Computing

Group members : Françoise Chaitin-Chatelin, Morad Ahmadnasab, CERFACS and Université Toulouse 1.

The work of the Qualitative Computing Group is an on-going collaborative effort to assess the validity of computer simulations. The central question is to assess the validity of computer results which are seemingly wrong such as in chaotic computations. This goal can be reached by discovering the laws of computation which govern finite-precision computations in the neighbourhood of algebraic singularities.
Some of these laws are now well understood for Numerical Linear Algebra. For example, one can cite i) the role of the normwise backward error to assess the reliability of numerical software in finite precision, ii) the role of nonnormality which makes approximated singularities appear much closer than they are in exact arithmetic.
These laws for finite-precision computations are derived from underlying laws for mathematical computation. Some of these more basic laws can be established by analytic tools (complex variables, matrix algebra). They include :

a) the basic role of $non\ linearities$ in computer simulations using floating-point arithmetic,

b) *inexact computing* and the associated homotopic deviation theory as a fruitful framework to understand approximate numerical methods, in exact arithmetic,

c) the unreasonable robustness of Krylov-type methods to perturbations in the data.

Their common feature is that the analysis of round-off is essentially 2-level (full versus machine precision). This 2-level analysis is sufficient for most matrix algorithms. But it cannot capture essential aspects of nonlinear computation such as chaotic iterations. These phenomena signal strong nonlinearities which are active at more than two levels. We currently explore such multiscale instability phenomena by means of Numerical Nonlinear Algebra.

Our research and understanding has been driven by work on practical numerical software applications in physics and technology, which come from CERFACS partners. In May 2004, Françoise Chaitin-Chatelin was one of the five external experts in charge of the review, for the EDF Scientific Council, of their ambitious programme to turn to "Numerical Simulation only" (Tout numérique) at the 2010 horizon.
We review below the work accomplished with respect to Qualitative Computing.

4.1 Homotopic Deviation in Linear Algebra

It is customary in Numerical Linear Algebra to analyse the robustness of a method/problem involving as data the matrix $A \in \mathbb{C}^{n\times n}$ by considering all (or a subset of) perturbations $\triangle A$ of A. This leads to perturbation theory and is successful when $\|\triangle A\|$ is not too large.
This approach finds its limits in the case of highly nonnormal matrices for example. A fruitful alternative is to consider a structurally fixed family $\triangle A = tE$, where $t \in \mathbb{C}$, $E \in \mathbb{C}^{n\times n}$. This leads to the $linear$ coupling $A + tE$.
The variation of the spectrum of linear operators and matrices under the influence of one or several parameters has long been an active domain of research, giving rise to the elegant analytic/algebraic

spectral theory initiated by Puiseux. The case of a linear dependence on a parameter $t \in \mathbb{C}$, of the form $A(t) = A + tE$ has been particularly studied [29, 30, 25]
We consider the resolvent field $z \mapsto R(t, z) = (A + tE - zI)^{-1}$ for $t \in \mathbb{C}$. Its singularities as t varies define the spectral field $t \mapsto \sigma(A(t))$ which denotes the spectrum of $A(t)$. For $z \in$ re$(A) = \mathbb{C} \setminus \sigma(A)$, we use the *multiplicative* representation

$$(A + tE - zI)^{-1} \quad = \quad (A - zI)^{-1} \left(I + tE(A - zI)^{-1}\right)^{-1}.$$

For a fixed z in re(A), the map $t \mapsto R(t, z)$ is analytic for $|t| < \frac{1}{\rho(E(A-zI)^{-1})} = \alpha$ [29, 30].
In Homotopic Deviation theory, we specifically look beyond analyticity in t, for $|t| > \alpha$. Our tools are elementary linear algebra, based on the Jordan structure of $0 \in \sigma(E)$. The rank deficient matrix E is called the *deviation*, and the term "perturbation" covers the case where $|t|\|E\|$ is limited, with $rankE = r \leq n$. Our work provides an elementary analysis for $z, t \in \widehat{\mathbb{C}} = \mathbb{C} \cup \infty$ of singular perturbation theory for matrices, since E is singular ($r < n$) in the case of interest, where the Sherman-Morrison formula plays a key role.
When $r = n$, $\lim_{|t|\to\infty} R(t, z) = 0$ and $\lim_{|t|\to\infty} \sigma(A(t)) = \infty$. But when $r < n$, a different and more interesting situation prevails, characterized by the spectral properties of the rational matrix :

$$z \to M_z \quad = \quad (\det(zI_n - A))^{-1} \; V^H \,\text{adj}\,(zI_n - A)\, U \in \mathbb{C}^{r\times r}$$

where $E = UV^H$, $U, V \in \mathbb{C}^{n\times r}$, $r < n$, and z varies in $\mathbb{C}$ outside $\sigma(A)$.
For almost all z in $re(A) = \mathbb{C}\backslash\sigma(A)$, M_z has rank r and $R(t, z)$ is analytic for $|t|$ large enough, $|t| > \beta = \frac{1}{min|\mu_z|}$, $\mu_z \in \sigma(M_z)$, such that $\lim_{|t|\to\infty} R(t, z) \neq 0$. For $\alpha < |t| < \beta$, the resolvent exists almost everywhere in $re(A)$. The spectrum $\sigma(M_z)$ represents the r $finite$ eigenvalues of the pencil $(A - zI) + tE$ for z fixed in $re(A)$, when $0 \notin \sigma(M_z)$.
The points in $re(A)$ such that M_z is singular are the $frontier$ points, where no analyticity at ∞ holds. At any frontier point, the pencil $(A - zI) + tE$ has $less$ than r finite eigenvalues. It may have none iff M_z is nilpotent. When $|t| \to \infty$, we can predict when some of the eigenvalues $\lambda(t) \in \sigma(A(t))$ converge to points in the frontier set, as proved in [27, 28, ALG42, ALG43, ALG46, ALG29].
Linearization of quadratic eigenproblems often leads to a situation where $0 \in \sigma(E)$ is semi-simple. The paper [26] treats an example from computational Acoustics, where t represents the complex admittance. This joint work with Martin Van Gijzen will appear in NLAA. It consists of a practical application where the homotopy parameter is $complex$. The points where the matrix pencils have no finite eigenvalues are given a physical interpretation : they are points where $no\ \ resonance$ can occur.
An application to the incomplete Arnoldi method (E singular defective of rank 1) has been made.
The paper [ALG42] is a written version of the *keynote presentation* that Françoise Chaitin-Chatelin was invited to present at NAA 2004 in Rousse, Bulgaria. The talk was actually delivered by Martin van Gijzen.
The restrictive conditions placed by the generic approach of Lidskii have been relaxed in [ALG46]. Numerical experiments were performed by Morad Ahmadnasab to illustrate how finite precision affects the mathematical theory.
Preliminary results indicate that finite precision computation tends, in this case, to reproduce the mathematical reality much more faithfully than we have been used to. If this is confirmed, this phenomenon is yet another reason to marvel at the "unreasonable" robustness of Krylov methods to perturbations.
The homotopic backward analysis of eigenvalues has been presented by Morad Ahmadnasab at the 2nd SMAI conference (Evian, May 2005) [24] and at the University of Versaille Saint-Quentin (July 2005) [23].

[23] M. Ahmadnasab, Homotopic Backward analysis for matrix eigenvalues. Presentation in CERFACS, and Université Versailles Saint-Quentin en Yvelines. 5 July 2005 .

[24] M. Ahmadnasab and F. Chaitin-Chatelin, Backward analysis for matrix eigenvalues. 2éme Congrés National de Mathématiques Appliquées et Industrielles, Evian - France 23 - 27 May 2005, Evian - France, Poster.

[25] F. Chaitin-Chatelin and V. Frayssé, (1996), *Lectures on Finite Precision Computations*, SIAM, Philadelphia.

[26] F. Chaitin-Chatelin and M. B. van Gijzen, Analysis of parameterised Quadratic Eigenvalue problems in Computational Acoustics with Homotopic Deviation, to appear in NLAA 2006.

[27] F. Chaitin-Chatelin, (2002), About Singularities in Inexact Computing, Technical Report TR/PA/02/106. Erratum : p.2, line 14, read 'associated with eigenvalues non equal to lambda'.

[28] F. Chaitin-Chatelin, (2003), Computing beyond analyticity. Matrix Algorithms in Inexact and Uncertain Computing., Technical Report TR/PA/03/110.

[29] F. Chatelin, (1983), *Spectral Approximation of Linear Operators*, Academic Press, New York.

[30] F. Chatelin, (1993), *Eigenvalues of matrices*, Enlarged Translation.

4.2 Numerical Nonlinear Algebra

Nonlinear Algebra is the required framework to deal with matrix computations which are strongly nonlinear and which do not lend themselves to a computationally reliable linearization. To exploit the algorithmic dynamics created by the nonlinearities (arising from multiplication), one is led to make full use of the inductive complex structure of multiplication which is a characteristic of (possibly non associative) Dickson algebras [34, 32, 33]. By doing so, one goes beyond the classical framework of (associative) Clifford algebras which is used so succesfully in Algebraic Geometry and Theoretical Physics to describe phenomena where multiplication is inherently non commutative, but remains associative.

Associativity puts an arbitrary limit to the type of nonlinearities which can be considered : they cannot be chaotic. The possibility to go beyond this limit is numerically very important to assess the validity of computer simulations in the chaotic regime. This ambitious goal implies going even beyond the framework of Dickson algebras where multiplication is neither associative nor isometric, but remains quadratic and flexible. A quadratic algebra is such that x^2 is a real linear combination of x itself and $\|x\|^2$, where $\|.\|$ denotes the Euclidean norm. This property can be related to the logistic equation (in real variables and under additive form) $x = x^2 + c$, making a significant connection between Dickson algebras and the quadratic polynomial iterations which can display chaos [38, 35]. A body of theory is developing [ALG39, 37, ALG40, ALG45, 38, 31, 36] together with experiments [35], which connect various aspects of Computation (Analysis, Algebra, Geometry and Arithmetics) in new $algorithmic$ ways. The first item in our agenda is to determine the number of hierachical levels to be taken into account in very unstable phenomena (leading to chaos), in order to adjust the targeted accuracy to the inherent instability, therefore minimizing the overall computing time.

[31] F. Chaitin-Chatelin, Calcul Matriciel : entre Algébre et Geométrie. Séminaire Université Montpellier 2, 27 January 2004, talk.

[32] F. Chaitin-Chatelin, Le rôle de la multiplication en Calcul Scientifi que. Séminaire du Dpt. de Physique Théorique, Université Paul Sabatier, Toulouse, 11 January 2005, talk.

[33] F. Chaitin-Chatelin, Le Sens des Nombres. Grand Séminaire d'Ouverture, Université Paul Sabatier, Toulouse, 5 February 2004, talk.

[34] F. Chaitin-Chatelin, (2000, pp. 83–92), The computing power of Geometry, In *Numerical Analysis*, D. F. Griffi ths and G. A. Watson, eds., CRC Press LLC.

[35] F. Chaitin-Chatelin and M. Ahmadnasab, (Work in progress to appear as Cerfacs Technical Report, January 2006), The logistics of Feigenbaum and Mandelbrot in real variables revisited.

[36] F. Chaitin-Chatelin, (2003), The Arnoldi method in the light of Homotopic Deviation theory, Technical Report TR/PA/03/15.

[37] F. Chaitin-Chatelin, (2003), Elements of Hypercomputations on $\mathbb{R}$ and $\mathbb{Z}_2$ with the Dickson-Albert inductive process., Technical Report TR/PA/03/34.

[38] F. Chaitin-Chatelin, (Working Notes December 2005, to appear as Cerfacs Technical Report), Computing lessons from the logistic iteration.

5 Nonlinear Systems and Optimization

5.1 Convergence properties of trust-region methods with application to multigrid optimization

S. Gratton : CERFACS, *France* ; **M. Mouffe** : CERFACS, *France* ; **A. Sartenaer** : FUNDP, *Belgium* ; **Ph. L. Toint** : FUNDP, *Belgium*

Following recent work on the convergence properties of a new recursive multiscale trust-region algorithm for unconstrained optimization [39], we present in [41] the numerical experience gained so far with a particular implementation of the considered algorithm applied to a few significant test problems. We illustrate the strength of methods of this type.
Convergence properties of trust-region methods for unconstrained nonconvex optimization is also considered in the case where information on the objective function's local curvature is incomplete, in the sense that it may be restricted to a fixed set of "test directions" and may not be available at every iteration [40]. It is shown that convergence to local "weak" minimizers can still be obtained under some additional but algorithmically realistic conditions. These theoretical results are then applied to recursive multigrid trust-region methods, which suggests a new class of algorithms with guaranteed second-order convergence properties.

[39] S. Gratton, A. Sartenaer, and P. Toint, A numerical exploration of recursive multiscale unconstrained optimization, In *In Oberwolfach Reports : Optimization and Applications*, J. Z. F. Jarre, C. LemarÃl'chal, ed. To appear.

[40] S. Gratton, A. Sartenaer, and P. L. Toint, (2005), Recursive Trust-Region Methods for Multiscale Nonlinear Optimization : Preliminary Numerical Experience, Technical Report in preparation, CERFACS, Toulouse, France.

[41] S. Gratton, A. Sartenaer, and P. L. Toint, (2005), Second-order convergence properties of trust-region methods using incomplete curvature information, Technical Report in preparation, CERFACS, Toulouse, France.

5.2 Sensitivity of some spectral preconditioners

L. Giraud : CERFACS, *France* ; **S. Gratton** : CERFACS, *France*

It is well known that the convergence of the conjugate gradient method for solving symmetric positive definite linear systems depends to a large extent on the eigenvalue distribution. In many cases, it is observed that "removing" the extreme eigenvalues can greatly improve the convergence. Several preconditioning techniques based on approximate eigenelements have been proposed in the past few years that attempt to tackle this problem. The proposed approaches can be split into two main families depending on whether the extreme eigenvalues are moved exactly to one or are shifted close to one. The first technique is often referred to as the deflating approach, while the latter is referred to as the coarse grid preconditioner by analogy to techniques first used in domain decomposition methods. Many variants exist in the two families that reduce to the same preconditioners if the exact eigenelements are used. In this work, we investigate the behaviour of some of these techniques when the eigenelements are only known approximately. We use the perturbation theory for eigenvalues and eigenvectors to investigate the behaviour of the spectrum of the preconditioned systems using a first order approximation. We illustrate the sharpness of the first order approximation and show the effect of the inexactness of the eigenelements on the behaviour of the resulting preconditioner when applied to accelerate the conjugate gradient method. We show how this analysis can be used to screen spectral information in the case of a sequence of SPD linear systems occuring in a nonlinear process. Such an application can be seen in variational data assimilation [42] where the Gauss-Newton methods consist in solving a sequence of normal equations.

[42] M. Fisher, (1998), Minimization algorithms for variational data assimilation, In *Recent Developments in Numerical Methods for Atmospheric Modelling*, ECMWF, 364–385.

5.3 An investigation of incremental 4D-Var using non-tangent linear models

A. Lawless : UNIVERSITY OF READING, *UK* ; **S. Gratton** : CERFACS, *France* ; **N. K. Nichols** : UNIVERSITY OF READING, *UK*

We investigate the convergence of incremental four-dimensional variational data assimilation (4DVar) when an approximation to the tangent linear model is used within the inner loop. Using a semi-implicit semi-Lagrangian model of the one-dimensional shallow water equations, we perform data assimilation experiments using an exact tangent linear model and using an inexact linear model (i.e. perturbation forecast model). We find that the two assimilations converge at a similar rate and analysis are also similar, with the difference between them dependent on the amount of noise in the observations. To understand the numerical results we present the incremental 4D-Var algorithm as a Gauss-Newton iteration for solving a least-squares problem and consider its fixed points.

5.4 Partial condition number for linear least-squares problems

M. Arioli : RUTHERFORD APPLETON LABORATORY, *England* ; **M. Baboulin** : CERFACS, *France* ; **S. Gratton** : CERFACS, *France*

We consider the linear least-squares problem $\min_{y \in \mathbb{R}^n} \|Ay - b\|_2$ where $b \in \mathbb{R}^m$ and $A \in \mathbb{R}^{m \times n}$ is a matrix of full column rank n and we denote its solution by x. We assume that both A and b can be perturbed and that these perturbations are measured using the Frobenius or the spectral norm for A and the Euclidean norm for b. We are concerned with the condition number of a linear function of x ($L^T x$ where $L \in \mathbb{R}^{n \times k}$) for which we provide a sharp estimate that lies within a factor $\sqrt{3}$ of the true condition number. Provided the triangular R factor of A from $A^T A = R^T R$ is available, this estimate can be computed in $2kn^2$ flops. We also propose a statistical method based on [43] that estimates the partial condition number by using the exact condition numbers in random orthogonal directions. If R is available, this statistical approach enables us to obtain a condition estimate at a lower computational cost. In the case of the Frobenius norm, we derive a closed formula for the partial condition number that is based on the singular values and the right singular vectors of the matrix A.
The theoretical results and numerical experiments related to this study are presented in [ALG33].

[43] T. Gudmundsson, C. S. Kenney, and A. J. Laub, (1995), Small-sample statistical estimates for matrix norms, *SIAM J. Matrix Analysis and Applications*, **16**, 776–792.

5.5 Distributed packed storage for large parallel calculations

M. Baboulin : CERFACS, *France* ; **L. Giraud** : CERFACS, *France* ; **S. Gratton** : CERFACS, *France* ; **J. Langou** : UNIVERSITY OF TENNESSEE, *USA*

Following a specific work on the Cholesky factorization [ALG6], we propose in [ALG36] a distributed packed storage format that exploits the symmetry or the triangular structure of a matrix. This format stores only half of the matrix while maintaining most of the efficiency compared to full storage for a wide range of operations. This work has been motivated by the fact that, contrary to sequential linear algebra libraries (e.g. LAPACK [44]), there is no routine that handles packed matrices in the currently available parallel distributed libraries. The proposed algorithms exclusively use the existing ScaLAPACK [45] computational kernels which proves the generality of the approach, provides easy portability of the code, efficient re-use of existing software and good load balance of the application even for high processor counts. We present performance results for the Cholesky factorization and for the updating of the R factor of a QR factorization.

[44] E. Anderson, Z. Bai, C. Bischof, S. Blackford, J. Demmel, J. Dongarra, J. D. Croz, A. Greenbaum, S. Hammarling, A. McKenney, and D. Sorensen, (1999), *LAPACK User's Guide*, SIAM. Third edition.

[45] L. S. Blackford, J. Choi, A. Cleary, E. D'Azevedo, J. Demmel, I. Dhillon, J. Dongarra, S. Hammarling, G. Henry, A. Petitet, K. Stanley, D. Walker, and R. C. Whaley., (1997), *ScaLAPACK Users' Guide*, SIAM.

5.6 Trust-region methods with dynamic accuracy and nonlinear least-squares

F. Bastin : CERFACS, *France* ; **S. Gratton** : CERFACS, *France* ; **C. Cirillo** : UNIVERSITY OF NAMUR, *Belgium* ; **Ph. L. Toint** : UNIVERSITY OF NAMUR, *Belgium*

We consider trust-region techniques with adaptive strategies for stochastic programming. We have constructed a convergent method designed for stochastic programs based on expected values [ALG65], and have applied it for mixed logit models, a class of problems encountered in discrete choice theory. We have however identified problems arising when using some popular classes of Hessian approximations, especially the BHHH one [46]. Such difficulties are similar to those that can be encountered with nonlinear least-square problems for the Gauss-Newton method. These similarities are at the origin of a project where we consider these problems inside an unified framework. We have identified the origins of the poor numerical performance and we consider hybrid strategies such as that developed by Dennis et al. [47], which can be shown to be convergent. The next step will be to complete the implementation that has been initiated in order to numerically validate the theoretical developments.

[46] F. Bastin, C. Cirillo, and Ph. L. Toint, (2006. In press), Application of an adaptive Monte Carlo algorithm to Mixed Logit estimation, *Transportation Research Part B*.

[47] J. E. Dennis, D. Gay, and R. E. Welsch, (1981), An adaptive nonlinear least-squares algorithm, *ACM Transactions on Mathematical Software*, **7**, 348–368.

5.7 Trust-Region algorithms applied to discrete choice modelling

Dick Ettema : UNIVERSITY OF UTRECHT, *The Netherlands* ; **Fabian Bastin** : CERFACS, *France* ; **John Polak** : IMPERIAL COLLEGE, *United Kingdom* ; **Olu Ahiru** : IMPERIAL COLLEGE, *United Kingdom*

In this research, we have considered the application of trust-region methods to discrete choice models involving random parameters, so that the problem can be viewed as a stochastic program. We have more specifically studied a model of activity and trip scheduling that combines three elements that have previously been investigated in isolation : the duration of activities, the time-of-day preference for activity participation and the effect of schedule delays on the valuation of activities. The model was tested using a 2001 data set from the Netherlands and results are presented in [48]. The method is convergent, and error components included in the model suggest that there is considerable unobserved heterogeneity with respect to mode preferences and schedule delay.

[48] D. Ettema, F. Bastin, J. Polak, and O. Ashiru, (2006), An error-components framework for joint choice models of activity timing and duration, Tech. Rep. TR/PA/06/2, CERFACS, Toulouse, France.

6 Signal processing

6.1 Phase Closure Imaging and Differential GPS

A. Lannes : CERFACS, *France*

The nearest lattice-point problems arising in Phase Closure Imaging (PCI) and in Differential GPS (DGPS) share a common feature. Their statement appeals to elementary notions of algebraic graph theory. In both cases, the original data are defined on the edges of the graph to be considered, the calibration graph in PCI, and the GPS graph in Global Navigation Satellite Systems (GNSS).

These data are biased by differences between unknown terms defined on the vertices of the graph : phase shifts in PCI and clock offsets in GNNS. The effective data are then closure terms in the sense of Kirchhoff : the sums of the original data on the directed edges of the n cycles defined by the choice of a spanning tree. By construction, these data are no longer biased. The original phase data are defined modulo 2π in interferometry, or modulo the carrier wavelengths in GPS. The "closure integers" involved in the related nearest lattice-point problems are associated with these cycles.

As summarized below, the studies performed at CERFACS in 2004-2005 have shown that the notion of spanning tree of maximal weight plays an essential part in the applications concerned by this approach. (Further details are to be found in [ALG20] for PCI, and in [ALG21] for DGPS.)

6.2 Phase Closure Imaging

A. Lannes : CERFACS, *France*

The edges of the calibration graph correspond to the baselines for which the phase Ψ_{s} of the Fourier transform of the calibration source can be regarded as relatively well known. On each connected component of this graph, the main entries of the problem are the closure phases $\Psi^{(i)} := \Psi_{\mathrm{d}}^{(i)} - \Psi_{\mathrm{s}}^{(i)}$; subscripts d and s stand for data and source, respectively. These closure phases are relative to the cycles defined by the selected spanning tree.

The calibration functional to be minimized is defined by a relation of the form $f(\Phi) := \|\operatorname{arc}(\Psi - \Phi)\|$ where Φ is an Optical Path Difference (OPD), a phase function which takes its values on the edges of the graph. At the end of the initialization step, the baseline phase function Ψ involved in the definition of f is of the form $\sum_{i=1}^{n} \Psi^{(i)}\xi_i$ with $\Psi^{(i)} \leftarrow \operatorname{arc}(\Psi^{(i)})$. Here, $\{\xi_i\}_{i=1}^{n}$ is the standard basis of cycle-entry phase space. The complexity of the correction step depends on the size of the residual closure phases $\Psi^{(i)}$.

As shown in [ALG20] , the minima of f correspond to particular points of $\mathbf{Z}^n$:

$a_\star \equiv (a_\star^{[1]}, \ldots, a_\star^{[n]})$ for the global minimum ;
$a_{\star\star} \equiv (a_{\star\star}^{[1]}, \ldots, a_{\star\star}^{[n]})$ for the nearest secondary minimum (if any) ;
etc.

These points lie in a convex set of $\mathbf{R}^n$ centered on the closure point $\widehat{a} \leftarrow (\psi^{(1)}, \ldots, \psi^{(n)})$ where $\psi^{(i)} \leftarrow \Psi^{(i)}/(2\pi)$; $a_\star$ is the point of $\mathbf{Z}^n$ closest to the float solution $\widehat{a}$, the distance being that induced by a given quadratic form q. The matrix of q is the inverse of the variance-covariance matrix of the closure phases.

When the residual closure phases are relatively large, say between $\pi/3$ and $2\pi/3$ (in absolute value), the correction step is delicate. The situations where $f(\Phi_{\star\star})$ is of the order of $f(\Phi_\star)$ with $\mathrm{arc}(\Psi - \Phi_{\star\star})$ very different from $\mathrm{arc}(\Psi - \Phi_\star)$ must be discarded. The calibration graph must then be truncated by removing the cycle-entry edges for which the residual closure phases are too large. The spanning tree to be selected is therefore the spanning tree of maximal weight.
The applications of this analysis concern, in particular, the situations where the self-calibration procedures must be conducted with much care. The delicate situations can be diagnosed and dealt with. It is thus possible to find a good compromise between the coverage of the calibration graph (which must be as complete as possible), and the quality of the solution (which must of course be reliable).

6.3 Differential GPS

A. Lannes : CERFACS, *France*

Once the observations have been screened for strong biases such as cycle slips, multipath, etc., the statistical modelling of the problem may still be unsatisfactory for some receiver-satellite pairs at certain epochs. The data validation tests developed at CERFACS are aimed at detecting these failures [ALG21].
In the process of finding a reliable solution for the DGPS integer ambiguity a, it is important to identify the epochs for which the reference physical modelling is not acceptable. Recursive testing procedures have already been developed for this purpose. One thus gets a first estimate $\widetilde{a}$ of the global float solution $\widehat{a}$. The next step is to find the integer ambiguity solution corresponding to this float estimate. The input for this last step must therefore be very reliable. The data validation tests developed at CERFACS refine the recursive procedures in question. The time to fix the optimal integer ambiguity $\check{a}$ should thereby be reduced.
Relying on the current estimate $\widetilde{a}$ of $\widehat{a}$, one tests, with regard to the model under consideration, the quality of the data obtained at some given epoch. The corresponding phase residual discrepancy is a function $\delta^{(\widetilde{a})}(r,s)$ whose values can easily be computed. Denoting by ℓ a relaxation parameter of the order of the standard deviation of the carrier-phase information, let us now assume that, for a given epoch, the phase discrepancy condition $|\delta^{(\widetilde{a})}(r,s)| \leq \ell$ is satisfied on all the edges of the GPS graph. Clearly, the corresponding data are then physically reliable. Evidently, the smaller ℓ, the more severe the criterion.
The phase residual discrepancy is obtained via the pseudo-inverse of the phase closure operator. The closure operation, which generalizes that of double differencing, depends on the selected spanning tree. The results (of course) do not depend on that choice. To identify the edges on which the GPS data are not reliable, it is however preferable to choose the spanning tree of maximal weight. This crucial point is clarified in [ALG21].

7 Publications

7.1 Journal Publications

[ALG1] P. R. Amestoy, T. A. Davis, and I. S. Duff, (2004), Algorithm 837 : AMD, an approximate minimum degree ordering algorithm, *ACM Trans. Math. Softw.*, **30**, 381–388.

[ALG2] P. Amestoy, I. Duff, and C. Vömel, (2005), Task scheduling in an asynchronous distributed memory multifrontal solver, *SIAM J. Matrix Analysis and Applications*, **26**, 544–565.

[ALG3] E. Anterrieu, S. Gratton, and B. Picard, (2004), Inverse problem in remote sensing by aperture synthesis imaging, *Traitement du Signal*, **21**, 1–16.

[ALG4] M. Arioli, D. Loghin, and A. Wathen, (2005), Stopping criteria for iterations in finite-element methods., *Numerische Mathematik*, **99**, 381–410.

[ALG5] M. Baboulin, L. Giraud, and S. Gratton, (2005), A parallel distributed solver for large dense symmetric systems : applications to geodesy and electromagnetism problems., *Int. J. High Speed Computing*, **19**, 353–363.

[ALG6] M. Baboulin, L. Giraud, and S. Gratton, (2005), A parallel distributed solver for large dense symmetric systems : applications to geodesy and electromagnetism problems., *Int. J. High Speed Computing*, **19**, 353–363.

[ALG7] A. Bouras and V. Frayssé, (2005), Inexact matrix-vector products in Krylov methods for solving linear systems : a relaxation strategy, *SIAM J. Matrix Analysis and Applications*, **26**, 660–678.

[ALG8] B. Carpentieri, I. S. Duff, L. Giraud, and M. M. monga Made, (2004), Sparse symmetric preconditioners for dense linear systems in electromagnetism, *Numerical Linear Algebra with Applications*, **11**, 753–771.

[ALG9] B. Carpentieri, I. S. Duff, L. Giraud, and G. Sylvand, (2005), Combining fast multipole techniques and an approximate inverse preconditioner for large electromagnetism calculations, *SIAM J. Sci. Comput.*, **27**, 774–792.

[ALG10] I. Duff and S. Pralet, (2005), Strategies for scaling and pivoting for sparse symmetric indefinite problems, *SIAM J. Matrix Analysis and Applications*, **27**, 313–340.

[ALG11] I. S. Duff and J. A. Scott, (2004), A parallel direct solver for large highly unsymmetric linear systems, *ACM Trans. Math. Softw.*, **30**, 95–117.

[ALG12] I. Duff and J. Scott, (2005), Stabilized bordered block diagonal forms for parallel sparse solvers, *Parallel Computing*, **31**, 275–289.

[ALG13] I. Duff, L. Giraud, J. Langou, and E. Martin, (2005), Using spectral low rank preconditioners for large electromagnetic calculations, *Int. J. Numerical Methods in Engineering*, **62**, 416–434.

[ALG14] I. S. Duff, (2004), MA57 – A code for the solution of sparse symmetric indefinite systems, *ACM Trans. Math. Softw.*, **30**, 118–144.

[ALG15] V. Frayssé, L. Giraud, S. Gratton, and J. Langou, (2005), A Set of GMRES Routines for Real and Complex Arithmetics on High Performance Computers, *ACM Trans. Math. Softw.*, **31**, 228–238.

[ALG16] L. Giraud, S. Gratton, and J. Langou, (2004), A rank-k update procedure for reorthogonalizing the orthogonal factor from modified Gram–Schmidt, *SIAM J. Matrix Analysis and Applications*, **25**, 1163–1177.

[ALG17] L. Giraud, J. Langou, and M. Rozložník, (2005), On the loss of orthogonality in the Gram-Schmidt orthognalization process, *Computer and Mathematics with Applications*, **50**, 1069–1075.

[ALG18] L. Giraud, J. Langou, M. Rozložník, and J. van den Eshof, (2005), Rounding error analysis of the classical Gram-Schmidt orthogonalization process, *Numerische Mathematik*, **101**, 87–100.

[ALG19] L. Giraud, A. Marrocco, and J.-C. Rioual, (2005), Iterative versus direct parallel substructuring methods in semiconductor device modelling, *Numerical Linear Algebra with Applications*, **12**, 33–53.

[ALG20] A. Lannes, (2005), A global analysis of the phase calibration operation, *J. Opt. Soc. Am.*, **22**, 697–707.

[ALG21] A. Lannes, (2005), On new data validation criteria in Differential GPS, *J. of Geod.*, **79**, 280–287.

[ALG22] A. Lawless, S. Gratton, and N. Nichols, (2005), Approximate iterative methods for variational data assimilation, *Int. J. Numer. Methods in Fluids*, **47**, 1129–1135.

[ALG23] A. Lawless, S. Gratton, and N. Nichols, (2005), An investigation of incremental 4D-Var using non-tangent linear models, *Quart. J. Royal Met. Soc.*, **131**, 459–476.

[ALG24] D. Loghin and A. J. Wathen, (2004), Analysis of preconditioners for saddle-point problems, *SIAM J. Scientifi c Computing*, **25**, 2029–2049.

[ALG25] A. Papadopoulos, I. Duff, and A. Wathen, (2005), A class of incomplete orthogonal factorization methods. II : implementation and results, *BIT*, **45**, 159–179.

[ALG26] J. van den Eshof, G. Sleijpen, and M. van Gijzen, (2005), Relaxation strategies for nested Krylov methods, *Journal of Computational and Applied Mathematics*, **177**, 347–365.

7.2 Theses

[ALG27] E. Martin, (2005), *Spectral two-level preconditioners for sequences of linear systems*, Ph.D. dissertation. Jury : G. Alléon, A. Bendali, A. Bunse-Gerstner (rapporteur), I. S. Duff, L. Giraud, S. Lanteri (rapporteur) and G. Meurant, INPT. TH/PA/05/57.

[ALG28] S. Pralet, (2004), *Constrained orderings and scheduling for parallel sparse linear algebra*, Ph.D. dissertation. Jury : P. R. Amestoy, I. S. Duff, J. Y. L'Excellent, E. Ng (rapporteur), A. Pothen (rapporteur), and J. Roman (Président), INPT. TH/PA/04/105.

7.3 Technical Reports

[ALG29] M. Ahmadnasab, F. Chatin-Chatelin, and N. Megrez, (2005), Homotopic deviation in the light of algebra, Technical Report TR/PA/05/05, CERFACS, Toulouse, France.

[ALG30] G. Alléon, S. Champagneux, G. Chevalier, L. Giraud, and G. Sylvand, (2005), Parallel Distributed Numerical Simulations in Aeronautic Applications, Technical Report TR/CFD-PA/05/44, CERFACS, Toulouse, France.

[ALG31] P. Amestoy, A. Guermouche, J. Y. L'Excellent, and S. Pralet, (2004), Hybrid scheduling for the parallel solution of linear systems, Technical Report TR/PA/04/140, CERFACS, Toulouse, France.

[ALG32] P. R. Amestoy, X. S. Li, and S. Pralet, (2004), Constrained Markowitz with local symmetrization, Technical Report TR/PA/04/137, CERFACS, Toulouse, France.

[ALG33] M. Arioli, M. Baboulin, and S. Gratton, (2004), Partial condition number for linear least squares problems, Technical Report TR/PA/04/111, CERFACS, Toulouse, France.

[ALG34] M. Baboulin, L. Giraud, and S. Gratton, (2004), A parallel distributed solver for large dense symmetric systems : applications to geodesy and electromagnetism problems., Technical Report TR/PA/04/16, CERFACS, Toulouse, France.

[ALG35] M. Baboulin, L. Giraud, and S. Gratton, (2005), GOCE, Méthode de résolution inverse pour le champ de gravité, Contract Report CR/PA/05/88, CERFACS, Toulouse, France.

[ALG36] M. Baboulin, L. Giraud, S. Gratton, and J. Langou, (2005), A distributed packed storage for large parallel calculations., Technical Report TR/PA/05/30, CERFACS, Toulouse, France.

[ALG37] F. S. V. Bazan, (2004), Matrix polynomials with partially prescribed eigenstructure, Technical Report TR/PA/04/64, CERFACS, Toulouse, France.

[ALG38] B. Carpentieri, L. Giraud, and S. Gratton, (2004), Additive and multiplicative two-level spectral preconditioning for general linear systems., Technical Report TR/PA/04/38, CERFACS, Toulouse, France.

[ALG39] F. Chaitin-Chatelin and E. Traviésas-Cassan, (Chapter 5 in B. Einarsson (ed.), *Accuracy and Reliability in Scientifi c Computing*, SIAM, Philadelphia, 2005, pp. 77-92), Qualitative Computing.

[ALG40] F. Chaitin-Chatelin, (2004), Beyond ideals in the Dickson ring of integral octonions, Technical Report TR/PA/04/96, CERFACS, Toulouse, France.

[ALG41] F. Chaitin-Chatelin, (2004), Beyond ideals in the rings of hypercomplex integers, Technical Report TR/PA/04/96, CERFACS, Toulouse, France. In Z. Li et al. (eds), Proceedings of NAA2004, Rousse Bulgaria, LNCS 3401, pp. 14-24.

[ALG42] F. Chaitin-Chatelin, (2004), The dynamics of matrix coupling with an application to Krylov methods, Technical Report TR/PA/04/29, CERFACS, Toulouse, France.

[ALG43] F. Chaitin-Chatelin, (2004), On Lidskii's algorithm to quantify the first order terms in the asymptotics of a defective eigenvalue. Part I, Technical Report TR/PA/04/129, CERFACS, Toulouse, France.

[ALG44] F. Chaitin-Chatelin, (2005), Inductive multiplication in Dickson algebras, Technical Report TR/PA/05/56, CERFACS, Toulouse, France.

[ALG45] F. Chaitin-Chatelin, (2005), Inductive multiplication in Dickson algebras, Technical Report TR/PA/05/56, CERFACS, Toulouse, France.

[ALG46] F. Chaitin-Chatelin, (2005), On Lidskii's algorithm to quantify the first order terms in the asymptotics of a defective eigenvalue. Part II, Technical Report TR/PA/05/04, CERFACS, Toulouse, France.

[ALG47] I. . S. Duff and S. Pralet, (2004), Experiments in preprocessing and scaling symmetric problems for multifrontal solutions., Technical Report WN/PA/04/17, CERFACS, Toulouse, France.

[ALG48] I. S. Duff and S. Pralet, (2004), Strategies for scaling and pivoting for sparse symmetric indefinite problems, Technical Report TR/PA/04/59, CERFACS, Toulouse, France.

[ALG49] I. S. Duff and S. Pralet, (2005), Towards a stable static pivoting strategy for the sequential and parallel solution of sparse symmetric indefinite systems, Technical Report TR/PA/05/26, CERFACS, Toulouse, France. Also available as RAL Report RAL-TR-2005-007 and IRIT Report RT/TLSE/05/08.

[ALG50] I. S. Duff, S. Riyavong, and M. B. van Gijzen, (2004), Parallel preconditioners based on partitioning sparse matrices, Technical Report TR/PA/04/114, CERFACS, Toulouse, France.

[ALG51] I. S. Duff, (2004), Combining direct and iterative methods for the solution of large systems in different application areas, Technical Report TR/PA/04/128, CERFACS, Toulouse, France.

[ALG52] L. Giraud and S. Gratton, (2004), On the sensitivity of some spectral preconditioners, Technical Report TR/PA/04/108, CERFACS, Toulouse, France.

[ALG53] L. Giraud, S. Gratton, and J. Langou, (2004), Convergence in backward error of relaxed GMRES, Technical Report TR/PA/04/132, CERFACS, Toulouse, France.

[ALG54] L. Giraud, S. Gratton, and J. Langou, (2004), A note on relaxed and flexible GMRES, Technical Report TR/PA/04/41, CERFACS, Toulouse, France.

[ALG55] L. Giraud, S. Gratton, and E. Martin, (2005), Incremental spectral preconditioners for sequences of linear systems, Technical Report TR/PA/05/17. Preliminary version of the paper to appear in Applied Numerical Mathematics.

[ALG56] L. Giraud, S. Gratton, and E. Martin, (2005), Incremental spectral preconditioners for sequences of linear systems, Technical Report TR/PA/05/17, CERFACS, Toulouse, France.

[ALG57] L. Giraud, J. Langou, and G. Sylvand, (2004), On the parallel solution of large industrial wave propagation problems, Technical Report TR/PA/04/52, CERFACS, Toulouse, France. Preliminary version of a paper to appear in Journal of Computational Acoustic.

[ALG58] L. Giraud, J. Langou, M. Rozložník, and J. van den Eshof, (2004), Rounding error analysis of the classical Gram-Schmidt orthogonalization process, Technical Report TR/PA/04/77, CERFACS, Toulouse, France.

[ALG59] L. Giraud, D. Ruiz, and A. Touhami, (2004), A comparative study of iterative solvers exploiting spectral information for SPD systems, Technical Report TR/PA/04/40, CERFACS, Toulouse, France.

[ALG60] D. Loghin, D. Ruiz, and A. Touhami, (2004), Adaptive preconditioners for nonlinear systems of equations, Technical Report TR/PA/04/42, CERFACS, Toulouse, France.

[ALG61] D. Loghin, M. B. van Gijzen, and E. Jonkers, (2004), Bounds on the eigenvalue range and on the field of values of non-hermitian and indefinite finite element matrices, Technical Report TR/PA/04/86, CERFACS, Toulouse, France.

[ALG62] D. Loghin, (2004), Boundary preconditioning for mixed finite-element discretizations of fourth-order elliptic problems, Technical Report TR/PA/04/43, CERFACS, Toulouse, France.

[ALG63] G. L. G. Sleijpen, J. van den Eshof, and M. B. van Gijzen, (2004), Restarted GMRES with Inexact Matrix–Vector Products, Technical Report TR/PA/04/75, CERFACS, Toulouse, France. In Z. Li et al. (eds), Proceedings of NAA2004, Rousse Bulgaria, LNCS 3401, pp. 494-501.

[ALG64] J. van den Eshof, G. L. G. Sleijpen, and M. B. van Gijzen, (2004), Iterative linear system solvers with approximate matrix-vector products, Technical Report TR/PA/04/133, CERFACS, Toulouse, France. To appear in the proceedings of the Third International Workshop on Numerical Analysis and Lattice QC.

7.4 Conference Proceedings

[ALG65] F. Bastin, (2005), An adaptive trust-region approach for nonlinear stochastic optimisation with an application in discrete choice theory, In *Algorithms for Optimization with Incomplete Information*, S. Albers, R. H. Möhring, G. C. Pflug, and R. Schultz, eds., no. 05031 in Dagstuhl Seminar Proceedings, Internationales Begegnungs- und Forschungszentrum (IBFI), Schloss Dagstuhl, Germany.

[ALG66] F. Chaitin-Chatelin, (2004), The dynamics of matrix coupling with an application to Krylov methods, In *Lecture Notes in Computer Science, Proceedings of NAA2004, Rousse Bulgaria*, Z. L. et al., ed., Springer-Verlag, 14–24.

[ALG67] L. Giraud and M. B. van Gijzen, (2004), Large scale acoustic simulations on clusters of SMPs, In *Integral Methods in Science and Engineering. Analytic and Numerical Techniques*, C. Constanda, M. Ahues, and A. Larguillier, eds., Boston, Birkhauser, 61–66.

[ALG68] G. L. G. Sleijpen, J. van den Eshof, and M. B. van Gijzen, (2004), Restarted GMRES with Inexact Matrix–Vector Products, In *Lecture Notes in Computer Science, Proceedings of NAA2004, Rousse Bulgaria*, Z. L. et al., ed., Springer-Verlag, 494–501.

2

Computational Fluid Dynamics

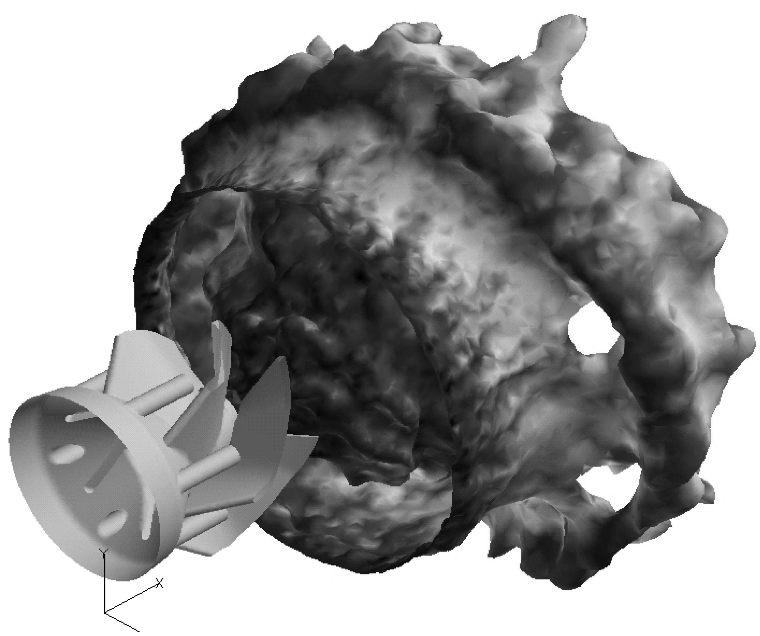

1 Introduction

The CFD team at CERFACS develops and applies high-performance codes for fluid mechanics applications in two main fields :

– *Aerodynamics.* Developing advanced simulation codes for aerodynamics applications in Europe was one of the initial goals of the CFD activity at CERFACS for Airbus and is still a central theme. After the NSMB code was stopped in 2003, most efforts have focused on elsA which is developed by ONERA and CERFACS. New collaborations with DLR in 2004 and 2005 have also started around the tau code. Unsteady aerodynamics, fluid structure interaction, vortex dynamics, efficient numerical methods on high-performance machines are central themes for the group. They are now accompanied by shape optimization, CFD for turbomachinery and aeroacoustics.
– *Combustion.* The LES tool developed by CERFACS and IFP (AVBP) has become a standard tool for reacting flows at many places in Europe (CNRS laboratories, ONERA centers, Universities in Spain, England, Netherlands or Germany, etc). Industrial partners (SNECMA, Turbomeca, Siemens, Alstom) have continued their collaboration with CERFACS to increase AVBP capabilities and validate it in multiple cases. LES is not yet industrialized but is used on a daily basis for industrial applications. LES tools are also being coupled to other solvers to predict acoustic fields or structure mechanical and thermal loading. A significant work of consolidation of CFD tools for combustion is also underway by comparing and coupling existing RANS (Reynolds Averaged Navier Stokes) tools with LES. This task is necessary to understand the respective strengths, limitations and potential combined use of RANS and LES

With more than 50 scientists (including PhD students), the CFD team is an active partner in various fields : research, teaching, formation, interaction with industry. In terms of man-power, the turn-over of the team remains high with only 10 permanent scientists and more than 40 others staying less than 4 years. Most scientists leaving CERFACS find positions right away and many keep in touch with CERFACS. The collaboration with french laboratories is also excellent : CERFACS provides codes to many CNRS or university laboratories and participates to multiple contracts with other research institutions. European support is very strong with multiple FP'6 programmes (Fluistcom, Fuelchief, Preccinsta, Intellect, FarWake, Vital, Molecules...) which were active in 2004 and 2005 and will be replaced by new projects (Quantify, Timecop, Eccomet, Simsac, TLC...). The EST Marie Curie project Eccomet is an excellent example of recent CERFACS success : it will allow CERFACS to hire 12 European PhD students in the next 4 years as well as 10 visitors. These scientists will be working on two-phase flow combustion at CERFACS, ONERA and IMFT and strongly contribute to the advancement of fundamental research in this field. The Eccomet project was initiated and is coordinated by CERFACS (Dr B. Cuenot) : it also shows that CERFACS is now well integrated in the research community.

2 Combustion

The combustion team at CERFACS develops fundamental models for reacting flows and applies them to real configurations. Fundamental research in combustion includes flame dynamics, chemistry, interaction with walls, heat transfer, radiation in reacting flows, multiphase reacting flows, flame / acoustic interactions... Most of these studies are performed using theory and Direct Numerical Simulation tools.
The application to real configurations is a direct extension of the results obtained from fundamental research where corresponding models are introduced in solvers usually developed at CERFACS (or in collaboration with CERFACS partners) for RANS (Reynolds Averaged Navier Stokes) and LES (Large Eddy Simulation) codes.
These two aspects (fundamental research versus applications in complex cases) must be balanced to fulfill the task of the team. The academic part, for example, is necessary to maintain the team expertise and attract high-level researchers from France but also from foreign universities. The contracts obtained in 2005 confirm that CERFACS can find funding for these fundamental aspects. These studies are described in Section 2.1. LES of two-phase flows is the fastest growing activity in the team and is described in Section 2.2 while the unsteady combustion work (in gaseous flows) is presented in Section 2.3. Since 2003, CERFACS has started working again on RANS methods, mainly to develop new numerical methods, to use RANS codes for optimization or to couple RANS and LES tools : these studies are described in Section 2.4. Finally, Section 2.5 describes the software engineering tasks needed to make all large LES studies at CERFACS possible : optimisation, parallelization, visualization, etc. Many of these tasks are the product of intense collaborations with national computing centers such as CINES or IDRIS and with companies : in 2005, for example, AVBP, the LES code of CERFACS was ported successfully on BlueGene machines achieving speed up of the order of 4900 on 5000 processors on applications provided by PSA, Siemens and Turbomeca.

2.1 Basic phenomena

To sustain the development of models for RANS or LES, and to understand the details of turbulent combustion and its interaction with other phenomena, a number of fundamental works are conducted by the team. Basic studies are performed on the role of liquid films in piston engines (in collaboration with IFP), the flow and flame structure in rocket engines, the modelling of perforated plates that can be found in gas turbines, and in parallel on the development of a two-phase flow version of AVBP, the structure and ignition of two-phase flames.

2.1.1 Interaction of a flame with liquid fuel on a wall (G. Desoutter, B. Cuenot, C. Habchi)

The Direct Injection Engine (IDE) is an interesting solution to reach a compromise between low fuel consumption and reduction of pollutant emissions. However direct injection of fuel in the combustion chamber causes important deposition on the walls, leading to an increase of unburnt hydrocarbons (HC) release. In IDE engines, especially during the starting regime, the fuel jet impacts directly on the piston and creates a liquid film that is a source of HC production and smoke during the combustion phase. If many studies can be found on the interaction of a flame with a dry wall, little is known about the flame behavior

when it approaches a liquid film. In particular the quenching of the flame and the distance of quenching are still open questions.
Here, Direct Numerical Simulations (DNS) of the flame-wall interaction with a liquid fuel film were performed with the code NTMIX3D and published in the last Symp. on Comb. [CFD2]. DNS allowed to understand the mechanisms involved in the interaction, like for example the film evaporation due to the presence of the flame and its impact on the flame structure. The role of the liquid film was also studied by comparing the interaction of the flame with a wet and a dry wall. Simulation results show that the flame quenches much further away from the walls when a liquid film is present, and that this effect is increased by high wall temperatures. The liquid film is mainly altered by the wall temperature and not by the flame. Based on these results, a new model for the evaporation of a liquid film in the presence of a flame has been established for RANS calculations and tested in the C3D code of IFP for piston engines.

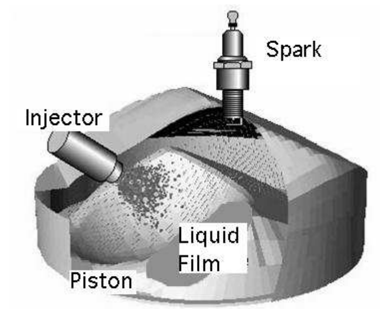

FIG. 2.1 – Deposition of a liquid fuel film in Direct Injection Engines (IDE).

2.1.2 H_2 - O_2 flame ignition and structure (A. Dauptain, B. Cuenot)

The ignition process of rocket engines must control ignition but also minimize the risk of explosion and destruction of the engine. In such systems, chemical phenomena are coupled to highly compressible flows, characterized by structures like shocks and slip lines. The numerical simulation of rocket ignition then requires robust and accurate methods, able to handle stiff chemistry and flow structures with strong pressure gradients.
In a first step, the autoignition of a mixing layer between hydrogen and hot oxidizer was simulated with Direct Numerical Simulations, using realistic transport laws, showing a behaviour which differs strongly from methane autoignition because of the high diffusivity of hydrogen. Results were reported in Comb. Sci. Tech. [1].

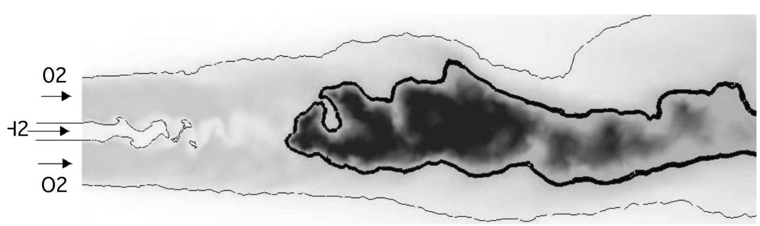

FIG. 2.2 – Supersonic H_2 - O_2 combustion : instantaneous temperature field.

In a second step, LES of underexpanded sonic jets were performed with AVBP after some adaptation to handle supersonic flows with shocks. This allowed a complete spectral study of the unsteady features that are the initial source of the acoustic noise, feeding the screech instability. The compression zone has been particularily studied, evidencing three different types of excitations [CFD40]. Finally LES was applied to supersonic combustion cases, such as the flame of Cheng [2]. The agreement between numerical and experimental results is fair : computations capture the lifted flame (Fig. 2.2), the mean values of speed, temperature and species concentrations, while the levels of RMS values are also correct. LES results confirm the influence of supersonic compressible pattern on combustion.

[1] R. Knikker, A. Dauptain, B. Cuenot and T. Poinsot, (2001), Comparison of computational methodologies for ignition in diffusion layers, *Combustion Science and Technology*, **175**(10), 1783-1806.

[2] T.S. Cheng, J.A. Wehrmeyer, R.W. Pitz, O. Jarrett and G.B. Northam, (1994), "Raman measurement of mixing and finite rate chemistry in a supersonic hydrogen-air diffusion flame", *Combustion and Flame*, **99** :157-173

2.1.3 Direct and Large Eddy Simulations of Effusion Cooling (S. Mendez, F. Nicoud, T. Poinsot)

In almost all combustion systems, solid boundaries must be cooled. One possibility often chosen in gas turbines is to use multiperforated walls. In this technique, fresh air coming from the casing goes through the perforations and enters the combustion chamber. The associated micro-jets coalesce to give a film that protects the internal wall face from the hot gases. The number of submillimetric holes on a perforated plate is far too large to resolve each hole and allow a complete description of the generation/coalescence of individual jets. Effusion is however known to have drastic effects on the whole flow structure, and to modify noticeably the flame position.

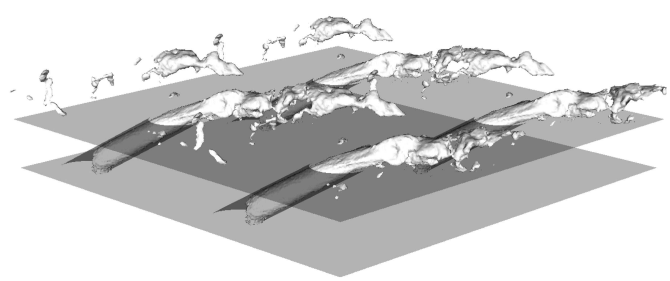

FIG. 2.3 – Visualization of the structure of the flow around a perforated plate obtained by Direct Numerical Simulation (velocity iso-surface).

As a consequence, new wall models for turbulent flows with effusion are required to perform predictive full scale computations. One major difficulty in developing new wall functions is that the boundary fluxes depend on the details of the turbulent flow structure between the solid boundary and the fully turbulent zone.
Measurements in realistic configurations are difficult to perform and generally do not provide enough detailed information to allow a complete understanding of the phenomena involved. This can be overcome by using numerical simulation. Although limited to very small domains, Direct Numerical Simulation is a first and crucial step to describe the details of the flow in the near zone of a perforation plate. Figure 2.3 shows an example of the velocity field obtained around one perforation (the domain has been duplicated four times for clarity). In this simulation, the main global characteristics of the flow have been validated by comparison with experimental data. A data base can then be generated on this configuration in order to

build an appropriate wall model for perforated walls. In a second step, RANS computations and Large Eddy Simulations of a full burner with the new perforated wall law is performed to validate the model [CFD53].

2.1.4 Ignition criteria of two-phase flames (N. Lamarque, G. Boudier, B. Cuenot

A critical issue for flames in liquid fuel combustors is the ignition process, that combines evaporation and combustion, and is significantly different from the ignition of gaseous flames. In this process and in addition to chemical kinetics data, parameters like the droplet size and its distribution have important impacts. The ignition of a reactive mixture in simulations is often obtained by unphysical methods. Here a realistic spark plug model has been implemented in AVBP, where the energy deposition due to spark discharge is modeled by a source term added to the total energy equation. A comprehensive theoretical

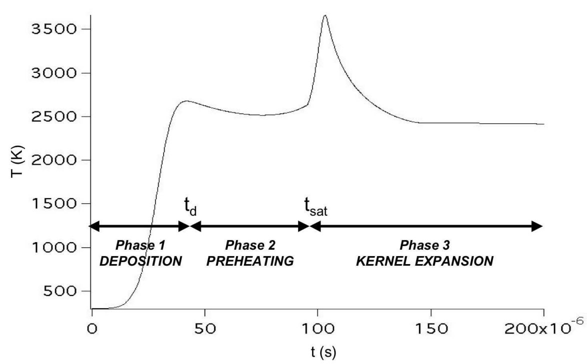

FIG. 2.4 – Typical temporal variation of gas temperature at the center of the flame kernel. t_d is the deposition time and t_{sat} is the time at which the liquid droplets reach the saturation temperature.

and numerical study of ignition in a one-dimensional configuration has been performed, starting from the spark energy deposition within the spray to the flame stabilisation. Figure 2.4 shows a typical time evolution of temperature at the center of the flame kernel. Three stages can be identified : in a first stage, the energy deposition results in a fast temperature increase ; then energy deposition is stopped and the main phenomenon of the following stage is the preheating of the droplets ; finally in the last stage, starting when the droplets have reached their staturation temperature, ignition occurs, leading to a sharp increase of temperature and a subsequent stabilisation on a value close to the flame temperature.
Two ignition criteria were determined, based on global parameters of the two-phase flow and the spark, that can therefore be calculated *a priori*. The relevance of these criteria has finally been evaluated against a series of one-dimensional ignition simulations [1].

[1] N. Lamarque, G. Boudier, B. Cuenot and T. Poinsot, "Numerical Study of Two-phase Flame Ignition by a Spark Plug", *submitted to Proc. of the Combustion Institute*, **31** (2006).

2.2 LES of two-phase reacting fbws

Most aeronautical combustors burn liquid fuel using injectors which atomise the liquid jet or film in small droplets of size $10 - 200\ \mu m$. These droplets are dispersed by the turbulent flow, partially vaporised and finally mixed with air. Modelling the liquid phase in a LES solver is a difficult issue for which two main classes of methods are available : the Euler framework (EF) and the Lagrange framework (LF).

The LF describes the liquid phase as a large but finite number of droplets with their own trajectory, velocity, temperature and diameter while the EF considers the dispersed phase as a continuous field whose characteristics are determined through a set of conservation equations for the liquid volume fraction, the liquid phase velocity and temperature, and the first/second order moments of the size distribution. Because it is easier to implement, parallelise and couple with the gas flow solver, the EF has been first chosen to study turbulent two-phase combustion with AVBP.
A first EF prototype (AVBP-TPF) has been validated in 2004 and allowed to demonstrate the feasability of two-phase reacting flow LES in industrial gas turbines. The potential of LES for these systems was particularly highlighted by the simulation of ignition sequences in helicopter and aircraft engines. In a second phase of development, a new version of AVBP-TPF has been written that includes a number of improved models, in particular for particle dispersion and polydisperse sprays, and a better control of numerical error. In 2005 the development of a LF solver has also been started with the PhD of M. Garcia, in collaboration with Stanford University.

2.2.1 Turbulent dispersion of particles (E. Riber, O. Simonin, B. Cuenot, T. Poinsot)

Large-Eddy Simulations (LES) of turbulent two-phase flows in combustion chambers with AVBP-TPF are based on the Mesoscopic formalism [1]. This approach uses first conditional ensemble averaging and then volume filtering. It leads to a transport equation for the so-called Mesoscopic Eulerian Particle Velocity (MEPV) which represents the local instantaneous velocity field shared by all the droplets or particles at the same spatial location. The remaining part of each single particle velocity, called the Random Uncorrelated

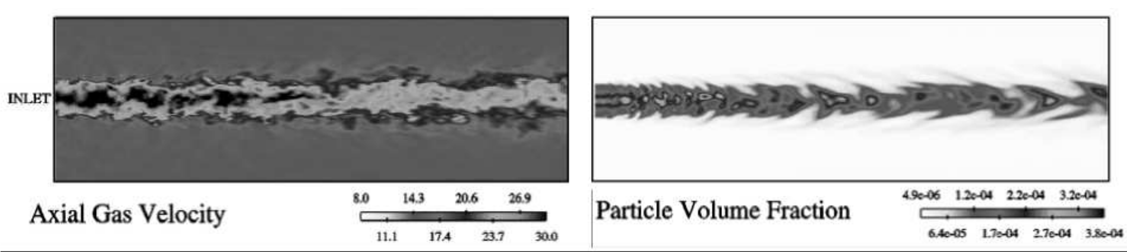

FIG. 2.5 – Instantaneous fields of axial gas velocity and particle volume fraction, configuration of Hishida et al. [2] (collaboration with IMF Toulouse).

Velocity (RUV), leads to a stress term in the MEPV equation which needs to be modelled. The volume filtering adds standard subgrid stress (SGS) terms, closed with a Smagorinsky-like model which proved to be successful in a priori testing on Homogeneous Isotropic Turbulence. Special care is required to solve the Eulerian equations because the dispersed phase implies the resolution of sharp particle concentration gradients. 3rd order accurate schemes (TTGC,TTG4A) have been implemented and tested in the code AVBP for the dispersed phase, while artificial dissipative terms have been adapted, to damp spurious modes in regions containing sharp gradients.
In collaboration with IMF Toulouse, two experimental configurations have been selected to study droplets dispersion and validate its modeling. One is the gas-solid turbulent confined round jet experimentally investigated by Hishida et al. [2]. The other configuration is a 'bluff body' type flow experimentally investigated by Boree et al. [3] which is closer to combustion chamber devices. Results are very encouraging : the particle mass flux and radial velocity fluctuation predicted profiles are used to characterize the effect and the accuracy of the particle RUV and subgrid stress modelling. Besides, the predictions are found to be very sensitive to particle inlet conditions and special care has been devoted to improve them. In particular, a turbulent velocity component, partially correlated with the fluid one, has

been added to the mean inlet MEPV.

[1] Février, P., Simonin, O. & Squires, K. D. , "Partitioning of particle velocities in gas-solid turbulent flows into a continuous field and a spatially-uncorrelated random distribution : theoretical formalism and numerical study", *J. Fluid Mech.*, in press (2006).
[2] Hishida, K., Takemoto, K. & Maeda, M., "Turbulent characteristics of gas-solids twophase confined jet", *Japanese Journal of Multiphase Flow*, **1(1)** :56-69 (1987).
[3] Borée, J., Ishima, T. & Flour, I., "The effect of mass loading and inter-particle collisions on the development of the polydispersed two-phase flow downstream of a confined bluff body", *J. Fluid.Mech.*, **443** :129-165 (2001).

2.2.2 LES of turbulent two-phase flames in aeronautical combustors (M. Boileau, S. Pascaud, B. Cuenot, T.Poinsot)

Depending on the droplets diameters, the flames observed in liquid-fueled combustors may be either purely gaseous (for small droplets) or non-homogeneous, in which case droplets may burn in clusters or even individually. But even in the simplest case of gaseous flames, the presence of a dispersed phase leads to very high local variation of the fuel vapor and therefore of equivalence ratio. To evaluate the capacity of AVBP to capture all these phenomena, a two-phase reacting LES of an industrial combustion chamber has been performed. Figure 2.6 shows the result of a calculation of the reacting flow inside one sector of a realistic aircraft combustor, fed with liquid kerosene. Like in the true geometry, air is entering through swirling inlets, cooling films and dilution holes. Results show that the overall shape of the flame is captured. The gaseous flame structure, behind the evaporation zone, is very similar to the classical gaseous flame found in a swirled burner. The main difference is in the stabilisation mechanism, controlled by the evaporation in the two-phase flame.

2.2.3 Ignition of two-phase combustors (M. Boileau, S. Pascaud, B. Cuenot, T.Poinsot)

In the performance of an aeronautical gas turbine, the capability of ignition and altitude re-ignition is a crucial criteria. For a helicopter or an aircraft engine, a fast and reliable lightup is required for various altitudes, i.e. different atmospherical conditions of pressure and temperature. In that context, a comprehensive understanding of the physics involved in the ignition process is a useful gain for combustor designers. The principle of ignition is to give an initial input of energy, able to initiate the combustion and set a stable flame. This energy can be provided either by a spark plug or by the use of an additional ignition injector. In both cases, ignition sequences are transient phenomena that can be computed by LES. To be accurate, such simulations have to take into account the effects of the presence of liquid fuel as a dispersed phase. AVBP has been used to compute two-phase ignition in realistic combustors. Figure 2.7 shows a snapshot of the ignition sequence calculation in one periodic sector of a helicopter annular combustor. In this simulation, the ignition burner injects hot gases on the left and right periodic planes of the computational domain. After a certain induction time, the main injector ignites and hot gases appear in this zone too. The complete ignition sequence lasts approximately 50 ms.

2.2.4 Polydisperse sprays (J. Lavédrine, J.-B. Mossa, B. Cuenot)

Sprays issued from the injectors used in gas turbines or in piston engines are not monodisperse and present diameter distributions of different shapes, depending on the atomisation process. The polydisperse characteristic of a spray has a great influence on all the variables describing the liquid phase, as the drag

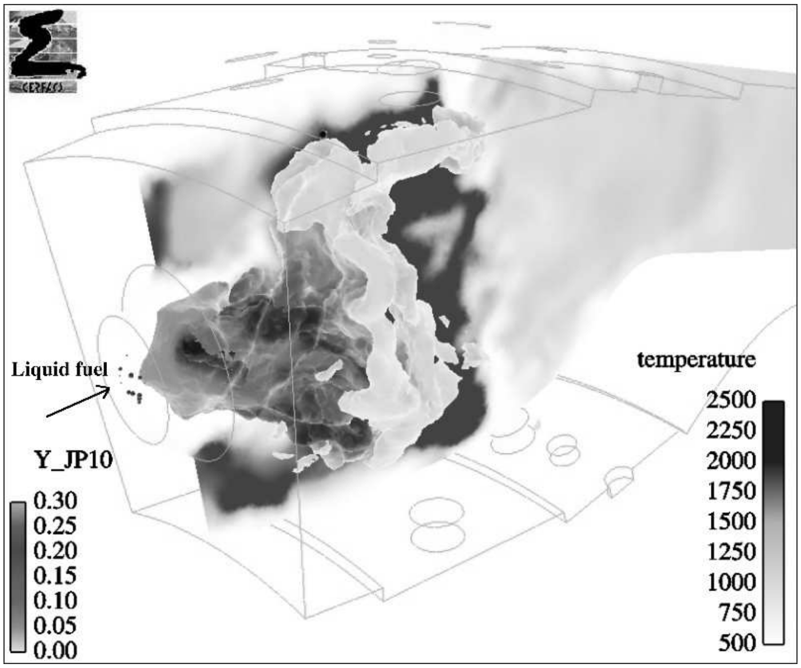

FIG. 2.6 – Steady two-phase combustion in a SNECMA combustor.

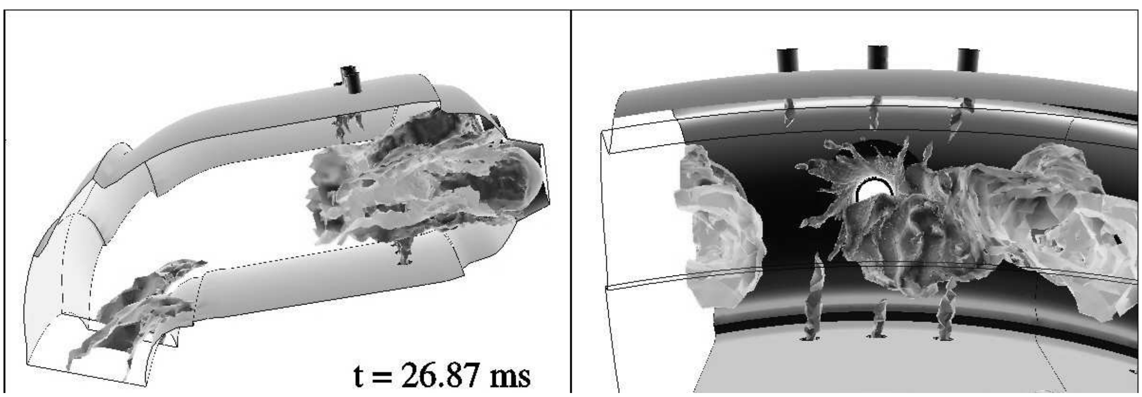

FIG. 2.7 – Snapshot of the ignition sequence in a Turbomeca combustor.

force and the evaporation are strongly linked to the size of the droplets.

In the eulerian framework described in the previous sections, there are two main ways to take into account a size distribution in a spray : either through a series of classes of droplets of the same size, or through the computation of evolution of the local size distribution. For compatibility and feasability reasons, the second approach has been retained (Thesis of J.-B. Mossa), assuming a presumed shape for the size distribution and computing its moments.

The methodology has been validated on the simple case of a liquid jet in a transverse gas flow, for which analytical results are available. It has been then applied to a full burner, which allowed to demonstrate its capability to capture the main effects of polydispersion. With this model, the implementation of droplets break-down and coalescence is straightforward.

2.3 LES of unsteady combustion

Unsteady combustion is now a major field of application for Large Eddy Simulations (LES) of reacting flows. These applications include predictions of combustion instabilities but also of ignition or quenching. In 2004 and 2005, CERFACS has lead multiple investigations around these topics and developed additional tools which are needed for these studies : LES tools but also acoustic analysis and sometimes RANS tools. Configurations computed at CERFACS were tested experimentally at the same time elsewhere in Europe, providing CERFACS with a unique data base for validation of the AVBP code. As a result, multiple papers have been produced since 2004 [CFD19, CFD20, CFD9, CFD15, CFD22] and the studies on unsteady combustion are a very important part of the team's work.

LES alone is not sufficient to understand turbulent combustion in confined chambers : theory and experiments show that acoustics play a very important role in many cases, especially in triggering combustion instabilities. Therefore writing codes able to describe the structure of acoustic modes in combustion chambers and their coupling with combustion is required : this is done at CERFACS and discussed in Section 2.3.4 and 2.3.5. In May 2005, CERFACS has organized a workshop in Toulouse on combustion instabilities and LES (with the support of the European Commission) which gatherered almost 100 scientists from 10 countries confirming the importance of this topic.

Section 2.3.1 recalls the submodels used for LES and Section 2.3.2 shows one example of LES validations for non-reacting flows where the CERFACS code AVBP was compared to experiments performed in DLR and with an LES code developed at Stanford. Acoustics are discussed in Sections 2.3.3 to 2.3.5. Ignition, quenching and flashback are discussed in Section 2.3.6 while multiburner computations are presented in Section 2.3.7. Effects of radiation and instability on NOx formation are discussed in a staged burner in Section 2.3.8. A ramjet LES is finally discussed in Section 2.3.9 before presenting LES applications in piston engines (Section 2.3.10).

2.3.1 LES models for combustion at CERFACS

Building an efficient LES tool in complex geometry chambers requires a compromise between precision and complexity : all submodels for turbulence, boundary conditions, turbulence / flame interaction, ignition, flame / wall interaction... are chosen to offer homogeneous performance and implementation costs which are compatible with the use of a compressible explicit solver on very large grids and large number of processors. Most models developed by CERFACS jointly with Institut Francais du Pétrole have been already published by CERFACS and are described in the literature.

The DTF (Dynamically Thickened Flame) model initially written by Colin et al (Phys. Fluids 12, 2000) continues to perform very well in the new configurations and has been used with virtually no modification [CFD20, CFD15, CFD4]. This model initially written for premixed flames is now used for diffusion flames with success. Note however, that many flames studied at CERFACS are categorized as diffusion flames because the fuel is injected through holes inside the chamber. However results show that these flames are usually lifted with significant mixing upstream of the flame so that very few diffusion flamelets are found.

An important submodel is the chemical scheme : initially many computations with the DTF model were performed with one-step schemes. Now two-step and four-step schemes are used and the DTF model has been modified to accomodate these multistep schemes [CFD35]. The construction of these schemes is performed by comparing their results on simple laminar premixed flames and using genetic algorithm techniques developed by C. Martin in his PhD [CFD29] to fit the results of the reduced schemes with the data obtained with full schemes. This was done for methane, propane, heptane, JP10 and kerosene. These

schemes have also been extended to include NOx in certain cases. For these cases, simple radiation models have also been developed in AVBP [CFD61, CFD33].
Boundary conditions and acoustic wave management of boundaries are still key issues for LES codes in which any error created at boundary will generally amplify in the domain. Selle [CFD18] has shown that the true reflection coefficient of a 'non-reflecting' boundary could be predicted analytically and that correct scalings for relaxation coefficients on non-reflecting boundaries have been proposed.
Important work was also required to extend LES from academic configurations to real combustion chambers. Being able to model multiperforated plates for example is mandatory for many chambers where multiperforation is used on a large portion of the chamber walls [CFD53]. Cooling films also raise additional difficulties. In most cases, models for these phenomena are based on separate DNS (see Section 2.1).

2.3.2 A small gas turbine burner (G. Lartigue, S. Roux, T. Poinsot)

During the PRECCINSTA EC programme, the accuracy of LES was tested for swirled flows by comparing LES velocity fields with measurements performed at DLR in a swirled premixed injector (Fig. 2.8) where swirl is produced by tangential injection downstream of a plenum. A central hub is used to stabilize the flame. Experiments include velocity measurements for the cold flow as well as a study of various combustion regimes.

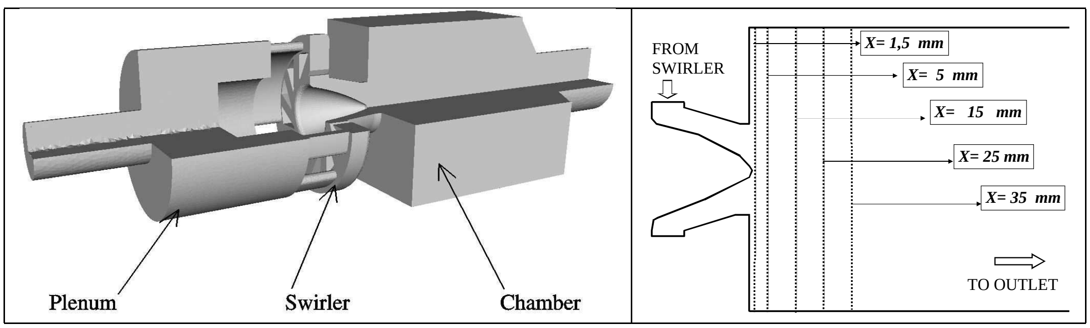

FIG. 2.8 – Configuration (left). Location of cuts for velocity profiles (right).

Cold and reacting premixed flows were computed successfully and published in Comb. and Flame [CFD15]. In 2004 and 2005, this study was used as a benchmark by Stanford and CERFACS to compare their LES codes. A typical example of result for non-reacting flow results is given in Fig. 2.9. The RMS axial velocity fields show very good agreement between the LES codes and the experiment. Even though small differences are observed (near walls for example), it is quite interesting to see that fully different codes lead to very similar accuracy on this configuration.

2.3.3 System identification of combustors (L. Selle, A. Giauque, A. Sengissen, K. Truffin, G. Staffelbach, Y. Sommerer, F. Nicoud, M. Brear, T. Poinsot)

System identification by forcing is a normal procedure during investigations of combustors stability : burners are forced in order to examine their response to acoustic waves entering the air or the fuel inlet. This identification can be performed experimentally or numerically using LES. But the cost of such experiments is high and LES are being developed to replace experiments for this task. At CERFACS, multiple studies of this type were devoted to system identifications in 2004 and 2005 :
– A theoretical study of how forcing should be performed and postprocessed was done by Truffin and Poinsot [CFD22] on a laminar premixed flame for which experimental results of the EM2C laboratory in EM2C Paris were available.

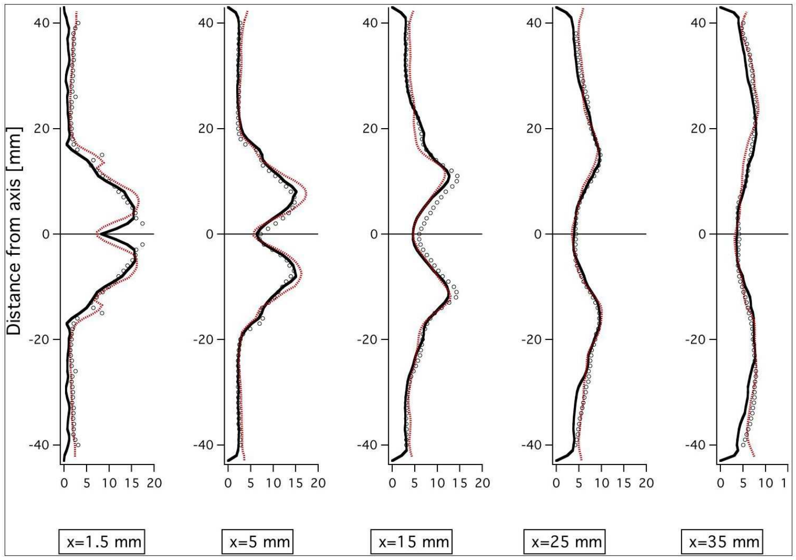

FIG. 2.9 – Cold flow : RMS axial velocity profiles. Circles : LDV ; solid line : LES (AVBP) ; dotted line : LES (Stanford).

- Chamber B : forced response of a large scale industrial gas turbine [CFD4] mounted in a square cross section chamber in Karlsruhe University (bilateral work with Siemens).
- Chamber C : an experiment built at Twente Univ. in the DESIRE EC project. The computation includes both mixing from the methane jets and combustion in the chamber. Fluid structure interaction between the oscillating combustion and the chamber wall is one goal of this work [CFD62] where wall vibrations can be monitored.

Studying the theoretical aspects of combustor forcing using a simple laminar flame proved to be a useful analysis [CFD22] which demonstrated that many similar studies (experimental or numerical) lack consistency and may lead to erroneous results when the point used to measure the fluctuating velocity is located too far upstream from the chamber.

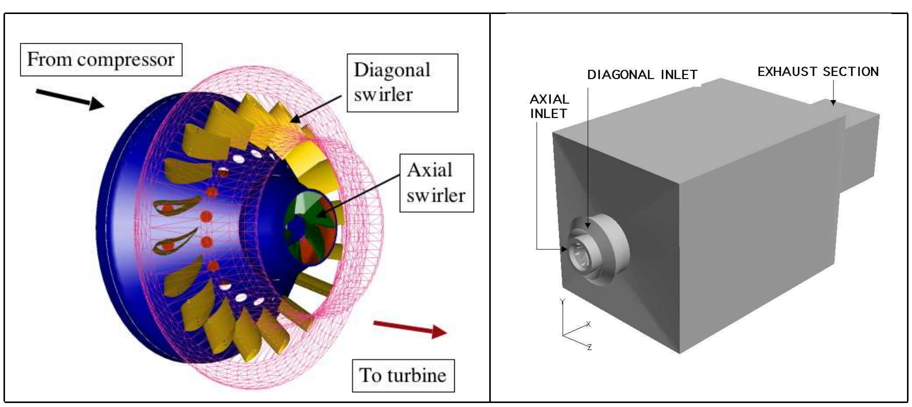

FIG. 2.10 – Chamber B : burner (left) and combustion chamber at ITS Karlsruhe (right).

Applying LES to measure flame response in Chamber B was a difficult challenge because it is a high-power swirled burner. It is installed in two different institutes in Karlsruhe, either in a square (ITS) or a circular (EBI) combustion chamber. Fig. 2.10 shows the main features of the burner in which this identification is performed : a central axial swirler (colored in dark) is used to inject and swirl a mixture of natural gas and preheated air. The main part of the combustion air as well as fuel is injected by the diagonal swirler through holes located on both sides of the vanes in order to achieve swirling. Perfectly mixed gases enter the diagonal swirler while pure air enters the axial swirler : the flame inside the chamber is in a partially premixed regime.

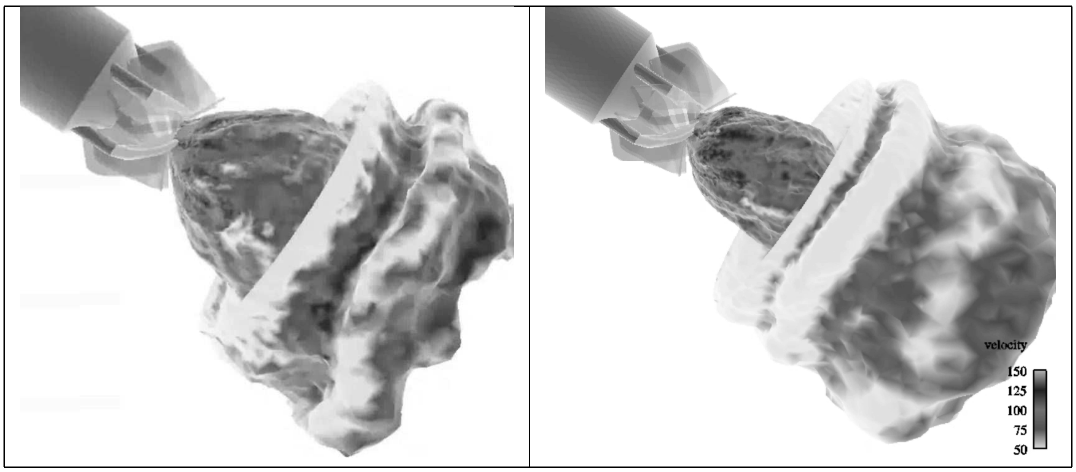

FIG. 2.11 – Chamber B (Fig. 2.10) with pilot flames on, forced by acoustic excitation. Snapshot of the flame visualized by an isosurface of temperature at $T = 1000$K. The left and right results correspond to different geometries of the swirler.

This burner and many of its evolutions have been analyzed in the PhD thesis of L. Selle (2004), G. Staffelbach and A. Giauque (2006). Comparisons of LES results with other methods and experimental results are given in [CFD4]. An example of results is presented here to illustrate the power of LES in predicting effects of geometrical changes on the flame response. For this study, the flame is pulsated at various frequencies by modulating the inlet velocity. Two configurations are computed to evaluate the response of the burner as a function of the geometry of the swirler. This response is the building block of acoustic solvers that predict the stability of combustors (see Section 2.3.4). Fig. 2.11 shows an instantaneous view of the flame front for a piloted flame during forcing for two different swirler geometries. The impact of this small geometrical modification on the flame response and shape is very strong.

The geometry of burner C (designed for the EC Desire project, PhD of A. Sengissen) is displayed in Fig. 2.12 : for this flame the computation must describe both mixing from the four methane jets with air and combustion in the chamber. This experiment was designed for LES validation : the set up can be meshed and computed entirely with LES. Another specificity of the Twente rig is that forcing is achieved by modulating the fuel flow rate and not the air. LES results predict the mean flow field with great accuracy as well as the flame transfer function over a wide range of forcing amplitudes [CFD62]. Unsteady wall pressure fields measured in the LES have also been compared with Twente measurements and shown good agreement, allowing to predict the vibration intensities of the chamber walls.

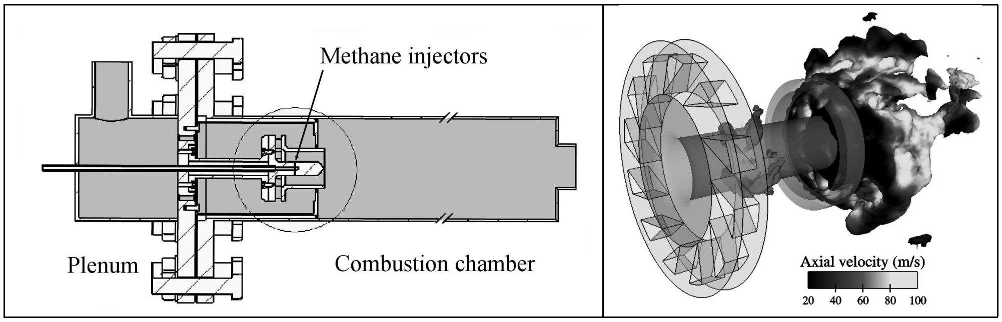

FIG. 2.12 – Combustor C. Left : geometry : the whole shaded area is meshed and computed. Right : isosurfaces of $Y_{CH4} = 0.1$ and isosurface of temperature $T = 1000$ K.

2.3.4 Acoustic / combustion numerical tools (A. Kaufmann, L. Benoit, C. Sensiau, F. Nicoud , T. Poinsot)

Acoustics play a key role in combustion and must be accounted for both experimentally and numerically. To understand confined flames, developing acoustic codes solving the wave equation in complex geometries for reacting flows is therefore a necessary step. CERFACS is developing such tools (PhDs of A. Kaufmann, L. Benoit and C. Sensiau).

The first tool called Soundtube provides the low-frequency longitudinal resonant modes in a network of interconnected ducts with variable sections and temperatures. The second tool is a full three-dimensional Helmholtz solver (called AVSP) solving the Helmholtz equation in the frequency domain. It is coupled to the LES code AVBP : they use the same grids ; the mean temperature and mass fraction fields required by AVSP (to know the sound speed) and the flame transfer function (to know the acoustic / flame coupling, see Section 2.3.3) are provided by AVBP.

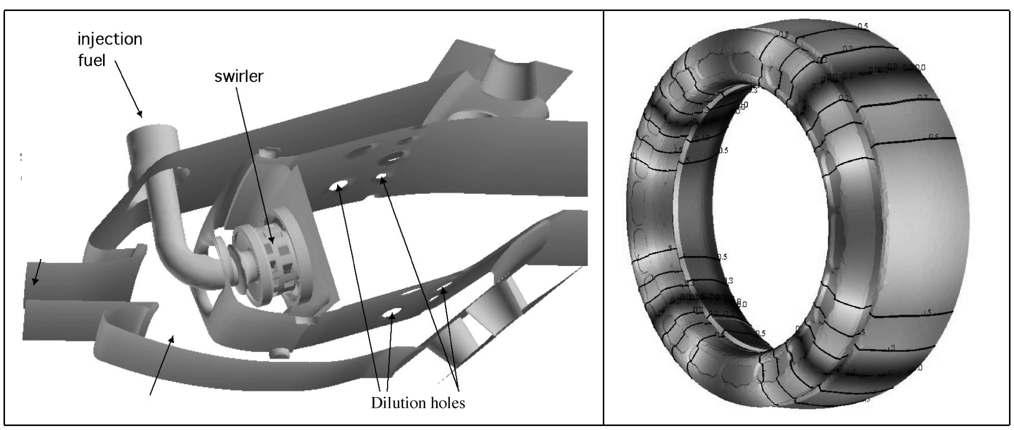

FIG. 2.13 – Acoustic analysis in a gas turbine annular chamber. Left : typical geometry for one burner Right : AVSP result for the 2nd annular mode (RMS pressure modulus on walls).

As an example, Fig. 2.13 shows a geometry of a single gas turbine burner and the structure of the second annular mode evidenced by AVSP in a full annular chamber with 18 burners. These modes are often crucial for the stability of the combustor.

2.3.5 Acoustic / combustion theoretical tools (C. Martin, A. Giauque, F. Nicoud , T. Poinsot, M. Brear)

At the moment, predicting at the design stage whether a given combustor will oscillate is still a challenge. If and when it oscillates, measurements and computations sometimes give indications of the reasons of the problem but it is usually too late. Being able to predict these phenomena requires the development of a new approach in which LES and acoustics tools are coupled : the joint usage of LES and Helmholtz solvers offers a new and powerful approach for such phenomena and has been exploited for various geometries in the last two years. In a Siemens case [CFD4], AVBP and AVSP were used together to understand the response of a chamber to forcing.
Section 2.3.4 has shown how acoustic codes were developed at CERFACS. In parallel, new theoretical tools must be built to analyze results : one approach is to look for proper 'energies' to analyze the growth of modes and to examine all terms in the budget of these energy equations. This method generalizes the usual Rayleigh criterion and was exposed in 2005 in a theoretical paper by Nicoud and Poinsot [CFD10] following initial ideas proposed by B.T. Chu in 1965. Among all possible energies tested at CERFACS, a classical choice is the acoustic energy e_1 (Poinsot Veynante, RT Edwards, Chapter 8) which follows a budget equation given by :

$$\frac{\partial e_1}{\partial t} = s_1 - \nabla \cdot (p_1 \vec{u}_1) \quad \text{with} \quad e_1 = \frac{1}{2}\rho_0 u_1^2 + \frac{1}{2}\frac{p_1^2}{\rho_0 c_0^2} \quad \text{and} \quad s_1 = \frac{(\gamma - 1)}{\gamma p_0} p_1 \dot{\omega}_T^1 \tag{2.1}$$

where the ^{0} subscript refers to mean quantities and the ^{1} to acoustic values. If integrated over the whole volume V of the combustor bounded by the surface A, it yields :

$$\frac{d}{dt}\int_V e_1 dV = \int_V s_1 dV - \int_A p_1 \vec{u}_1 . \vec{n} dA \tag{2.2}$$

where $\vec{n}$ is the surface normal vector. The surface A consists of walls, inlet and outlet sections. The RHS source term $\int_V s_1 dV$ corresponds to the well-known Rayleigh criterion and is the source of the oscillations. But there are other terms like acoustic fluxes on outlets and inlets $\int_A p_1 \vec{u}_1 . \vec{n} dA$ which also have a very strong effect on the instabilities : these terms can not be measured experimentally and most studies consider only the term they can quantify (the Rayleigh term) which is clearly just one part of the problem [CFD50]. LES offers a new approach by giving access to all terms of Eq. (2.2). In the PhD of C. Martin [CFD50, CFD29], a full closure of the acoustic energy equation for a burner developed by Ecole Centrale within the Fuelchief project was performed for the first time (AIAA J. 2006 in press). In the same study LES was used to compute the self-excited unstable modes of the device and AVSP was able to recover these modes and to predict their occurrence. In 2005, Pr M. Brear (Melbourne Un.) has spent 5 months at CERFACS to study energy equations for combustion stability. This study should be continued in 2006 at Stanford during the Summer Program.

2.3.6 Ignition, quenching and flashback (Y. Sommerer, G. Staffelbach, M. Boileau, T. Poinsot)

Unsteady combustion is a major field of research for applications. Igniting a combustor is a central issue for helicopter or aircraft engines. Predicting quenching or flashback is another important issue during transients. By improving mixing upstream of the combustion chamber, many devices used to reduce pollution by increasing mixing can also create the possibility for the flames to propagate upstream of their normal stabilization zone, thereby risking the destruction of the injector or a part of it. Predicting such phenomena is also a challenge for modelling because, during flashback, the flame regime changes considerably from partially premixed to almost purely non premixed flames. CERFACS and EM2C Paris have developed a joint experimental / numerical project which lead to the demonstration that LES can indeed predict quenching and flashback in swirled burners. Results were published in J. of Turb. [CFD20].

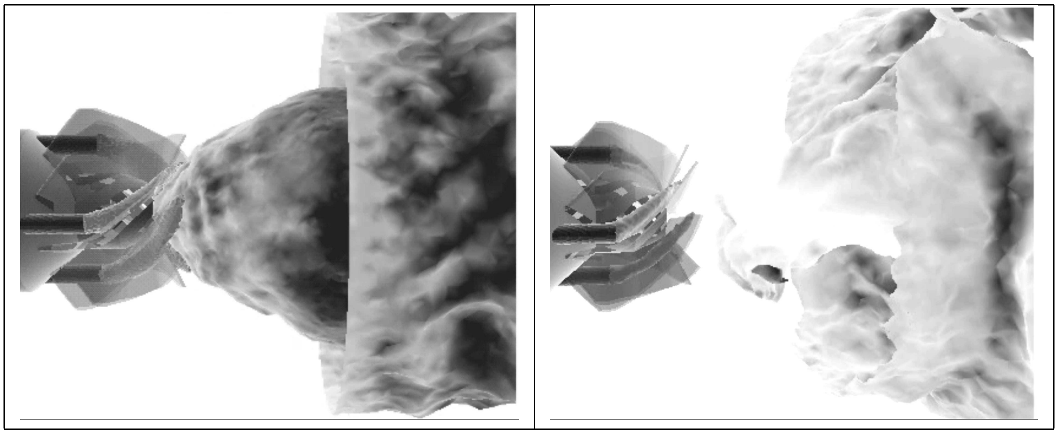

FIG. 2.14 – Effects of pilot flame flow rate on flame stabilization in Chamber C. When the pilot fuel flow rate is not adequate (right picture), the flame lifts from the central hub and oscillates.

This study was extended to more complex cases in 2005 : Fig. 2.14 shows an example where the effects of piloting on flame stabilization were studied in Chamber B (Fig. 2.10). For this burner, decreasing the fuel flow rate going through the pilot injection (left picture to right picture) leads to a loss of stabilization which is a major problem for operability.
Additional studies of ignition have been performed in helicopter engines for full configurations (Section 2.5) and in spark-ignited piston engines (Section 2.3.10). For these studies, the thickened flame model was coupled to a spark model. At the same time, other models for spark ignition (based on flame surface approaches) have also been coded by IFP in AVBP (PhD of S. Richard), leading to similar results.

2.3.7 Multiburner computations (Y. Sommerer, M. Boileau, G. Staffelbach)

Most academic studies of combustion in gas turbines are performed using a single gas turbine burner and installing it into a laboratory combustion chamber. However real gas turbines use 16 to 24 burners installed in the same annular chamber. In such situations coupling may occur between burners : in regions where the issuing flames from neighbouring burners meet, strong turbulence and heat release can take place and lead to instabilities which cannot be observed in single burners configurations. In cooperation with Siemens PG and DLR, within the EC project DESIRE, CERFACS is studying a chamber equiped with three burners (PhD of G. Staffelbach). This LES has been performed for three burners (5 million cells) and started for the full machine (40 million cells : see Section 2.5). It is the largest computation ever performed with combustion in such a geometry. It requires typically 64 to 128 processors to run efficiently for the 3 burner rig and it was performed with up to 5000 processors on the full geometry on a BlueGene architecture. Fig. 2.15 shows an instantaneous isosurface of temperature.

2.3.8 Radiation, instability and pollutants (P. Schmitt, T. Poinsot)

Nitric oxide formation in gas turbine combustion depends on four key factors : flame stabilisation, heat transfer, fuel-air mixing and combustion instability. The design of modern gas turbine burners requires delicate compromises between fuel efficiency, emissions of oxides of nitrogen (NO_X) and combustion stability. Burner designs allowing substantial NO_X reduction are often prone to combustion oscillations. These oscillations also change the NO_X fields. Being able to predict not only the main species field in a burner but also the pollutant and the oscillation levels is now a major challenge for combustion modelling.

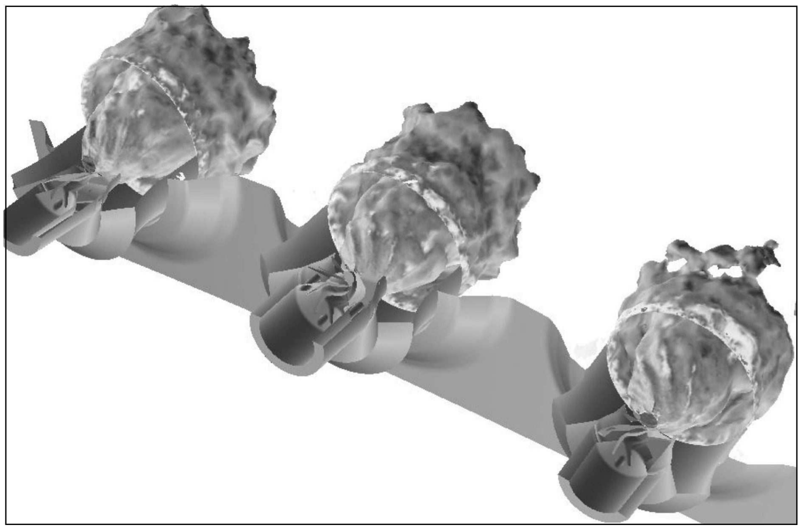

FIG. 2.15 – Three-burner combustion chamber of DLR. Isosurface of temperature T=1000 K.

This must include a realistic treatment of unsteady acoustic phenomena (which create instabilities) but also of heat transfer mechanisms (convection and radiation) which control NO_X generation.

In this study, LES was applied to a realistic gas turbine combustion chamber configuration where pure methane is injected through multiple holes in a cone-shaped burner. Mixing and combustion are handled simultaneously using the DTF model and a two-step chemical scheme. Simulations have shown the impact of cooling air and heat transfer on nitric oxide emissions as well as the effects of combustion instability on nitric oxide emissions. Additionally, the combustion instability is analysed in detail, including the evaluation of the terms in the acoustic energy equation and the identification of the mechanism driving the oscillation. Fig. 2.16 shows the geometry of the burner and a typical flow snapshot during combustion instability displaying an isosurface of fuel mass fraction (0.1) (showing the methane jets) and an isosurface of reaction rate (showing the flame position). This regime corresponds to a pulsating flame. The comparison of the LES data with experiments is also good as shown in Fig. 2.17 (J. Fluid Mech. 2006 ; paper under revision).

2.3.9 Ramjet (Y. Sommerer, L. Gicquel, A. Roux, T. Poinsot)

Combustion instabilities are common in ramjet engines : they can lead to vehicle damage and still remain a difficult problem to solve at the design stages. The LES tools of CERFACS allow to investigate flame dynamics and predict combustion instabilities for highly compressible flows as found in ramjet engines. The research ramjet studied for MBDA is a two-inlet side-dump ramjet combustor experimentally investigated by ONERA and the flight case corresponds to a high-altitude flight condition. Boundary conditions are 'exact' because the inlet is perfectly non-reflecting and the outlet is a choked nozzle. Fig. 2.18 shows the complexity of the flame topology. Two distinct flames are observed and stabilized by different processes : the first flame is located in the head-end and anchored by the recirculation zone due to jet impingement while the second flame is located in the combustion chamber and fed by hot rich burned gases coming from the head end and fresh gases directly coming from the air intakes. Comparisons between LES and LDV fields are good both for mean and RMS fields. LES reveals a high frequency 'screech-like' mode often observed in such side-dump configurations. The frequency observed by LES matches exactly the second transverse

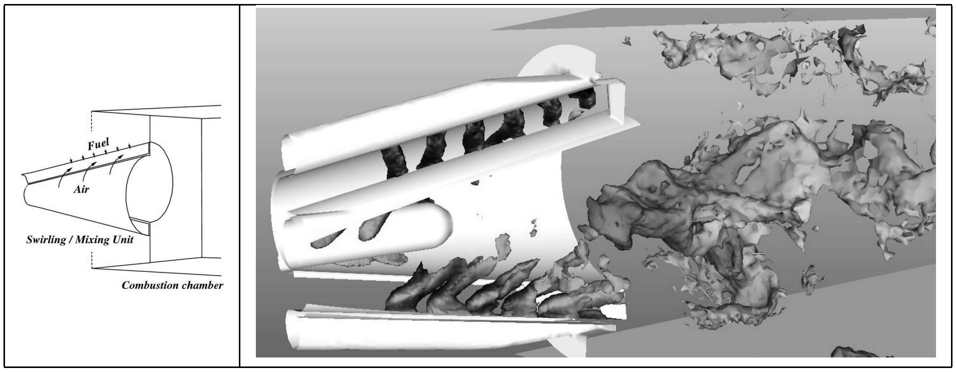

FIG. 2.16 – LES of combustion in a staged burner.

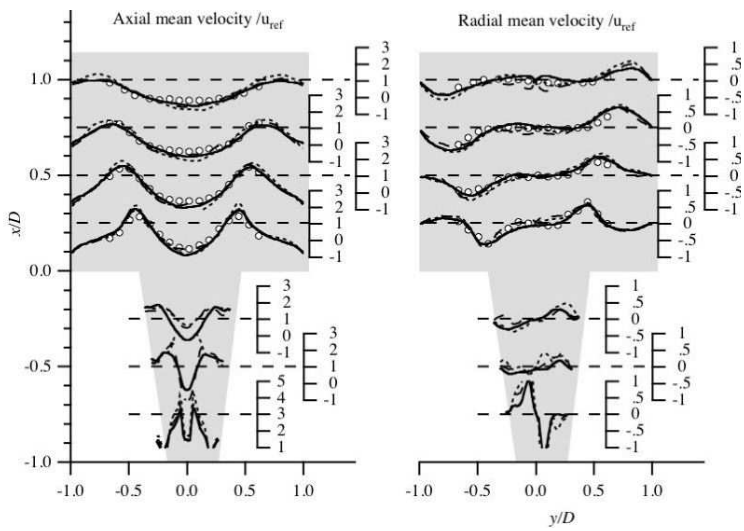

FIG. 2.17 – Comparison of LES and experiment : mean axial (left) and radial (right) velocity fields on transverse axis for various distances to inlet. Circles : experiments (DLR), solid line : LES.

mode of the chamber predicted by AVSP suggesting that this oscillation is probaly due to thermo-acoustic resonances.

2.3.10 LES in piston engines (L. Thobois, O. Vermorel, T. Poinsot)

Another field where LES is developing fast is flow in piston engines. Together with IFP, CERFACS has extended its LES tools to piston engines. Two main directions have been pursued : computing multiple successive cycles and computing steady flow with LES through valves. Of course, being able to develop high-fidelity computations on moving grids and managing grid displacements in complex geometries were the major difficulties in this task : AVBP was modified in depth to allow moving mesh computations and new numerical techniques were required to handle these problems. Solutions used now in AVBP are described in a JCP paper published in 2005 [CFD9].
With this tool, for the first time, CERFACS and IFP have produced in 2005 a computation of all phases of combustion in engines (intake, compression, combustion and exhaust) over multiple cycles with LES.

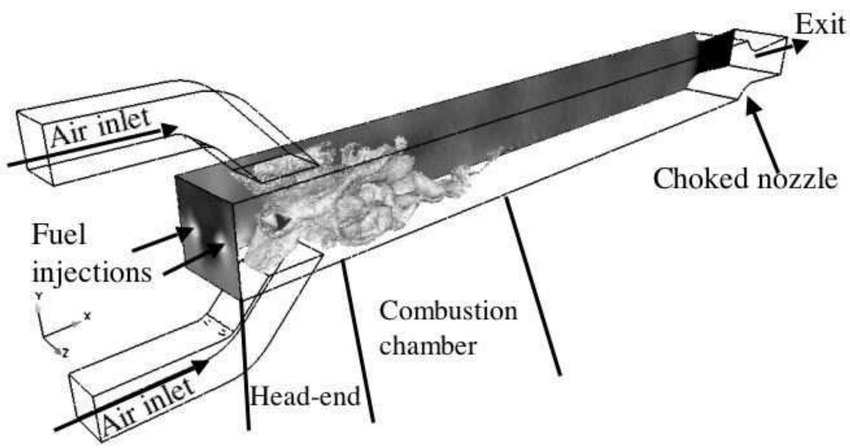

FIG. 2.18 – Ramjet configuration and instantaneous visualization of the flame (white iso-surface). x-plane : fuel mass fraction ; z-plane : pressure field.

Results open a path which has never been followed before : investigate cycle-to-cycle variations in engines. Fig. 2.19 shows an example of the flame front position in an engine at the same crank angle for four successive cycles. Obviously LES does capture variations between cycles.

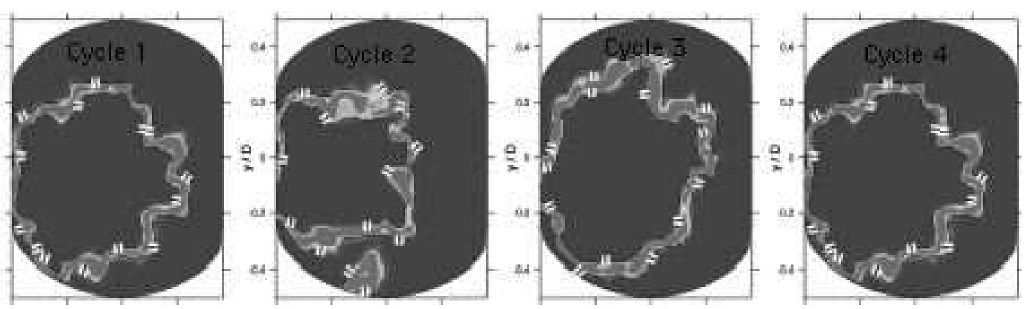

FIG. 2.19 – Fields of reaction rate (marking the flame position) in a plane normal to cylinder axis for four cycles at the same crank angle : all cycles are different (LES with AVBP).

LES was also used to predict pressure losses and flow structure during intake in a joint study with PSA and Ford (Fig. 2.20). It was shown to be much more accurate than RANS for this type of flow [CFD64, CFD21]. This configuration was run on CERFACS computers but was also tested with a 20 million cell grid on a BlueGene configuration (Section 2.5).

2.4 Advanced RANS tools for combustion

Despite the progress of LES, many industrial applications are still easier to handle with classical RANS (Reynolds Averaged Navier-Stokes) methods. CERFACS develops activities in this field along three directions : (1) hybrid numerical methods for RANS combustion codes, (2) coupling tools for shape and regime optimization using RANS tools and (3) cross comparison of RANS and LES codes. RANS codes can be used to initialize LES for example or in an integrated design chain : this can be done efficiently only

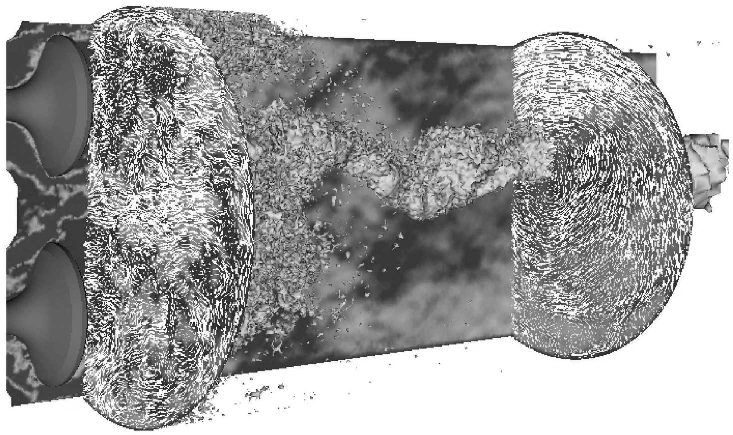

FIG. 2.20 – LES of the flow field in a steady bench for 4 valve engine tests.

if both approaches give sufficiently close results. Therefore understanding the limits of RANS and LES is important.

2.4.1 Hybrid numerical methods for RANS (V. Auffray, L. Gicquel, G. Puigt)

The RANS code used by SAFRAN for RANS computations is N3S-Natur (developped by INCKA-SIMULOG). It is routinely employed for the evaluation of the next generation of aeronautical gas turbines. However, current N3S-Natur versions are limited to triangular and tetrahedric cell topologies. In an effort to reduce the associated computational cost when applied to ever more complex geometries, CERFACS participates in the development of advanced numerical schemes to handle various cell topologies. This work constitutes the bulk work of the PhD dissertation of Valérie Auffray conducted in conjunction with the INCKA specialists and under the supervision of the SAFRAN group. A strong link with the methods used at CERFACS for LES in AVBP is favored for future interaction between the two codes.

2.4.2 Shape and regime optimization for reacting flows (F. Duchaine, L. Gicquel)

Present operating conditions of combustion chambers are essentially dictated by mechanical limits of the components located downstream of the chamber ; the chamber design must be tuned so as to satisfy pre-requisites on the temperature profile at the outlet of the chamber for example. The aim of this work (performed within the EC project INTELLECT DM) is to apply to combustion, closed loop optimisation methods already developed and validated in other fields (aircraft, structures and antenna designs). The coupling device PALM (develop within CERFACS by the Algo team) is used to develop an optimisation loop based on RANS calculations : N3S-Natur - SAFRAN's production code. Suitable test configurations have already been evaluated to assess the automatic chain and the optimisation algorithms implemented at CERFACS. Different cost functions and optimization methods are available [CFD44] and 3D optimization tests on real combustors are currently conducted.

2.4.3 Comparison of RANS and LES (F. Duchaine, A. Roux, L. Gicquel, T. Poinsot)

Comparing RANS and LES results on the same burner is an interesting exercice. A direct comparison of the time averaged solutions obtained with the two approached and for the same configuration constitutes

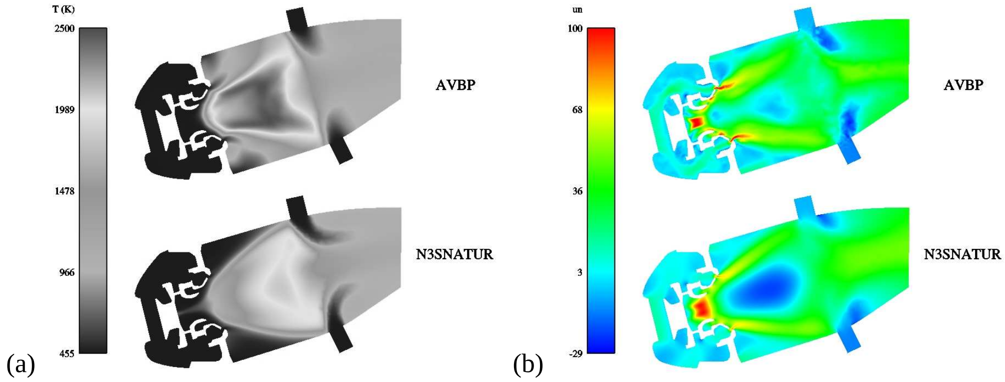

FIG. 2.21 – Comparisons of (a) mean temperature and (b) mean axial velocity obtained with N3S-Natur and AVBP for an aircraft burner.

a first step toward the proper use of both methods by industry. Figure 2.21 presents solutions from RANS and LES computations (N3S-Natur and AVBP respectively) for an industrial gas turbine of SAFRAN. Such an assessment allows gauging of each approach when compared with the experiment but also evidences the necessity of a proper treatment if RANS is to be considered as an initial solution for LES.

2.5 Software engineering

Developing and using large LES and DNS codes requires specific efforts : the codes but also the associated pre and post-processing tools required to prepare LES runs and examine results make software engineering a critical task at CERFACS. Multiple actions took place in the last two years.

2.5.1 Source management (Y. Sommerer)

AVBP is developed jointly by CERFACS and Institut Francais du Petrole (IFP) and used by many European institutions. Multiple laboratories also bring specific sub models to the code. The source management is performed by CERFACS using CVS in order to manage this multi-sites and multi-developers environment. A software quality practice is established to minimize the development risks. Regular meetings take place between IFP and CERFACS to define the versions evolutions. Two levels of non-regression test cases are used :
- CTEA (Automatic Elementary Test Cases) run on a weekly basis during development,
- QPF (Quality Program Form) performed for each new version (every nine months).

Another specific benchmark is run frequently on various computational architectures to verify both single-processor efficiency and parallel performances. The AVBP documentation (User's Manual and Handbook) evolves in parallel with the source code and is available for the users via a web site maintained by CERFACS. This is a significant task for CERFACS : CTEA, QPFs and information management require more than 5 man years for the CFD team every year.

2.5.2 Source optimisation (Y. Sommerer, M. Garcia, G. Staffelbach)

The previous sections have shown an increase of problems size and complexity of most LES at CERFACS. Simultaneously, the new generation of super computers opens the path for studies which were not possible up to now, such as ignition sequences or complete annular chambers computations. The recent evolution of massively parallel clusters (up to thousands processors) reinforces the importance of sustaining high performance levels on thousands of processors :

– CPU and Message passing : optimization, using the most modern profiling tools, is done jointly with the CERFACS Parallel algorithm team to use the most efficient MPI functions and minimize CPU cost. This work is a key to reach linear speedups up to 5000 processors.
– Domain decomposition : the algorithm used for domain decomposition controls the speed up for massively parallel cases. AVBP is linked with the most modern decomposition domain algorithms in order to minimize the frontier interface between neighbors domains (i.e. minimize the point-to-point communications).

2.5.3 Frontier computations (Y. Sommerer, G. Staffelbach)

CERFACS collaborations with computer companies and computing centers allow to extend LES to 'frontier' simulations, thereby testing these super computers and anticipating the problems linked to very large computations in terms of memory, parallelism and pre/post-processing. Two application fields were used in 2005 for these tests :

– Piston engines
– Full gas turbines (aeronautical and industrial)

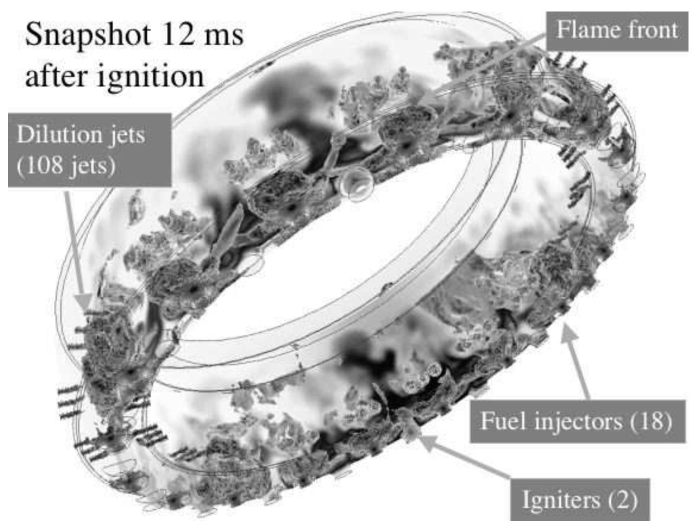

FIG. 2.22 – LES of ignition in a helicopter gas turbine using jets of hot gases. Computation with AVBP on 2048 processors (BlueGene configuration).

High-resolution LES of turbulent flows in Diesel intake pipes (10 millions cells ; 1024 processors) were performed on an IBM eServer Blue Gene made available to CERFACS by IBM. test cases data were provided by PSA. In DI engines aerodynamics play a key role : the design of intake pipes is crucial, requesting significant optimizations and especially with CFD. For such flows, classical turbulence methods lack for accuracy : the revolution introduced by Large Eddy Simulation (LES) methods in the last ten years, allows now a precise computation of the flows but the size of the models makes them impossible to be run on most of the computers with classical architectures.

In 2005, AVBP was ported on a BlueGene machine and LES was run on a high-resolution mesh, in order to compute a typical Diesel intake geometry (see Fig. 2.20). Instantaneous velocity fields exhibit many structures on the valve jets and show that the high-resolution LES reveals flow features which were never computed before.

In the field of aeronautic gas turbines, a full combustion chamber was computed with LES on BlueGene and CINES computers (20 millions cells cases, 2048 processors IBM BG/L and 32 to 128 processors CINES SGI O3800 in a joint CINES/CERFACS project). Computing combustion in a full combustion chamber had long been out of reach of Computational Fluid Dynamic tools. In 2005, AVBP was used on BlueGene on high-resolution meshes, in order to compute ignition and flame propagation in the combustor of an helicopter turboshaft engine from Turbomeca (Safran group). In this geometry (Fig. 2.22), all fuel injectors (18) and dilution jets (108) are included and a full ignition sequence starting from two igniters is computed. Industrial gas turbine (40 millions cells ; 1000 to 5120 processors IBM BG/L) were also computed as test cases for massively parallel machines. For such turbines, recent CERFACS LES studies show the importance of burner - burner interaction and azimuthal acoustic modes to accurately predict the flame stability. This requires full chamber computations with all burners (24 usually) and huge CPU capacities. A Siemens PG configuration was run on IBM BlueGene/L (Thomas Watson Research Center and Rochester respectively 2d and 22th in the 26th top500 list) and linear speedup up to 5000 processors were measured (Fig. 2.23). Typically, a speed up of 4078 on 4096 processors was obtained.

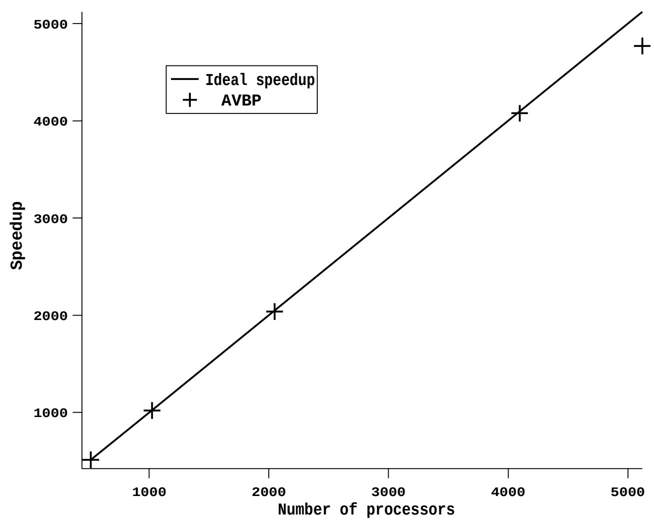

FIG. 2.23 – Speed-ups obtained with AVBP on BlueGene (Thomas Watson Research Center)

2.5.4 Collaboration with French national computing centers (CINES and CEA) and computer companies (Y. Sommerer)

CERFACS continues to collaborate with French national computing centers CINES, IDRIS and CEA. Because of their excellent parallel scalability, AVBP and/or NTMIX are often used to benchmark machines for those three institutions in order to stress the whole configuration machine. In parallel, a joint effort with constructors like IBM [1] or Cray as been done in 2005 to optimize AVBP on specific processors and interconnection networks : Power PC 440 - IBM BlueGene/L and Opteron - Cray XD1.

[1] IBM Red Book (Chapter 8.4) : http ://www.redbooks.ibm.com/abstracts/sg246686.html ?Open

3 Aerodynamics

The core activity of the AAM (Aerodynamic and Applied Methods) team is concentrated on developping aerodynamics numerical tools that are in used either in industry or in research laboratories. The close link with research laboratories allows to rapidly transfer advanced technologies to the industrial world. Most of the effort is dedicated to improve the multibloc structured solver called *elsA*. This solver is an ONERA project which aims to gather aerodynamics methods and algorithms in an Object Oriented framewok. Due to an official agreement with ONERA, CERFACS is involved in the *elsA* developement since 2001. This code is now daily used in an industrial environment such as Airbus and SNECMA, which implies that the majority of developments is now dedicated to increase the computing performances (this activity is described in Section 3.3 and Section 3.4).

Besides *elsA*, the CERFACS has the opportunity to work with numerous others solvers either on structured approach (in-house cartesian code : NTMIX) or unstructured ones (TrioU from CEA, Tau from DLR, AVBP from CERFACS). Such a diversity of tools enables to study different applications ranging from wake vortex to aerothermal simulation (work presented in Section 3.1).

During the past two years, CERFACS has started a new activity in the field of optimization (detailed in Section 3.2). The work done can be splitted in two main branches. Firstly, the construction of metamodel for A/C design and interdisciplinary data exchange has been developed making use of POD, Kriging and Neural Networks. Secondly, different optimization algorithms have been evaluated in order to build an efficient optimization loop.

All the works describe in the following sections have been done in collaboration with industrials such as Airbus and SNECMA and also research centers among which : ONERA, DLR (through MIRACLE), IRPHE, Paris VI and the university of Montpellier.

3.1 Modelling

3.1.1 Wake vortex simulation (L. Nybelen)

CERFACS has developed a strong expertise on the topic of wake vortex dynamics, which is now widely recognized in the scientific community. Numerous studies have been conducted investigating the stability of different vortex systems by means of Direct Numerical Simulations (DNS) or Large-Eddy Simulations (LES). These studies are both a mean of characterizing the wake of an aircraft in the near-field and a way to determine the decay in the far-field, which is important in predicting the behaviour of the wake for large transport aircraft. A PhD student at CERFACS investigates wake vortex dynamics through a collaboration with Airbus -Deustchland and IMFT (Institute of Fluids Mechanic of Toulouse). CERFACS is also active in the framework of European programs such as AWIATOR (FP5) and FAR-Wake (FP6).
CERFACS has been involved in studying the merging process of two co-rotating vortex, which governed principally the wake vortex dynamic in the near- extended field ($1 < x/B < 10$). These co-rotating vortices correspond to the vortices shed by the flap and the wing tip. In certain cases depending on the Reynolds number and the position of the vortices, the system may be subject to the development of a very short

wavelength/elliptic instability ($\lambda_i = 0(r_{core})$) which amplifies rapidly within the inner vortices. Thus, the merging process becomes unstable. The development of elliptic instability is characterized by an oscillation of the vortex core position. The vortices finally exchange their vorticity and lose their structure coherence, leading to the merging by a reorganization of turbulent structures. The unstable merging process is faster than the stable merging [CFD120]. Unstable and stable merging mechanisms have been analyzed using two analytical vortex models, namely the Lamb-Oseen and the Jacquin VM2 model which describes better a realistic vortex in the extended near-field.

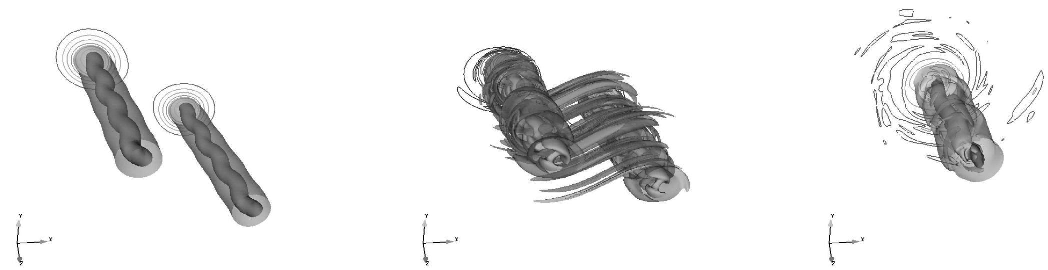

FIG. 3.1 – Isocontours of vorticity magnitude $||\vec{\omega}||$: the dynamic flow of the unstable merging with Lamb-Oseen vortex model as initial condition. Left to right : $t^* = t/(2\pi^2 b^2/\Gamma) \sim 1.95, 2.45, 3.25.$

The phenomena caused by the generation and propagation of pressure waves in vortex cores have also been investigated with DNS and LES approaches [CFD8]. The propagation of pressure waves is responsible for the generation of axial velocity, which under certain conditions leads to the development of helical instabilities and to an abrupt change of flow topology in the vortex core. Involved dynamics may explain vortex bursting and end-effects, which are phenomena observed in smoke visualization of real aircraft wakes as well as in small-sacle experiments that are not well understood.
Numerous analyzes have been made of the interaction between an exhaust jet and trailing vortex in two phases, the jet regime then the entrainment case.

3.1.2 Aerothermal Simulations

3.1.2.1 Improvement of $k-\varepsilon\ v^2-f$ turbulence model simulations (A. Celic)

Durbin's $k-\varepsilon\ v^2-f$ turbulence model theoretical basis [1] consists in a construction of the turbulent eddy viscosity in order to reproduce more accurately the behavior of μ_t in the boundary layer. The model contains three transport equations coupled with an elliptic one (for f). At CERFACS, the activity began with comparisons of turbulence models behaviors for several applications (including Durbin original turbulence model) and lead to the implementation of a new variant of Durbin's $k-\varepsilon\ v^2-f$ turbulence model in elsA. This model contains [CFD88] :

- a new version of the realizability condition which is adapted from Durbin's one,
- an extra source term on f equation for a better conditionning of f wall boundary condition,
- a dissipation term for v^2 constructed from Sveningsson one.

This new version of Durbin's turbulence model was first validated over a flat plate [2] (Fig. 3.2) and lead to interesting results for the computation of cold jets impinging on a hot wall [3], as shown on Fig. 3.3. This work has been done in the framework of MAEVA project ('Aerothermal Modelling of Fluids for Ventilation of Planes').

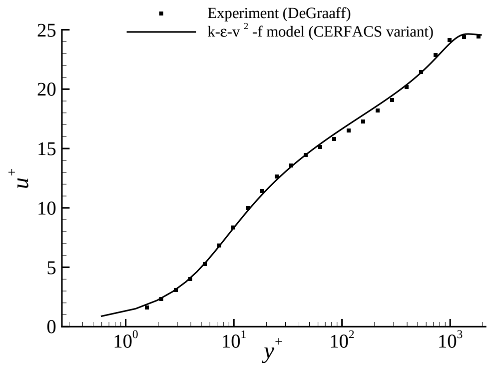

FIG. 3.2 – Flat plate : non dimension velocity as function of the non dimension distance to the wall. The experimental data and the test case are proposed in [2].

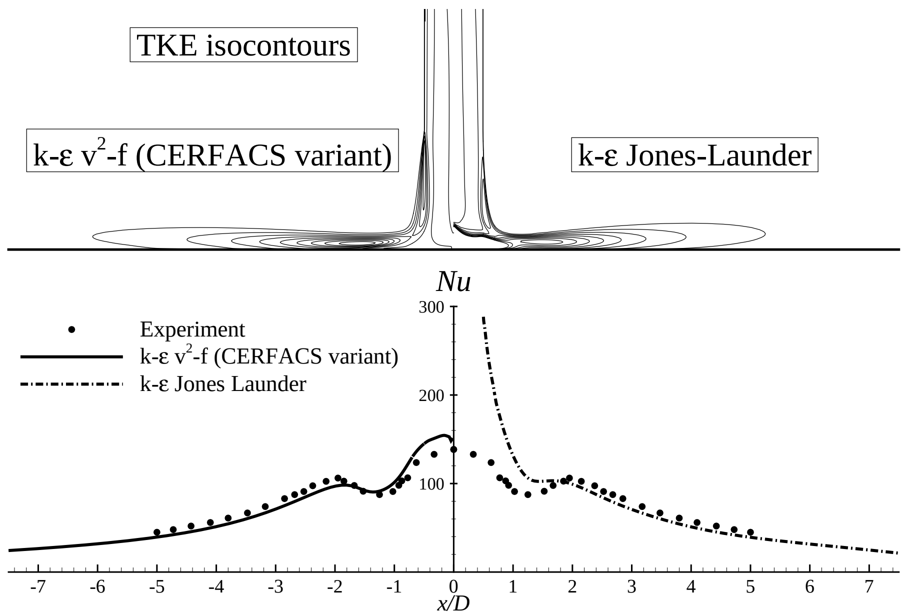

FIG. 3.3 – Jet impinging on a plate : comparison of turbulent kinetic energy distribution for Durbin's modified and Jones Launder turbulence models ; Nusselt coefficient computed on the flat plate and experimental data.

[1] P. A. Durbin, (1991), Near-Wall Turbulence Closure Modeling Without "Damping Functions", *Theoretical and Computational Fluid Dynamics*, **3**, 1-13.

[2] D.B. DeGraaff and J.K. Eaton, (2000), Reynolds-Number Scaling of the Flat-Plate Turbulent Boundary Layer, *Journal of Fluid Mechanics*, **422**, 319-346.

[3] J. Baughn, A. Hechanova and X. Yan, (1991), An experimental Study of Entrainment Effects on the Heat Transfer from a Flat Surface to a Heated Circular Impinging Jet, *Journal of Heat Transfer*, **113**,

1023-1025.

3.1.2.2 Jet in cross flow (J.C. Jouhaud)

The 'Jet in Cross Flow' topic represents for CERFACS an initiative to strengthen the fundamental scientific aspect in the field of turbulence modelling for aerothermal applications [CFD13]. More precisely, this topic concerns here the development of a reliable simulation tool for the computation of industrial configurations which involves warm jets exhausting in cold cross-flows, i.e. turbojet anti-ice exhaust flows. This type of aerothermal flow is a major stake for AIRBUS France.

FIG. 3.4 – Square Jet in Cross-Flow Produced by a Scoop - Instantly Temperature Field (Y=0 plane).

In the MAEVA framework ('Aerothermal Modelling of Fluids for Ventilation of Planes'), our recent LES computations with AVBP solver (see Fig. 3.4) have shown that LES appears like an efficient tool for aerothermal predictions [CFD102]. In fact, only these types of computations are able today to predict very precisely the right thermal profiles (see Fig. 3.5) compared to U-RANS methods, without an excessive CPU cost (good turnover). In the future our objective could be to develop hybrid LES/U-RANS methods in a production code dedicated to AIRBUS aerothermal computations.

3.1.2.3 Wall modeling for unsteady dilatable flows (A. Devesa, F. Nicoud)

This research topic corresponds to A. Devesa's on-going PhD thesis that started at the end of 2003. It is the result of a collaboration between three entities : CEA, the French Agency for Nuclear Energy based at Grenoble (France), University Montpellier II hosting F. Nicoud (PhD advisor) and CERFACS. The objective is to model accurately and reliably the fluid / solid interaction in energetical industrial applications, *e.g.* nuclear reactor safety, where strong temperature gradients exist. For those flows, the correct prediction of thermal fluxes at the wall is a crucial problem, because materials can be subject to contraction, to dilatation and to ablation phenomena, leading to a possible destruction. In this study, the CEA in-house Trio_U CFD code is used, as well as Matlab. Crossed comparisons were systematically undertaken between the two numerical approaches.
First, the study was limited to a steady state approach. Under the classical law-of-the-wall assumptions, density changes in the boundary layer, virtually due to strong temperature gradients were taken into account in a new non-isothermal wall law. The analytic derivation of this new wall function was deduced from Van Driest's transform [1]. Implementation in Trio_U code was carried out and results showed significant

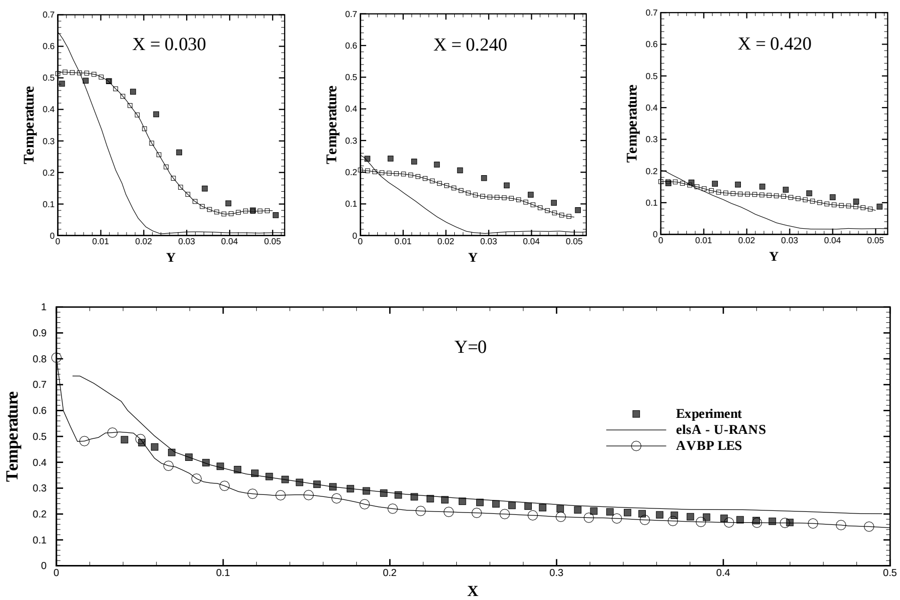

FIG. 3.5 – Comparisons between LES, U-RANS and MAEVA Experiment - Average Temperature Curves.

improvement compared to the standard law-of-the-wall (logarithmic law for the velocity and Kader's formula for the temperature) [CFD42].

The following step was to adopt an unsteady approach in the wall modeling, using a two-layer model, namely the TBLE (Thin Boundary Layer Equation) model [2]. The concept of this model lies on solving a set of simplified equations in a one dimensional fine mesh embedded between the first off-wall point and the wall. The work consisted in adapting this model, previously validated in incompressible cases, to dilatable fluid cases and in implementing it into Trio_U software. At the end of 2005, the validation process was still under progress, but showed (Fig. 3.6) that, for steady state quasi-isothermal flow, the "dilatable version" of the TBLE model recovered the standard law-of-the-wall, while in non-isothermal case, it behaved like the non-isothermal wall function previously described [CFD42].

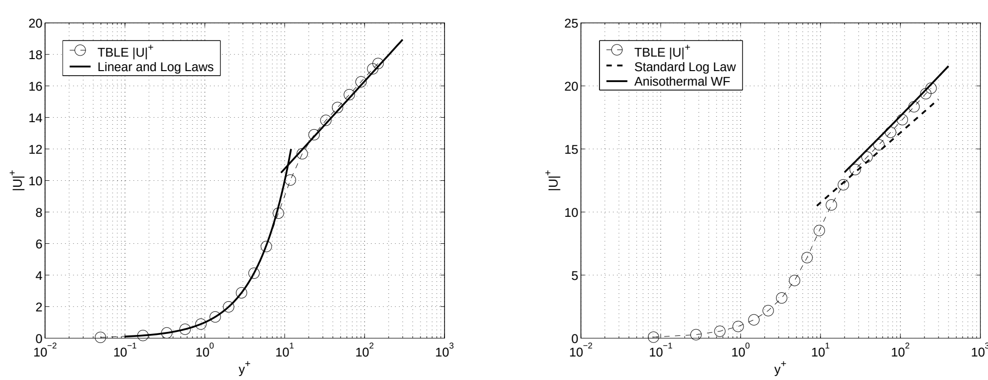

FIG. 3.6 – Velocity profiles from TBLE model. Left : isothermal case, right : non-isothermal.

Finally, the problem of unsteady effects in wall modeling was adressed. Even if two-layer models are developed for unsteady turbulent flows, there must exist a critical frequency beyond which the model can not be used in an accurate way. To answer this question, a Direst Numerical Simulation (DNS) of turbulent channel flow with 6 passive scalars submitted to a temporal varying forcing term was set up.

[1] E.R. Van Driest, 1951, Turbulent boundary layers in compressible fluids, *Journal of Aeronautical Sciences*, **18**(3).

[2] E. Balaras, C. Benocci and U. Piomelli, (1996), Two-layer approximate boundary conditions for Large-Eddy Simulations, *AIAA Journal*, **34**(6), 1111-1119.

3.1.3 Detached eddy simulation

3.1.3.1 Detached Eddy Simulation with $k-\omega$ turbulence model (J.-C. Jouhaud, X. Toussaint, P. Sagaut)

Since 2004, the aerodynamic team is involved in the development of hybrid U-RANS/LES techniques for complex aeronautical configurations. In fact, these techniques when combined with wall functions and grid strategies (automatic mesh refinement, non-coincident interface boundary conditions ...) could push further away the actual limits of unsteady computations by optimizing the 'precision/cost computations' ratio.

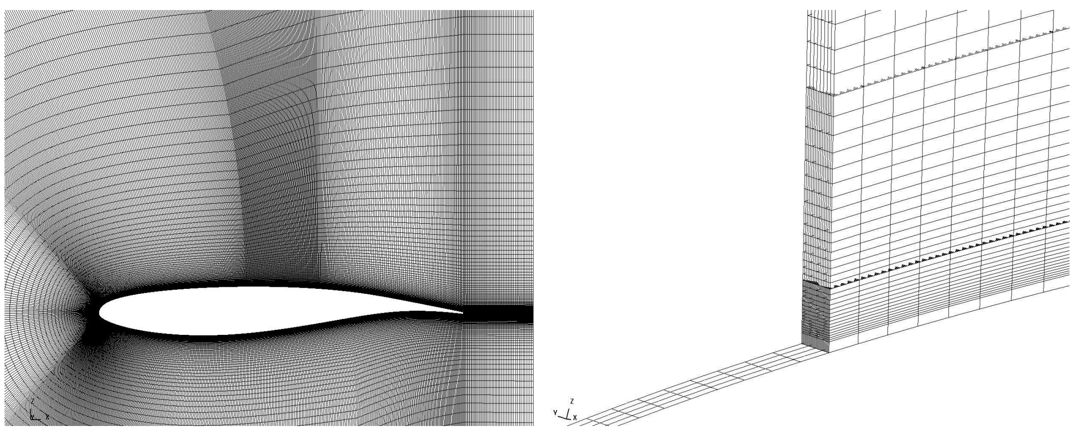

FIG. 3.7 – Buffet phenomenon over the OAT15A airfoil - View of the mesh around the airfoil and zoom on the non-coincident part.

Our first subject of investigation has concerned the development of a turbulence model that exploits the concept of Detached Eddy Simulation (DES) [1]. More precisely, the formulation proposed by H. Bush and M. Mani [2] with a primary inspiration from Strelets [3] has been considered. In this formulation, the near wall boundary layer predictive capabilities of the Wilcox $k-\omega$ turbulence model is combined with LES behaviour for large scale separated regions of the flow. This is done by comparing the length scales of the turbulence with the resolved scales of the grid.

To evaluate this DES with $k-\omega$ turbulence model, we have focused on aerodynamics buffet on the rigid OAT15A airfoil that is characterised by a periodic motion of the shock over the airfoil (see Fig. 3.7 and Fig. 3.8). In order to decrease the computational costs, two strategies were considered : wall functions and conservative non-coincident interface boundary conditions [4]. This computation is still under investigations.

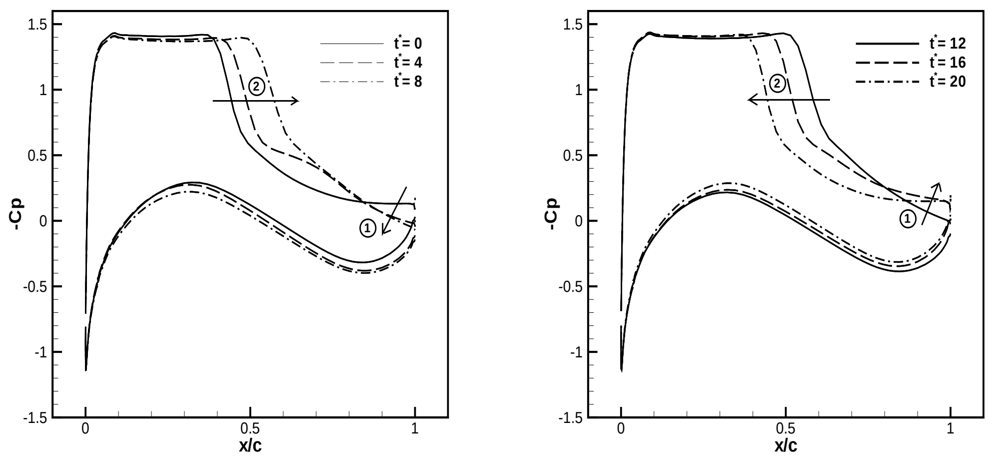

FIG. 3.8 – Buffet phenomenon over the OAT15A airfoil ($M = 0.15$ and $\alpha = 3.4$ deg) - Rising and descendant phases of the pressure coefficient.

[1] P.R. Spalart, W.H. Jou, M. Strelets and S.R. Allmaras, (1997), Comments on the Feasability of LES for Wings, and on a Hybrid RANS/LES Approach, *1st AFOSR International Conference on DNS/LES*, Aug. 4-8, Ruston, LA.

[2] R.H. Bush and M. Mani, (2001), A Two-Equation Large Eddy Stress Model for High Sub-Grid Shear, 15th AIAA Computational Fluid Dynamics Conference, 11-14 June, *AIAA paper 2001-2561*, Anaheim, CA.

[3] M. Strelets, (2001), Detached Eddy Simulation of Massively Separated Flows. 39th AIAA Aerospace Sciences Meeting and Exhibit, 8-11 January, *AIAA paper* 2001-0879, Reno, Nevada.

[4] A. Benkenida and J. Bohbot and J.-C. Jouhaud, (2002), Patched grid and adaptive mesh refinement strategies for Vorticies transport calculation, *International Journal Numerical Methods in Fluids Dynamics*, **40**, 855-873.

3.1.3.2 Zonal Detached Eddy Simulation (J.-F. Boussuge, V. Brunet, S. Deck)

In addition to the work done in section 3.1.3.1, the buffet phenomenon has been studied with a zonal Detached Eddy Simulation approach based on the Spalart-Allmaras model [1]. The zonal approach decouples the determination of LES zone from the mesh characteristics. The user can define the RANS and LES zones, so the attached boundary layer regions are explicitly treated in RANS mode regardless of the grid resolution which avoids grid induced separation.This method has been implemented in *elsA* in collaboration with the Applied Aerodynamics Department from ONERA. Moreover, in order to optimize the computational cost, a study has been done on time integration schemes. The Dual Time Stepping technique and the GEAR scheme were evaluated in term of CPU cost on a 2,5D supercritical airfoil. Both schemes were able to capture the buffet phenomenon with the right frequency and at the right experimental angle. In term of CPU cost, the GEAR scheme appeared to be more efficient than the DTS.

[1] S. Deck, (2005), Numerical simulation of transonic buffet over a supercritical airfoil,*AIAA Journal*, Vol 43, No 7

3.2 Optimization

3.2.1 Meta Models

Aerodynamic models are largely used in a lot of applications in A/C design and interdisciplinary process (loads, MDO, Identification). In that context, CFD based metamodels are developed at Cerfacs making use of Proper Orthogonal Decomposition (POD), Kriging and Neuronal Networks. These models are designed to give quickly the main features of aerodynamic system and are well adapted to interdisciplinary exchange.

3.2.1.1 Aerodynamic Metamodel using Proper Orthogonal Decomposition (POD) (J.-Ph. Boin)

The Proper Orthogonal Decomposition has been applied to a set of CFD computations in order to extract global information and build a metamodel. According to one or several parameters (time for unsteady flows or flight parameters for steady flows), a set of CFD computations are performed, called snapshots. The POD decomposition is applied to these snapshots, solving the eigenvalue problem of the auto-correlation matrix. The proper modes of this problem are orthogonal and build up the POD basis. The POD basis could be understood as an optimal basis which contains more information than any other ones. Each mode represents a characteristic of the set of snapshots. For unsteady turbulent flows, it represents the coherent structures. With that basis, it is also possible to reconstruct all the snapshots and to extrapolate solutions for a different set of parameters (metamodel). Introduced in Fluids Mechanic by Lumley [1], the POD is mainly applied on experimental data for unsteady flow analysis, Delville and al. [2]. More recent applications have been done for numerical steady flows in Optimization, Bui-Thanh and al [3].
CERFACS has developed a basic functioning POD module in Python. This module has been applied to the analysis of a turbulent flow in a combustion chamber on unstructured meshes in collaboration with the CERFACS Combustion-CFD team and in the reconstruction of pressure distribution on a high lift configuration in a polar computation context on multi-block structured meshes (Fig. 3.9).
The quality of the POD-based metamodel is first linked to the good choice of the snapshot distribution (for steady problem). We aimed at putting forward systematic strategies to achieve the optimal distribution of CFD evaluation, using sampling methods and design of experiments. Another aspect is the use of an efficient interpolation process for the reconstruction step such as linear and quadratic interpolation, Radial Based Function (RBF) and Neuronal Network (NN). For the two latest topics, collaborations with the CERFACS Algo team have started.

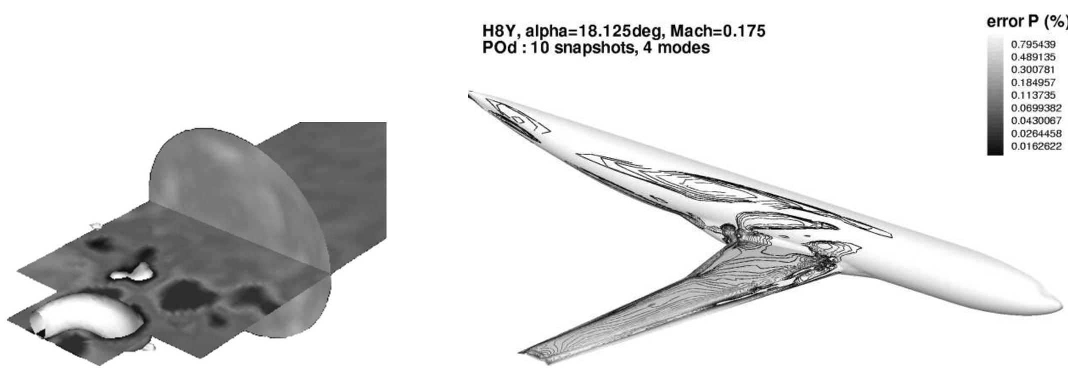

FIG. 3.9 – POD : Turbulent flow analysis in a combustion chamber(left), data reconstruction of Cp (right).

[1] Lumley J., (1967), The structure of inhomogeneous turbulent flows, *Atmospheric Turbulent and Radio Wave Propagation*, 166-178.

[2] Delville J., Ukeiley L.,Cordier L., Bonnet J. and Glauser M., (1999), Examination of large-scale structures in a turbulent plane mixing layer. part1. proper orthogonal decomposition, *Journal of Fluid Mechanics*, **391**, 92-122.
[3] Bui-Thanh T., Damodaran M. and Willcox K.,(2004), Aerodynamic Data Reconstruction and Inverse Design using Proper Orthogonal Decomposition, *AIAA Journal*, **42**(8), 1505-1516.

3.2.1.2 Kriging surrogate-model (J.C. Jouhaud, M. Montagnac, J. Laurenceau, P. Sagaut)

The term "Kriging" denotes a family of interpolation methods where weighting coefficients are chosen to minimize the variance of the error [1]. First applied in geological analysis, it has been extended to many fields of application, including agriculture, human geography, epidemiology, biostatistics or archelogy. The Kriging method is a linear interpolation method that predicts values at unknown locations (i.e. response surface construction) from data observed at known locations (control points).

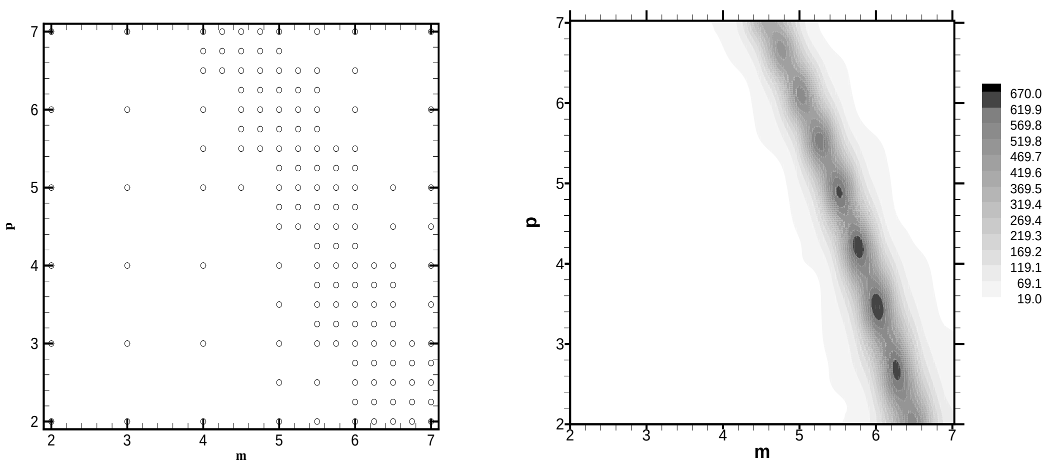

FIG. 3.10 – NACA (m,p,16) profile - Sample points in the parameter space with two levels of refinement (left part) and corresponding isolines of the cost function (right part).

Recently, a Kriging method has been implemented in a *Kriging Computational Suite* which is coupled with elsA solver. This suite is divided in four stages :

1. Definition of the following data :
   - Range of variation of the uncertain parameters.
   - Sampling in the selected subspace for uncertain parameters.
2. CFD Computations with elsA :
   - Realization of the simulations for each sampling point in the uncertain parameter space.
3. Data Processing :
   - Computations of the values taken at sampling points by the function to be interpolated.
   - Creation of data files for Kriging method.
4. Kriging Method :

- Reconstruction of the *Response Surface*.
- Computation of the *Mean Square Error* of Kriging method.
- Visualization of the *Response Surface*.
- Determination of the zone to be refined in the uncertain parameter space.

5. Return to the first stage.

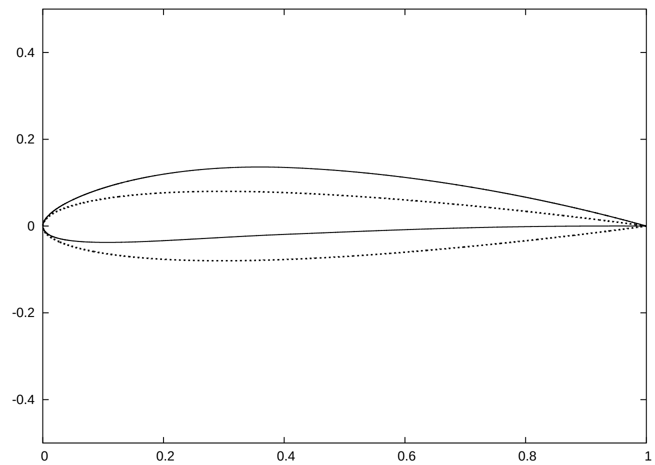

FIG. 3.11 – NACA (m,p,16) profile - Robust solution of the shape optimization (solid line) compared to symmetric shape (dashed line).

Firstly, Kriging computational suite was considered to compute the corrections needed to recover equivalent free-flight conditions from wind-tunnel experiments. Using this approach, optimal corrected values of the free-stream Mach number and the angle of attack from the compressible turbulent flow around the RAE2822 wing were computed [2]. It appeared that such a tool makes possible to compute optimal corrections for wind-tunnel parameters.

Secondly, the computational suite has been applied to the case of the multidisciplinary shape optimization of a 2D NACA airfoil [3]. The cost function is designed so that both the far-field radiated noise and the aerodynamic forces are controlled. In order to increase the efficiency of the method, a dynamic Kriging method has been developed, which can be interpreted as an Adaptive Mesh Refinement method in the shape optimization parameters (see Fig. 3.10 and Fig. 3.11).

[1] D. G. Krige, (1951), A Statistical Approach to some Basic Mine Valuations Problems on the Witwatersrand, *Journal of Chemistry, Metal. and Mining Soc. of South Africa*, **52**, 119-139.
[2] J.C. Jouhaud, P. Sagaut and B. Labeyrie, (2006), A Kriking approach for CFD/Wind Tunnel Data Comparion, *Journal of Fluids Engineering*, in press.
[3] J.C. Jouhaud, P. Sagaut, M. Montagnac and J. Laurenceau, (2005), A surrogate-model based multi-disciplinary shape optimization method with application to a 2D subsonic airfoil, Submitted for publication to *Computers and Fluids*.

3.2.1.3 Neural networks (F. Blanc)

Neural networks, based on a sampling, are widely used in the field of statistics to automatically build models descibing complex relations between inputs and outputs with a low computational cost. The basic principle

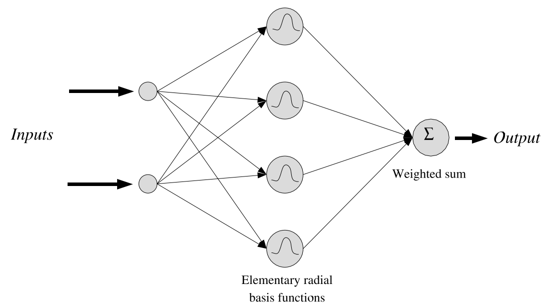

FIG. 3.12 – Representation of a radial basis neural network

of neural networks is to create an approximation of a complex function by combining simple elementary functions — called *neurons* — through a network.

There's a lot of different structures of neural networks, each having its own advantages and drawbacks. Among these structures, the *Radial Basis Functions Network*[CFD83] has been chosen after comparative tests, because of its simplicity and its robustness. A *Radial Basis Functions Network* is based on a layer of elementary radial functions. The output of each radial basis function depends on the distance between an input data of the neural network and a list of elements called *centers* which are defined for each elementary function. Outputs of the neural network are computed using a weighted sum of elementary output functions.

To create an approximation of a function, some parameters of the network (number and type of radial functions, position of their centers, coefficients of the weighted sum) have to be computed through a process called *learning* of the neural network. A completely automatic learning algorithm has been created : given a set of samples of a function, it builds a neural network which approximates this function.

In order to reduce the cost of a genetic optimization process, neural networks have been used to predict airfoil aerodynamic coefficients (lift and drag). The neural network inputs were 6 parameters defining the shape of the airfoil.

3.2.2 Optimization algorithms

Efficient optimization algorithms are the key features to manage computational cost since each objective evaluation called optimizer iterates is a cfd calculation sometimes involving gradients computation. That is why optimizer must be adapted to each type of optimization problem : DOT or CONMIN when gradients are available, trust region or pattern search for local gradient-free optimization, genetic algorithm for global gradient-free optimization.

3.2.2.1 CONMIN/DOT (J. Laurenceau)

DOT (Design Optimization Tools from Vanderplaats R&D) or CONMIN (the free version) are the gradient-based optimizers used to drive the adjoint method of elsA and allow finding local minima in a constraigned design space. The process, using discrete adjoint state of NS equations and quasi-Newton optimization algorithm, is very efficient and precise. These optimizers are also able to compute gradients 'internally' by finite differences.

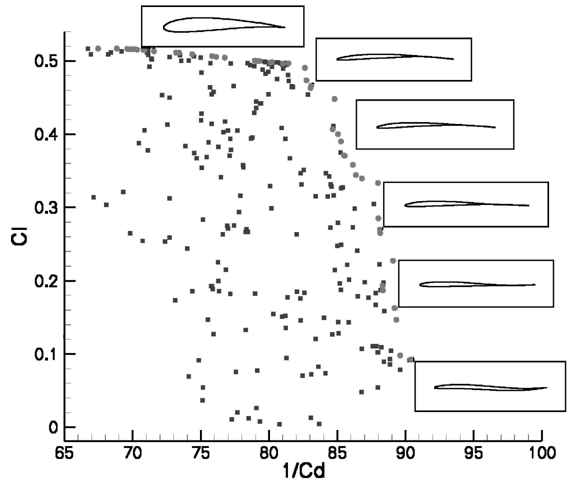

FIG. 3.13 – Pareto front achieved by solving the multi objective problem : Optimizing an airfoil shape to minimize its drag and maximize its lift

3.2.2.2 Gradient-free local optimization (J. Laurenceau)

When local minimum found by a quasi-Newton method is not satisfying or gradient can not be computed by an adjoint method, trust region (Cerfacs Algorithm Team) or pattern search (Sandia's AsynchronousParallel Pattern Search) algorithms can be more suited. Despite their higher number of evaluations to achieve convergence, these optimizers are less sensitives to local minima. Moreover, APPS is a parallel algorithm.

3.2.2.3 Genetic algorithms (F. Blanc)

During spring and summer 2005, some work on genetic algorithms has been done to evaluate their suitability for solving optimization problems in aerodynamics. A multi objective genetic algorithm has been used as a basis for these tests. This algorithm is an evolution of the famous genetic algorithm GADO [1] (Genetic Algorithm for Design Optimization). It has been coupled with the software elsA to solve multi objective problems. Experiments have been performed on a test case which consists in the optimization shape of an airfoil shape to maximize its lift and minimize its drag.

This test has shown that the genetic algorithm coupled with elsA was able to find the Pareto's front which is the solution of this problem, see Fig. 3.13. But the computational cost of this optimization process was too hight, even by using all possibilities offered by parallel computation. It was then decided to test two techniques to improve the computational efficiency of the genetic algorithm : the use of *variable fidelity* and the use of *surrogates*[CFD83].

– *Variable fidelity* : With this technique, elsA is not used to evaluate the performances of all designs. Some performances are evaluated by a low cost and low fidelity software. The technique key point is the indicator that is needed to determine which software to use for evaluating the performance of a given design. For the airfoil test case, a singularity method was used for the low fidelity method. The *variable fidelity* technique allowed to solve this optimization problem roughly 5 times faster than with the original genetic algorithm.

– *Use of a surrogate* : The original genetic algorithm has been modified to solve the optimization problems by using a neural network to perform rapid evaluations of the performances of some designs. This new version of the genetic algorithm is able to automatically build the neural network. It can add samples to data base of the neural network to increase its accuracy when necessary. This genetic algorithm enabled to solve the airfoil optimization problem 2 times faster than with the original one.

[1]Khaled Mohamed Rasheed, (1998), *Gado : A Genetic Algorithm For Continuous Design Optimization*, PhD. thesis, New Brunswick.

3.3 Numerical aerodynamics

3.3.1 Numerical methods

3.3.1.1 Coupling turbulence and multigrid methods (J.-F. Boussuge)

Initially, *elsA* was developped for solving steady RANS equations with classical convergence acceleration methods such as local time stepping and multigrid. However, the latter method was applied to mean flow equation only which implies a convergence shift between turbulence and mean flow. This shift

To correct this behaviour, a more efficient implicit method can be used on turbulence only (work desribed in Section 3.3.1.2) or the FAS algorithm can be extended to the set of turbulence equations.
A work has been done in that direction and ends up to a significant improvement of the turbulence quantities convergence without improving the convergence of mean flow field. In fact, this technique appeared to be usefull only when the mesh presents a very high degree of anisotropy in the direction perpendicular to the flow. For such a configuration turbulent informations does not propagate easily and turbulence multigrid can overcome this problem. More over, different behaviours has been observed with respect to the turbulence model. The one equation transport model from Spalart-Allmaras being the more robust.

3.3.1.2 Gauss Seidel line (F. Lörcher, M. Montagnac, C. Gacherieu, J.-F. Boussuge)

In elsA software, the linear system coming from the time integration implicit method can be solved by different techniques among which the Lower-Upper Symmetric Successive OverRelaxation (lussor) method. In this method, the solution is updated point by point as in a point Gauss-Seidel method. Many other algorithms can be stated depending on the order in which grid points are updated. On an other hand, convergence acceleration through a multigrid algorithm is only triggered for the mean flow part of equations. Therefore, the propagation of information is slower for turbulence equations that do not benefit from the multigrid method. On top of that, industrial configurations lead to complex meshes that include most of the time huge anisotropic zones. In these part, stretched cells prevent a good convergence on turbulence equations since information can not propagate easily and quickly in the direction corresponding to the smallest cell dimension.

In this context, a line lussor method has been implemented and validated on several configurations. The principle of this method consists in using a line relaxation in the direction of the smallest cell dimension. For each line of points to be updated, a tridiagonal linear system has to be solved in the scalar lussor version. In the matrix lussor version, the linear system can be block tridiagonal or pentadiagonal. In industrial applications, it is too hard to define a unique favored direction and all directions are alternated in the process.

Fig. 3.14 shows the convergence of global coefficients for an AS28 configuration at a Reynolds number $R_e = 1.4\,10^6$, a Mach number $M_\infty = 0.8$ and an angle of attack $\alpha = 2.2$. Turbulence is modeled by Spalart-Allmaras equations. The dotted line is the convergence of the line lussor applied on turbulence equations only. The plain line is the convergence of the reference computation.

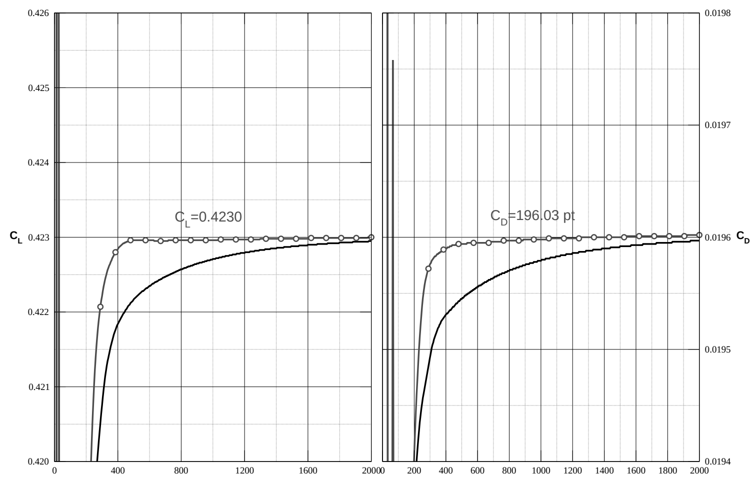

FIG. 3.14 – Convergence of lift (left) and drag (right) coefficients for an AS28 wing configuration.

3.3.1.3 Preconditioning for low-speed fbws (Y. Colin)

Preconditioning techniques involve the alteration of the time-derivatives used in time-marching CFD methods with the objective of enhancing their convergence and accuracy. The original motivation for the development of these techniques arose from the need to compute low speed compressible flows efficiently. At low Mach numbers, the performances of traditional time-marching algorithms suffer because of the wide disparity that exists between the particle and acoustic wave speeds. Preconditioning methods introduce artificial time-derivatives which alter the acoustic waves so that they travel at speeds that are comparable in magnitude to the particle waves. Thereby good convergence characteristics may be obtained at all speeds. One of the major problems concerning low-Mach preconditioners is that they loose robustness in the neighborhood of stagnation points or in boundary layers[1].
The Weiss-Smith preconditioner[2] is theoretically the most robust preconditioner due to its eigenvector structure[3] and it has been implemented and validated in elsA. Besides, it turns out that the low Mach number preconditioning does not only improve the convergence of the system, but is also responsible for maintaining accuracy at low speeds. Thus the Roe and Jameson schemes have been modified to have a correct conditioning of the artificial dissipation terms and to ensure reliable accuracy at all speeds.

[1] E. Turkel, (1999), Preconditioning Techniques in Computational Fluid Dynamics, *Annual Review in Fluid Mechanics*, **31**, 385-416.

[2] J.M. Weiss and W.A. Smith, (1995), Preconditioning Applied to Variable and Constant Density Flows, *AIAA Journal*, **33**.

[3] D.L. Darmofal and P.J. Schmid, (1995), The importance of eigenvectors for local preconditioning of the Euler equations, *AIAA paper*, AIAA-95-1655.

3.3.2 Meshing technics

3.3.2.1 Nomatch boundary conditions (M. Montagnac)

Grid generation is a crucial problem for the computation of complex aircraft configurations using a body-fitted structured-block solver. A key point is the type of interface between two zones or grids used during the geometry meshing. In case of one-to-one abutting or matching interface, local refinements around the geometry and flow regions of special interest (boundary layers, stagnation lines, wakes) tend to spread through the whole configuration domain even in zones where gradients are expected to be weak. This can lead to very large grids, especially for complex geometries. CERFACS has developed the efficient technique of conservative non coincident adjacent interface boundary condition or mismatched abutting interfaces to simplify the grid generation. Two domains must have a common adjacent interface, but grid points of both interfaces do not have to be at the same location or coincident. Grid lines through the interface may be not continuous. Therefore, this approach prevents mesh points from spreading from a block to others. It is also possible to mesh independently two parts of a geometry and just to abut the two resulting meshes to get the whole mesh. This meshing technique has already been implemented and validated in the elsA software and Airbus fully exploits this numerical feature in its production environment. Nearly all their meshes now includes non-matching interfaces. CERFACS now improves and supports this approach to still help Airbus in decreasing simulation turn-around times.
The non coincident interface boundary condition is the core of the sliding mesh feature. This functionality could be helpful in turbomachinery activities or in aerodynamics around advanced high-speed propellers for aeroelastic analysis. The actuator disk boundary condition often used to model a propeller can then be replaced by the mesh of a propeller itself.

3.3.2.2 Compatibility of wall-laws with other numerical methods(J.-Ph. Boin)

Wall laws appear to be useful for global cost reduction of high Reynolds RANS computations. Their use is more and more current in complex CFD configuration and they are systematically associated with other numerical methods and meshing technics. A validation work has been done at CERFACS around the wall law implementation in the elsA code [CFD87]. The tested wall laws are Houdeville's ones based on an apriori agglomeration of near-wall cells [1]. Compatibilities with low speed preconditioning, with Adaptive Mesh Refinement and with no-match boundary conditions have been look into.
Low speed preconditioning have been already studied and validated for a 3D profile in a wind tunnel, ONERA test-case AG29. To use wall laws, a specific mesh is built from the fine low-Reynolds meshes using Airbus France tools damas, EDM and Quickview. The 24 first cells are concatenated for wall adjacent blocks. Comparisons are made with and without wall laws for local quantities, pressure and friction coefficients. Wall laws run smoothly with the preconditioning even if some differences appear for the friction coefficient.
Compatibility of wall laws with AMR has been tested on wing-body configuration AS28G_WB. An anisotropic AMR block is used on the extrados of the wing to capture the shock. This test-case puts forward some limitations of the elsA solver regarding to the use of AMR in parallel. Nevertheless these problems are not related to the wall laws and results with and without wall laws are similar. During that work, no-match boundary conditions have been tested. Indeed that kind of boundary conditions have less limitations both for mesh generation and for multi-processor computations.
This study has been carried on with another test-case wing-body and nacelle AS28G_NCT. Here the no match boundary conditions are strictly around the nacelle. Figure 3.15 shows the isocontours of ρE in a slice normal to the spanwise. The no match boundary are represented with bold line. We have checked that these boundary introduce few perturbations. For these three approaches, the compatibility with wall laws is guaranteed. Further studies should be done to valid wall laws with other numerical methods such as grid sequencing, ALE formulation and Chimera.

[1] E. Goncalves,(2001), *Implantation et validation de lois de paroi dans un code Navier-Stokes*, PhD thesis, Ecole Nationale Supérieure de l'Aéronautique et de l'Espace.

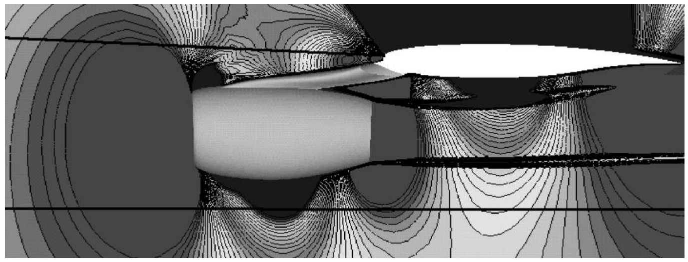

FIG. 3.15 – No match BC - Wall laws, isocontours of ρE

3.3.2.3 Wall functions (S. Champagneux)

It is well-known that turbulent flows computations for 3D multi-blocs configurations need an important effort, since global quantities such as distance to the wall,... are generally needed by the turbulence models. In the framework of DTP Modèles de Données Aérodynamiques (models for aerodynamic data) [CFD80], and in order to decrease the numerical cost of turbulent 3D computations, the aerodynamic team has been involved in the implementation and in the validation of a wall function approach for Reynolds Averaged Navier-Stokes (RANS) computations in elsA. The principle of wall functions is to decrease the numerical cost of the computations, replacing the classical non-slip boundary condition by more sophisticated relations between the variables and their derivatives. The wall function model is coupled with the high-Reynolds reduction of the turbulence models, which generally does not need the distance to the wall. Contrarily to classical implementations based on a large cell above the wall, our implementation is based on a fictitious wall, translated from the real one. We choose this technique because it is easy to couple with computational cost decreasing techniques, such as multigrid schemes, and with methods to increase the precision of the computation (Automatic Mesh Refinement -AMR- for instance). Our formulation is only sensitive to one parameter : the distance between real and fictitious walls.
In practice, there is no difference between the real wall and the computational one. To construct a mesh adapted for wall function computations, we need the same mesh topology as for low-Reynolds computations (up to the wall). The formulation impact on the mesh generation appears only in the choice of the cell height h for the first row above the wall : we typically choose for wall-laws computations a non-dimensioned cell height h^+ such that $h^+ \simeq 50$. The mesh obtained is less refined than for low-Reynolds computation and contains about 20% cell fewer.

3.3.3 Applications

3.3.3.1 Fluid/Structure interactions (J. Delbove)

The field of aeroelasticity studies the interaction between inertial, elastic and aerodynamic forces acting on a flight vehicle. Industrial partners make significant efforts to introduce this field in an early phase of the design process in order to minimize costs and production delays. CFD simulations play a major role in this objective. This activity is often divided in two sub-domains : static and dynamic aeroelasticity.
The first area of interest is the static fluid-structure interaction. In steady flight condition, the shapes of aircraft wings are deformed by the constraint of aerodynamic loads. CERFACS [CFD26], in collaboration with Airbus, has developed an algorithm which, for a given flexibility matrix representing the wing structure and for a set of flight conditions, computes the deformed wing shape and the fluid flow. It implies that a

robust mesh deformation algorithm must be available in elsA. An analytical deformation method coupled with a transfinite interpolation method has been successfully developed (see Fig. 3.16 for an example of mesh deformation).

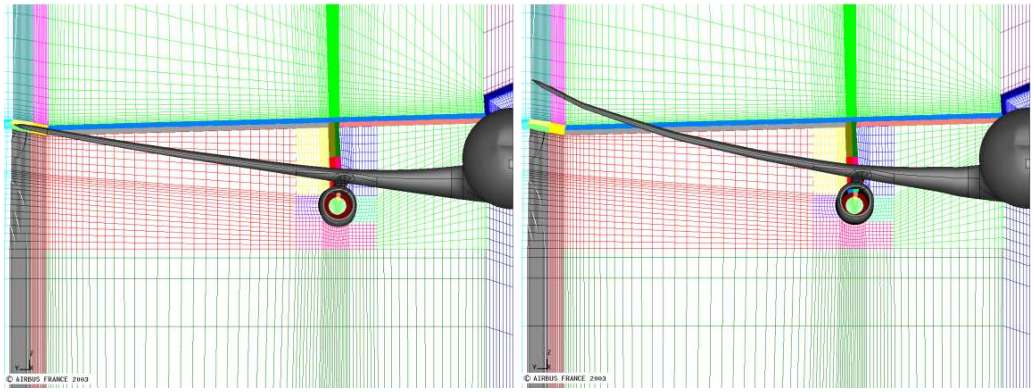

FIG. 3.16 – Wing bending of an AS28G configuration.

The second area of interest is the dynamic aeroelasticity and direct industrial application is the flutter prediction. Flutter is a destructive fluid-structure interaction due to a transfer of energy from the fluid to the aircraft structure. It is characterized by a growing oscillation which can lead to the destruction of the aircraft. It can be predicted either with the use of unsteady aerodynamic loads provided by unsteady simulations or with a direct temporal fluid structure simulation. CERFACS has improved numerical methods for unsteady simulations in the elsA software to get reliable loads in non linear regions. These loads are then used by the PK method [1] to predict the flutter phenomena. Fig. 3.17 shows a good agreement between flutter results obtained with the PK method and direct aeroelastic simulations. However, the latter are too expensive to be affordable in an industrial environment.

[1] C. A. Irwin and P. R. Guyett, (1965), The subcritical response and flutter of a swept wing model, *Royal Aircraft Establishment*, August 1965, Rept 65186, Farnborough, England, U.K.

3.3.3.2 Air intake computations (Y. Colin)

Nacelles design must fulfill geometrical constraints and engine requirements. One of the engine requirement is focused notably on the homogeneity of the flow in front of the compressor which is quantified by the distortion levels of the total pressure in the fan plane. Plane on the ground with crosswind inlet flows is a critical case for the nacelle : it occurs a subsonic or supersonic separation in the inlet depending on the engine mass flow. The resulting heterogeneity of the flow may account for the outbreak of aerodynamic instabilities of the fan blades. CERFACS, in collaboration with Snecma, is working on the numerical simulation of such crosswind inlet flows in order to predict distortion levels. This application is featured by the cohabitation of incompressible and transsonic areas along with turbulent stagnation areas on the inlet lip. The numerical issue due to low Mach number crosswind flows may be solved by preconditioning techniques and an accurate description of the separation requires turbulence model investigations. Figure 3.18 shows a preconditioned RANS computation on the Lara nacelle using the Spalart-Allmaras model. The crosswind speed is set to 35kt (corresponding to Mach numbers of 0.05) and the engine mass flow rate is about $750kg.s^{-1}$. It turns out that the subsonic separation is pretty well predicted by the model and gives levels of distortion close to the experiment.

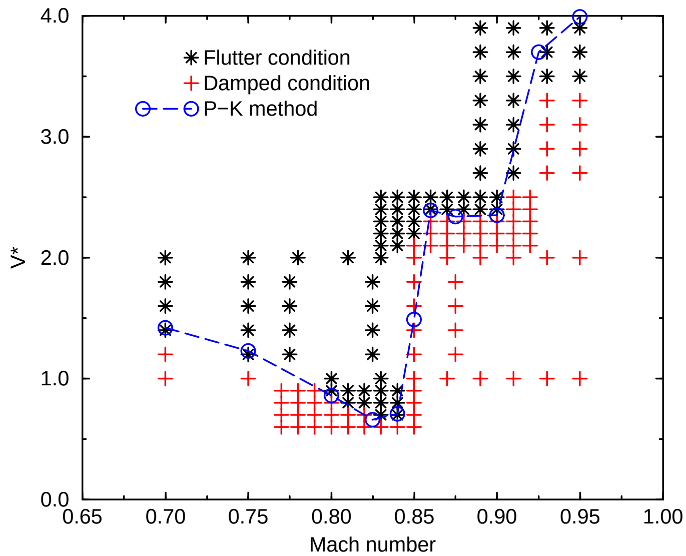

FIG. 3.17 – Flutter boundary computed by the P-K method and direct aeroelastic simulations on a 2D configuration.

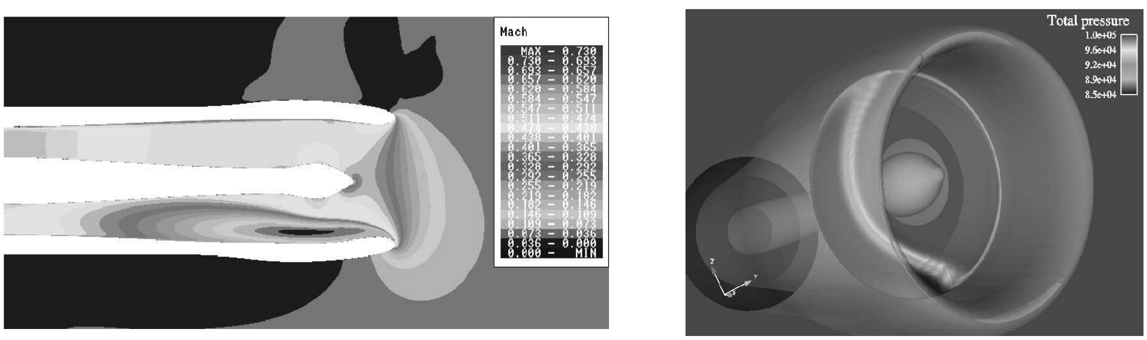

(a) (b)

FIG. 3.18 – Preconditioned RANS Lara nacelle computations : (a) Mach and (b) total pressure isocontours

3.3.3.3 Dynamic derivatives of full Aircraft Configuration(J.-Ph. Boin)

The use of advanced CFD computation to determine aerodynamic features of a full aircraft configuration has been carried on within the European program AWIATOR(FP5) [CFD109]. Prediction of full set of aerodynamic coefficients including dynamic derivatives is of great interest for flight mechanics problems such as stability, maneuverability and global behavior of an Aircraft Configuration (A/C).

elsA-RANS computations have been done on full A340 grids with finite fuselage and engine installation (see Fig. 3.19). Results of α-effect and pitching effect have been compared to wind tunnel data from our project partner Airbus-EGAG. In order to deal with non-symmetric configurations (β-effect), wall laws have been used on 12 million nodes grid. As a conclusion, the advanced CFD has given good results since viscosity effects are taken into account. The next step will be to match efficient wall laws with Arbitrary Lagrangian Eulerian (ALE) formulation and to take advantage of Full Multi-Grid Sequencing (FMG).

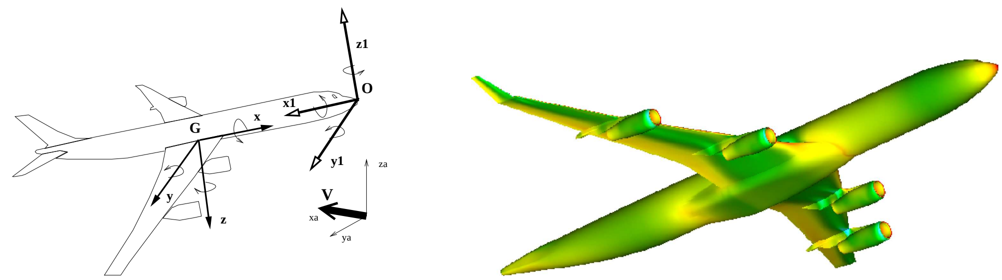

FIG. 3.19 – A340 A/C : Flight Mechanics axis definition (left) and pressure distribution, α=2 (right).

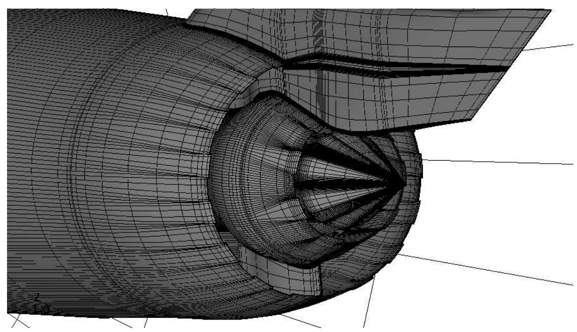

FIG. 3.20 – Mesh of a low noise exhaust nozzle

3.3.3.4 VITAL project (F. Blanc)

VITAL project is an European project which began at the beginning of 2005. The goal is to reduce commercial aircraft engines noise and emissions. Using the RANS software elsA, CERFACS is involved in the computation of several jets on different complex configurations of bypass jet engine nozzles.

Among the challenges raised by the computations, one is mesh sizes required to precisely compute jets (more than 11 millions of cells), see Fig. 3.20. In order to decrease the numerical cost, we first extract coarser meshes from the original one and compute the flow on the coarser mesh using multi-grid technique, and then, we use the solution obtained on the coarse mesh to initialize the flow on the refined one. This is what we call the *Full Multi-Grid Technique*. Thanks to this technique, high convergence levels can be achieved at a low numerical cost. VITAL project is an opportunity to use elsA on new and realistic industrial configurations.

3.4 Software engineering

3.4.1 Management and Support (M. Montagnac, J.-F. Boussuge, S. Champagneux)

CERFACS industrial partners require not only performance, reliability and robustness of softwares but also high turnaround time response in the software development process. Furthermore, CERFACS researchers also ask for code simplicity and clearness as well as for a highly-tunable and scalable code. As a consequence, software management and code engineering are topics of the primary importance both in a research and an industrial working environment.

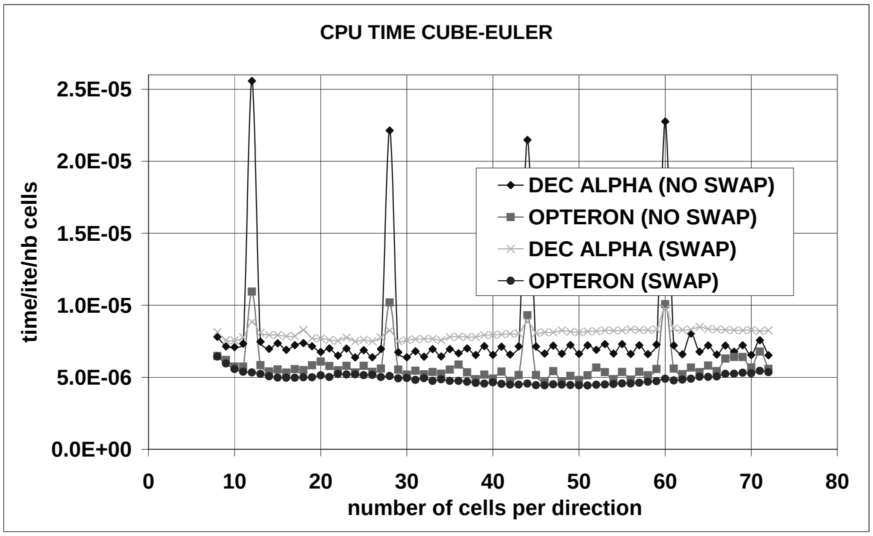

FIG. 3.21 – Evolutions of CPU time.

Therefore, the aerodynamics group takes in charge a lot of such activities mainly in the ONERA elsA software. This software is jointly developed by ONERA and CERFACS but is deployed in many european research and industrial partners. It comes along with procedures to enhance productivity in a multi-user and multi-platform environment : cvs management tools, software quality program, documentation, unitary test cases, non regression and validation databases, training sessions.
Common works include checkings of new version compliance with the non regression and validation databases, integration of new developments in the cvs repository, contributions to debugging and to quality reviews and the writing of user's and developer's guides and theoretical manuals.
Portability tests, optimization and benchmarking actions are also frequent activities to ensure the reliability and the efficiency of the code on many different computer platforms, and to enable smooth transitions whenever industrial partners renew their computing facilities.
Finally, the installation at CERFACS by the team members of the industrial environment delivered by Airbus leads to a real synergy between the two partners.

3.4.2 Code performance (J. Tournier, M. Montagnac)

The performance improvement of the elsA software has been an important objective. In the current project, a reorganization of the memory management on the entire code was carried out. The results are exposed on Fig. 3.21. This figure presents the evolution of the CPU time (Y-coordinate) and the number of cells per direction (X-coordinate) for the study of isotropic blocks.
This modification of the code completely removes the peaks of CPU time for the two computers with the Dec Alpha processor and the Opteron processor. On the other hand, the behavior is different away from the peaks. With the Dec Alpha processor, a CPU time increase of 20% is noted between the elsA reference version (NO SWAP) and the elsa modified version (SWAP). With the Opteron processor, an improvement of 5% to 30% is obtained.

This difference comes from the better memory management of DEC Alpha compiler in version NOSWAP than in version SWAP. For example, vectorization cannot be carried out in version SWAP. This remark does not apply to the pgi compiler on the Opteron machine.
A second test-case was studied on the S3Ch configuration (wing+pylon+nacelle). On this case, the DEC Alpha processors provide an improvement of the performance by 5%. An improvement of 17% with the Opteron processors is obtained.
These results are very dependent on the architecture of the computing platform. The positive point is the removal of CPU time peaks, which remains desirable, but others techniques such as padding are possible. In conclusion, it appears difficult to state definitively on the need for applying this memory reorganization in the elsA software.

3.4.3 Software architecture (M. Montagnac, J.-P. Boin, J.-F. Boussuge, S. Champagneux)

As co-developer of the elsA software, CERFACS maintains a constant effort to ensure its improvement and evolution. Indeed, many specific actions have been conducted through projects to enhance, upgrade and provide new numerical features and methods. These activities are described all along section 3.3.
In an industrial context, the aerodynamic numerical simulation tool is only a component in a whole multidisciplinary design and data process that includes many different tools as post-processing, visualization, mesh generator, mesh deformation... Airbus has defined a proprietary common software architecture for its numerical simulation needs. This flow simulation system should fulfill many requirements as performing fully parallel simulations and scenarios in a reliable and efficient way with a high-level of automation. With this approach, it would also enable to couple solvers to perform multi-physics simulations. A common data manager implemented in langage Python will held all information concerning the simulation and will dispatch them to third-party tools.
In this topic, CERFACS cooperates with ONERA to write specifications in order to adapt the elsA software to this new flow simulation architecture. With these specifications, the common data manager could provide the fluid solver with the correct information needed by the elsA interface.
CERFACS is also involved in a project that aims at building a component-oriented version of the elsA software. Indeed, many numerical functionalities coded in this solver are independent of the Navier-Stokes solver itself. By example, some grid deformation algorithms are implemented but they could be used by other solvers if they were available through a public interface. Other examples include computation of connectivity coefficients in chimera method or for non abutting adjacent zonal boundaries and distance calculation. The major work consists then in analyzing the different parts of the software that can be gathered and redesign the elsA architecture to form coherent and independent components usable by other solvers or tools.
The previous task was partly begun through an ONERA-DLR collaboration in which CERFACS was invited to participate. The goal was to introduce a common shared view between the elsA software and the TAU code.
Lastly, the increasing availability of massively parallel processing systems with relatively small memory for each processor leads CERFACS to be particularly involved in the reduction of the elsa software memory requirement. Indeed, this software handles really memory intensive applications and must run on a broad range of computer systems. Therefore, refactoring work has been initiated to decrease memory storage in the software.

3.4.4 Parallelism (M. Montagnac)

On multi-processor computer architectures with shared memory (SMP), two main parallel programming models are available to increase the parallel performance of a code : OpenMP and MPI.

OpenMP provides a simple and flexible interface for developing parallel applications. In collaboration with the CERFACS "Parallel Algorithms" team, a strategy has been elaborated to parallelize elsA efficiently with OpenMP. It has been implemented on some of the most CPU-time consuming functions of the elsA software, especially the implicit time integration method. Even if performances obtained could not reach a perfect speedup, this approach is still worth considering since it could avoid an extensive mesh splitting that could degrade convergence and robustness of computations.
Using the MPI message passing library needs a deeper knowledge of the code than with OpenMP but it is also often more efficient. To adapt the code to run on massively parallel processing systems, CERFACS has proposed to ONERA some technical solutions that need to be implemented in order to increase the scalability of the elsA software. Consequently, some design refactorings are under investigations in order to reduce the number of synchronous communications and the size of messages to decrease significantly the data traffic over the communication network. The use of asynchronous communications and the reduction of collective parallel operations should also be promising to avoid processor idle time.
These high performance computing activities are carried out with the CERFACS internal computing facilities but also with external computing resources as supercomputers from the French national centers CINES and CCRT.

4 Publications

4.1 Journal Publications

[CFD1] L. Benoit and F. Nicoud, (2005), Numerical assessment of thermo-acoustic instabilities in gas turbines, *International Journal of Numerical Methods in Fluids*, **47**, 849–855.

[CFD2] G. Desoutter, B. Cuenot, C. Habchi, and T. Poinsot, (2004), Interaction of a premixed flame with a liquid fuel film on a wall, *Proc. of the Combustion Institute*, **30**.

[CFD3] V. Faivre and T. Poinsot, (2004), Experimental and numerical investigations of jet active control for combustion applications, *Journal of Turbulence*, **5**, 025.

[CFD4] A. Giauque, L. Selle, T. Poinsot, H. Buechner, P. Kaufmann, and W. Krebs, (2005), System identification of a large-scale swirled partially premixed combustor using LES and measurements, *jot*, **6**, 1–20.

[CFD5] D. Joseph, H. El, R. Fournier, and B. Cuenot, (2005), Comparison of three spatial differencing schemes in discrete ordinate method using three-dimensional unstructured meshes, *International Journal of Thermal Sciences*, **44**, 809–913.

[CFD6] J. Jouhaud, M. Montagnac, and L. Tourette, (2005), Multigrid Adaptive Mesh Refinement for Structured Meshes for 3D Aerodynamic Design, *International Journal of Numerical Methods in Fluids*, **47**, 367–385.

[CFD7] G. Lartigue, U. Meier, and C. Bérat, (2004), Experimental and numerical investigation of self-excited combustion oscillations in a scaled gas turbine combustor, *Applied Thermal Engineering*, **24**, 1583–1592.

[CFD8] H. Moet, F. Laporte, G. Chevalier, and T. Poinsot, (2005), Wave propagation in vortices and vortex bursting, *Physics of Fluids*, **17**, 054109 (15 pages).

[CFD9] V. Moureau, G. Lartigue, Y. Sommerer, C. Angelberger, O. Colin, and T. Poinsot, (2005), Numerical methods for unsteady compressible multi-component reacting flows on fixed and moving grids, *Journal of Computational Physics*, **202**, 710–736.

[CFD10] F. Nicoud and T. Poinsot, (2005), Thermoacoustic instabilities : should the Rayleigh criterion be extended to include entropy changes ?, *Combustion and Flame*, **142**, 153–159.

[CFD11] R. Paoli, J. Hélie, and T. Poinsot, (2004), Contrail formation in aircraft wakes, *Journal of Fluid Mechanics*, **502**, 361–373.

[CFD12] T. Poinsot and D. Veynante, (2004), *Encyclopedia of computational mechanics - Fluids*, vol. 3 of Encyclopedia of computational mechanics - Fluids, Wiley & Sons, ch. Combustion, 499–525.

[CFD13] C. Prière, L. Gicquel, P. Gajan, A. Strzelecki, T. Poinsot, and C. Bérat, (2005), Experimental and Numerical Studies of Dilution Systems for Low Emission Combustors, *AIAA Journal*, **43**, 1753–1766.

[CFD14] C. Prière, L. Gicquel, A. Kaufmann, W. Krebs, and T. Poinsot, (2004), LES predictions of mixing enhancement for jets in cross-flows, *Journal of Turbulence*, **5**, 005.

[CFD15] S. Roux, G. Lartigue, T. Poinsot, U. Meier, and C. Bérat, (2005), Studies of mean and unsteady flow in a swirled combustor using experiments, acoustic analysis and Large Eddy Simulations, *Combustion and Flame*, **141**, 40–54.

[CFD16] J. Schlüter, (2004), Axi-symmetric and Full 3D LES of Swirl Flows, *International Journal of Computational Fluid Dynamics*, **18**, 235–246.

[CFD17] L. Selle, G. Lartigue, L. Benoit, and T. Poinsot, (2004), *Clean combustors for industrial gas turbines*, vol. Lecture series 2004-03 of Clean combustors for industrial gas turbines, Rhode Saint Genèse, Belgium, ch. Recent methods for numerical simulation of turbulent combustion in gas turbines, 3–46.

[CFD18] L. Selle, G. Lartigue, T. Poinsot, R. Koch, K.-U. Schildmacher, W. Krebs, B. Prade, P. Kaufmann, and D. Veynante, (2004), Compressible Large-Eddy Simulation of turbulent combustion in complex geometry on unstructured meshes, *Combustion and Flame*, **137**, 489–505.

[CFD19] L. Selle, F. Nicoud, and T. Poinsot, (2004), The actual impedance of non-reflecting boundary conditions : implications for the computation of resonators, *AIAA Journal*, **42**, 958–964.

[CFD20] Y. Sommerer, D. Galley, T. Poinsot, S. Ducruix, F. Lacas, and D. Veynante, (2004), Large eddy simulation and experimental study of flashback and blow-off in a lean partially premixed swirled burner, *Journal of Turbulence*, **5**, 037.

[CFD21] L. Thobois, G. Rymer, T. Soulères, T. Poinsot, and B. Van Den Heuvel, (2005), Large-eddy simulation for the prediction of aerodynamics in IC engines, *Int. J. Vehicle Design*, **39**, 368–382.

[CFD22] K. Truffin and T. Poinsot, (2005), Comparison and extension of methods for acoustic identification of burners, *Combustion and Flame*, **142**, 388–400.

[CFD23] C. Westbrook, Y. Mizobuchi, T. Poinsot, P. Smith, and J. Warnatz, (2004), Computational combustion - Plenary Session, *Proc of the Comb. Institute*, **30**.

[CFD24] Y. Wu, D. Haworth, M. Modest, and B. Cuenot, (2004), Direct numerical simulation of turbulence/radiation interaction in premixed combustion systems, *Proc. of the Combustion Institute*, **30**.

4.2 Theses

[CFD25] L. Benoit, (2005), *Prédictions des instabilités thermoacoustiques dans les turbines à gaz - TH/CFD/05/41*, PhD thesis, UNIVERSITE DE MONTPELLIER II.

[CFD26] J. Delbove, (2005), *Contribution aux outils de simulation aéroélastique des aéronefs : prédiction du flottement et déformation statique des voilures - TH/CFD/05/34*, PhD thesis, Ecole Nationale Supérieure de l'Aéronautique et de l'Espace.

[CFD27] A. Kaufmann, (2004), *Towards Eulerian-Eulerian large eddy simulation of reactive two phase flow - TH/CFD/04/11*, PhD thesis, Institut National Polytechnique de Toulouse.

[CFD28] G. Lartigue, (2004), *Simulation des grandes échelles et instabilités de combustion - TH/CFD/04/98*, PhD thesis, Institut nationale polytechnique de Toulouse.

[CFD29] C. Martin, (2005), *Etude énergétique des instabilités thermo-acoustiques et optimisation génétique des cinétiques réduites - TH/CFD/05/84*, PhD thesis, INPT.

[CFD30] A. Massol, (2004), *Simulations numériques d'écoulements à travers des réseaux fixes de sphères monodisperses et bidisperses, pour des nombres de Reynolds modérés - TH/CFD/04/12*, PhD thesis, Institut National Polytechnique de Toulouse - Dynamique des fluides.

[CFD31] J.-B. Mossa, (2005), *Extension polydisperse pour la description euler-euler des écoulements diphasiques réactifs - TH/CFD/05/74*, PhD thesis, Institut National Polytechnique de Toulouse.

[CFD32] C. Prière, (2005), *Simulations aux grandes échelles : application au jet transverse - TH/CFD/05/2*, PhD thesis, Institut National Polytechnique de Toulouse, France.

[CFD33] P. Schmitt, (2005), *Simulation aux grandes échelles de la combustion étagée dans les turbines à gaz et son interaction stabilité - polluants-thermique - TH/CFD/05/45*, PhD thesis, Institut National Polytechnique de Toulouse.

[CFD34] L. Selle, (2004), *Simulation aux grandes échelles des interactions flamme-acoustique dans un écoulement vrillé - TH/CFD/04/35*, PhD thesis, Institut National Polytechnique de Toulouse.

[CFD35] K. Truffin, (2005), *Simulation aux grandes échelles et identification acoustique des turbines à gaz en régime partiellement prémélangé - TH/CFD/05/37*, PhD thesis, Institut National Polytechnique de Toulouse.

4.3 Conference Proceedings and Book Chapters

[CFD36] D. Bissières, C. Bérat, and L. Gicquel, (2005), Large eddy simulation predicitons and validations of a gas turbine combustion chamber, In *ISABE 2005, 17th International Symposium on Airbreathing Engines*, Munich, Germany.

[CFD37] M. Boileau, J.-B. Mossa, B. Cuenot, T. Poinsot, D. Bissiéres, and C. Bérat, (2005), Toward LES of an ignition sequence in a full helicopter combustor, In *First Workwhop INCA 2005*, SNECMA, Villaroche, France.

[CFD38] J.-F. Boussuge, S. Champagneux, G. Chevalier, L. Giraud, F. Loercher, and M. Montagnac, (2004), How to maintain efficiency on vector and SMP platforms for large aerodynamic calculations, In *ECCOMAS*, Jyvaskyla - Finland, Session CFD–1067.pdf.

[CFD39] A. Celic, G. Chevalier, and C. Negulescu, (2005), Comparison of Modern Turbulence Models for Aero-Thermal Applications, In *European Conference for Aero-space sciences*, Moscou - Russie.

[CFD40] A. Dauptain and B. Cuenot, (2005), Large Eddy Simulation of a Supersonic Hydrogen-Air Diffusion Flame, In *The Cyprus International Symposium on Complex Effects in Large Eddy Simulation*, Limassol, Cyprus.

[CFD41] L. Debiane, B. Ivorra, B. Mohammadi, F. Nicoud, A. Ern, T. Poinsot, and H. Pitsch, (2004), Temperature and pollution control in flames, In *Proceeding of the Summer Program*, Center for Turbulence Research, NASA AMES/Stanford University, USA, 367–375.

[CFD42] A. Devesa and F. Nicoud, (2005), Anisothermal Wall Functions for RANS and LES of Turbulent Flows With Strong Heat Transfer, In *ERCOFTAC Workshop, Direct and Large-Eddy Simulation*.

[CFD43] A. Devesa, J. Moreau, J. Helie, and T. Poinsot, (2004), Large Eddy Simulations of a jet / tumble interaction in a GDI model engine flow, In *SAE Spring Fuels and Lubricants Meeting*, Centre de congrés P. Baudis, Toulouse - France.

[CFD44] F. Duchaine, L. Gicquel, D. Bissiéres, C. Bérat, and T. Poinsot, (2005), Automatic Design Optimization Applied to Lean Premixed Combustor Cooling, In *1er Workshop INCA*, SNECMA Villaroche, France.

[CFD45] G. Fillola, M.-C. LePape, and M. Montagnac, (2004), Numerical simulations around wing control surfaces, In *24th international congress ot the aeronautical sciences*, Yokohama, Japan.

[CFD46] D. Galley, A. Pubil-Melsio, S. Ducruix, F. Lacas, D. Veynante, Y. Sommerer, and T. Poinsot, (2005), Dynamics of Lean Premixed Systems : Measurements for Large Eddy Simulation, In *Proceedings of the ERCOFTAC Int. Symposium on Engineering Turbulence Modelling and Measurements - ETMM6*, M. W. R. . M., ed., Sardinia, Italy, Chapter 13.

[CFD47] M. García, Y. Sommerer, and T. Schönfeld, (2005), Assessment of Euler-Euler and Euler-Lagrange Strategies for Reactive Large-Eddy Simulations, In *1er Workshop INCA*, SNECMA Villaroche, France.

[CFD48] M. García, Y. Sommerer, T. Schönfeld, and T. Poinsot, (2005), Evaluation of Euler-Euler and Euler-Lagrange strategies for Large-Eddy Simulations of turbulent reacting flows, In *ECCOMAS thematic conference on computational combustion*, Lisbon, Portugal.

[CFD49] A. Kaufmann, O. Simonin, and T. Poinsot, (2004), Direct Numerical Simulation of Particle-Laden homogeneous isotropic turbulent flows using a two-fluid model formulation, In *5th International Conference on Multiphase Flow - Paper No.443*, Yokohama, Japan.

[CFD50] C. Martin, L. Benoit, F. Nicoud, and T. Poinsot, (2004), Analysis of acoustic energy and modes in a turbulent swirled combustor, In *Proceeding of the Summer Program*, Center for Turbulence Research, NASA AMES/Stanford University, USA, 377–394.

[CFD51] S. Mendez and F. Nicoud, (2005), Large-Eddy Simulations of a Periodic Turbulent Flow over a Perforated Plate, In *1st Workwhop INCA*, SNECMA, Villaroche, France.

[CFD52] S. Mendez, F. Nicoud, and P. Miron, (2005), Direct and Large-Eddy Simulations of a Turbulent Flow with Effusion, In *ERCOFTAC Workshop on Direct and Large Eddy Simulation-6*, Université de Poitiers, France.

[CFD53] S. Mendez, F. Nicoud, and T. Poinsot, (2005), Large-Eddy Simulations of a Turbulent Flow around a Multi-Perforated Plate, In *The Cyprus International Symposium on Complex Effects in Large Eddy Simulation (CY-LES2005)*, Limassol, Cyprus.

[CFD54] V. Moureau, I. Barton, C. Angelberger, and T. Poinsot, (2004), Towards large eddy simulation in internal combustion engines : simulation of a compressed tumble flow, In *SAE Spring Fuels and Lubricants Meeting*, Centre de congrés P. Baudis, Toulouse - France, SAE Paper 2004–01–1995.

[CFD55] V. Moureau, O. Vasilyev, C. Angelberger, and T. Poinsot, (2004), Commutation errors in Large eddy simulation on moving grids : Application to piston engine flows, In *Proceedings of the Summer Program*, Center for Turbulence Research, NASA AMES/Stanford University, USA, 157–168.

[CFD56] S. Pascaud, M. Boileau, B. Cuenot, and T. Poinsot, (2005), Large Eddy Simulation of turbulent spray combustion in aeronautical gas turbines, In *ECCOMAS Thematic Conference on computational combustion*, Lisbon, Portugal.

[CFD57] S. Pascaud, M. Boileau, L. Martinez, B. Cuenot, and T. Poinsot, (2005), LES of steady spray flame and ignition sequences in aeronautical combustors, In *1er workshop INCA*, SNECMA, Villaroche, France.

[CFD58] T. Poinsot and L. Selle, (2005), LES and acoustic analysis of combustion instability in gas turbines, In *PLENARY LECTURE - ECCOMAS Computational Combustion Symposium*, Lisbonne, Portugal.

[CFD59] E. Riber, M. Moreau, O. Simonin, and B. Cuenot, (2005), Towards Large Eddy Simulation of Non-Homogeneous Particle Laden Turbulent Gas Flows Using Euler-Euler Approach, In *11th Workshop on Two-Phase Flow Predictions*, Merseburg, Germany.

[CFD60] M. Saudreau and H. Moet, (2004), Characterization of Extended Near-Field and Crow Instability in the Far-Field of a Realistic Aircraft, In *European Congress on Computational Methods in Applied Sciences and Engineering*, Jyvaskyla, Finland, Session STS–909.pdf.

[CFD61] P. Schmitt, B. Schuermans, K. Geigle, and T. Poinsot, (2005), Effects of radiation, wall heat loss and effusion cooling on flame stabilisation and pollutant prediction in LES of gas turbine combustion, In *ECCOMAS thematic conference on computational combustion*, Lisbonne, Portugal.

[CFD62] A. Sengissen, T. Poinsot, K. Van, and J. Kok, (2005), Response of a swirled non-premixed burner to fuel flow rate modulation, In *The Cyprus International Symposium on Complex Effects in Large Eddy Simulation (CY-LES2005)*, Limassol Cyprus.

[CFD63] G. Staffelbach, L. Gicquel, and T. Poinsot, (2005), HIGHLY PARALLEL LARGE EDDY SIMULATIONS OF MULTIBURNER CONFIGURATIONS IN INDUSTRIAL GAS TURBINES, In *Complex Effects in Large Eddy Simulation*, Limassol, Cyprus.

[CFD64] L. Thobois, G. Rymer, T. Soulères, and T. Poinsot, (2004), Large Eddy Simulations in IC engine geometries, In *SAE Fuels and Lubricants Meeting*, Centre de congrés P. Baudis, Toulouse - France.

[CFD65] B. Wegner, D. Bissières, L. Gicquel, B. Janus, A. Sadiki, A. Dreizler, and J. Janicka, (2005), Enclosed swirling flows as a bench mark for LES of gas turbine combustors, In *1st Workshop on Quality Assessment of Unsteady Methods for Turbulent Combustion Prediction and Validation*, DARMSTADT (Seeheim -Jugenheim), GERMANY.

4.4 Technical Reports

[CFD66] L. Artal and F. Nicoud, (2005), Direct Numerical Simulation of a Multi-SpeciesTurbulent Channel Flow, Tech. Rep. TR/CFD/05/86, CERFACS.

[CFD67] L. Artal and F. Nicoud, (2005), Direct Numerical Simulation of Reacting Turbulent Multi-Species Channel Flow, Tech. Rep. TR/CFD/05/85, CERFACS.

[CFD68] L. Artal, (2004), Modélisation des flux de chaleur stationnaires pour un mélange multi -espèce avec transfert de masse à la paroi - (année 2), Contract report CR/CFD/04/113, CERFACS.

[CFD69] L. Artal, (2005), Modélisation des flux de chaleur stationnaires pour un mélange multi-espèce avec transfert de masse à la paroi, Contract report CR/CFD/05/79, CERFACS.

[CFD70] V. Auffray, (2005), Dossier de modélisation (ref. N3SNATUR3.0/DM01/02), Contract report CR/CFD/05/91, CERFACS.

[CFD71] I. Barton, (2004), A Bug Investigation of the Undesirably Fast Grid Velocities, Working notes WN/CFD/04/21, CERFACS.

[CFD72] I. Barton, (2004), The Cause and Correction of Undesirably Fast Grid Velocities, Working notes WN/CFD/04/22, CERFACS.

[CFD73] I. Barton, (2004), How to Move the Grid without a Target Grid using ITC, Working Notes WN/CFD/04/26, CERFACS.

[CFD74] I. Barton, (2004), Improved Input Files for Running the ITC Approach, working notes WN/CFD/04/24, CERFACS.

[CFD75] I. Barton, (2004), Initial Efficiency Tests for the ITC Approach Running Moving Mesh Simulations, Working notes WN/CFD/04/20, CERFACS.

[CFD76] I. Barton, (2004), The Main Status Report for the Development of the First Version of ITC into AVBP, Contract report CR/CFD/04/23, CERFACS.

[CFD77] I. Barton, (2004), Status Report of ITC Implementation for AVBP (Version 5.3Beta) and a Presentation of a Complete Laminar, Working note WN/CFD/04/25, CERFACS.

[CFD78] A. Beer and B. Cuenot, (2005), Numerical simulation of an underexpanded sonic jet, Contract report AIR LIQUIDE CR/CFD/05/10, CERFACS.

[CFD79] A. Beer, (2004), Simulation numérique d'un jet sonique sous-détendu, Contrat Air Liquide CR/CFD/04/106, CERFACS.

[CFD80] S. BenKhelil, M.-C. LePape, J.-F. Boussuge, S. Champagneux, N. Denève, and G. Hanss, (2004), Contribution au DTP Modèles de données aérodynamiques - Rapport d'avancement à un an - RT 223/07401 DAAP, Rapport contractuel CR/CFD/04/15, ONERA/CERFACS.

[CFD81] L. Benoit, (2004), AVSP_V1.8.3 handbook, Users guide WN/CFD/04/123, CERFACS.

[CFD82] L. Benoit, (2004), Calculations of thermo-acoustic eigenmodes of an annular combustion chamber, Technical report TR/CFD/04/44, CERFACS.

[CFD83] F. Blanc, (2005), Couplage code aérodynamique et algorithme génétique, rapport de stage DEA - ENSICA WN/CFD/05/60, CERFACS.

[CFD84] G. Boudier, (2004), Allumage des foyers aéronautiques en combustion diphasique, rapport de stage fin d'étude WN/CFD/04/57, CERFACS.

[CFD85] G. Boudier, (2004), Allumage des foyers aéronautiques en combustion diphasique, Rapport de stage DEA - Institut National Polytechnique de Toulouse - Energétique et transferts WN/CFD/04/83, CERFACS.

[CFD86] J.-F. Boussuge, (2004), DTP Modèles de données aérodynamiques, rapport d'avancement à 18 mois, contract report ONERA/AIRBUS/CERFACS CR/CFD/04/146, CERFACS.

[CFD87] J.-F. Boussuge, (2005), DTP Modèles de données aérodynamiques, rapport de synthèse, contract report ONERA/AIRBUS/CERFACS CR/CFD/05/103, CERFACS.

[CFD88] A. Celic, (2005), Implementation of a k-e-v'v'-f Turbulence Model into ElsA, Contract report CR/CFD/05/42, CERFACS.

[CFD89] B. Cuenot and T. Poinsot, (2005), Simulation aux grandes échelles de la configuration ORACLES, Tech. Rep. TR/CFD/05/89, CERFACS.

[CFD90] B. Cuenot, L. Benoit, K. Truffin, A. Kaufmann, J.-B. Mossa, M. Boileau, E. Riber, S. Pascaud, G. Boudier, M. García, and T. Poinsot, (2004), Rapport final PRC - Année 3, Contract Report CR/CFD/04/127, CERFACS.

[CFD91] F. Duchaine, L. Gicquel, D. Bissières, and C. Bérat, (2005), Automatic chain optimization for low NOx injection system and combustors, Contract report CR/CFD/05/54, CERFACS.

[CFD92] F. Duchaine, (2004), Optimisation de turbomoteur d'hélicoptère - Stage en collaboration avec TURBOMECA, Rapport de stage de Mastère Mécanique des Fluides Numérique WN/CFD/04/76, CERFACS.

[CFD93] F. Duchaine, (2005), Palmérisation de N3SNatur, Tech. Rep. TR/CFD/05/8, CERFACS.

[CFD94] A. Giauque, L. Selle, T. Poinsot, H. Buechner, A. Kaufmann, and W. Krebs, (2004), System identification of a large scale swirled premixed combustor using LES and comparison to measurements, Tech. Rep. TR/CFD/04/6, CERFACS.

[CFD95] L. Gicquel, M. Boileau, and T. Poinsot, (2004), LES monophasiques réactives - Makila 2a, Rapport contractuel CR/CFD/04/88, CERFACS.

[CFD96] L. Gicquel, G. Boudier, and T. Poinsot, (2005), Evaluation de la méthode "large eddy simulations" pour la prédiction du profil FRT, contract report CR/CFD/05/93, CERFACS.

[CFD97] L. Gicquel, C. Prière, and T. Poinsot, (2004), Final report on the LES computations of jets incross-flow in relation with WP3, Contract report CR/CFD/04/60, CERFACS.

[CFD98] L. Gicquel, Y. Sommerer, and T. Poinsot, (2005), LES monophasiques réactives et non-réactives - calculs de STATO-MBDA, Contract report CR/CFD/05/11, CERFACS.

[CFD99] L. Gicquel, K. Truffi n, and T. Poinsot, (2004), Software AVBP LES code validation report : prediction of the aerodynamic behavior of the primary zone, Contract report CR/CFD/04/50, CERFACS.

[CFD100] L. Gicquel, (2004), Final report on the LES computations of jets incross-fbw in relation with WP3, Contract report CR/CFD/04/131, CERFACS.

[CFD101] F. Jaegle, (2005), Etude numérique de l'écoulement autour d'un cylindre circulaire utilisant la 'Detached Eddy Simulation' (DES), rapport de stage - 3ème année Ingénieur WN/CFD/05/51, Ecole Polytechnique.

[CFD102] J. Jouhaud, (2005), Interaction dún Jet Débouchant avec un écoulement Transverse de Couche Limite - Simulation des Grandes échelles à lÁide du Code AVBP, Rapport MAEVA TR/CFD/05/95, CERFACS.

[CFD103] B. Labeyrie, (2004), Optimisation en calculs aérodynamiques avec une méthode de krigeage, Tech. Rep. WN/CFD/04/82, CERFACS.

[CFD104] B. Labeyrie, (2004), Une méthode de krigeage pour l'optimisation multi-critères en calculs aérodynamiques, rapport de stage de fi n d'études WN/CFD/04/55, CERFACS.

[CFD105] N. Lamarque, (2004), Ecriture et validation d'un code permettant le calcul de l'impédance d'entrée d'une tuyère, Rapport de stage de fi n d'études ENSEEIHT WN/CFD/04/51, CERFACS.

[CFD106] N. Lamarque, (2004), Ecriture et validation d'un code permettant le calcul l'impédance d'entrée d'une tuyère, Rapport de stage DEA - Institut National Polytechnique de Toulouse - Dynamique des Fluides WN/CFD/04/78, CERFACS.

[CFD107] J. Lavedrine, (2004), Simulation aux grandes échelles d'une chambre de combustion diphasique, Rapport DEA Dynamique des Fluides et des Transferts - Université Paris XI WN/CFD/04/80, CERFACS.

[CFD108] F. Loercher, (2004), Couplage elsA/ens++ à l'aide du logiciel PALM, Technical report TR/CFD/04/66, CERFACS.

[CFD109] D. Margerit, J.-P. Boin, and G. Chevalier, (2005), Prediction of dynamic derivatives of full A/C including large winglets, Contract Report CR/CFD/05/98, CERFACS.

[CFD110] C. Martin, (2004), EPORCK User Guide V1.8, Tech. Rep. TR/CFD/04/84, CERFACS.

[CFD111] L. Martinez, (2005), Vers la simulation des écoulements diphasiques denses en formulation Euler-Euler, Rapport de stage Mastère Mécanique des Fluides Numériques - ENSEEIHT WN/CFD/05/59, CERFACS.

[CFD112] A. Massol, O. Simonin, and T. Poinsot, (2004), Steady and unsteady drag and heat transfer in fi xed arrays of equal sized spheres, Tech. Rep. TR/CFD/04/13, CERFACS.

[CFD113] S. Mendez, (2004), Simulation numérique d'écoulements dans les plaques multiperforées : Etude préliminaire, Rapport DEA - Institut National Polytechnique de Toulouse - Dynamique des Fluides WN/CFD/04/79, CERFACS.

[CFD114] S. Mendez, (2004), Simulation numérique directe d'écoulements dans les plaques multiperforées. Etude préliminaire, rapport de stage de fi n d'études WN/CFD/04/56, CERFACS.

[CFD115] S. Mendez, (2005), Methodology for performing wall-resolved numerical computations of a periodic turbulent fbw with effusion, Contract report INTELLECT CR/CFD/05/35, CERFACS.

[CFD116] M. Montagnac, J.-P. Boin, and J.-F. Boussuge, (2005), Programme FLOWSIM, Réponse au Cahier des Charges du 20/10/2005, Number D05025044, Contract report FLOWSIM CR/CFD/05/99, CERFACS.

[CFD117] M. Montagnac, J.-F. Boussuge, S. Champagneux, G. Chevalier, L. Giraud, F. Loercher, J. Delbove, G. Hanss, and X. Toussaint, (2004), Rapport fi nal ParelsA : consolidation de la parallélisation du logiciel elsA, Rapport Technique RT 3/07380 ONERA/DSNA CR/CFD/04/145, CERFACS.

[CFD118] M. Montagnac, (2005), Note d'avancement T0P6 ANANAS, Contract report ANANAS CR/CFD/05/100, CERFACS.

[CFD119] M. Montagnac, (2005), Rapport d'avancement T0P12 ANANAS, Contract report ANANAS CR/CFD/05/101, CERFACS.

[CFD120] L. Nybelen and G. Chevalier, (2005), Analysis of Reynolds number effects, Contract report CR/CFD/05/102, CERFACS.

[CFD121] L. Nybelen, (2004), Simulations numériques du mécanisme de fusion de tourbillons de sillage dans le champ proche étendu, rapport de stage WN/CFD/04/101, CERFACS.

[CFD122] R. Paoli and B. Cuenot, (2005), Rapport final COS-3eme appel, contract report TR/CFD/05/9, CERFACS.

[CFD123] A. Roux, (2005), Comparaison des logiciels de CFD N3SNATUR et AVBP en géométrie complexe, rapport de stage DEA Energetique et Aeronautique, Ecole Nationale Supérieure de l'Aéronautique et de l'Espace WN/CFD/05/65, CERFACS.

[CFD124] M. Saudreau, (2004), Développement logiciel N3S NATUR version 3.0 - tâche 5.1, Contract report SIMULOG CR/CFD/04/134, CERFACS.

[CFD125] M. Saudreau, (2004), Etude de l'influence du critère de convergence du système linéaire sur la qualité et le temps de restitution d un calcul de chambre, SNECMA Contract Report pdf file and CD-ROM CR/CFD/04/104, CERFACS.

[CFD126] M. Saudreau, (2004), Outils LES et RANS pour les turbine à gaz - LOT 1 Rapport à 6 mois, contract report CR/CFD/04/117, CERFACS.

[CFD127] M. Saudreau, (2004), Outils LES et RANS pour les turbines à gaz - Lot 2.1.2 à 8 mois, Contract report SNECMA CR/CFD/04/121, CERFACS.

[CFD128] M. Saudreau, (2004), Outils LES et RANS pour les turbines à gaz - Lot 2.1.4 - Rapport à 8 mois, Contract report SNECMA CR/CFD/04/120, CERFACS.

[CFD129] M. Saudreau, (2005), Outils LES et RANS pour les turbines à gaz : lot 2.2 PTF ref 2004/SN/04, Contract report CR/CFD/05/22, CERFACS.

[CFD130] M. Saudreau, (2005), Outils LES et RANS pour les turbines à gaz : lot 3.2 PTF ref 2004/SN/04, Contract report CR/CFD/05/21, CERFACS.

[CFD131] T. Schmitt and B. Cuenot, (2005), Simulation aux grandes échelles d'un cas test du banc Mascotte, Contract report CR/CFD/05/36, CERFACS.

[CFD132] T. Schmitt, (2005), Vers la simulation aux grandes échelles de la combustion supercritique, Rapport de stage DEA - ENSEEIHT WN/CFD/05/62, CERFACS.

[CFD133] C. Sensiau, (2005), Calculs thermoacoustiques dans les chambres de combustion, Master Recherche Energétique et Transferts - Ecole Nationale Supérieure d'ingénieurs de Constructions Aéronautiques WN/CFD/05/64, CERFACS.

[CFD134] Y. Sommerer, J. Lavedrine, and T. Poinsot, (2005), Mise en données d' un calcul de pertes de charge contournement du foyer DEM21 avec le code AVBP, Contract report CR/CFD/05/63, CERFACS.

[CFD135] Y. Sommerer, J. Lavedrine, T. Poinsot, and F. Nicoud, (2005), COS : rapport final du 3ème appel à propositions. Simulations aux grandes échelles de foyers turbulents à carburant diphasique, Contract report CR/CFD/05/6, CERFACS.

[CFD136] Y. Sommerer, L. Selle, L. Benoit, M. Boileau, and T. Poinsot, (2004), Calcul LES de la chambre DEM21, Contract report CR/CFD/04/47, CERFACS.

[CFD137] K. Truffin and T. Poinsot, (2004), Comparison and extension of methods for acoustic identification of burners, Tech. Rep. TR/CFD/04/126, CERFACS.

[CFD138] K. Truffin, B. Varoquié, D. Veynante, T. Poinsot, and F. Lacas, (2004), Large Eddy Simulations and experimental characterization of the unsteady response of partially premixed flames, Tech. Rep. TR/CFD/04/36, CERFACS.

[CFD139] K. Truffin, (2004), Simulation aux grandes échelles de la combustion partiellement prémélangée dans une configuration industrielle, Contract Report CR/CFD/04/124, CERFACS.

[CFD140] B. Varoquié, M. Saudreau, A. Beer, and T. Poinsot, (2004), Initialisation de simulations LES en combustion à partir de solutions moyennes RANS, Contract report TR/CFD/04/139, CERFACS.

[CFD141] B. Varoquié, (2004), Large Eddy Simulation of auto-ignition in gas turbines with sequential combustion, Contract report CR/CFD/04/19, CERFACS.

[CFD142] M. Willemse, (2005), Modelling complex cemistry in large eddy simulation and the interaction between combustion and acoustics, Rapport de stage WN/CFD/05/83, CERFACS.

3

Electromagnetism Team

1 Overview Presentation

Let us first recall the main objectives of the "*Computational Electromagnetism Project*" :

- deal with the large size problems related to propagation and scattering of time-harmonic electromagnetic waves arising in real world industrial applications,
- face the demand in fast, reliable and accurate algorithms coming from this area of activities.

This demand is expressed in a concrete manner through the following collaborations with industrial partners :

- scattering of electromagnetic waves by a large metallic structure with an electrically deep cavity : MBDA-EADS ;
- interaction of a satellite with an inboard antenna : CNES – Antenna Department ;
- treatment of general geometrical and/or physical symetries with general sources : CNES – Antenna Department ;
- scattering by imperfectly conducting surfaces modelled by an impedance boundary condition : Dassault-Aviation ;
- coupling of a Finite Element Method with a Boundary Element Solution by means of the adaptive radiation condition : CEA-CESTA ;
- electromagnetic compatibility of a wind turbine with a civil aviation antenna : DGAC. This study was carried out in collaboration with ENAC.

The first two items answer a demand of CERFACS shareholders. The first topic has benefited from a grant, jointly supported by MBDA-EADS and ANRT, for the Ph.D. thesis of N. Balin. Similarly the second topic has benefited from a joint support of CNES and CERFACS for the Ph.D. thesis of N. Zerbib. These two theses are now finished.

Besides the approaches specifically developed for the above topics, some more fundamental studies have been conducted. They concern

- some theoretical aspects of Domain Decomposition Methods (DDM),
- hybridization of different solution procedures,
- the resonance phenomena,
- numerical microlocal analysis of harmonic fields,
- Shape reconstruction of buried objects in collaboration with INRIA-Rocquencourt,
- construction of preconditionners by means of analytical tools.

As well-known, the methodology developed for the electromagnetic waves can apply, with generally some slight modifications, to acoustic waves. Moreover, because acoustic waves can be merely characterized by a scalar unknown, the methods developed for them can be considered as a first step before handling the electromagnetic case. This explains why some of the studies conducted during the two last years have been dedicated to acoustic problems.

Apart from some very basic theoretical studies like the above first and last item, one of the main concern of the team is to translate the activities in terms of new functionalities of the CERFACS Electromagnetism Solver Code (CESC). Recall that CESC is highly tuned to fully take advantage from the capabilities of High Performance Computing (HPC) parallel platforms. In this respect, two other functionalities have been added to CESC. The first one concerns the possibility to hybridize a Finite Element Method (FEM) and a Boundary Element Method (BEM) with several coupling procedures developed to deal as efficiently as possible with various practical cases. The second functionality is related to the possibility to take advantage of general geometrical and physical symetries, with or without symetric excitations, to significantly reduce

the amount of computations. The study on the wind turbine benefited from this new functionality in a essential manner.
The Multi Level Fast Multipole Method (MLFMM) is the most advanced technique for solving the formulation of the basic equations of electromagnetism in terms of Boundary Integral Equations (BIE). The team has gained a great expertise in this technique, particularly in its implementation within the framework of HPC platforms. The advances achieved in this domain concern the hybridization with a FEM and the particularization to the cavity problem. The new challenge is now to extend this solving technique to the case of an impedance boundary condition.
The studies undertaken the last three years on the scattering by a large structure with a deep cavity can be considered as finished for the case of a perfectly conducting cavity.
The members of "*Computational Electromagnetism Project*" made creditable efforts to reconcile their obligations as regards development of codes and cooperation with the industrial sector with a constant policy of publication and communication.

2 Domain Decomposition and Hybridation Methods

2.1 Electrically deep cavity (N. Balin, A. Bendali)

Air intakes significantly contribute to the overall Radar Cross Section (RCS) of aircrafts. The determination of such a kind of RCS is reduced to the computation of the electromagnetic field scattered by an electrically large structure with a deep cavity. This important issue in stealth technology is characterized by several difficulties preventing to address it by standard techniques even the MLFMM which is the most powerful of them.

In collaboration with MBDA-EADS, the team has conducted in the last years a systematic study to develop appropriate methods for solving this kind of problems. In some meaning, the defence of N. Balin's Ph. D. thesis has concretely expressed the end of a first significant step : the case of a metal cavity can be considered as completely solved.

We report to N. Balin's Ph. D. thesis [CEM7] for the detailled description of the various methods which have been devised and implemented. Let us only mention that

- the interior of the cavity is treated by a substructuring approach solved by a BIE method in order to avoid the usual dispersive flaws of FEM,
- an overlapping decomposition method is used for coupling an exact method for a limited area containing the opening of the cavity with a high-frequency asymptotic method to handle the rest of the structure.

Figure FIG. 2.1 gives a side view of a “COBRA” cavity within a large fuselage. It constitutes a case-test specially designed to benchmark the performances reached by methods and codes dedicated to electromagnetic scattering problems for this kind of scatterers.

Figure FIG. 2.2 depictes a schematic view of the decompositions of the cavity and of the exterior boundary which are used in the framework of the hybrid method.

At a frequency of 10 GHz and for approximately 5 points by wavelength, the numerical solution of this problem has required about 230,000 degrees of freedom. The plot in FIG. 2.3 shows that the hybrid procedure well agrees with an exact solving.

The hybrid approach can be compared to a standard MLFMM solving in terms of the respective computational cost of these methods :

- **The Multi Level Fast Multipole Method**
  - Computation of the near interactions matrix : 2 h
  - Computation of the Radar Cross for one incidence : 9.5 h
  - Total CPU time : 1723 h
- **The Hybrid Method**
  - Elimination of the degrees of freedom at the intrior of the cavity : 1 h 20mns
  - Ray tracing : 272 h
  - Total CPU time : 343 h

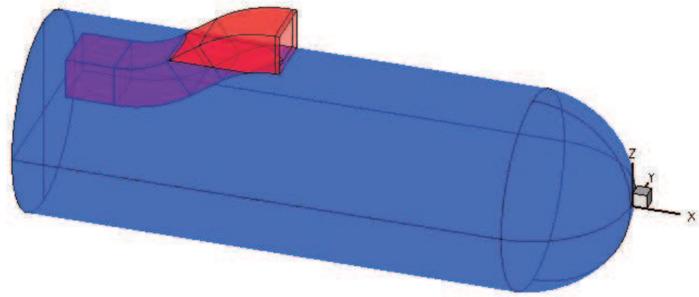

FIG. 2.1 – Cobra cavity within a large fuselage

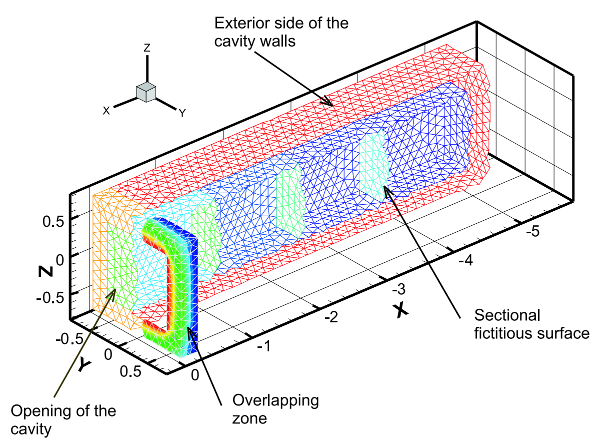

FIG. 2.2 – Schematic view of the various decompositions involved in the hybrid method.

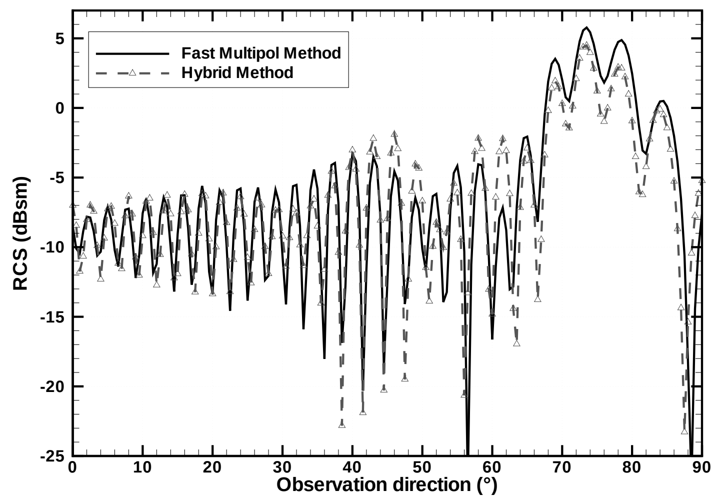

FIG. 2.3 – Radar Cross section of the "COBRA" cavity within a fuselage computed by the hybrid and the exact method.

2.2 Domain Decomposition Method and Hybridation of a Finite Element and an Integral Equation Method (A. Bendali, M. Fares)

The problem that is addressed concerns the numerical computation, using the FEM, of a radiated or a scattered time-harmonic acoustic field in the presence of a rigid obstacle surrounded by a finite region inhomogeneoulsy filled with penetrable materials. A second characteristic of the problem is that it is related to relatively high-frequency situations, so that it becomes necessary to resort to HPC on massively parallel platforms to be able to perform the actual computations.

The main issue herein, arguably, is to find a suitable way to efficiently treat the unbounded region beyond the finite element mesh. Two classes of such treatments have been developed and intensively used.

The first class can be called "approximate methods" in the sense that, an inherent error remains present even without any error of discretization. The main advantage of these methods lies in the fact that they lead to a linear system with a purely sparse matrix (e.g., [9]). However, these methods have a major disadvantage. It is not possible in general to control the accuracy of the solution they deliver in the end.

For the second class of methods, the only errors are coming from the discretization. They are hence called "exact methods" and are generally based on a coupling of a FEM with a BEM (e.g., [8]) like it is done in this study. A major disadvantage of these methods, in the context of HPC, is that they lead to a matrix which is partly dense, due to the part of the discrete equations related to the FEM, and partly sparse, for the ones concerning the discretization by a BEM. More precisely the general linear system solvers in the HPC context are tailored for either one of these two types of matrices. To the best of our knowledge, it seems that to-date there is neither a suitable method nor a HPC code specially adapted to deal with a matrix partly dense and partly sparse.

To overcome this difficulty, a quite obvious approach is to use a DDM to uncouple the part of the equations related to the BEM from that concerning the discretization by the FEM by means of an iterative procedure as this is done in (e.g., [11, 3]). However, as explained below, the most natural procedures which consist of transmitting either Dirichlet or Neumann data from one domain to the other, do not work in the framework of problems with weak coerciveness properties like those related to waves propagation. The correct way to deal with this kind of problems was introduced by Després [6]. In this study, we followed this way to proceed since, at least at the level of the continuous problem, that is, without considering any discretization error, the convergence of the algorithm can be established theoretically [6, 5, 3]. However, we departed from this previous work in two fundamental directions :

1. Only standard BEM are used instead of those doubling the unknowns based on another principle than the utilization of the usual Green kernel [4, 2] ;
2. The procedure we develop is a FETI-like method in the sense that the DDM can be interpreted exactly as an efficient iterative process to solve the coupling of the FEM and the BEM formulation.

A detailled description of the approach can be found [CEM13] which will appear in a special issue of *Computers & Structures*.

Another issue which was addressed concerns the use of a DDM once more for solving the sparse system related to the FEM instead of the parallel library `MUMPS`. A new approach has been developped to overcome the well-known difficulty met in this context for degrees of freedom shared by more than two subdomains. A theoretical study establishing convergence and stability of the approach is reported in [CEM12] which has been accepted for publication. Some preliminary promising results for the coupling with a BIE are already available for the 2D case, the 3D one being presently in progress.

2.3 Extension of the far-to-near transformation to an antenna close or posed on a structure (A. Bendali)

The radiating properties of an antenna can be sometimes documented only by measurements in the far-field zone. Is it possible nevertheless to obtain the field that it radiates in the presence of a large structure like a satellite. In collaboration with CNES, the team has previously published a study [CEM2] which has completely answered this issue when the antenna is separated from the structure by at least a quater of wavelength.

The next issue was to determine if it would be possible to extend the procedure so that it can deal with an antenna directly posed on the structure. This question was tackled in a prospective study in the two-dimensionnal case.

The first conclusion that can be drawn is that it is not possible even to assume that the structure does not modify the field emitted by the antenna. Figure FIG. 2.4 depictes the far-field pattern for a completely coupled formulation and that obtained by assuming that the structure only reflects the field emitted by the antenna but does not modify its radiation characteristics when the antenna is separated by a distance of one wavelength from the structure. Clearly, the approximation is valid in this case.

If now the antenna is placed at a distance of a tenth of a wavelength, figure FIG. 2.5 shows that even the effect of the structure on the field emitted by the antenna can no longer be neglected.

We have then tried the following setup. We have placed the antenna on periodically distributed slots as depicted in figure FIG. 2.6 whose role is to trap the near field energy of the antenna.

It was next possible for the numerical simulation to fictitiously move away the traps at a distance of $\lambda/4$ from the antenna and to use only the far field emitted by the antenna without any significant modification of the field obtained for the exact setup with an exact solving as indicated in FIG. 2.7.

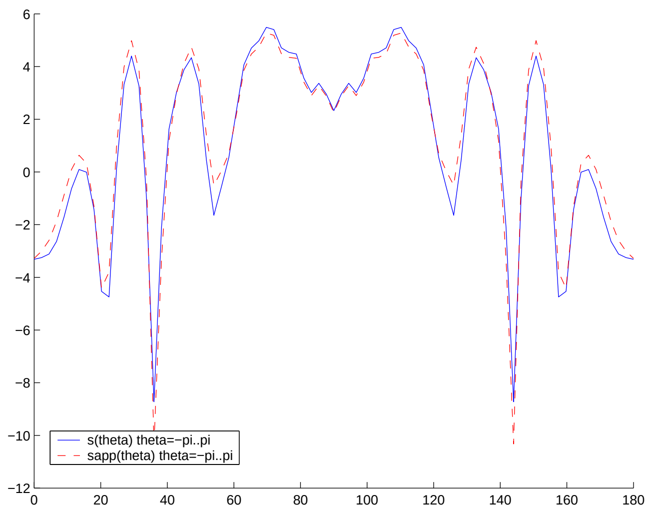

FIG. 2.4 – Far field pattern of an antenna separated by λ from a structure : exact and approximate modeling.

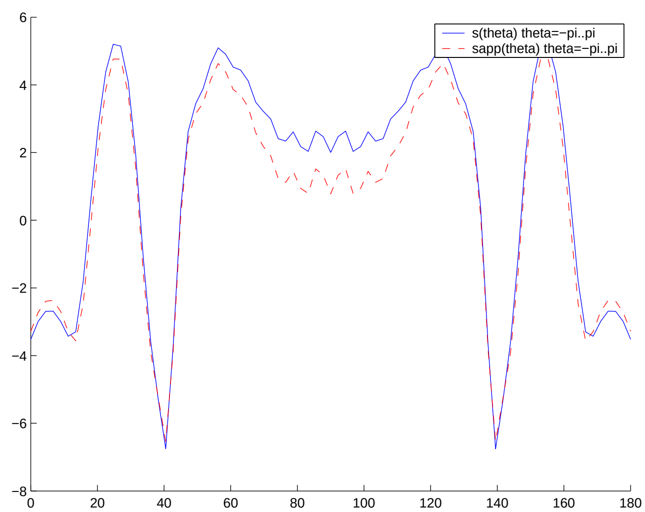

FIG. 2.5 – Far field of an antenna separated by $\lambda/10$ from a structure : exact and approximate modelling

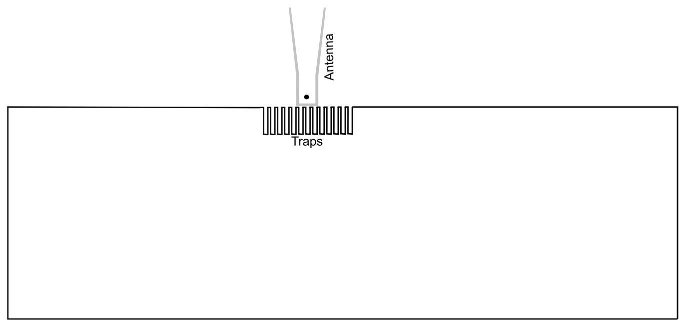

FIG. 2.6 – Antenna mounted on traps

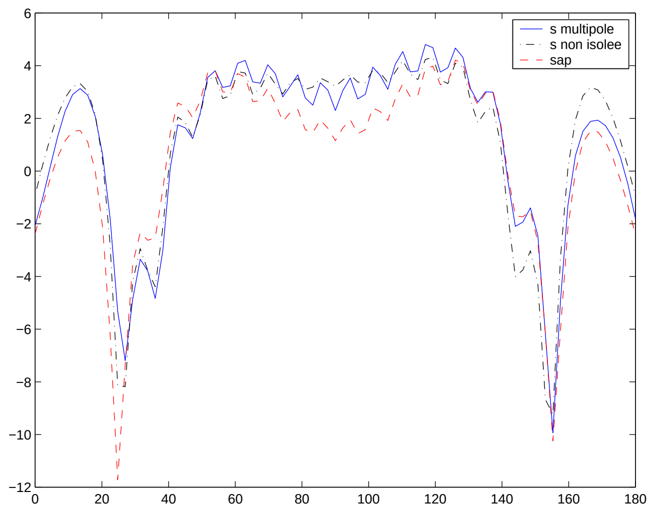

FIG. 2.7 – Far field pattern computed in an exact way (point/dashed curve), assuming that the field radiated by the antenna is not modified by the structure (dashed line) and fictitiously moving away the traps and using only the far field of the antenna (continuous line).

2.4 Coupling FEM and BIE solutions with an Adaptive Absorbing Boundary Condition (N. Zerbib)

We consider a large perfectly conducting structure on which is posed an inhomogeneous dielectric in a restricted zone as depicted in FIG. 2.8a. To solve electromagnetic scattering and radiation problems for this kind of configuration, an efficient hybridization of a FEM with a BIE based on an Adaptive Absorbing Boundary Condition (AABC) was developped. The standard approach presented in [1, 10, 7] consists in truncating the computational domain by using an fictitious surface on which is set an AABC derived from a BIE as depicted in FIG. 2.8b. Unlike the standard FEM-BIE approach, this FEM-AABC coupling constitutes a really powerful method :

- The proposed method is free of interior resonance ;
- It produces a purely sparse linear system matrix.
- Only the right-hand side of the linear system is changed from one iteration to another one.
- All the integrals involved in the formulation are not singular and therefore can be determined by quadrature formulas only ;
- Finally, the radiation condition, set on an arbitrarily shaped fictitious surface which can be placed very close to the scatterer/antenna, is exactly satisfied as for standard FEM-BIE approaches at convergence.

However, despite these very attractive properties, the dispersion errors inherently attached to a FEM approximation of a wave phenomenon can become prohibitive : even if the fictitious surface can be set close to the scatterer/antenna, it must wrap up all the structure.

As depicted in FIG. 2.8c, the formulation designed in [12], is typically characteristic of an overlapping DDM. It enables for the reduction of the FEM discretization to a localized zone only while the exterior computational domain is dealt with by a BIE. There is a difficulty in the above extension comparatively to the initial method, as this is mentionned in [7, 10]. The FEM allows for the determination of the currents only inside the dielectrics. In the rest of the structure, it is the Electric Field Integral Equation (EFIE) which has to be used to this purpose. However, this BIE then becomes expressed by means of hypersingular integrals. This difficulty is overcome by performing an integration by parts to remove all the integrals that do not converge in the usual meaning. While keeping the main attractive properties of the FEM-AABC approach, the FEM-BIE-AABC method reduces the computational domain attached to the FEM approximation and also the number of iterations of the standard FEM-AABC. The required evaluation of boundary integrals in the calculation of the AABC and the resolution of the exterior BIE can be carried out using the MLFMA. Unlike the standard FEM-BIE approach, it only requires the solution of two completely uncoupled systems : one purely sparse and the second purely dense. The capabilities of the FEM-BIE-AABC procedure are illustrated in FIG. 2.9 which depicts the results obtained from the standard FEM-BIE, the standard FEM-AABC and this approach for the determination of the field radiated by a circular patch antenna mounted on a large perfectly conducting structure.

2.5 Using the MLFMM algorithm to compute the scattered fields by an electrically deep cavity (N. Zerbib)

It is well-known that the internal resonances inside a cavity severely slow down the convergence of the iterative process coupled with the MLFMM despite the use of high performing preconditioners. Thanks to the aforementionned substructuring process to deal with the equations and the degrees of freedom inside the cavity, the scattering problem is now set on a closed surface consisting of the exterior boundary and the aperture of the cavity. This makes it possible to use a Combined Field Integral Equation (CFIE) for an efficient determination of the exterior field [12]. More particularly, the problem set at the exterior of the cavity can be solved by means of a Krylov method using the MLFMM to speed up the matrix vector

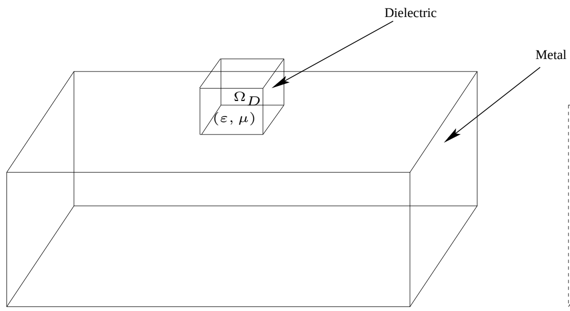

(a) Schematic view of a large perfectly conducting structure on which is posed a piece of inhomogeneous dielectric.

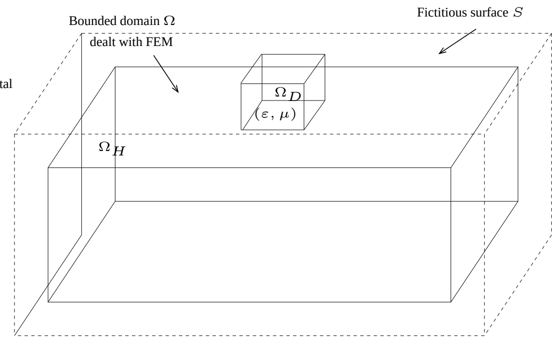

(b) The FEM-AABC standard approach : the fictitious surface S wrapping up all the obstacle.

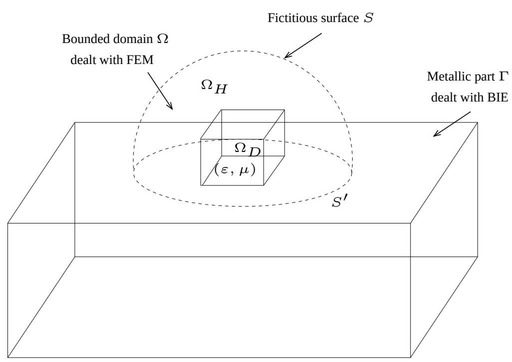

(c) The FEM-BIE-AABC approach : the fictitious surface S enclosing only the domain Ω modelled by FEM.

FIG. 2.8 – Description of the model problem and the two approaches.

product. The elimination of the unknowns inside the cavity significantly improves the iterative process. For example, figure FIG. 2.10 indicates that the method is scalable in the sense that the number of iterations remains approximately independent of the depth of the cavity whereas it grows almost linearly for the usual CFIE.

2.6 Domain Decomposition Method versus Liu-Jin Method (F. Collino)

In the framework of a collaboration with CEA-CESTA, we have developed a 2-D code to compare two methods for the solution of harmonic scattering problems in unbounded domains. The first one mimics the algorithm used by the CEA-CESTA code `ODYSSEE`, which couples a FEM with some BIE ; the solution is obtained iteratively via the DDM proposed by B. Despres ; its main drawback is that it requires to solve at each iteration a large complex linear system associated to the integral equation. The second method

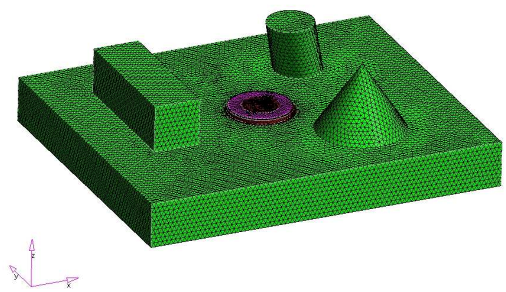

(a) Mesh of a circular patch antenna posed on a large perfectly conducting structure.

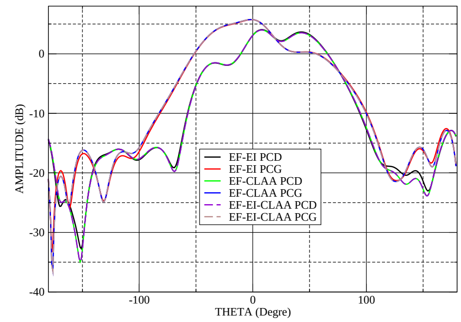

(b) Circular polarisations of a circular patch antenna posed on a large perfectly conducting structure.

FIG. 2.9 – Comparison between three approaches for the determination of the radiation pattern of a circular patch antenna posed on a large perfectly conducting structure.

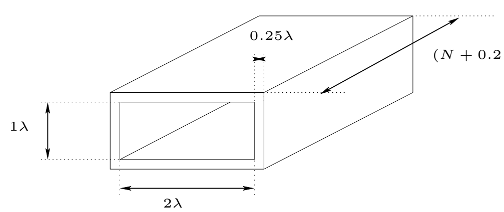

(a) The rectangular cavity.

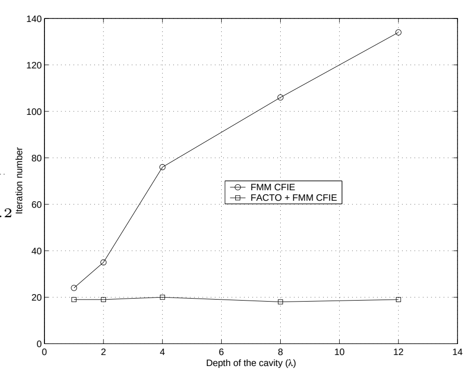

(b) The convergence curve versus the depth for a rectangular cavity (GMRES(30) solver, 10^{-3} residual).

FIG. 2.10 – Coupling a substructuring method with a FMM to to solve the scattering problem by a rectangular perfectly conducting cavity.

was introduced by Liu-Jin. It consists in determining iteratively some impedant boundary condition of a scattering problem posed in a bounded domain enclosing the obstacles. At each iteration, the impedant problem is first solved by means of FEM, then, a new impedant condition is simply constructed through an explicit formula which can be computed in a fast way by techniques from the MLFMM. The results we have obtained on examples of large 2-D obstacles clearly demonstrate the advantage of the second method : the solution is obtained much faster with no loss of accuracy (see [CEM20]).

[1] S. Alfonzetti, G. Borzì, and N. Salerno, (1998), Iteratively-Improved Robin Boundary Conditions for the Finite Element Solution of Scattering Problems in Unbounded Domains, *Int. J. Numer. Meth. Engng*, **42**, 601–629.

[2] N. Bartoli and F. Collino, (2000), Integral Equations VIA Saddle Point Problem for 2D Electromagnetic Problems, *Mathematical Modelling and Numerical Analysis (M2AN)*, **34**, 1023–1049.

[3] Y. Boubendir, (2002), *Techniques de Décomposition de Domaine et Méthodes d'Equations Intégrales*, PhD thesis, INSA of Toulouse.

[4] F. Collino and B. Després, (2002), Integral Equations Via Saddle-Point Problems for Time-Harmonic Maxwell's Equations, *Journal of Computational and Applied Mathematics*, **150**, 157–192.

[5] F. Collino, S. Ghanemi, and P. Joly, (2000), Domain Decomposition Method for Harmonic Wave Propagation : a General Presentation, *Computer Methods in Applied Mechanics and Engineering*, **184**, 171–211.

[6] B. Després, (1991), Domain decomposition method and the Helmholtz problem, In *Mathematical and numerical aspects of wave propagation phenomena (Strasbourg, 1991)*, G. Cohen, L. Halpern, and P. Joly, eds., Philadelphia, PA, SIAM, 44–52.

[7] C. Hazard and M. Lenoir, (1996), On the Solution of Time-Harmonic Scattering Problems for Maxwell's Equations, *SIAM J. Math. Anal.*, **27**, 1597–1630.

[8] G. C. Hsiao, P. B. Monk, and N. Nigam, (2002), Error analysis of a finite element-integral equation scheme for approximating the time-harmonic Maxwell system, *SIAM J. Numer Anal*, **40**, 198–219.

[9] J. Jin, (2002), *The Finite Element Method in Electromagnetics, Second Edition.*, John Wiley & Sons, New York.

[10] J. Liu and J.-M. Jin, (2001), A Novel Hybridization of Higher Order Finite Element and Boundary Integral Methods for Electromagnetic Scattering and Radiation Problems, *IEEE Transactions on Antennas and Propagation*, **49**, 1794–1806.

[11] B. Stupfel and B. Després, (1999), A Domain Decomposition Method for the Solution of Lare Electromagnetic Scattering Problems, *Journal of Computational Waves and Applications*, **13**, 1553–1568.

[12] N. Zerbib, (2006), *Méthodes de sous-structuration et de décomposition de domaine pour la résolution des équations de Maxwell Application au rayonnement d'antenne dans un environnement complexe*, PhD thesis, Université Paul Sabatier.

3 Integral equations and Fast Multipole Method

3.1 Symmetries in CESC (F. Collino, M. Fares)

It is well known that it is possible to take advantage of symmetries to put the matrix of the linear systems associated to BIE in a block diagonalize form and consequently reduce the computational cost of the solution. In an industrial context, many situations can be encountered : antennas composed with different pieces of dielectrics or conductors possibly including wires and junctions. Defining a practical method for taking into account all kinds of symmetries (plane symmetries, invariance by rotation and composition of several of them) in such a general context is a challenging problem. The abstract theory of linear representations of finite groups is the appropriate tool to adequately solve this problem.
Assume that the object under consderation is invariant by a group of symmetries. We have proposed an algorithm that first consists in constructing a mesh of a part P of the object, P being generic in the sense that it is possible to reconstruct the whole object by the group of symmetries. When the mesh connection is proceeded, we transform the mesh of P by the symmetries, thus obtaining a mesh of the whole object which, by construction, is invariant by each of these symmetries ; we construct the usual connectivity table of the developed mesh and either construct two integer arrays $\sigma(d)$ and $D(d)$ indexed by the degrees of freedom d of the developed mesh[1]. This information is then enough to carry out the assembly process and to solve, for each representation of the group, a linear system and its right-hand side of size $\simeq N/G$ where N is the number of degrees of freedom of the whole mesh and G is the number of representations (which is the number of elements of the group of symmetries for commutative groups). It is then easy to recover the whole solution on the developed mesh through simple sums over the representations.
The program we wrote (CESC 4.1) works with an abstract notion of group that allows us to treat a large number of situations : invariance by a single, two or three symmetries or by a rotation of angle $2\pi/G$ around an axis or composition of this rotation with a symmetry with respect to a plane perpendicular to the axis...) It has been parallelized, optimized and validated on a large number of examples. A documented version of the code was delivered to CNES.

3.2 Inverse Scattering Solution via the Linear Sampling Method (F. Collino, M. Fares, H. Haddar (INRIA), F.Cakoni (Delaware Univ.))

We have continued our investigation of the linear sampling method (LSM) for solving scattering inverse problems at resonant frequencies. The object reconstruction by the LSM is carried out in several steps :

- From the collection of some scattering data, a matrix M is constructed and its singular value decomposition computed ;

[1]The meaning of the two arrays is as follows : a degree of freedom d of the whole mesh is obtained by the action of the symmetry number $\sigma(d)$ on the degree of freedom $D(d)$ on P (there is an additional sign in $D(d)$ to take into account orientation problems but it is just a matter of details).

– At each point x of the investigated domain, a linear system of the form $Mu_x = g_x$ is solved by means of regularization techniques ;
– The norm of the solutions $\|u_x\|$ provides a criterion to distinguish the points x located inside the object from those outside.

H. Haddar and F. Cakoni have proposed and analyzed two methods theoretically, related to the LSM, for determining the shape of a perfectly conducting object buried in a conducting ground from the knowledge of scattering data. The data are the observations, recorded at points located on a line above the ground, to point sources located along the same line.

We have extended the flexibility of CESC to handle objects embedded in a conducting ground, the main difficulty being to compute in a fast way the related Green function. Both the performance of CESC and the parallelization of the LSM code have allowed us to test and compare those methods on large significant examples. Fig 3.5 presents a comparison between the true object and its reconstitution obtained by one of the two methods.

3.3 Comparison of two feed models of a patch antenna fed by a coaxial cable. (M. Fares, N. Zerbib)

The most critical and difficult part in the numerical simulation of the functionning of a patch antenna is related to the determination of its impedance, especially at a resonance frequency. Inside the coaxial cable and far enough from its junction with the patch, only the fundamental TEM mode is propagating. The determination of the reflection coefficient of this mode directly yields the impedance of the antenna.

For a hybrid method coupling a FEM with a BEM, an impedance boundary condition can be used to truncate the coaxial cable as a mesh terminating booundary condition. However, such a boundary condition results in hard difficulties in the context of a BIE solution. Another approach based on the expression of the boundary condition in terms of the fundamental TEM mode has been developed to overcome this difficulty. Figure FIG. 3.6b depicts the impedance obtained from measurements and from the two previous feed models in the case of the circular patch antenna represented in FIG. 3.6a.

Electromagnetic scattering solutions by BIE methods lead to dense systems of linear equations. When the characteristic size of the obstacle is about six times the wavelength, the solutions can be computed by direct methods with high performance and massively parallel codes. However, for lager sizes, the solutions can only be obtained by means of some iterative methods. The computation of the matrix-vector product then becomes the basic part of the iterative algorithm. It can be done efficiently by means of the MLFMM. This method reduces the complexity of the matrix vector product from $O(N^2)$ to $O(NlogN)$ where N is the number of unknowns.

3.4 Parallelization of the MLFMM code (F. Millot)

Advances in computing have demonstrated that the future of HPC lies in parallel computing. It is clear that a parallel version of the MLFMM algorithm must be built. It uses the Message Passing Interface (MPI) for communication. We shall briefly describe the parallel version. During the MLFMM algorithm, some quantities called the near and the far fields are needed. They are defined for all the directions of the unity sphere. Their computations can be done independently except during the interpolation and anterpolation phases. These last phases consist in a FFT operation plus a matrix-vector product and at the end an inverse FFT operation. So, it may be possible to distribute this matrix-vector product on the processes. We have implement this distribution and tested on some cases [CEM16, CEM9]. We observed a good scalability which doesn't depend on the type of the machine (see Tab 3.1).

machine	2 processes	4 processes	8 processes
compaq	7 min 35 s 96	4 min 47 s 24	3 min 55 s 46
PC cluster	21 min 10 s 34	10 min 38 s 44	7 min 26 s 20

TAB. 3.1 – CPU time needed to solve the scattering by a sphere with $100,000$ unknowns

3.5 A MLFMM algorithm for solving imperfectly conducting problems (F. Collino, F. Millot and S. Pernet)

A BEM is used to solve electromagnetic scattering problems in the frequency domain relative to an impedance boundary condition. This impedance condition was first proposed by Leontovich. It is used for example to address scattering problems by an imperfectly conducting obstacle or a obstacle covered by a thin layer of dielectric materials. The impedance relation can be written in form $\mathbf{n} \times (\mathbf{E} \times \mathbf{n}) = Z_0 \eta (\mathbf{n} \times \mathbf{H})$ where $\mathbf{E}$ and $\mathbf{H}$ are the electric and magnetic fields respectively, $\mathbf{n}$ is the unit normal to the surface of the object, Z_0 is the intrinsic impedance of vacuum and η is the impedance operator not necessarily constant.
The total electromagnetic field is expressed in terms of the equivalent electric and magnetic currents on the scatterer surface and compelled to satisfy the boundary condition. Several boundary integral formulations can be built for this purpose. Most representatives are the formulation using one current as unknowns proposed by A. Bendali., M. Fares and J. Gay [13], the system of integral equations (FDESPRES) based on the minimisation of a quadratic functional proposed by B. Despres and F. Collino [14] and a formulation keeping the two currents as unknowns (FBACHL) obtained, in particular, by Bachelot, Gay and Lange [15]. It is the last formulation which seems to have the best assets for solving a big size problems (in term of the number of unknowns) bringing into play a impedance boundary condition. Section 3.5.1 is devoted to this formulation. In particular, an efficient MLFMM calculation and a thorough study of its behavior are presented.
However, it has been observed that for various reasons all these formulations lead to a linear system with a condition number very sensitive to the variations of the impedance values. We have been led to seek some cure to curb this phenomenon. Section 3.5.2, is devoted to this investigation. We propose there several solutions and compare them to determine the most efficient one.

3.5.1 Two unknowns formulation (F. Millot)

One possibility to solve the scattering problem with an impedance condition is to keep the two currents as unknowns. The equivalent currents are discretized by a BEM built as usual on a triangular mesh of the surface. In the end, the problem is reduced to the solution of a dense linear system. The main advantages are that the BIE formulation involves only “classical” integral operators and the difficulty related to the conservation of both the electric and magnetic charges associated to the equivalent currents is avoided. The impedance condition is prescribed in an implicit manner. The main drawback of this approach is that the order of the linear system is twice larger than for the perfect conductor case. Moreover, this formulation is sensitive to the variations of the impedance operator. The condition number deteriorates and for an impedance operator equal to zero, the equation degenerates into the EFIE.
When the characteristic size of the obstacle is about six times the wavelength, the currents can be computed by direct methods with HPC parallel codes. This method was implemented and its accuracy tested [CEM19]. Its validation was carried out from available analytical solutions.
However, for obstacles of larger size, the solutions can only be obtained by means of some iterative methods coupled with the MLFMM. For the impedant problems, the matrix-vector product is done by applying eight times the MLFMM algorithm in the usual implementation (four times for each unknown). Another implementation of the MLFMM for the computation of the matrix-vector product can be built. In fact, from a

suitable combination of the unknowns, the matrix can be put in a diagonal form. By changing the numerical integration formulae, it is possible to do the matrix-vector product using only twice the MLFMM algorithm [CEM17]. This method was implemented. We have tested the accuracy of the product. We compared its performances relatively to the standard solution of the perfectly conducting case solved by means of the EFIE formulation. The CPU times for performing a matrix-vector product are nearly the same for the two methods. The required memory for the near interactions matrix is twice larger.

3.5.2 Comparison of various formulations for the impedance boundary condition. (S. Pernet)

The BIE methods lead to the solution of a linear system with a dense matrix. One has hence to resort to the use of an iterative solver for large size problems. It is well-known that the rate of convergence of most of the iterative methods depends among other things, of the condition number of the linear system matrix and on the clustering of its eigenvalues. We have observed that the impedance operator, especially if it is varing, produces a dispersion of the eigenvalues (see the figure of left-hand side of 3.7) hence deteriorating the rate of convergence significantly.

We first made a comparative study of several formulations classically used to solve impedance problems. The guiding line of this study concerned the accuracy, each of these formulations deliver, as well as their robustness and their adaptation relatively to an iterative solving. We highlighted, both analytically for spherical geometry and numerically with 3D codes, that the presence of a variable impedance operator mostly results in a significant deterioration of the performances of these methods and this even for problems of small sizes. In particular, this can lead to very low rates of convergence. Moreover, we come to the conclusion that the formulation with two currents studied in the previous subsection seems to be the most accurate.

In order to improve the efficiency of the iterative solving, we have studied two possibilities. First, we proposed several techniques based on both the introduction of an operator of reflexion coefficient type and the use of a double iterative process to solve systems which are well conditioned for all the possible values of the impedance operator. More precisely we propose formulations leading to a system in the form :

$$(I + A_0^{-1} N_R)u = A_0^{-1} b$$

where A_0 is the matrix associated either to FBACHL or FDESPRES for an impedance equal to 1 and N_R is a matrix taking into account the real surface impedance. So, one needs an internal loop to solve $A_0^{-1} N_R u$ and an external loop to compute u. The internal loop is an iterative solving of a pivot problem related to a constant impedance boundary condition, relatively well-conditioned. Regarding the external loop, we show that its eigenvalues are gathered around the point 1 in the complex plan and is contained in the window $[0, 2] \times [-1, 1]$ (see the figure of right-hand side of 3.7) for all impedance operators. For this loop we obtain also a good iterative behavior.

We have next studied a formulation with one current. More precisely, we have introduced a CFIE for solving the electromagnetic scattering problems relative to an impedance boundary condition. We have proposed several efficient techniques to remove one of the currents during the iterative process, as well as to treat the composition of the EFIE integral operator with the rotation around the unit normal to the surface. Thanks to that, we remain within a traditional functional framework for the electromagnetism. We lead to a system which is better conditioned than for FBACHL. Moreover it is less sensitive to the variations of the impedance.

A part of these studies are reported in [16].

3.6 Resonances (F. Millot)

In the frequency domain, the response of the antenna to some excitation is proportional to the inverse of the impedance matrix and also depends on the wavenumber in vacuum. At some frequencies F_c, a sharp variation of this response can be observed. These frequencies are called the resonant frequencies. Close to these frequencies, the response of the antenna is sensitive to the perturbations. In fact, the linear system becomes close to be not invertible and has a bad condition number. The purpose of this study is to compute the resonant frequencies with a good accuracy. The first idea is to sweep over k and to evaluate the response of the antenna with the help of for example a direct computation. Plotting the impedance versus the wavenumber k enables for the determination of the resonant frequencies expressed as peaks in the plot. If the peak is too sharp or/and if the sweeping step too large, it is not possible to be ensured that no resonance frequency was missed. Moreover, even when one succeeds in localizing a resonance frequency, the accuracy of its determination depends on the sweeping step and cannot easily be improved.
The second idea is to use the definition of the resonant poles in the complex plane. The real part of the resonant pole determines the value of the resonant frequency and the imaginary part is linked with the quality factor of the antenna. We propose to compute these resonant poles following ideas of Poisson and Labreuche. The resonant poles are obtained by searching the zeros of the determinant of the matrix related to the underlying scattering or radiation problem. In this way, the modes containing the main part of the information on the scattering or the radiation problem can be also recovered. This method was applied to the case of two plates in front of each other (see Fig 3.8). The resonant frequencies are obtained with a good accuracy. However for setups involving dielectrics, the determination of the resonant frequencies is more complicated and requires more investigations.

3.7 Panels and Satellite interaction (F. Millot)

The problem under consideration is to determine the inflence of a satellite on the far-field emitted by an inboard antenna. We want to do this as quickly as possible. The satellite is composed by metallic structures and solar panels. These panels can be considered as plates with a zero thickness. The structure as well as the panels are considered as perfectly conducting scatterers. Various types of surface integral equations can be considered for solving this scattering problem. We can use the EFIE. However this kind of formulation suffers from two main flaws. First, for some values of the wavenumber (related to the so-called interior resonance frequencies), the uniqueness of the solution is lost. Next, if the solution is carried out by means of an iterative process, the presence of the panels which are open surfaces drastically slows down the convergence. In order to avoid this drawback, we can choose the CFIE for solving our scattering problem. It is well known that this equation has a better condition number and the rate of the iterative convergence is faster. But this kind of equation is valid for closed surfaces only. A possible cure is to assume that the solar panels have a small fictitious thickness. A first consequence of this handling of the panels is that the number of degrees of freedom is increased, thus augmenting the computing time and the memory storage. The purpose of this study is to write a suitable equation combining the advantages of the two formulations. The new formulation can be solved by a iterative process very quickly. Some hypotheses are needed to be able to apply this formulation. First, the panels are assumed to be separated from the rest of the structure. The surface of the scatterer is next decomposed into two surfaces : one on which the EFIE is set and the other dealt with by the CFIE. Now the system to be solved is under the form

$$\begin{bmatrix} Z_{\text{CFIE}}^{\text{CFIE}} & Z_{\text{CFIE}}^{\text{EFIE}} \\ Z_{\text{EFIE}}^{\text{CFIE}} & Z_{\text{EFIE}}^{\text{EFIE}} \end{bmatrix} \begin{bmatrix} I_{\text{CFIE}} \\ I_{\text{EFIE}} \end{bmatrix} = \begin{bmatrix} U_{\text{CFIE}} \\ U_{\text{EFIE}} \end{bmatrix}. \tag{3.1}$$

The unknowns I_{EFIE} and I_{CFIE} represent the degrees of freedom for the currents, and U_{EFIE} U_{CFIE} are linked to the incident field.

Only the I_{CFIE} is kept after I_{CFIE} was removed from for (3.1) by means of a Schur complement technique.

A GMRES solver is finally used to obtain I_{CFIE}. The number of iterations is practically identical to this observed when the satellite has no panel. It is smaller than this one obtained for panels with a small thickness. A good accuracy on the current and the far-field is obtained (see Tab 3.2 and [CEM11], [CEM10]).

	EFIE GMRES	CFIE - EFIE Schur-GMRES
Number of iterations	43	12
Error obtained on the current	0.22%	5.83%
Error obtained on the RCS	0.04%	3.85%

TAB. 3.2 – Relative errors obtained for the different formulations

3.8 Electromagnetic Compatibility of large wind turbine blades (M. Fares)

The process of obtaining planning permission to build a wind turbines farm involves many considerations, including consultation with various aviation stakeholders. These parties may raise objections for a variety of reasons, with a known source of objections being that the wind turbine farm may appear on the display of air traffic control radar.

So, there is a strong need to predict electromagnetic perturbation caused by wind turbines farm over traffic control radar and on VOR (VHF Omnidirectionnel Radio) antennas.

DGAC has launched a first initiative with CERFACS and ENAC to develop a first study on the numerical simulation of the electromagnetic perturbations due to the implementation of wind turbine blades close to an airport.

This study is focused on the development and validation of a computer model that can be used to predict the radar reflection characteristics (Radar Cross Section) of wind turbines and understand the complex interaction between radar and wind turbines.

The most significant parameters that influence the RCS of a wind turbine can be listed as follows :

- Blade design (shape, size and construction materials) ;
- Tower design ;
- Nacelle design.

Figure FIG. 3.9 and Figure FIG. 3.10 show the CAD model of the blade.

Nowadays, the highly parallel codes make it possible to determine the perturbation of the field emitted by a VOR antenna (300 MHz) by a wind turbine blade composed of a metallic mast of 65 m and three dielectric blades of 30 m. Actually, even for this case, it was necessary to uncoupled the effect of the mast and each of the blades to be able to carry out the computation. The real challenge is to perform a complete coupled computation for a mast of 100 m blades of 75 m at a frequency of a few GHz. This would require an increase by a factor 1000 to 10000 of the computing power.

Our planned objective is to perform a complete coupled formulation for a wind turbine blades device at a frequency 1 Ghz.

3.9 Numerical Microlocal Analysis of harmonic wavefields (J.D. Benamou (INRIA), F. Collino, O. Runborg (KTH))

We have presented and tested a numerical method which, given an analytical or numerical solution of the Helmholtz equation in a neighborhood of a fixed observation point and assuming that the geometrical optics approximation is relevant, determines at this point the number of crossing rays and compute their directions and associated complex amplitudes. Obtaining our solution is cheap : $\mathcal{O}(M \log M)$ operations is needed, where M is the number of sample points on a small circle around the observation point. The accuracy of the method increases with the frequency. It is easy to implement and can be applied both for heterogeneous media and homogeneous media. A remarkable feasibility is its ability to capture scattered rays. These results are reported in the journal paper [CEM3].

[13] A. Bendali, M. Fares, and J. Gay, (1999), A Boundary-Element Solution of the Leontovitch Problem, *IEEE Transaction on antennas and propagation*, **47**.

[14] F. Collino and B. Despres, (2003), Integral equations via saddle point problems for time-harmonic Maxwell's, *Journal of computational and Applied Mathematics*, **150**.

[15] V. Lange, (1995), *Equations intégrales espace-temps pour les équations de Maxwell. Calcul du champ diffracté par un obstacle dissipatif*, PhD thesis.

[16] S. Pernet, F. Collino, M. Fares, and F. Millot, (2006), Comparaison de formulations intégrales adaptées à la résolution des problèmes de diffraction d'ondes électromagnétiques avec condition d'impédance, Tech. Rep. CR/EMC/06/06, C.E.R.F.A.C.S, *42,av. G. Coriolis,31057 Toulouse Cedex France*.

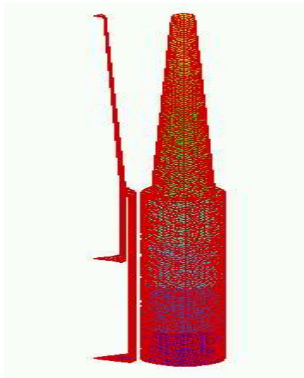

FIG. 3.1 – mesh of the generic part of a septet of candles. The left part corresponds to the candle in the middle, the shifted candle produces six candles around the central axis by symetry.

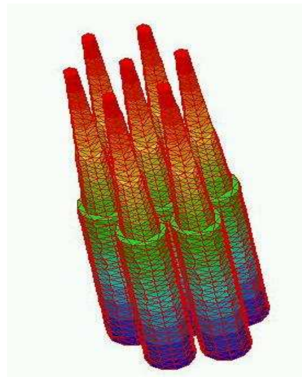

FIG. 3.2 – developped mesh : it is obtained by applying the group of rotational symetries of angle $2\pi/6$ around the vertical axis

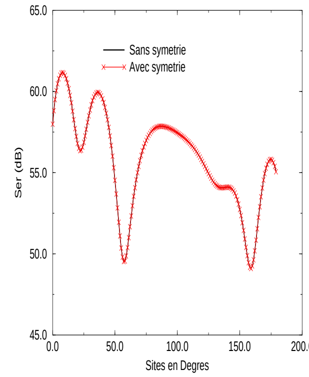

FIG. 3.3 – RCS of the candle obtained by CESC.4

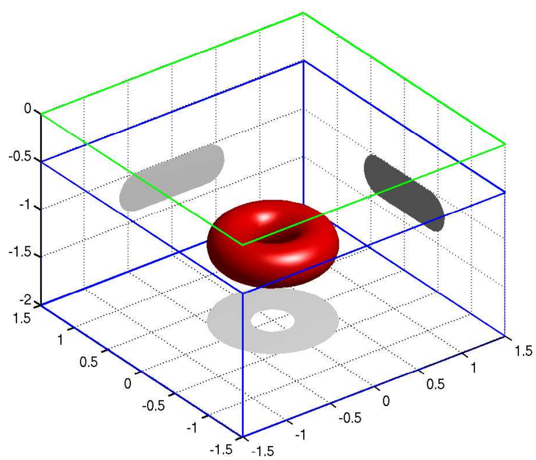

FIG. 3.4 – Exact geometry of the perfect conductor in the second example. The interface earth-air is at $z_3 = 0$. The box indicates the boundary of the probed region.

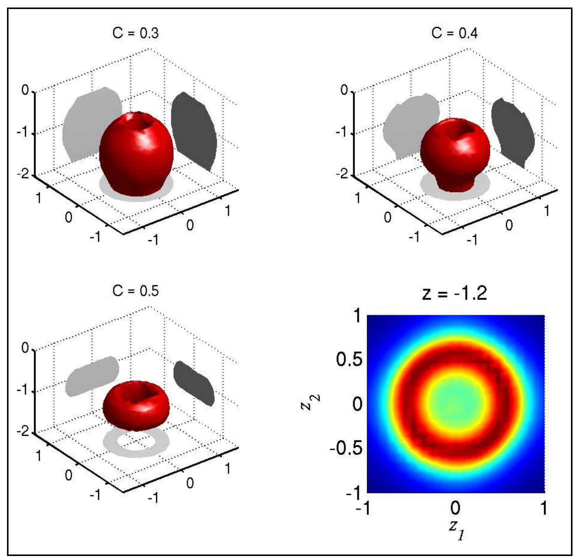

FIG. 3.5 – Reconstructed geometries for $n = 2 + 0.5i$ and an added 1% random noise (see exact geometry in Figure 3.4). The wave length in the air is $\lambda = 1$. LSM : left 4 figures ; RG-LSM : right 4 figures. Each 3-D plot corresponds to a different choice of the isosurface value. The 2-D plot corresponds to a horizontal cross section of $\mathcal{G}$ at $z_3 = -1.2$.

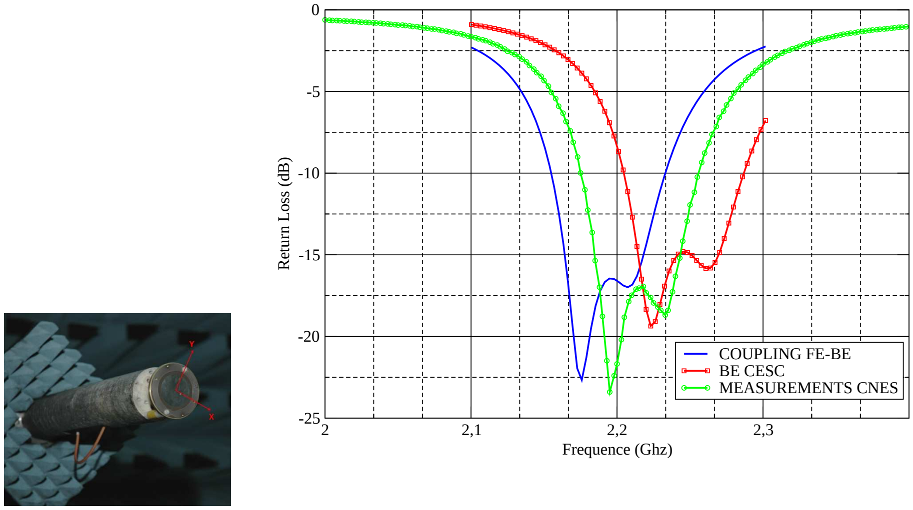

(a) The circular patch antenna.

(b) Impedance curve versus the frequency from measurements, code CESC and code coupling FEM-BIE.

FIG. 3.6 – Comparison between two models of the feeding of a circular patch antenna by a coaxial cable.

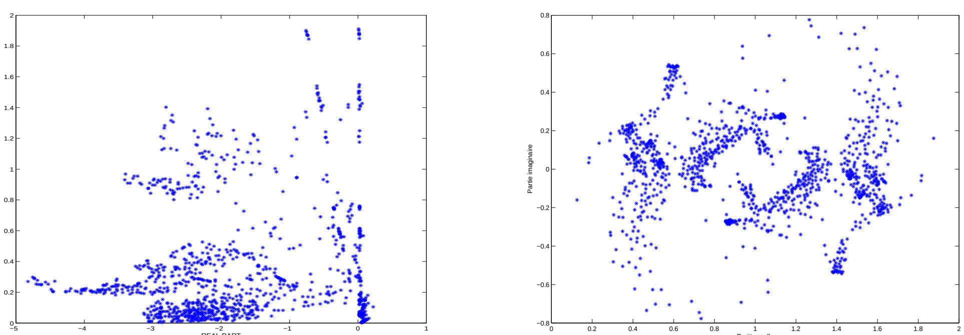

FIG. 3.7 – Left : spectrum of FBACHL for a variable impedance operator on a box. Right : example of spectrum obtained for the external loop for a variable impedance operator

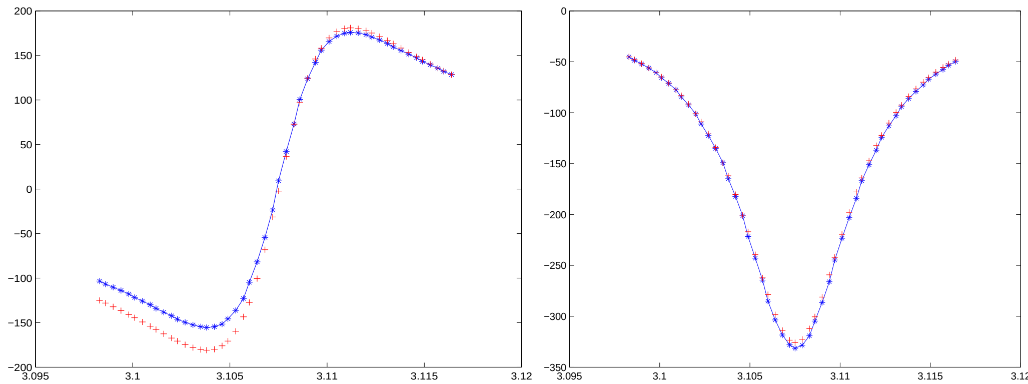

FIG. 3.8 – Variation of the inverse of the impedance matrix versus k (+ :obtained with sweeping, * : computed) Left : real part . Right : imaginary part

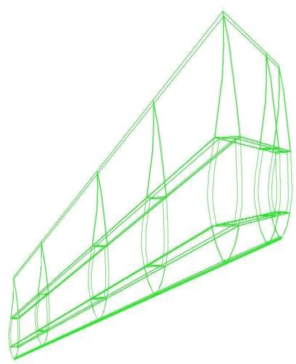

FIG. 3.9 – CAO of the Blade

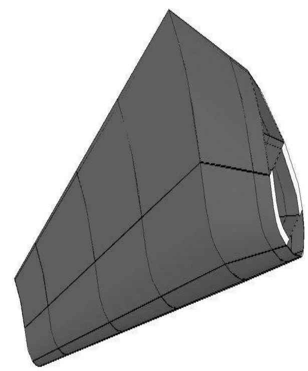

FIG. 3.10 – Mesh of the Blade

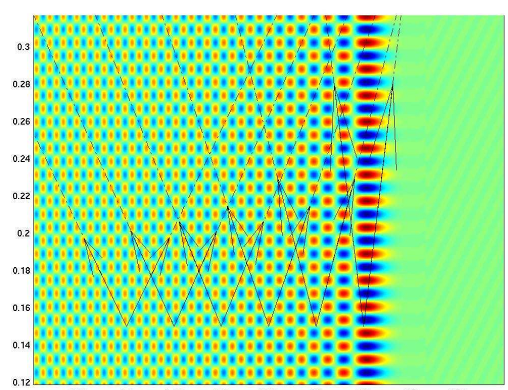

FIG. 3.11 – Determination of rays near a caustic in a stratified media

4 Publications

4.1 Journal Publications

[CEM1] X. Antoine, A. Bendali, and M. Darbas, (2005), Analytic preconditionners for the boundary integral solution of the scattering of acoustic waves by open surfaces, *Journal of Compuational Acoustics*, **13**, 477–498.

[CEM2] N. Bartoli, F. Collino, F. Dodu, and T. Koleck, (2004), A far-near fi eld Transformation using the Fast Multipole Techniques, *EEE Transactions on Antennas and Propagation*, **52**, 3329–3336.

[CEM3] J.-D. Benamou, F. Collino, and O. Runborg, (2004), Numerical microlocal analysis of harmonic wavefi elds, *Journal of Computational Physics*, 717–741.

[CEM4] A. Bendali and Y. Boubendir, (2004), Méthode de dÃl'composition de domaine et éléments fi nis nodaux pour la résolution de l'équation d'Helmholtz, *C. R. Acad. Sci, Paris, Ser. I*, **339**, 229–234.

[CEM5] Q. Carayol and F. Collino, (2005), Error estimates in the Fast Multiupole Method for Scattering Problems. Part 2 : Truncation of the Gegenbauer Series, *ESAIM : Mathematical Modelling and Numerical Analysis*, **39**, 183–221.

[CEM6] N.Zerbib, M. Fares, T. Koleck, and F. Millot, (2005), Some numerical models to compute electromagnetic antenna-structure interactions, *C. R. Physique*, **6**, 647–653.

4.2 PhD Thesis

[CEM7] N. Balin, (2005), *Etude de méthodes de couplage pour la rśolution des équations de Maxwell. Application au calcul de la signature radar d'eéronifs par hybridation de méthodes exactes et asymptotiques*, PhD thesis, Université Paul Sabatier.

4.3 Technical reports

[CEM8] N. Balin, A. Bendali, M. Fares, F. Millot, and N. Zerbib, (2005), Some recent applications of substructuring and domain decomposition techniques to radiation and scattering of time-harmonic electromagnetic waves, Technical Report TR/EMC/05/80, CERFACS.

[CEM9] N. BARTOLI, F. COLLINO, and F. MILLOT, (2004), CODE CESC-FMM : manuel d'utilisation, Tech. Rep. TR/EMC/04/33, C.E.R.F.A.C.S, *42,av. G. Coriolis,31057 Toulouse Cedex France*.

[CEM10] N. BARTOLI, (2004), Documentation technique pour le module CFIE - EFI , Tech. Rep. TR/EMC/04/116, C.E.R.F.A.C.S, *42,av. G. Coriolis,31057 Toulouse Cedex France*.

[CEM11] N. BARTOLI, (2004), Etude du couplage CFIE - EFIE, Tech. Rep. CR/EMC/04/115, C.E.R.F.A.C.S, *42,av. G. Coriolis,31057 Toulouse Cedex France*.

[CEM12] A. Bendali and Y. Boubendir, (2005), Non-overlapping domain decomposition method for a nodal fi nit element method, Technical Report TR/EMC/05/107, CERFACS.

[CEM13] A. Bendali, Y. Boubendir, and M. Fares, (2005), A FETI-like Domaine Decomposition Method for coupling Finite Elements and Boundary Elements in large-size problems of acoustic scattering, Technical Report TR/EMC/05/108, CERFACS.

[CEM14] F. Cakoni, M. Fares, and H. Haddar, (2005), The Electromagnetic Inverse Scattering Problem for Buried Objects in an Inhomogeneous Background, Technical Report TR/EMC/05/105, CERFACS.

[CEM15] F. Collino and M. Fares, (2005), Exploitation des symétries dans le code CESC, Technical Report TR/EMC/05/14, CERFACS.

[CEM16] F. COLLINO and F. MILLOT, (2004), ParallÃl'lisation du code mulitpole, Tech. Rep. TR/EMC/04/142, C.E.R.F.A.C.S, *42,av. G. Coriolis,31057 Toulouse Cedex France*.

[CEM17] F. COLLINO and F. MILLOT, (2005), Mise en oeuvre d'un calcul multipôle pour obstacle impédant, Tech. Rep. CR/EMC/06/05, C.E.R.F.A.C.S, *42,av. G. Coriolis,31057 Toulouse Cedex France*.

[CEM18] F. Collino and F. Millot, (2005), Modélisation numérique de phénomènes de résonance électromagnétique, Technical Report TR/EMC/05/23, CERFACS.

[CEM19] F. Collino and F. Millot, (2005), Résolution des problèmes de diffraction d'ondes électromagnétiques avec condition d'impédance par méthodes intégrales, Technical Report TR/EMC/05/53, CERFACS.

[CEM20] F. Collino, (2005), Etude comparative de deux méthodes pour la résolution de la diffraction d'une onde par un obstacle, Technical Report TR/EMC/05/82, CERFACS.

[CEM21] M. Fares, A. Bendali, and D. Clesse, (2005), Etude sur la modélisation de l'alimentation des antennes patch, Technical Report TR/EMC/05/78, CERFACS.

[CEM22] J. WOJAK, (2005), Calcul du rayonnement d'une antenne posee sur une structure à partir de la donnee du champ lointain de l'antenne seule, Technical Report TR/EMC/05/109, CERFACS.

[CEM23] N. Zerbib, F. Collino, and F. Millot, (2005), Etude tridimensionnelle de la condition absorbante adaptative proposée par Liu et Jin pour la résolution des problèmes de diffraction, Technical Report TR/EMC/05/81, CERFACS.

4.4 Proceedings

[CEM24] N. Balin and A. Bendali, (2004), New Numerical Methods for the Prediction of EM Scattering by Electrically Deep Cavities, EEE AP-S/URSI Symposium - Monterey, CA, USA.

[CEM25] N. Balin, (8-10 Novembre 2004), Couplage de Méthodes Exactes et Asymptotiques pour le Calcul de la SER de Cavités Profondes, JINA2004, 13èmes Journées Internationales de Nice sur les Antennes.

[CEM26] N. Bartoli and F. Collino, (2004), Numerical method applied to the antenna-satellite interactions, PIERS - Pisa, Italy.

[CEM27] A. Bendali and M. Fares, (2004), A FETI-like domain decomposition procedure for coupling large scale finite element-boundary element in acoustic scattering, Interdisciplinary Workshop on Developments in Boundary Element Methods for Acoustics and Electromagnetics - University of Reading, UK.

[CEM28] A. Bendali, N. Balin, and N. Zerbib, (2004), Hybridation d'une formulation intégrale pour le système de Maxwell, Congrés International sur les Mathématiques Appliquées à l'Industrie et à la Physique, CIMAIP'04 - El Jadida, Maroc.

[CEM29] A. Bendali, (2004), Presentation of the activities of CERFACS and MIP and scattering by a rough surface, Workshop on Computational Electromagnetism - Oberwalfach, GERMANY.

[CEM30] A. Bendali, (2004), Traitement des points de jonction dans une méthode de décomposition de domaine sans recouvrement, Workshop Méthodes numériques pour les fluides incompressibles - Alger.

[CEM31] F. Collino and F. Millot, (2004), A MLFMM algorithm for solving imperfectly conducting problems, PIERS - Pisa, Italy.

[CEM32] T. Koleck, N. Bartoli, and F. Millot, (2005), Calcul d'interaction antenne/structure par les méthodes multipôles rapides, JOURNEES SCIENTIFIQUES DU CNFRS - Paris.

[CEM33] T. Koleck, N. Mailhat, N. Bartoli, and F. Millot, (8-10 Novembre 2004), Antenna/Structure Interaction Computation by Using Fast Multipole Methods, JINA2004, 13èmes Journées Internationales de Nice sur les Antennes.

[CEM34] N.Zerbib, N. Balin, M. Fares, and F. Millot, (2005), Domain decomposition method for electromagnetic scattering by electrically deep cavities, Waves, Providence, USA.

[CEM35] N. Zerbib and A. Bendali, (2005), Méthodes de décomposition de domaine pour le couplage Antenne-Satellite, JOURNEES SCIENTIFIQUES DU CNFRS - Paris.

[CEM36] N. Zerbib, A. Bendali, and M. Fares, (2004), Application of the fast multipole method and a new procedure for the computation of CFIE matrices to a hybrid Finite element-boundary element solution of an electromagnetic scattering problem, Developments in Boundary Element Methods for Acoustics and Electromagnetics - University of Reading, UK.

4

Climate Modelling and Global Change

1 Introduction

Olivier Thual

Nine projects, active for the “Climate Modelling and Global Change Team” (GLOBC) during at least part of the 2004-2005 two year period, are described in this report.

The first three projects have been sustained by the “Climate” Group made of two researchers (L. TERRAY and C. CASSOU), two reasearch engineers (S. VALCKE and E. MAISONNAVE) and several post-doc or PhD students. There are described in the three following sections and are entitled :
– Climate variability and predictability
– Climate change and related impacts
– The OASIS coupler and its applications
This group of projects is characterized by a high level research on a large scope of actual topics on climate modelling. The continued development effort of the OASIS coupler is pursued through the PRISM project which has become a European platform for climate modelling.

The following four projects have been sustained by the “Data Assimilation” Group, made of three researchers (A. WEAVER, Ph. ROGEL and S. MASSART), three research engineers (Th. MOREL, S. BUIS and N. DAGET) and several short term engineers or PhD students. There are described in the four following sections and are entitled :
– Oceanic data assimilation for climate studies and seasonal prediction
– Data assimilation for atmospheric chemistry
– Data assimilation for nuclear plant modelling
– The PALM coupler
During the 2004-2005 period, the first project has focused on the oceanic data assimilation aspects while the seasonal prediction topic has been merged within the “Climat Group”. Recently, the project on “atmospheric chemistry” has moved to the new “Aviation and Environnement” team since it was mature for a further expansion. Thus, the “Data Assimilation Group” is now combining a high level scientific activity on oceanic modelling, involvement with the application of data assimilation approaches in several domains (neutronics, hydrology, ...) and development of generic software (PALM).
There are strong connections between these two groups of projects. The Climate group uses and validates the oceanic analysis of the Data Assimilation group through several experiences, which, in return, provide useful feed-backs. Both groups also interact strongly with the software development project from which the PALM and OASIS couplers serve a large community of users in the world.

Until recently, a project on “Synthetic Aperture Imaging” has been hosted in the framework of the GLOBC team. It is described in a section entitled :
– SMOS mission
Interesting exchanges between this project and the other ones have happens, such a better knowledge of the sea surface salinity data which will be produced by the SMOS mission.

The last project corresponds to development activities which are directly included in the MERCATOR project which deals with operational oceanography. The CERFACS contribution to this project is described in the last section and is entitled :

– The CERFACS contribution to the MERCATOR project

2 Climate variability and predictability

2.1 Introduction

The Earth climate is rapidly changing in response to a wide range of anthropogenic forcings. To assess confidence in the detection, attribution and prediction of this global and regional change (See Chapter 3), deeper understanding of the intrinsic variability and stability properties of the main climate variability modes is needed. The analysis of the physical mechanisms associated with seasonal to decadal natural climate fluctuations also appears as a prerequisite step to improve seasonal forecasts and to understand the shortcomings of current prediction systems.

Within this global framework, the scientific objectives of the Climate Variability and Predictability project, in very close collaboration with the Climate change and related impact project, are as follows :

- To advance understanding of climate processes underlying the natural variability of the main climate modes, such as the North Atlantic Oscillation (NAO), the decadal Atlantic interhemispheric tropical oceanic mode etc. Emphasis is laid on spatio-temporal scale interaction from synoptic dynamical entities (weather regimes for instance) to multi-decadal patterns (rainfall fluctuations of the West African Monsoon etc.).
- To explore the multiple sources of low frequency predictability with a specific focus on an extended European domain. A special attention is devoted to the tropical-extratropical connections, since most of the predictability is expected to rise from a broad tropical band at least at seasonal to interannual timescales.
- To participate tp the evaluation of the representation in models of the mechanisms underlying potential long range forecasts or responsible for observed low frequency variability.
- To provide a solid physical background in the interpretation of any climate change signals attributed to anthropogenic forcings.
- To assess the risk of abrupt climate change, with emphasis upon the possible collapse of the thermohaline circulation due to its own natural variability.

Over the past two years, the main activity has been devoted to the analysis and the understanding of the tropical-extratropical connection associated with the exceptionally hot summer of 2003 in Europe. Observations and model experiments have been combined to extract a robust forcing of the tropical Atlantic climate on the variability of the European heatwaves occurrence. The low frequency variability of the West African monsoon (WAM) system has been also studied to better understand the steady decrease of the Sahelian precipitation from the 1960's to the mid-1990's, and its recent recover. The low-frequency variability of the NAO has finally been investigated. The oceanic re-emergence processes at work at the beginning of winter is found to contribute to the winter-to-winter persistence of the same NAO phase. At longer timescale, a connection is found between the steady warming of the Indian Ocean and the upward NAO trend.

2.2 Tropical – Extratropical connections (C. Cassou, L. Terray, A. Phillips, E. Sanchez, M. Minvielle, E. Maisonnave)

2.2.1 Tropical Atlantic influence on European heatwaves (C. Cassou, L. Terray, A. Phillips, E. Sanchez)

The North Atlantic-European dynamical signature of the summertime atmospheric variability is examined through a non-linear approach known as cluster analysis (Cassou et al 2004). This method based on classification techniques seeks preferred and/or recurrent quasi-stationary atmospheric patterns or weather regimes that are spatially well defined and limited in number. The partition algorithm we applied here to NCEP reanalysis data identifies four summertime regimes that are about equally excited (Fig. 2.1). The relationships between station-based temperature data for 1950-2003 and regime occurrence indicate that European heat waves can be associated with the *Blocking* and *Atl.Low* regimes. These two regimes clearly favor extreme warm days, whereas *NAO−* and *Atl.Ridge* clearly inhibit their occurrence.

We then analyze the possible driving impact of the alteration of the 2003 Atlantic Inter Tropical Convergence Zone upon the frequency of the North Atlantic regimes using the NCAR CAM2/CLM2 atmospheric/land models, coupled to a simple mixed layer oceanic component. Convective heating anomalies derived from the observed 2003 anomalous Outgoing Longwave Radiation (proxy for convection) are imposed in the atmospheric model in the the sole tropical Atlantic band. Based on model outputs, we present evidence that during the record warm summer of 2003, the excitation of the *blocking* and *Atl.Low* regimes was significantly favored by the anomalous tropical Atlantic heating related to wetter-than-average conditions in both the Caribbean basin and the Sahel.

Given the persistence of tropical Atlantic climate anomalies, their seasonality and their associated predictability, the suggested tropical-extratropical Atlantic connection is encouraging for the prospects of long-range forecasting of extreme weather in Europe. The knowledge of such a physical mechanism and the strong similarities between conditions of late spring of 2003 and late spring of 2005 in the tropical Atlantic helped us predicting a warmer-than-average summer for 2005, in collaboration with Météo-France.

2.2.2 Indian Ocean warming influence on the upward trend of the NAO (M. Minvielle, C. Cassou, L. Terray, E. Maisonnave)

The low-frequency wintertime NAO is characterized by a significant upward trend, especially over the last two decades. Preliminary results from literature have suggested a possible connection between the steady warming of the Indian Ocean and the NAO trend. Several mechanisms have been proposed but none of them were carefully tested.

Within the VIMA PNEDC project, we used the ARPEGE model and conducted two ensembles of 20-year forced simulations. Those only differ by their SST forcing over the Indian Ocean corresponding, in the first set, to the climatological conditions over the 1950-1975 period (cold Indian), and, in the second set, to those over 1976-2001 (warm Indian). Contrasting the two periods, the model response strongly projects on the positive phase of the NAO in the Northern Hemisphere in winter and confirms the hypothesis obtained from observations for the trend.

We show that the tropical-extratropical connection is explained in the model by the alteration of the local Pacific Hadley cell leading to changes in the jet position and stormtrack activity over the entire North Pacific. The latter is associated with a planetary anomalous Rossby wave extending downstream up to the North Atlantic following the upper-tropospheric jet wave guide. The North hemispheric changes associated with the Indian Ocean warming therefore leads to the strengthening of the wintertime subtropical Highs and to the deepening of a broad Icelandic Low.

When comparing model results from the forced idealized experiments with those from IPCC scenarios, we suggest that the observed Indian Ocean warming could be a signature of the anthropogenic forcing over the last century or so. Projections for the current century based on classical scenario show a continuation of the Indian Ocean warming and consistently, a clear dominance of the positive phase of the NAO. Note that a careful investigation of the coupled models shows a clear interaction between the model mean biases and its simulated variability. The Indian-northern hemisphere connection is intrinsically dependent on the tropical mean state, which appears crucial to correctly simulate the midlatitude changes. Such a remark has a strong impact for decadal time-scale prediction, whose skill will clearly depend on the ability of the model to get a correct mean climate state for good reasons.

2.3 Role of the re-emerging SST anomalies on the winter-to-winter persistence of the NAO (C. Cassou, C. Deser, M. Alexander)

In the extratropics, thermal anomalies stored in the deep winter oceanic mixed layer persist at depth through summer where they are insulated from surface fuxes. They become reentrained back in the deepening mixed layer during the following winter and their reemergence explains part of the winter-to-winter persistence of the extratropical Sea Surface Temperature anomalies. The forcing of the oceanic reemergence on the atmosphere is investigated here in the North Atlantic using a simplified coupled model (Atmospheric Global Circulation Model coupled to a Mixed Layer Ocean Model and to a thermodynamical ice component). Such a model configuration takes the vertical oceanic processes into account and correctly represents the physics of the ocean-atmosphere interaction at the interface. Estimation of the thermal anomalies created by late-winter/early spring atmosphere and stored below the hightly stratified summer thermocline are obtained from a long control simulation. They strongly project on the so-called North Atlantic tripole associated with the phase of the NAO.

These thermal anomalies are applied below 40meter depth and north of 25N, in the oceanic initial conditions of a 60-member ensemble of 1yr integration starting in August. We show that their reemergence occurs in November/December and has a significant impact on the model atmosphere. The reentrainment of the subsurface oceanic anomalies tends to favor the same phase of the NAO which created them during the previous winter. The simulated atmospheric response would confirm the hypothesized role of the oceanic reemergence in the weak but significant year-to-year persistence of the wintertime NAO. Model results suggest a probable role of the high-frequency atmospheric eddies. Storminess is clearly modify in the perturbed ensemble and eddy-mean flow interactions would explain the large-scale and persistent atmospheric response to the extratropical North Atlantic reemergence.

In terms of seasonal to interannual predictability, our study suggests that the model should be able to correctly simulate the reemergence of the midlatitude SST anomalies. It highlights the need for decent oceanic assimilation both in the Tropics as known for a few years now, but also for the midlatitudes.

2.4 Influence of global ocean SST forcing upon the low frequency variability of the West African Monsoon (C. Caminade, L. Terray, E. Maisonnave, C.Cassou)

The low frequency variability of the WAM is studied using a new ensemble of SST-forced ARPEGE simulations integrated from 1901 to 1999. The simulated variability of the WAM is first separated into internal (noise) and external parts (signal forced by SST) using the traditional analysis of variance method. At interannual timescale, the SST-forced fraction of variability captures about 30% in average and slightly more for decadal fluctuations. The model exhibits a good skill at decadal scale as it correctly reproduces the observed shift between the wet period in the $1950-60$'s and the very dry one in the $1970-90$'s. The associated SST pattern is remarkably similar to the one deduced from the observed data. It is very close to the so-called Global Extratropical mode, which captures the multidecadal balance in SST between the two hemispheres, with maximum loading in the Indian and Southern Atlantic basins.

At interannual timescale, lagged singular value decomposition analysis further allows us to document the dominant influence of El Niño Southern Oscillation. The role of the mediterranean SSTs is also suggested : warm conditions there are associated with stronger monsoon due to a significant increase of the moisture advection by the Etesian northerly wind. A significant link between the so called Atlantic Niño and the guinean coast increase has been highlighted for precipitation. The latter however appears overestimated in the model. It might be related to the artificial decoupling simulated in the model between the Western African Monsoon system and its easward extension (Ethiopian and Soudan regions). Rainfall over these areas seems to be too much connected to the broad Indian Monsoon system. Again, the mean bias of the model interact with its variability and very likely degrade its forecast skill at low frequency.

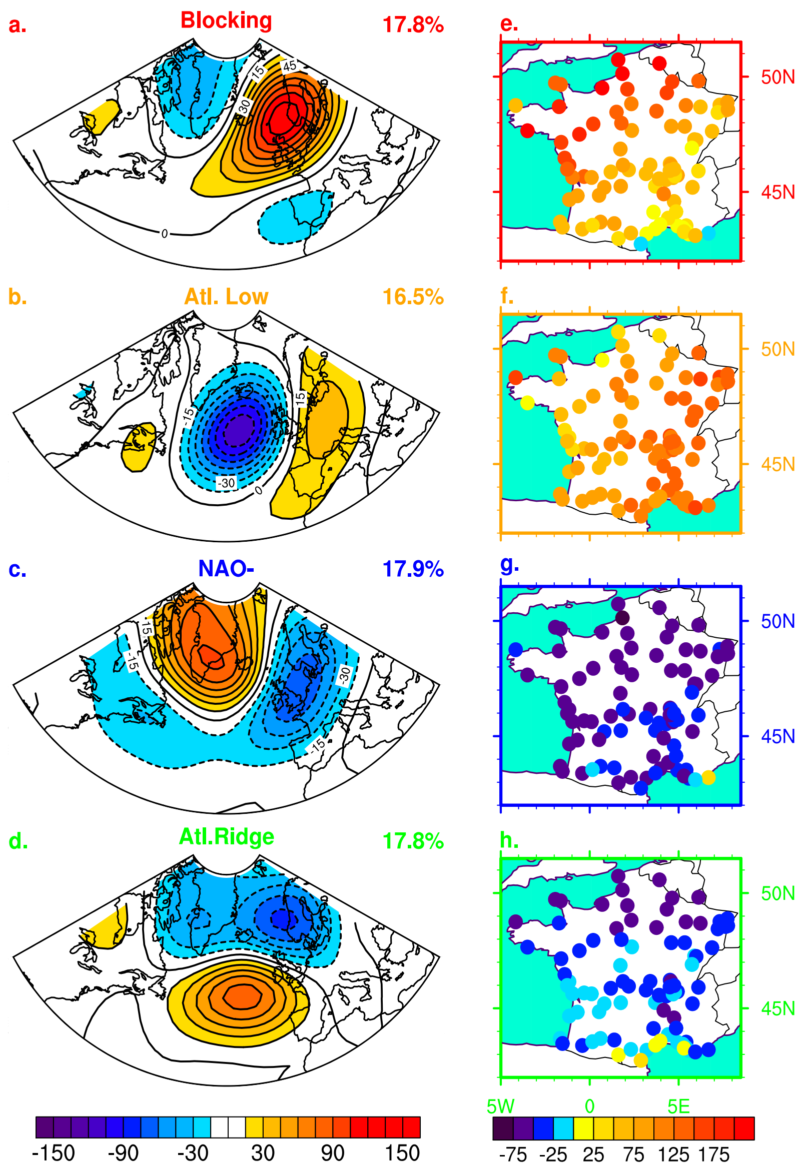

FIG. 2.1 – **(abcd)** Summer weather regimes of anomalous geopotential height at 500 hPa (Z500) estimated from the National Centers for Environmental Prediction-National Center for Atmospheric Research (NCEP-NCAR) reanalysis product over 1950-2003. Daily summer maps (from June 1^{st} to August 31^{st}) are used for decomposition and the geographical domain is limited to [90^oW-30^oE/20^oN-80^oN]. Contour interval is 15m. **(efgh)** Relative changes (%) in the frequency of extreme warm days for each individual regime. Color interval is 25% from -100% to 200%, red above (maximum equal to 233%). As an example, 100% corresponds here to the multiplication by 2 of the likelihood for extreme warm days to happen.

3 Climate change and related impacts

3.1 Introduction

The world climate is currently changing due to the human-induced increase in the atmospheric concentrations of CO_2 and other greenhouse gases. In order to optimally define the adaptation and mitigation strategies needed to cope with the potential impacts of this expected climate change, a deeper understanding of the intrinsic variability of the climate system is needed to assess confidence in the detection, attribution and prediction of global and regional climate change due to anthropogenic causes.
Within this global framework, the scientific objectives of the Climate Change and Related Impacts project are as follows :

– To detect, attribute and describe anthropogenic climate change on global to regional scales with a focus upon Europe and West Africa, using high resolution atmospheric models and long-term, high quality, observations.
– To assess the impacts of anthropogenic climate change at regional scale with specific interest in the changes of extreme events distribution and hydrological cycle properties, with a focus upon Europe and West Africa, and to provide uncertainty bounds in future climate projections.
– To assess the risk of abrupt climate change, with emphasis upon the possible collapse of the thermohaline circulation due to anthropogenic forcing and its regional impacts particularly over Europe.

For the past two years, work has concerned essentially the first two objectives. The main activity has been devoted to the development of the methodological and numerical framework related to the DISCENDO project on Detection and Attribution studies at the regional scale. Another major activity was the study of extreme events distribution and its potential changes in the future climate perturbed by anthropogenic forcing. This work is part of the GICC IMFREX project. Some preliminary assessment of the mean and seasonal changes to the West African Monsoon system due to the anthropogenic forcing has been performed. Finally some preliminary work has also started to develop a new downscaling approach for the studies of hydrological cycle changes at the regional and sub-regional scale.

3.2 Detection and Attribution of Climate Change at the Global and Regional Scale : the DISCENDO project(M. Allen, C. Cassou, J.M. Epitalon, V. Lorant, E. Maisonnave, D. Stone, L. Terray)

The main objective of the DISCENDO project is to develop and validate an original methodology to carry out detection and attribution studies at the regional scale. The impact of global warming on society is largely determined by spatial scales far smaller than those considered in current detection and attribution studies. It is thus very important to begin to focus on sub-global to regional scales. The approach followed in DISCENDO to assess the regional influence of external forcings is to apply the detection and attribution formalism (based on the optimal fingerprint methodology, which can be seen as a simple multiple linear regression scheme) to observations in specific regions (on continental scale, Europe and West Africa ; on smaller scale, France). This choice is based on the existence of high-quality and homogenized observed datasets for these regions in terms of temperature and precipitation. The next ingredient in the detection process is the estimation of the signal due to the external forcing. In DISCENDO, the different signals are estimated with ensembles of simulations performed with a variable resolution of the ARPEGE atmospheric general circulation model (AGCM) with high horizontal resolution over the region of interest. This allows for a better representation of the regional climate and its sensitivity. These various ensembles of simulations are all forced with observed SST for the 1950-2000 period, but differ in terms of the applied external forcings. The aim of the AGCM-based approach is to test the null hypothesis that the observed climate change can be explained by a combination of variations due to changing SSTs and seaice extents and internal atmospheric variability alone. This is basically done by showing that the differences between the ensembles are unusual in a statistical sense, by comparing them against the model intrinsic variability or noise. As the noise is estimated by the intra-ensemble variance, the use of the ensemble technique is a further vital property of the methodology. The effect of the design on the signal-to-noise ratio is crucial as it determines if the AGCM-based is more efficient to detect a climate change signal. The main point here is the idea that the noise is significantly reduced in the AGCM-based approach as the oceanic component of natural variability (noise) has been converted to a common signal (the one due to the SST forcing).

To estimate the different external forcings, we have performed six ensembles of simulations with the variable resolution version of the ARPEGE model at T106 spectral truncation for the 1950-1999 period. For the case of Europe, four different ensembles have been realized while only two have been performed for the case of West Africa (CTRL and GS-Nat). For Europe, these ensembles are defined as follows :

– CTRL(6 members) : the simulations are forced with observed SSTs and fixed (to their 1950 values) greenhouse gases (GHG) and sulfate aerosols (SUL) concentrations. The solar forcing (SOL) is also constant and fixed to the 1950 value.
– G(6 members) : forced with observed SST and GHG ; SUL and SOL fixed to their 1950 values.
– GS(6 members) : forced with observed SST, GHG and SUL ; SOL fixed to the 1950 value
– GS-NAT(4 members) : forced with observed SST, GHG, SUL and SOL

For West Africa, both CTRL and GS-NAT have been performed with 4 members. The model uses a different grid with the maximum in the Gulf of Guinea in order to have high resolution over the tropical Atlantic and West Africa. The mean state and seasonal cycle of the two versions (Europe and West Africa) have been extensively validated by comparing to observed (mainly CRU) and reanalysis (for the dynamical variables) datasets. Furthermore, we have developped a Live Access Server (LAS) to access through the web the various simulated datasets performed within the framework of the DISCENDO project. In addition to the partners of the DISCENDO project, this server will be opened to the french and international AMMA project community.

The various ensembles provide signal estimates for the relevant combination of forcings by using the ensemble means of each ensemble (the role of each individual forcing can then be derived with a linearity assumption). The estimation of the covariance matrix of atmospheric internal variability is performed by using the intra-ensemble variability of the CTRL and G ensembles simulations. The other part of intra-ensemble variability is used to carry out the consistency checks between the residuals of the regression algorithm and internal atmospheric variability. As a first detection study, the case of the summer T_{min} over France has been considered. The observed dataset is a high-quality and homogenized dataset of 91 meteorological stations over France. As a first step, we use a time-evolving signal pattern consisting of decadal averages of minimum temperature anomalies relatively to the 1961-1990 climatology. The detection analysis shows that the combined influence of the SST, GHG and SUL signals can be detected at the 95% level in the observed T_{min} dataset over France. The dominant part of the SST signal seems to be associated to a low frequency mode called the Atlantic Multi-decadal Oscillation (AMO). The anthropogenic signals strongly emerge from the internal atmospheric variability in the last two decades. Next steps include the investigation of the physical mechanisms underlying the detection of the three signals as well as the application of the detection algorithm to other seasons, variables and regions.

3.3 Influence of the anthropogenic forcing upon the West African Monsoon system : mean climate and seasonal cycle changes (C. Caminade, C. Cassou, E. Maisonnave, L. Terray)

The impact of increased greenhouse gases (GHG) and aerosols concentrations upon the West African monsoon (WAM) has been investigated for the late 21^{st} century period using the Météo-France ARPEGE-IFS high-resolution atmospheric model. Perturbed (2070-2100) and current (1961-2000) climates are compared using the model in time-slice mode. The model is forced by global sea surface temperatures (SST) provided by two transient scenarios performed with low-resolution coupled models and by two GHG evolution IPCC scenarios, SRES-A2 and SRES-B2. Comparing to reanalysis and for observed data sets, the model is able to reproduce a realistic seasonal cycle of WAM despite a clear underestimation of the African Easterly Jet (AEJ) during the boreal summer. Mean temperature change indicates a global warming over the continent (stronger over North and South Africa). Simulated precipitation change at the end of the 21^{st} century shows an increase in precipitation over Sudan-Sahel linked to a strong positive feedback of surface evaporation. Along Guinea Gulf coast, rainfall regimes are driven by large-scale advection humidity process. Moreover, results show a mean precipitation decrease (increase) in the most (less) enhanced GHG atmosphere over this region. Modification of the seasonal hydrological cycle consists in a rain increase during the monsoon onset. While the linear links between precipitation variability and SST modes are not significantly modified in the moderate emission scenario experiment, an only dependence to the Atlantic basin is shown in the most enhanced GHG atmosphere. Enhanced precipitation over Sahel is linked to large-scale circulation changes, namely a weakening of the AEJ and an intensification of the Tropical Easterly Jet.

3.4 Study of extreme events changes due to anthropogenic forcing based on the weather regime approach (C. Cassou, G. de Coetlogon, A. Joly, E. Maisonnave, E. Sanchez, L. Terray)

Increase in concentration of greenhouse gas has been shown to produce non negligible shifts in the global mean climate. An important question is whether modifications in the statistical properties of climate extremes are also to be expected in the future climate perturbed by the anthropogenic forcing. These changes would have a profound impact on human society and natural environment as weather hazards can cause tremendous economic and life losses. We have investigated the links between the large-scale environment and extreme events with a new approach based on the concept of weather regimes. This work was part of the GICC IMFREX project on extreme events. The idea is to relate the extreme events occurrence to their specific large-scale environment and to use the latter as a predictor of the former in climate experiments such as scenarios of the 21^{st} century. The relationships between the large-scale weather regimes and local climate extremes have been established for a region covering France. The weather regimes (at the daily timescale) have been derived from the ERA40 reanalysis time series of the geopotentiel at 500 hPa using the k-means algorithm. The local climate variables (minimum and maximum temperature as well as precipitation) come from an extended dataset (SQR) provided by Météo-France which covers the entire ERA40 period. The summer and winter seasons are both considered separately. Winter is defined by the period from October 15th until April 15th while summer represents the standard June-July-August (JJA) period. The determination of extreme temperature and precipitation events occurrence is simply based upon exceedence of a threshold value given by the 95^{th} (warm or heavy precipitation days) or 5^{th} (cold days) quantile of the distribution function defined for each calendar day. The daily regime partition is optimal with the four classical regimes for both summer and winter : Greenland Anticyclone(GA), Atlantic Ridge(AR), Blocking(BL) and Zonal(ZO). The residence frequency indicates that the ZO regime is the dominant one in winter (30%) while the partition is almost uniform in summer. In summer, the patterns are very similar to the winter ones with slight differences regarding the location and amplitude of the anomaly centers. Trends in weather regime occurrence are significant only in the cold season and suggest a strong increase of the ZO regime occurrence during the last 30 years. This strong rise is linked to the observed tendency towards high North Atlantic Oscillation index values for the same period. During winter, the risk of cold days increases markedly (in particular for Northern France) when GA and BL characterize the large-scale environment. The ZO regime is associated to a reduced risk of cold days over all locations. In summer, the risk of high temperature episodes is enhanced(decreased) with the presence of the BL and ZO (GA and AR) regimes. For precipitation, enhanced occurrence of intense precipitation episodes are associated to the presence of GA (southern France) and ZO (western France) regimes. All these relationships exhibit very distinct patterns reflecting the strong influence of the large-scale flow upon extreme event occurrence at the local scale. Finally, simple linear multiple regression can then be used To build a relationship the number of extreme events for one season and the regimes occurrence during the same period. The explained variance is usually around 20% and can be as high as 45% depending on location, season and considered climate variable (Fig. 3.1). In order to suggest the possible changes in extreme events occurrence due to anthropogenic forcing, we have used two ensembles of time slice experiments for the current and future climate respectively. The experiments were performed by M.Déqué at CNRM within the PRUDENCE european project. They use the variable resolution of the ARPEGE AGCM at T106 spectral truncation. The first ensemble (CTRL) includes three 40-year (1960-1999) simulations forced with observed SST and GHG concentrations. The second ensemble (scenario-SCEN) includes three 30-year (2070-2099) simulations forced by the predicted SST changes (from the HadCM3 coupled model forced by the A2 IPCC-SRES scenario) combined with observed SST for the period 1960-1989, and the A2 IPCC-SRES scenario. Under the assumption that the regime spatial structures in the future climate remain identical to those of the current climate, one may obtain the regime residence frequency for both CTRL and NCEN experiments by projecting modelled daily atmospheric maps onto an Empirical orthogonal Function (EOF) space derived from the reanalysis. Each modelled day can then be attributed to a given observed weather regime by minimization of a similarity criterion in the reduced phase space (the first 10 principal components of the EOF analysis). The model regime results for the CTRL ensemble compares very well with the reanalysis in terms of structure and residence frequencies. Analysis of the NSCEN ensemble shows large changes for both cold and warm season. For the cold season, there is a strong increase in the occurrence of the ZO and BL regimes and a moderate(dramatic) decrease for the AR(GA) regime. For the warm season, the BL regime becomes the dominant one while the GA and AR regimes are almost absent in the future summers. Then, these modelled changes can be used as the predictors for the multiple regression scheme described previously in order to quantify the changes in extreme events distribution linked to modifications of weather regime occurrence. These prove non negligible as for instance, changes in regime occurrence for the summer period indicate an increase of 5 to 10 warm days in the northwest of France(Fig. 3.1). Direct estimation from model results is on the order of 25 days meaning dynamical changes can be responsible up to 20 per cent on average of the extreme warm event distribution changes.

Finally, we have also investigated the role of regime transition upon the occurrence of extreme events. We have shown that the large-scale circulation patterns associated with intense precipitation episodes (IPE) over a specific domain (in this case, western France) can be identified using clustering algorithms applied to a set of daily maps of 500 hPa geopotential height selected on the basis of precipitation threshold exceedence. In the case of western France, the large scale circulation pattern linked to the IPE occurrence displays a strong anomaly over Great Britain. Furthermore, this pattern corresponds to the structure observed during the transition from ZO to GA standard weather regimes. Moreover, this is the least likely transition from the ZO regime, suggesting potential links between atmospheric dynamics and the occurrence of extreme precipitation events.

3.5 Development of a new methodology for the downscaling problem : application to hydrological changes upon the Seine watershed due to anthropogenic forcing (J. Boé, F. Habets, E. Martin, L. Terray)

In the context of enhanced anthropogenic forcing due to the rise in greenhouse gases emission, the question of water cycle changes is of primary importance both at the global and regional scales. To quantify the impacts of hydrological changes at the watershed scale, one must first solve the resolution problem. While the standard coupled ocean-atmosphere general circulation models (GCM) typically have a horizontal resolution on the order of 300 kms, hydrometeorological models require forcing data with a much higher resolution (10 kms or less). This is the well-known downscaling problem. Two main approaches exist : the dynamical and the statistical downscaling techniques. Dynamical downscaling is a model-based approach that allows to reach sub-GCM scales by using a finer-scale (50 kms) limited area model (LAM) within a GCM. Statistical downscaling is based on the following paradigm : the regional climate is dependent on two factors : the large-scale environment, reasonably described by climate models, and small-scale features (land use, topography, land sea distribution) which are not adequatly resolved in GCMs. Empirical relationships linking large-scale variables (predictors) and local or regional parameters (predictands) must then be derived for the current climate using observed and/or reanalysis datasets. These relationships can then be applied to the large-scale variables changes in future climate conditions to assess modifications of the regional climate. These two approaches rely on the following hypothesis : empirical relationships and physical parameterizations derived for the present climate must remain valid under a modified climate (low frequency natural variability or anthropogenic climate change). We are currently developping an hybrid dynamical/statistical methodology to solve the downscaling problem related to the estimation of high-resolution forcings required for a future study of the impacts of climate change on the Seine basin hydrology. The hydrometeorological model is the Safran-Isba-Modcou model developped at Météo-France which requires atmospheric forcing data at a 8-km resolution. Previous work performed within the project has shown that high horizontal resolution may be necessary to achieve reliable projections of anthropogenic climate change upon european climate, in particular the ones related to circulation changes. Thus, the dynamical part of the methodology relies upon the use of a variable resolution model (with high resolution over the region of interest, 50 kms) to simulate the predictors (large-scale circulation parameters, 500 hPa height or mean sea level pressure) and their changes in the modidied climate. The statistical part relies upon the weather typing (or regime) approach. The approach is based on a bottom-up strategy where one starts from regional climate properties to establish discriminative daily weather types for local variables (such as temperature or precipitation). Moreover, possible changes in intra-type variations in surface climate are accounted for by using the phase space distances to the weather types within a multivariate regression procedure associated to a resampling strategy. The methodology has been validated using the ERA40 reanalysis fields as predictors. The construction period of the statistical relationships is based on a 17-year period (1985-2002) and the validation is performed on an independent dataset over the full ERA40 period (1957-2002). The new methodology has been shown to be globally more performant than the well known analog approach. In particular, it is able to successfully reproduce the daily statistical properties of precipitation (including a good representation of the persistence properties of climate variables). Furthermore, and in contrast with the analog method, low-frequency variations of downscaled temperature and precipitation are close to the obverved ones. Next steps include sensitivity tests to various options in the statistical technique (metric used, weather typing method, etc ...) as well as an indirect validation applying the downscaled forcing to the Safran-Isba-Modcou model for the 1985-2002 period.

[1] U. Ulbrich and M. Christoph, (1999), A shift of the NAO and increasing storm track activity over Europe due to anthropogenic greenhouse gas forcing, *Clim. Dyn.*, **15**.

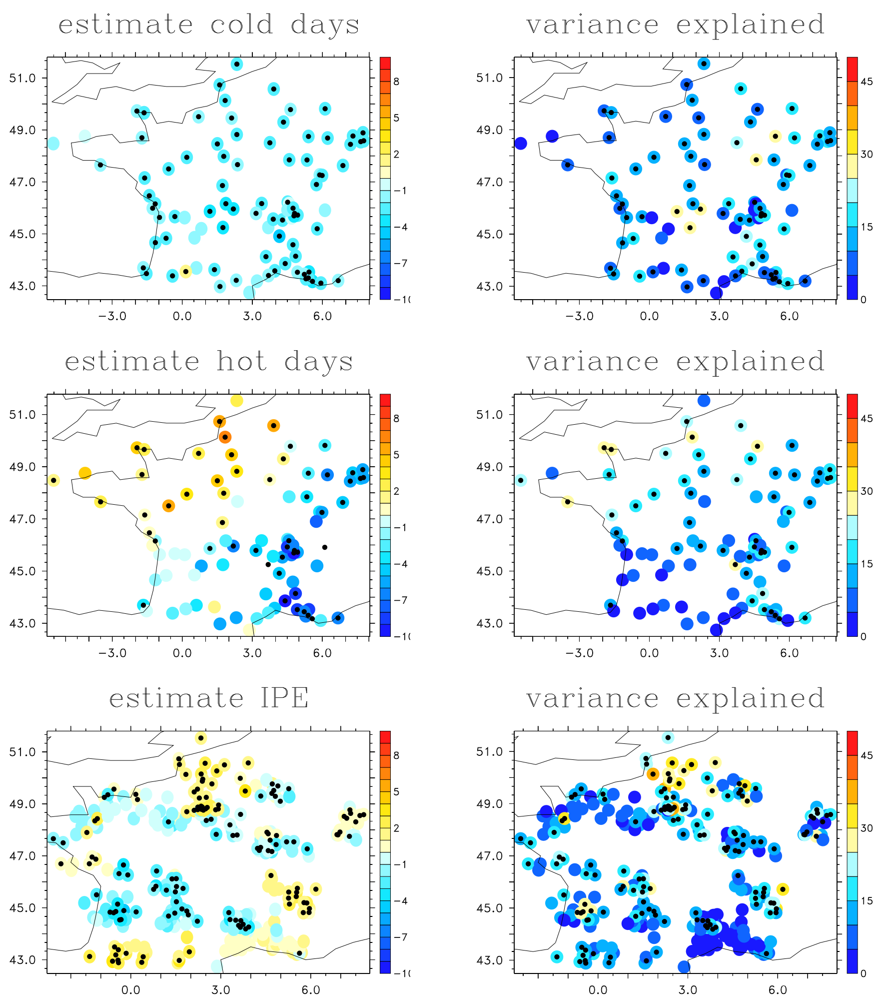

FIG. 3.1 – **Left** Changes in the number of cold, hot and intense precipitation days between the control (CTRL) and scenario (NSCEN) experiments due to the modifications of weather regime occurrence and obtained by multiple regression analysis. **Right** The percentage of variance (in %) explained by the regression model. Stations where the multiple regression is statistically significant are indicated by a black dot.

4 The OASIS coupler and its applications

Coupling numerical models, i.e. exchange information in a synchronised way between the models, is a central issue in the climate modeling community and in other research fields such as electromagnetism and computational fluid dynamics.

The OASIS coupler is an open source software developed at CERFACS since 1991, used for coupling independent General Circulation Models (GCMs) of the atmosphere (AGCMs), of the ocean (OGCMs), as well as other climate modules (sea-ice, land, hydrology, etc).

Most of the OASIS developments in the last two years was done within the PRISM project [GLO29] and in the framework of the PRISM Support Initiative (PSI). Recognising the need for a shared software infrastructure, the European Network for Earth System Modelling (ENES) organised the PRISM project, which gathered 22 partners and was funded by the European Union under the 5th Framework Programme (FP5) in 2001-2004 for 4.8 MEuros. In October 2004, a core group of PRISM participants decided to sustain the FP5 PRISM developments, investing their own resources into a shared software infrastructure, the PRISM Support Initiative (PSI). Today, the partners (CERFACS, CNRS, NEC-CCRL, MPI M&D, UK Met Office, and ECMWF) and associate partners (MPI-Met, SMHI, CGAM, and computer manufacturers CRAY, NEC-HPCE, SGI) are planning to invest a total of about 8 persons-years per year for the next 3 years in the maintenance, support, and further development of the PRISM software.

OASIS is therefore at the core of the PRISM standard software infrastructure used to assemble, run and post-process Earth System models. During the PRISM project, the OASIS3 version of the coupler, product of about 15 years of evolution in CERFACS, was finalized ; its last release is available since December 2004 [GLO99]. As the climate modelling community is progressively targeting higher resolution climate simulations run on massively parallel platforms with coupling exchanges involving a higher number of (possibly 3D) coupling fields at a higher coupling frequency, a new fully parallel coupler, OASIS4, has also been developed within the PRISM project [GLO60]. The first official OASIS4 version was released in November 2004 [GLO101].

Each version of the OASIS3 and OASIS4 couplers is composed of a Driver which monitors the coupled system, a Transformer which performs the interpolation, and a PRISM System Model Interface Library (PSMILe) which is used in the component models to communicate with the rest of the coupled system and which also includes a file input and output (I/O) library. The OASIS4 PSMILe Application Programming Interface (API) was kept as close as possible to OASIS3 PSMILe API ; this should ensure a smooth and progressive transition between OASIS3 and OASIS4 in the climate modelling community.

4.1 The OASIS3 coupler

4.1.1 Development and maintenance (S. Valcke)

During the last two years, different versions of the OASIS3 coupler (“prism_2-1”, “prism_2-2”, “prism_2-3”, and “prism_2-4”) were released within the PRISM infrastructure. The main improvements included in the OASIS3 coupler during that period are :

– Driver modification to support the new grid writing PSMILe routines ;
– Driver modifications to output fully NetCDF CF-compliant files (variable name and units, grid definition, etc.) ;

– Transformer modification to support interpolation of a variable having a time dimension (in interpolator-only mode) ;
– Revalidation of SIPC (Unix System V Inter Process Communication) technique ;
– Interfacing with the GOSSIP communication layer based on Unix sockets from Direction de la Recherche en Météorologie du Canada ;
– Porting and testing of OASIS3 and associated toy model on IBM Power4 ;
– Appropriate treatment of vector fields ;
– Writing of a User Guide for each OASIS3 version.

4.1.2 OASIS3 Users and applications (S. Valcke)

– Today, OASIS is used by about 15 climate modelling groups in France, in other European countries, in the USA (the International Research Institute for Climate Prediction, the NASA Jet Propulsion Laboratory, etc.), in Japan on the Earth Simulator super computer (the Japan Marine Science and Technology Center), and in Australia (the Bureau of Meteorology Research Center and the University of Tasmania).
– In the last few years, the OASIS coupler has been regularly used by our team and at Centre National de Recherches Météorologique (CNRM) of Météo-France to assemble various Coupled GCMs (CGCMs), based on the atmospheric model ARPEGE (CNRM, Météo-France) and on the ocean model OPA (Laboratoire d'Océanographie Dynamique et de Climatologie, LODYC, CNRS), which were validated and exploited through a series of climate experiments as part of the PREDICATE and DEMETER European projects.
– In 2004, active user's support was provided to the PRISM Community using the OASIS3 coupler for the PRISM demonstration runs in 2004 : different ocean models (ORCA2LIM from LODYC, MPI-OM from the MPI-Met, and a toy ocean component) and atmosphere models (ARPEGE V4 from Météo-France, ECHAM5 from the MPI-Met, LMDZ from the Laboratoire de Météorologie Dynamique, HadAM3 from the UK Met Office, and a toy atmosphere component) were combined with OASIS3 and run on different platforms (NEC SX6, SGI IRIX4, VPP5000, IBM Power4).
– Finally, OASIS3 is currently being used in our team to set-up a new CGCM based the atmospheric model ARPEGE V4 and the oceanic model OPA9 in the framework of the FP6 projects ENSEMBLES and DYNAMITE.

4.2 The OASIS4 coupler

4.2.1 Development (S. Valcke, D. Declat)

The development of the fully parallel OASIS4 coupler, which specifications were established in 2003, summoned up an important part of coupler development efforts in the last two years. The first official OASIS4 version was delivered in November 2004. The following aspects were developed :
– Development of OASIS4 Driver :
  – in OASIS4, the XML standard is used to configure the coupled model (Specific Coupling Configuration -SCC- and Specific Model Input and Output Configuration -SMIOC- files) ; the "SASA" tools were developed (in collaboration with Institut Pierre-Simon Laplace, IPSL) and used to access the SCC and SMIOC configuring information ;
  – analysis of this XML information, translation into coupler structures, and transfer to component model PSMILes.
– Development of OASIS4 Transformer :
  – Development of PSMILe-Transformer interface routines (transfer of neighborhood search results, coupling fields, etc.) ;
  – Transformer parallelisation ;

  - Support of 3D linear interpolation.
- Development and finalization of OASIS4 PSMILe (in collaboration with NEC Europe Ltd C & C Research Laboratories, NEC-CCRL) :
  - Finalization of PSMILe Application Programming Interface (scale factor definition, mesh corner definition, etc.) ;
  - Interaction with the Driver to get the XML configuring information ; internal use of this information to perform appropriate coupling actions ;
  - Implementation of internal calendar routines to perform coupling and I/O action (put and get) at appropriate time ;
  - Development of PSMILe calendar routines to be used by the model (calculation of new date, inquiry of calendar type, etc.) ;
  - Completion of 3D linear and 2D1D linear parallel neighborhood search ;
  - Implementation of PSMILe-Transformer interface routines (transfer of neighborhood search results, coupling fields, etc.) ;
  - Support of coupling restarts.
- Implementation of OASIS4 toy coupled model, tests and debugging.
- Writing of OASIS4 User Guide.

4.2.2 OASIS4 Users and applications

- OASIS4 was first run with different toy models, on different platforms demonstrating its portability and scalibilty : SGI Origin and ALTIX, NEC SX6, AMD Athlon PC-Cluster, and Fujitsu AMD Opteron PC-Cluster.
- A real ocean model MOM4 has also been successfully coupled with toy atmosphere model via OASIS4.
- The Institute for Marine Science at the Research Center for Marine Geosciences (IFM-GEOMAR), is using OASIS4 with pseudo models to interpolate high resolution data onto high resolution model grids.
- Active user support is also currently provided to the FP6 GEMS project community (ECMWF, Météo-France, and Koninklijk Nederlands Meteorologisch Instituut -KNMI) for 3D coupling between atmospheric and chemistry models, and to the Swedish Meteorological and Hydrological Institute (SMHI) for regional coupling.

5 Oceanic data assimilation for climate studies and seasonal prediction

The ocean data assimilation project at CERFACS spans three main research activities : (1) the development of a variational data assimilation system for the OPA ocean general circulation model (a system called OPAVAR) ; (2) the application of OPAVAR to global ocean reanalysis ; and (3) the use of OPAVAR to produce ensembles of ocean analyses for seasonal climate prediction. This chapter summarizes some of the main developments that were made in each of these three areas during the past 2 years.

5.1 Recent developments to the global OPAVAR system (A. Weaver, N. Daget, S. Ricci)

The OPAVAR system was initially developed for a tropical Pacific configuration of OPA. That system has been documented and extensively validated in several studies ([3], [2], [GLO31], [GLO22]). The global OPAVAR system was developed from the tropical Pacific system and adapted to a newer version of OPA (version 8.2). The development of the global system was initiated in the ENACT project (EC-FP5 : Jan. 2002–Dec. 2004) and the first applications of OPAVAR to multi-annual global ocean reanalysis were performed in ENACT, as described in section 5.2.

5.1.1 Reformulation of the control vector

The control vector has been reformulated to allow for a more general representation of the background error covariances. This has been a major new improvement to the OPAVAR system. In its new formulation ([GLO106]), OPAVAR produces an ocean analysis by approximately minimizing a cost function of the general form

$$J[\mathbf{v}] \;=\; \frac{1}{2}\,[\mathbf{v}-\mathbf{v}^b]^T\,[\mathbf{v}-\mathbf{v}^b] \;+\; \frac{1}{2}\,[\,G(\mathbf{v})-\mathbf{y}^o\,]^T\,\mathbf{R}^{-1}\,[\,G(\mathbf{v})-\mathbf{y}^o\,] \tag{5.1}$$

where $\mathbf{v}$ is the control (analysis) vector, $\mathbf{v}^b$ is the background estimate of the control vector, $\mathbf{y}^o$ is the vector of observations, $\mathbf{R}$ is an estimate of the observation error covariance matrix, and G is a nonlinear operator that maps the control vector onto the space of the observation vector. The background error covariance matrix of the control vector is assumed to be the identity matrix ($\mathbf{B}_{(\mathbf{v})} = \mathbf{I}$) as evident by the use of the canonical inner product for the background term in (5.1). In other words, background errors for $\mathbf{v}^b$ are assumed to be uncorrelated and to have unit variance. The control vector must be constructed carefully for this to be a reasonable assumption. In OPAVAR, $\mathbf{v}$ is assumed to be related to the model (initial) state vector $\mathbf{x}$ through a transformation of the form

$$\mathbf{v} = U^{-1}(\mathbf{x}) \tag{5.2}$$

where U^{-1} is a block-matrix operator, with possibly nonlinear blocks, which is split into three basic operators : a transformation K^{-1} that produces a set of approximately mutually uncorrelated variables by removing any known dynamical or physical balance relationships between model state variables ; a diagonal matrix D^{-1} of normalization factors ; and a roughening operator F^{-1} (the inverse of a smoothing operator) that acts separately on each of the uncorrelated variables.

There are two important advantages that result from this formulation of the cost function in which the background term takes on a very simple form. First, it generally results in a minimization problem with reasonably good conditioning, particularly when the number of observations is small compared with the number of control variables. Second, multivariate and smoothness constraints that are usually imposed in conventional matrix formulations of background error covariances are no longer required to be linear as they are now transferred to the observation term via the nonlinear transformation U which is embedded within the nonlinear observation operator G. This feature has been exploited in the current version of OPAVAR to employ nonlinear balance relationships (temperature-salinity relations, equation of state) in defining the control vector ([GLO106]). It also opens the way for generalizing the diffusion-based smoothing algorithm used in OPAVAR to a flow dependent, adaptive algorithm based on nonlinear diffusion. Nonlinear smoothing algorithms can be expected to be particularly advantageous in regions of strong ocean gradients (e.g., near fronts and coastlines).

Two examples are presented below to illustrate how the control variable transformation developed for OPAVAR can be used to produce analysis increments with physically sensible structures. Figure 5.1 shows a zonal-vertical section at the equator of the temperature (T) increment (Fig. 5.1) and salinity (S) increment (Fig. 5.1) generated by 3D-Var when a single SSH observation, chosen to be 5cm higher than the background SSH, is assimilated on the equator in the central tropical Pacific. To fit the SSH observation, 3D-Var produces T and S increments with largest amplitude at the level of the thermocline. The vertical structures are noticeably anisotropic. The T increment displays a pronounced upward tilt from west to east commensurate with the tilt of the background isotherms in this region. This anisotropic response is produced by a gradient-dependent parameterization for the standard deviations of T. The S increment has a dipole-like structure where the transition from negative to positive values occurs at the level of the salinity maximum in the background state. This feature of the salinity analysis increment arises from the flow-dependent formulation of the T-S constraint used in the balance operator ([GLO22]).

The previous example illustrates the fundamental importance of the control variable transformation in establishing a physically sensible (multivariate) response in 3D-Var. The balance operator also plays an important role in 4D-Var. This is illustrated in Fig. 5.2 which x@shows the SSH increments produced from two 4D-Var single T observation experiments performed without and with the balance operator activated (Figs. 5.2a and b, respectively). The geographical location of The single T observation is located in the thermocline (100m) at the same longitude and latitude as in the previous example. In these 4D-Var experiments, the control variables are a function of the model initial conditions which are taken to be 10 days before the observation time. The increments shown in Figs. 5.2a and b are those produced at the observation time (day 10) and have been computed by using the tangent-linear model to propagate forward the analysis increment at initial time. The 4D-Var SSH increment without the balance operator is remarkably similar to that obtained by 3D-Var with the balance operator (figure not shown). When the balance operator is included, however, the temperature observation projects much more effectively onto large-scale equatorial wave-modes as clearly illustrated in Fig. 5.2b by the presence of a westward-propagating baroclinic Rossby wave and an eastward-propagating Kelvin wave to the west and east of the observation location, respectively. Contrary to the experiment without the balance operator, the observation is able to have a much wider impact than in 3D-Var.

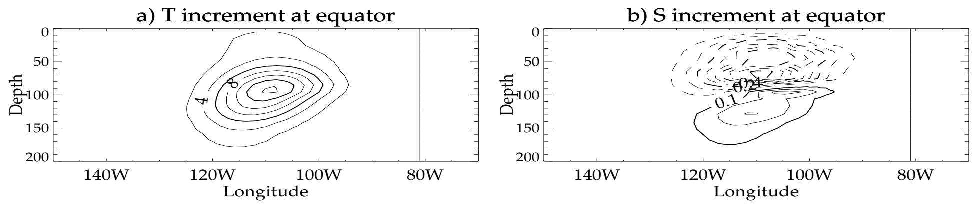

FIG. 5.1 – Vertical cross section at the equator of the analysis increments for a) temperature and b) salinity generated by the 3D-Var assimilation of a single SSH observation (positive innovation) located on the equator in the central Pacific. The fields have been multiplied by a factor 100. Solid (dashed) contours indicate positive (negative) values.

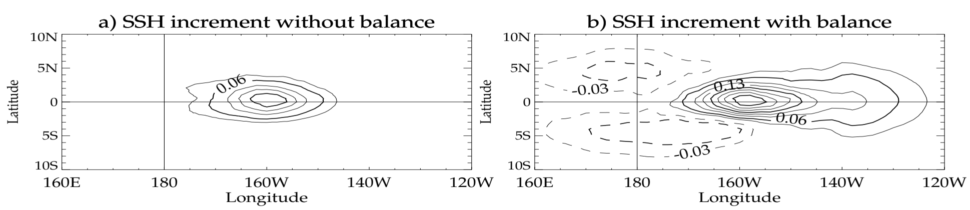

FIG. 5.2 – Horizontal section of the SSH analysis increments generated by the 4D-Var assimilation of a single temperature observation (positive innovation) located 10 days into an assimilation window located in the thermocline on the equator in the central Pacific. The increments are displayed on day 10 for a 4D-Var experiment a) without and b) with the balance operator activated. The fields have been multiplied by a factor 100 and the same contour interval has been used in a) and b). Solid (dashed) contours indicate positive (negative) values.

5.1.2 Improved minimization strategies

The minimization of (5.1) is achieved iteratively by minimizing a sequence, $k = 1, ..., K$, of quadratic cost functions

$$
\begin{aligned}
J^k[\delta \mathbf{v}^k] \;&=\; \frac{1}{2}\left[\mathbf{v}^{k-1} + \delta \mathbf{v}^k - \mathbf{v}^b\right]^T \left[\mathbf{v}^{k-1} + \delta \mathbf{v}^k - \mathbf{v}^b\right] \\
&+\; \frac{1}{2}\left[G\left(\mathbf{v}^{k-1}\right) + \mathbf{G}^{k-1}\delta \mathbf{v}^k - \mathbf{y}^o\right]^T \mathbf{R}^{-1}\left[G\left(\mathbf{v}^{k-1}\right) + \mathbf{G}^{k-1}\delta \mathbf{v}^k - \mathbf{y}^o\right]
\end{aligned}
\tag{5.3}
$$

where $\mathbf{v}^{k-1}$ is a reference state, $\delta\mathbf{v}^k$ is an increment defined by $\mathbf{v}^k = \mathbf{v}^{k-1} + \delta\mathbf{v}^k$, and $\mathbf{G}^{k-1}$ is a linearized operator defined such that $G(\mathbf{v}^{k-1} + \delta\mathbf{v}^k) \approx G(\mathbf{v}^{k-1}) + \mathbf{G}^{k-1}\delta\mathbf{v}^k$ (when this equation is satisfied exactly, (5.3) is identical to (5.1)). The difference $\mathbf{y}^o - G(\mathbf{v}^{k-1})$ in (5.3) is the innovation vector. The superscript $k-1$ indicates that $\mathbf{G}^{k-1}$ is the result of linearizing G about $\mathbf{v}^{k-1}$. The sequence $k = 1, ..., K$ are called outer iterations while the minimization iterations performed within each outer loop are called inner iterations. In practice, it is customary to set $\mathbf{v}^0 = \mathbf{v}^b$ and $\delta\mathbf{v}^0 = 0$, and to choose $\mathbf{v}^{k-1}$ for $k = 2, ..., K$ to be the solution obtained at the end of the previous outer loop. The minimum of (5.3) after the K-th outer iteration defines the analysis increment, $\delta\mathbf{v}^a = \delta\mathbf{v}^K$. The analysis in model space is then given by $\mathbf{x}^a = U(\mathbf{v}^a)$ where $\mathbf{v}^a = \mathbf{v}^{K-1} + \delta\mathbf{v}^a$. This formulation encompasses both 3D-Var (FGAT version) and 4D-Var which are distinguished by the type of linear model used in $\mathbf{G}^{k-1}$ to evolve the increments between observation times. In 3D-Var the increments are persisted whereas in 4D-Var they are evolved by a dynamical model that closely approximates the tangent-linear model. By distinguishing 3D-Var and 4D-Var at the incremental level, they can be viewed as two different algorithms for solving approximately the same 4D assimilation problem described by the nonquadratic cost function (5.1).

Several interesting properties of the incremental minimization algorithm are illustrated in Figure 5.3. Both panels show the cost (J^k), normalized by its initial value, as a function of iteration number for three experiments : 3D-Var with Incremental Analysis Updating (IAU), 3D-Var without IAU, and 4D-Var (IAU is not used with 4D-Var). In IAU the analysis increment is introduced smoothly into the nonlinear model, compared to the usual procedure of adding the analysis increment directly to the model background state. The assimilated data were *in situ* temperature measurements from the ENACT data-set. The assimilation window was 10 days in all experiments, and covered the period 01 January 1987 to 11 January 1987 (the first cycle of the ENACT Stream 1). In the left panel of Fig. 5.3 no outer iteration is performed; in the right panel an outer iteration is performed after 10 iterations as evident by the jump in J^k. It is not possible to make absolute comparisons between curves corresponding to different incremental cost functions (e.g., those used in 3D-Var and 4D-Var) so one must be careful in interpreting these figures. It is possible, however, to compare the values of the nonincremental cost function computed in the outer loop since this cost function is the same for each experiment and described by (5.1). In other words, the 6 different experiments (3D-Var/4D-Var, with/without outer iteration, with/without IAU) can be viewed as different approximate algorithms for minimizing the same nonincremental cost function. The value of the normalized nonincremental cost on the final outer iteration is indicated by the coloured symbols.

These figures illustrate several points. First, in both 3D-Var and 4D-Var, the use of two outer iterations results consistently in a much better simultaneous fit to the observations and background state than when only one outer iteration is performed (21% improvement in 4D-Var; 12% in 3D-Var with IAU; 15% in 3D-Var without IAU). The use of more than one outer iteration in 3D-Var was not made in the original 3D-Var system of [3] and [2] but has now become a standard feature in our global 3D-Var system. Sensitivity experiments have shown that the closer fit achieved with an extra outer iteration in 3D-Var comes mainly from changes to the nonlinear term $G(\mathbf{v}^{k-1})$ in (5.3) rather than from improvements to the linearization states for $\mathbf{G}^{k-1}$. Performing more than two outer iterations does not lead to further significant improvements in the fit, particularly in 3D-Var, and therefore does not appear to justify the extra computational cost involved (more integrations of the nonlinear ocean model). The second point is that 4D-Var produces a

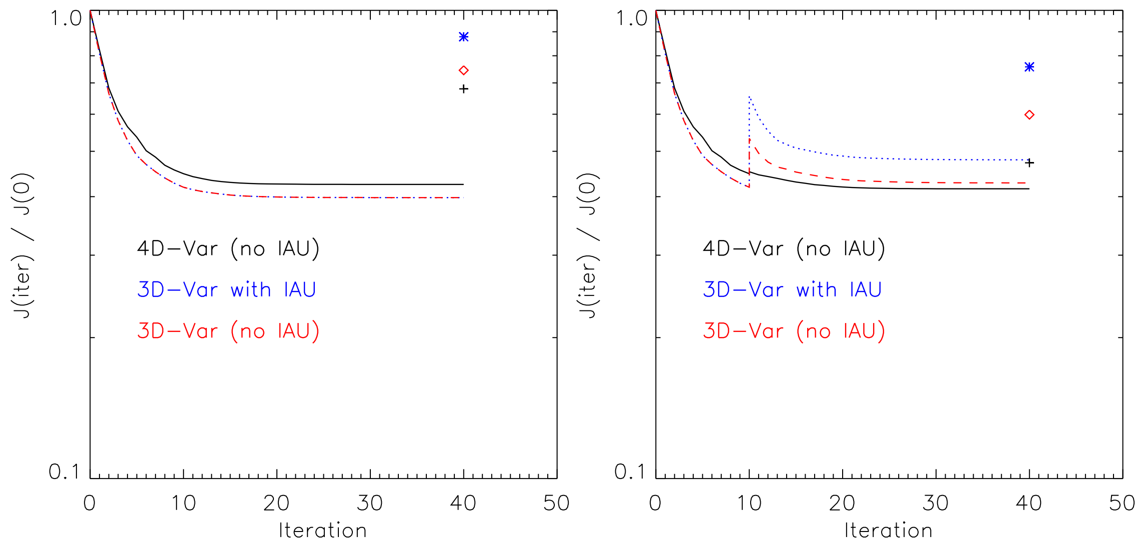

FIG. 5.3 – The value of J^k, normalized by its initial value, for assimilation experiments without (left panel) and with (right panel) an outer iteration. The solid black curves correspond to 4D-Var, the dotted blue curve to 3D-Var with Incremental Analysis Updating (IAU), and the red dashed curve to 3D-Var without IAU. The black cross, blue asterisk and red diamond correspond to the (normalized) values of the non-incremental cost function at the end of minimization for these different experiments, respectively.

much reduced value of the cost function compared to that of 3D-Var (13% improvement over 3D-Var with IAU ; 28% over 3D-Var without IAU). The small discontinuity in the 4D-Var cost after the update is a clear indication that the incremental cost function is a good approximation to the nonincremental cost function. Both 3D-Var experiments, on the other hand, display a much larger discontinuity after the update which simply illustrates that on a 10-day window the persistence assumption in 3D-Var FGAT is a poor approximation compared to the tangent-linear assumption used in 4D-Var. The final point worth remarking is that the final cost reduction achieved by 3D-Var with IAU is worse than that achieved by 3D-Var without IAU. This tendency was already observed in the tropical Pacific study of [3]. While IAU produces temporally smoother analyses than direct initialization, it does so at the expense of degrading the fit to the data achieved during minimization. It is possible, however, that the results could be improved by using a different forcing function for IAU than the constant forcing currently used.

In order to reduce the computational cost of 4D-Var, a hybrid 3D-Var/4D-Var strategy is currently being explored whereby the 3D-Var algorithm is used in the initial stages of minimization to obtain a good initial “guess” for a 4D-Var minimization. Preliminary results with a such a scheme are very promising and suggest that the efficiency of incremental 3D-Var can be combined with the theoretical advantages of incremental 4D-Var to produce an overall cost-effective 4D-Var algorithm.

5.1.3 Improved modularity using the PALM coupler

In order to improve the modularity of OPAVAR and to open up possibilities for parallelizing different parts of the system, a new version has been made developed which exploits the PALM-MP coupler. Using PALM-MP, OPAVAR has been separated into a set of independent “units” where each unit corresponds to a specific task in the assimilation algorithm (e.g., the control variable transformation (5.2) would constitute a unit). The independence of the unit is ensured by a well-controlled management of its data-inflow and -outflow, as illustrated in Fig. 5.4. The PALM-MP version of OPAVAR has been integrated into the existing version of OPAVAR as an option that can be activated via CPP key. This has been done to facilitate comparisons between the PALM and non-PALM versions of OPAVAR for both validation and performance-evaluation purposes. The current PALM version of OPAVAR can be used to perform a 3D-Var analysis of *in situ* temperature and salinity data but does not yet support the 4D-Var or altimeter data options which exist in the non-PALM version.

5.2 Global ocean reanalysis (A. Weaver, N. Daget)

Several multi-annual (re)analysis experiments have been performed with OPAVAR using the experimental framework established in ENACT. The analysis experiments were divided into three streams : Stream 1 from 1987–2001 (the altimeter period starting from GEOSAT) ; Stream 2 from 1962–2001 (the full ERA-40 period from which daily atmospheric forcing fields were available) ; and Stream A from 1993–2001 (a shorter altimeter period starting from TOPEX/Poseidon). During ENACT, control (no data assimilation) experiments and 3D-Var experiments assimilating temperature data only were performed for Streams 1 and 2, and 4D-Var experiments assimilating temperature data only and altimeter data only were performed for Streams 1 and A, respectively (see the ENACT final report which is available at http ://www.ecmwf.int/research/EU_projects/ENACT/index.html). Since the end of ENACT in December 2004, several improvements have been made to the assimilation system and a new set of 3D-Var analyses have been performed using the improved system. Some results from the latest Stream 1 3D-Var analysis experiment, which assimilates temperature and salinity data, are presented below.

Statistics derived from the observation-minus-background (OmB) and observation-minus-analysis (OmA) vectors yield valuable information about the internal consistency and performance of the assimilation system. The OmA corresponds to the residual in the observation term of the *nonincremental* cost function, and can be compared to the residual in the observation term of the *incremental* cost function, which will be denoted by OmA_inc in the following, in order to allow us to check the validity of the linear approximation in the incremental algorithm. For the *in situ* data, the OmB, OmA and OmA_inc vectors are stored in the same (NetCDF) format as the original data. This has been found to be very convenient for post-processing.

Figures 5.5 and 5.6 show vertical profiles of the mean and standard deviation of the OmB (black dotted curve), OmA (blue dashed curve) and OmA_inc (pink dashed curve) from a Stream 1 3D-Var reanalysis in which both *in situ* temperature and salinity from the ENSEMBLES-ENACT data-set have been assimilated. The 3D-Var was cycled with a 10-day assimilation window. Two outer iterations were performed per cycle, with 10 inner iterations within the first outer loop and 30 inner iterations within the second. The figures shown are based on statistics computed over all 549 cycles of the 15-year period from 01 January 1987 to 31 December 2001. For reference, the observation-minus-control (OmC) vector (red solid curve) is also shown on these plots. The OmC was computed using exactly the same data that were assimilated in the 3D-Var experiment. The mean statistics (left panels) are useful for detecting biases in the system, while the standard deviation statistics (right panels) illustrate how well the model fits the observed variability. Statistics are shown for the global average and two focus regions : Nino3.4 - a well-observed region in the tropical Pacific which is important for forecasting *El Niño* ; and NE_extratrop_atl - a region of direct interest to Europe.

Several interesting features can be deduced from these figures. First, the mean OmC indicates that the model without data assimilation has a pronounced temperature and salinity bias. In the upper 200m of Nino3.4 the control is too warm by up to $1°$C and too salty by up to 0.11 psu (on a global average the warm bias reaches $0.6°$C and the salt bias 0.2 psu). In NE_extratrop_atl the bias is the reverse of that in Nino3.4 : in the upper ocean there is a cold bias (max. $0.4°$C) and freshwater bias (max. 0.44 psu), whereas below 300m, the bias is warm (max. $0.4°$C) and salty (max. 0.08 psu). The 3D-Var reduces this bias significantly in all regions but not completely (e.g., in the OmA in Nino3.4 there is a maximum warm bias of up to 0.1°C near 150m and a maximum salt bias of 0.02 psu near 100m). This is not surprising since, by construction, the 3D-Var system has not been designed to correct for a bias in the background (background errors have been assumed to be random, which is clearly not the case especially near the start of the stream) so that a biased background will necessarily result in a biased analysis. In a realistic system we should always expect some degree of bias in the analysis.

The right panels in Fig. 5.5 show that the 3D-Var analysis (OmA) improves the fit to the observed temperature variability in all regions, particularly in NE_extratrop_atl. In this region, the OmB is also notably reduced relative to the OmC. In Nino3.4, on the other hand, the OmB is similar to the OmC at most depths, except near 100m where it is slightly larger. This indicates that error growth during the “forecast” (background) integration that follows each assimilation cycle is much more rapid in this region, and is possibly associated with an imbalance between the analysis and the surface forcing. The right panels in Fig. 5.6 show that the 3D-Var analysis (OmA and OmB) also improves the fit to the observed salinity variability at all depths in all three regions, but that, in Nino3.4, the fit is lost more quickly in the upper ocean during the forecast step.

Finally, it is interesting to note that the OmA and OmA_inc are similar everywhere except in the upper 200m of Nino3.4. This similarity illustrates that the fit to the observations achieved during minimization is not significantly degraded by the IAU procedure. The extra outer iteration used in 3D-Var has been shown to be essential for preserving this property of the 3D-Var analysis.

5.3 Use of ocean data assimilation for seasonal climate prediction (P. Rogel)

5.3.1 Design of an ensemble generation method for seasonal prediction in the presence of data assimilation

Building perturbed ocean analyses

In analogy to the DEMETER ensemble generation strategy for constructing ocean initial conditions for seasonal climate prediction, we have designed a strategy that preserves the dynamical balance of the ocean. The former has been constructed by perturbing the wind stress and sea surface temperature forcing of an ocean model. The other set is constructed by assimilating perturbed *in situ* temperature data using a multivariate 3D-Var version of OPAVAR. The OPAVAR system has been used to produce ensembles of analyses using the ECMWF ocean *in situ* observation data-base. SST perturbations have been interpolated to all temperature observation locations and extrapolated at depth. The original vertical profile properties have been conserved in the mixed layer and the perturbation progressively fades to zero underneath. Ensemble statistics are computed for the period 1990 to 1999.

Impact of the assimilation on the ensembles of ocean states

Due to nonlinear effects, the ensemble mean temperature has a significant subsurface cold bias when no data are assimilated, thus indicating that some part of the DEMETER hindcast systematic error may be explained by the way ensembles are generated. Constraining the temperature through data assimilation contributes to reduce this subsurface bias. The dispersion of the initial conditions is supposed to sample the uncertainty associated with the ocean state estimate. Therefore, a smaller spread in the assimilation case than in the forced only case is consistent with the idea that ocean uncertainty has been reduced by constraining the ocean state through data assimilation. Figure 5.7 illustrates this point and also displays how data assimilation impacts the interannual variability (see also [GLO24]). However, some qualitative estimates indicate that ocean uncertainty may be overestimated by the ensemble spread in the nonassimilated case, and that the opposite occurs in the assimilated case. It is also shown that wind stress perturbations mainly control the spread amplitude in the nonassimilated case, but that temperature perturbations have a stronger relative impact in the assimilated case.

5.3.2 Impact of 3D-Var analyses on seasonal hindcasts

Building seasonal hindcasts

Production of a 3D-Var-initialised set of coupled 6-month, 9-member hindcast ensembles has been completed for the period 1990-1999. The coupled system consists of the ARPEGE-Climat-V3 and the ORCA2 version of the OPA model coupled through OASIS. This same system has been used for the DEMETER project ([GLO20]). This experiment has been designed as much as possible as a sensitivity experiment with respect to the ocean initial conditions, so that the latter will be considered in the following as the control (reference) to which we compare the scores changes. The data have been stored on MARS, as part of the first phase of the phase 1 of the ENSEMBLES project.

Results

The results have been extensively examined in terms of climatology, tropical scores and global scores.

1. *Climatology :* The first source of error of any seasonal prediction system is a systematic error due to imbalances between components (ocean, atmosphere,...) at the beginning of the coupled integration. In [GLO16], we have shown that this systematic error is due to imbalances in the initial conditions, which explains most of the first month systematic error, and to fast varying systematic error, primarily controlled by the atmosphere. In this respect, the impact of the 3D-Var initial conditions is globally very positive since it substantially reduces the first source of error. The climate drift is thus significantly reduced in the whole tropical band as well as outside the tropics. As the improvement of the climatology is not sufficient to obtain a better behaviour of the model, we verified that the model variability is improved at all lead times in the tropical regions. This is probably due to the fact that data assimilation is able to impose subsurface anomalies that are not present when the ocean is forced only by winds and fluxes. Deep anomalies, especially at the thermocline level, can persist and be advected over a 6-month period and thus improve SST variability when they outcrop.

2. *Tropical Scores :* Tropical scores show in general good behaviour of the 3D-Var initialised experiments. In the Nino3 region of the Pacific, scores are better at months one and two, and at month six of the forecasts, suggesting that the impact of ocean information is effective at long time scales. This suggests that they could be even more important at time scales of one year. During the 1997 event (see Fig. 5.8), the 3D-Var initialised forecasts clearly outperform the control and other DEMETER forecasts.

3. *Global Scores :* In order to have a general overview of the impact of ocean initial conditions on the seasonal hindcasts, a systematic evaluation of the impact of ocean initial conditions for all seasons, all lead times, three climate variables (temperature, precipitation and MSL pressure) and all over the globe (divided in 6 regions) has been carried out. This has been done using Economic Value scores for above normal anomalies (in most cases, the effect is the same for upper terciles). An example of the results can be found in Fig. 5.9, where we can see for example that the impact over Europe is globally positive in Summer, Spring and Fall, but negative in Winter. The global balance is in favour of the 3D-Var hindcasts, with 67 cases where there is a gain, against 56 losses, and 20 neutral cases.

5.3.3 Regional seasonal prediction study over West Africa

Due to errors in modelling precipitation in atmospheric models, seasonal prediction of this quantity is often of poor quality and is not able to outperform statistical predictions when they exist. In Western Africa, where seasonal prediction is crucial in several domains (crop yield or malaria), the DEMETER multi-model has almost no skill. We have evidenced a significant statistical relationship between the dominant modes of observed precipitation and a combination of ERA-40 reanalysed large-scale atmospheric fields, namely the humidity convergence in the lower troposphere. We have shown that the dominant modes of precipitation of the rainy season can be more accurately forecasted when precipitation is estimated from the forecasted humidity convergence through this statistical relationship associated. This method has shown that the probabilistic ROC scores for the three dominant modes could be improved by 0.2, which makes them significantly more skilful than climatology in almost all cases.

[2] J. Vialard, A. T. Weaver, D. L. T. Anderson, and P. Delecluse, (2003), Three- and four-dimensional variational assimilation with an ocean general circulation model of the tropical Pacific Ocean. Part 2 : physical validation., *Mon. Wea. Rev.*, **131**, 1379–1395.

[3] A. T. Weaver, J. Vialard, and D. L. T. Anderson, (2003), Three- and four-dimensional variational assimilation with an ocean general circulation model of the tropical Pacific Ocean. Part 1 : formulation, internal diagnostics and consistency checks., *Mon. Wea. Rev.*, **131**, 1360–1378.

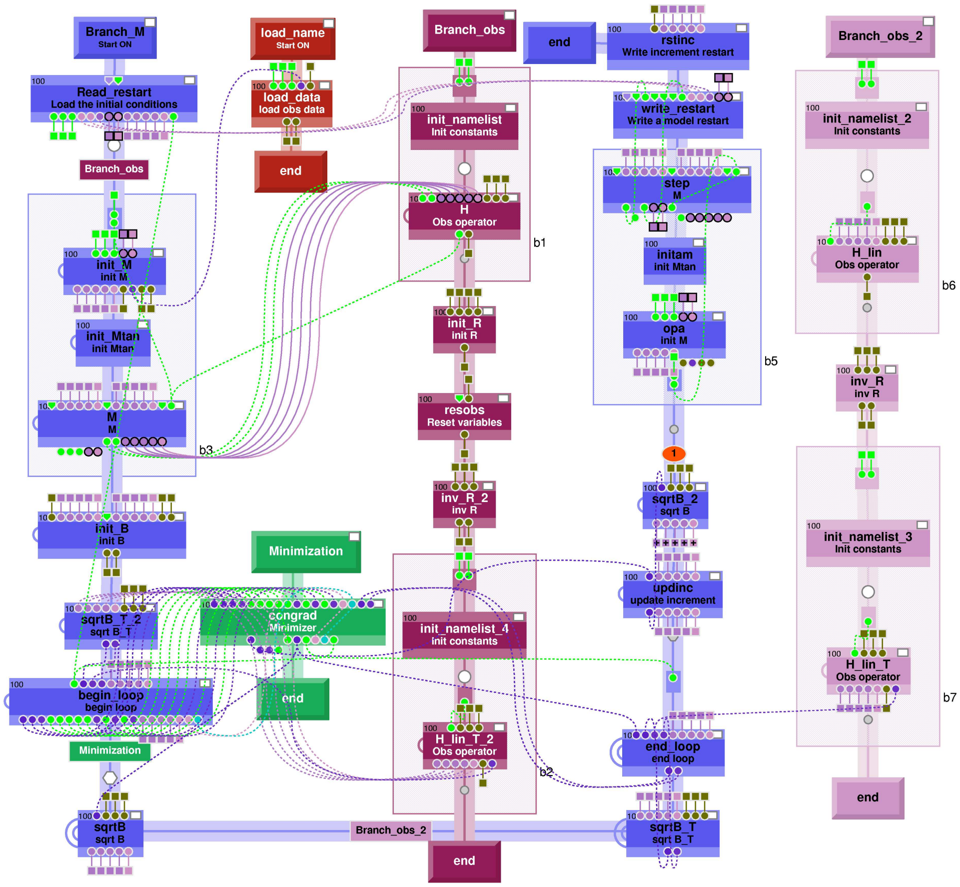

FIG. 5.4 – The PALM-MP modular configuration of an incremental 3D-Var (FGAT) version of OPAVAR. The coloured boxes correspond to different "units" used in 3D-Var. They are located on one of five "branches" which are distinguished by a different colour. Each branch executes the sequence of units on that branch. Units belonging to different branches can run in parallel. In this configuration, for example, the units "load data" and "read restart" are run in parallel. Each unit is a separate executable, except for those blocks of units enclosed by an outer box (e.g., the block containing the "step", "initam" and "opa" units) where it is the entire block that constitutes an executable. The inputs (outputs) for each unit are indicated by the circles at the top (bottom) of each box. The lines joining the output of one unit with the input of another indicate a direct "data" exchange between these units. Alternatively, the output (input) can be stored on (retrieved from) the PALM-MP buffer, indicated by the small squares. Loops are indicated by large circles on the thick line connecting units on a given branch : the start (end) of a loop is defined by a white (grey) circle. Units contained within a loop have a half-circle attached to the left-hand-side of the box. Several half-circles indicate that the units are contained within nested loops. For example, the two half-circles on the "sqrtB" box indicates that this unit, which corresponds to the control variable transformation (5.2), is called within the inner loop of the outer loop of the incremental 3D-Var algorithm.

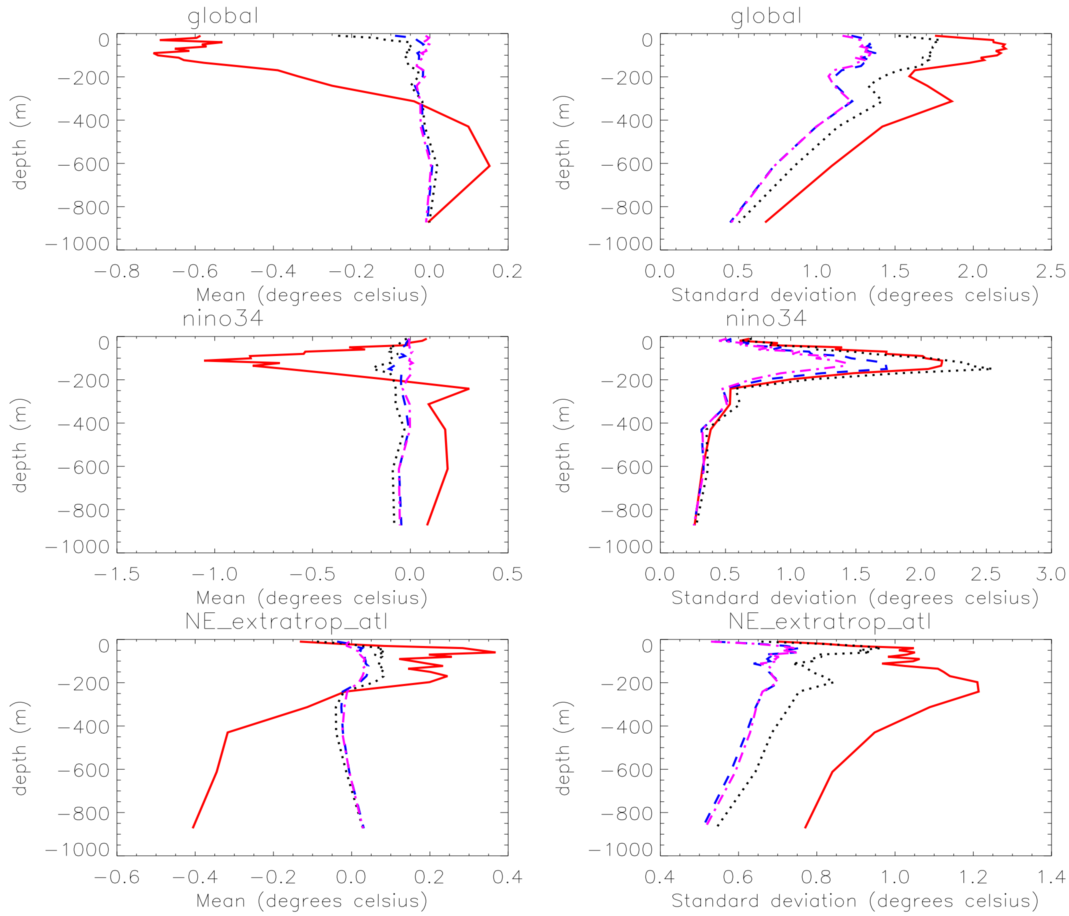

FIG. 5.5 – Vertical profiles of the mean (left panels) and standard deviation (right panels) of the OmC (solid red curve), OmB (dotted black curve), OmA (dashed-dotted pink curve) and OmA_inc (dashed blue curve) for temperature from a 15-year global 3D-Var reanalysis (01 January 1987 to 31 December 2001) in which both temperature and salinity profiles have been assimilated. The OmC, OmB etc. have been averaged within each model level. The statistics are displayed for the global average (top panels) and for two focus regions : the tropical Pacific (middle panels) and the north-east extra-tropical Atlantic (bottom panels).

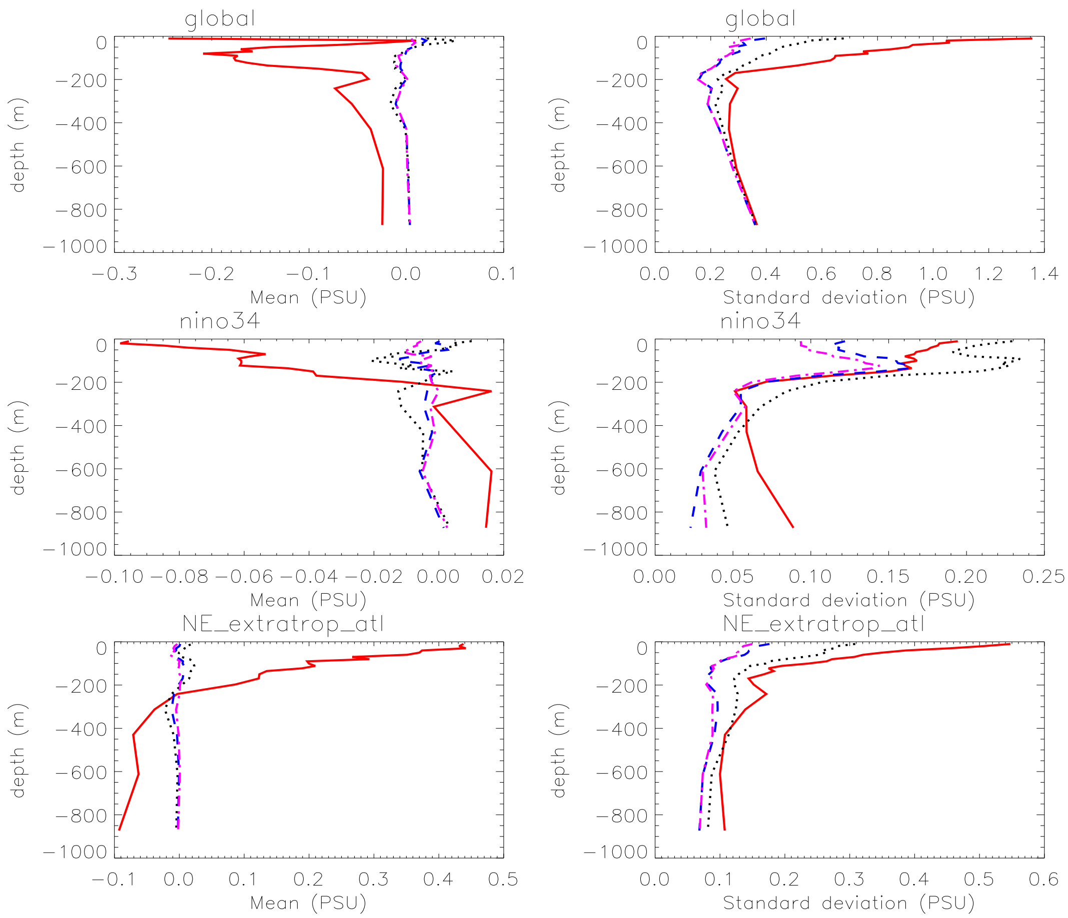

FIG. 5.6 – As Fig. 5.5 but for salinity.

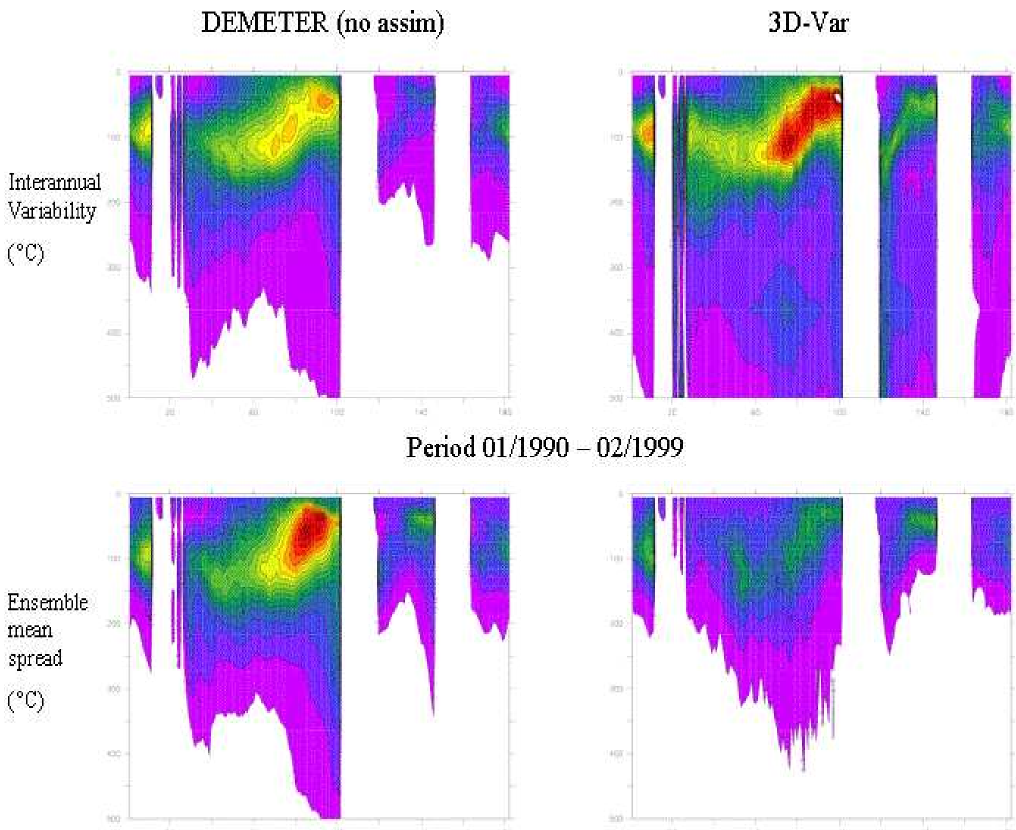

FIG. 5.7 – Vertical section at the equator of the interannual variability (top row) and ensemble spread (bottom row) deduced from the DEMETER (no assimilation) ocean initial conditions (left column) and from the 3D-Var experiments (right column).

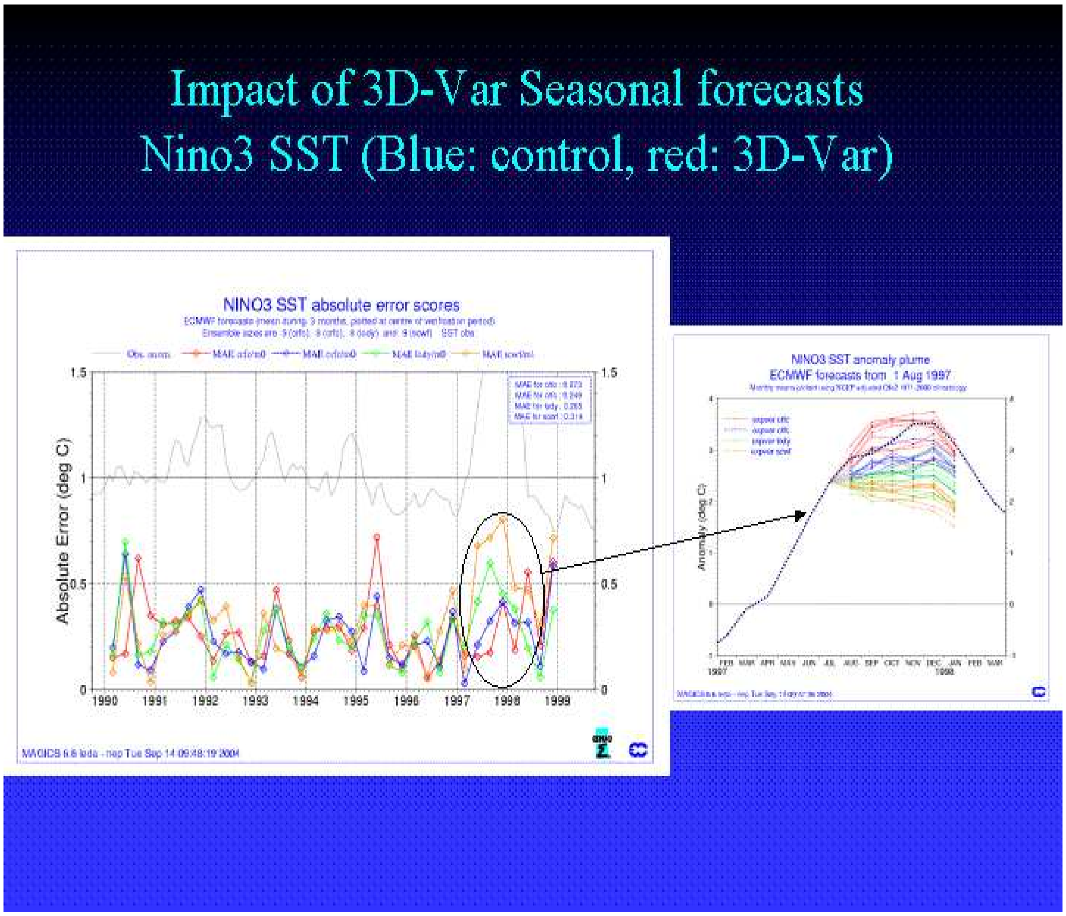

FIG. 5.8 – Prediction of SST anomalies in the Nino3 region ; left : absolute error ; right : prediction of the peak ENSO97 event started in August 1997.

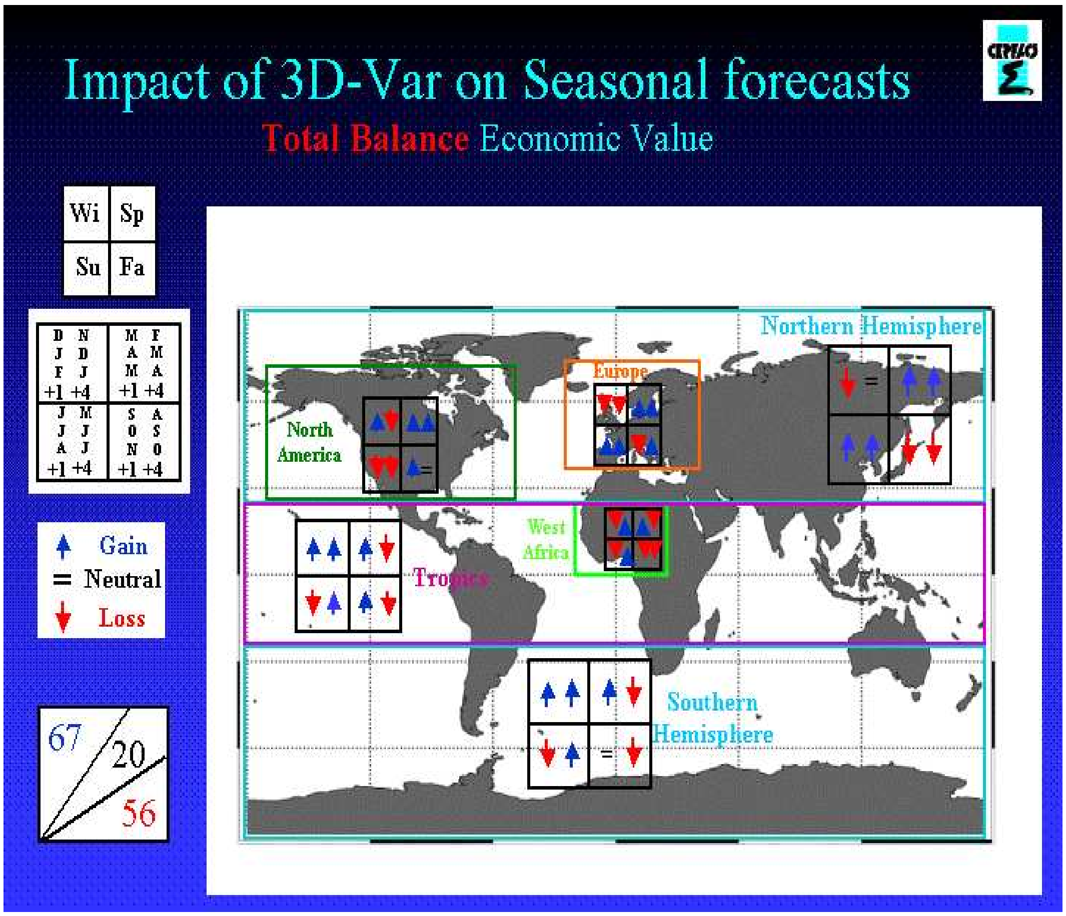

FIG. 5.9 – Gain in terms of Economic Value for predictions of temperature, precipitation and MSL pressure anomalies.

6 Data assimilation for atmospheric chemistry

The atmospheric chemistry project has started in January 2003, with the EC-FP5 ASSET project as a new application for the Palm software. The main part of the activity was the development of a variational data assimilation system for the global chemistry-transport model (CTM) Mocage from CNRM, Météo-France. The data to be assimilated into the ASSET project come from the Envisat satellite and they were not available at the beginning of the project. Due to their similarities with the ozone profiles from the spectrometer MIPAS onboard Envisat, the Gome data had been chosen to develop the assimilation system named Mocage-Palm. Interesting results were obtained at the end of the year 2003 (ref rapport 2003) and had encouraged us to improve this system as a new research activity and not only as an application for the Palm software.

6.1 Improvement of the ozone profiles assimilation system

The developments of the Mocage-Palm assimilation system are separated into three main ways : (1) the chemistry transport model used to assimilate the ozone profile, (2) the assimilation scheme and (3) the diagnostics to validate the analyzed ozone fields.

6.1.1 Chemistry transport model (S. Massart, H. Teyssedre)

The chemistry scheme used to assimilate Gome data into the CTM Mocage was Racmobus, the state of the art chemistry model with around 120 species. This model results from the combination of the Reprobus model for the stratosphere and the RACM model for the troposphere forced by an inventory of pollutants surface emission. Nevertheless, the numerical cost of this complete chemistry model is too high to analyze data during several months. The Mocage-Palm system was then adapted to two lightest chemistry models : Reprobus and Cariolle schemes.
The Cariolle scheme is a linear chemistry model devoted to only stratospheric ozone. The low cost of this scheme allows us to test and adjust the assimilation system when we receive new set of data to assimilate. Being validated with this scheme, we reanalyze the data using the Reprobus scheme in order to have a more detailed atmospheric chemistry state with 55 species solved in the stratosphere.

6.1.2 Assimilation scheme (S. Massart, H. Manzoni)

In the 3D-Fgat (First Guess at Appropriated Time) assimilation scheme, the misfit (difference between an observation and the model equivalent) is calculated by considering the model state for each specific time an observation is available. This is of great interest since satellite observations are not just performed at synoptic hours, but rather are continuous. The 3D-Fgat algorithm adjusts an increment constant in time, which minimizes simultaneously the model-background distance and all the model-observation distances over the entire assimilation window. The 4D-Var algorithm obtains an increment at the initial time, which is integrated in time using the tangent linear model and minimizes the model-observation distances all over the assimilation window. In this respect, the 4D-Var technique is more flexible than the 3D-FGAT, but it is also much more costly as it necessitates many integrations of the linear model and of its adjoint.

Assessing the relative strengths and weaknesses of 3D-FGAT and incremental 4D-Var in a chemical data assimilation context has seldom been demonstrated. Both methods have been implemented using the Palm software and the same CTM. Nevertheless, the choice of the chemical scheme in the incremental 4D-Var is restricted to the Cariolle one that is the only scheme we have developed an adjoint. We also had to develop the linear and adjoint model of the transport module of Mocage. The incremental 4D-Var currently works with three linear model : (1) the identity to be compared to the 3D-Fgat, (2) the semi-lagrangian transport model and (3) the transport and the Cariolle linear chemistry. Comparison between this several version of the 4D-Var and the 3D-Fgat has not still been performed over a long period of assimilation.

6.1.3 Diagnostic tools (S. Massart)

A key step in the assimilation procedure is the validation of the analyzed fields. Several diagnostics were developed following three ways. The first one consists on the calculation of the distance between dependent data (those that are assimilated) and model outputs before and after the assimilation procedure. As expected, the analysis is closer to the analyzed observations. However, it does not necessarily mean that the result obtained is consistent with the prescribed error statistics.

In order to evaluate the overall global consistency of any assimilation algorithm, a very simple diagnostic provided by Talagrand (1998) on the statistical expectation of the objective function taken at its minimum has also been implemented.

Nevertheless, according to Talagrand (1998), the only objective measure of the quality of an assimilation algorithm is a comparison of the fields produced by the assimilation with independent data. Thus, analyzed ozone profiles were lastly compared to available soundings and to the TOMS (Total Ozone Mapping Spectrometer) total ozone measurements.

6.2 Valorization of the assimilation system

The Mocage-Palm assimilation suite includes a 3D-Fgat and an incremental 4D-Var able to assimilated ozone profiles and a number of diagnostic tools. The direct CTM model used to compute the model equivalent to observations is Mocage that can be run in any of its chemical configuration for the 3D-Fgat and only with the linear Cariolle scheme for the 4D-Var. This suite is currently employed to assimilated ozone profiles from the MIPAS instrument onboard Envisat and SMR instrument onboard Odin.

6.2.1 Assimilation of MIPAS data (S. Massart, H. Manzoni)

Being involved into the Asset project that aims to assimilate the data from the European Space Agency (ESA) satellite Envisat, the assimilation suite was applied to the Michelson Interferometer for Passive Atmospheric Sounding (MIPAS) instrument. Operating in the near to mid-infrared, MIPAS provides concentration profiles of a number of target species (O_3, HNO_3, CH_4, and N_2O) in the upper troposphere and stratosphere. A typical limb elevation scan of MIPAS starts at about 50 km height and descends in 3 km steps to 8 km. With around 600 profiles per day during day and night time the MIPAS data has a good global coverage allowing a high-quality global analysis.

As an exemple, the figure 6.1 presents the zonal mean ozone distributions for the control simulation, the analysis with the 3D-Fgat using the Cariolle scheme and the MIPAS data averaged over September 2003. As expected the assimilated field is even closer to the data than the control run. In particular the larger corrections to the control simulation are mostly brought in two regions. The first one is located in the southern hemisphere, in the 40–$60°$S latitude band. The assimilation corrects the model by lowering the north-south gradient above 100 hPa. The second region is located in the northern hemisphere up to $40°$N. The ozone maximum around 50 hPa is increased. Moreover, an unusual secondary maximum appears in the analyzed fields at 200 hPa that is only sketched in the MIPAS data. Additional comparisons with sondes have justified this secondary maximum.

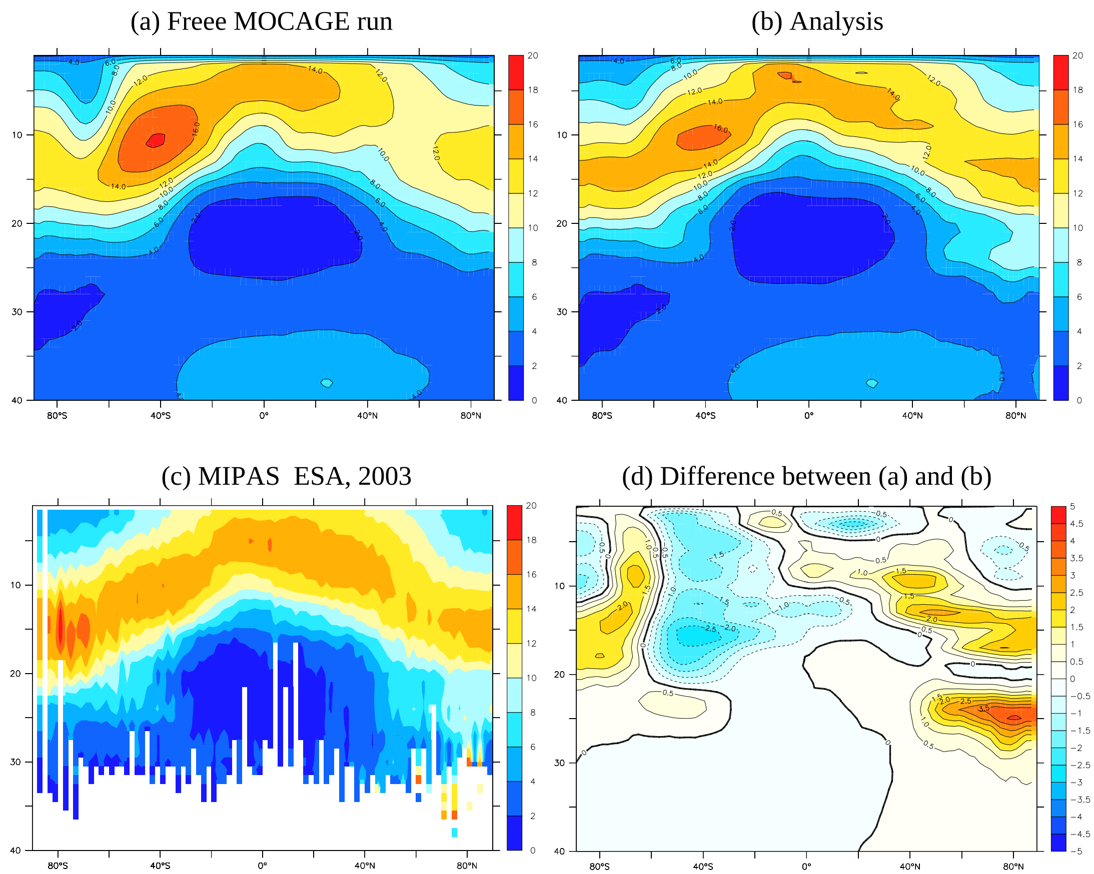

FIG. 6.1 – Zonal mean ozone in mPa averaged over July 2003 as a function of pressure levels for the control run (top left), the analysis with the 3D-Fgat-Cariolle (top right), the MIPAS data (bottom left) and the difference between analysis and control run (bottom right).

More validations have been performed for the 3D-Fgat-Cariolle scheme in particular with TOMS (figure 6.2). The analysis globally maintains larger values compared to the TOMS total ozone measurements with a difference close to 20 DU from the morth midlatitudes to the south midlatitudes. In the high latitudes of the northern hemisphere, the difference reaches 40 DU. Even if the absolute accuracy between MIPAS and TOMS data can not be concluded, our results clearly demonstrate the ability of the assimilation techniques to compare measurements that have very different characteristics like limb soundings in the IR and nadir UV measurements.

The 4D-Var assimilation of MIPAS data is in progress and still have to be validated but first results can already be compared to the 3D-Fgat analysis (figure 6.3). Before producing interesting scientific results, the 4D-Var have to be adjusted. In particular, the size of the assimilation window can be increased for the

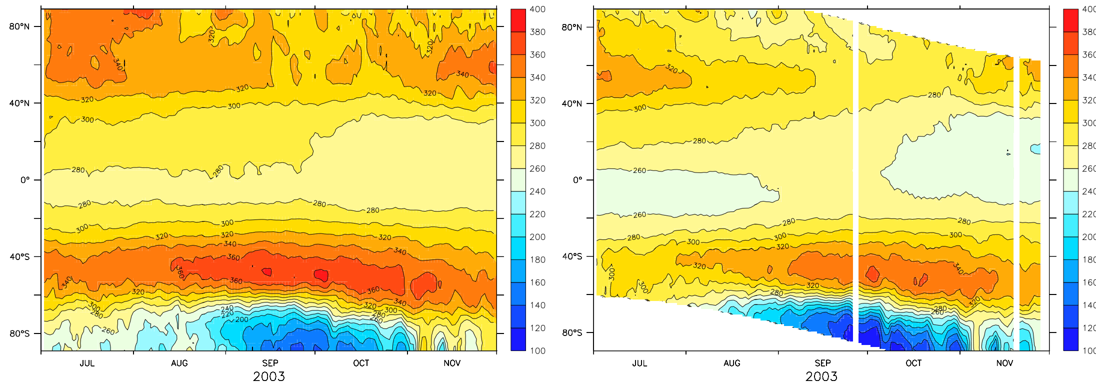

FIG. 6.2 – Zonal total ozone time evolutions in DU over the Asset intercomparison period (July-November 2003) from the 3DFGAT analysis (left) and measure by TOMS (right).

4D-Var, that means that the background error is different from the 3D-Fgat since the background is provided by an integration of the CTM.

6.2.2 Assimilation of SMR data (S. Massart, L. El Amraoui)

In order to extend the variety of data to be assimilated by the Mocage-Palm suite, collaboration between the CERFACS, the LA and the CNRM has been initiated around the data from the Odin satellite, that is dedicated to both astronomy and aeronomy. The Sub-Millimeter Radiometer (SMR) is one of its two instruments that detects simultaneously many species in the stratosphere such as O_3 and N_2O. For the aeronomy part of the Odin mission, approximately one day over three, SMR scans the limb of the atmosphere from 17 to 70 km and provides O_3 and N_2O profiles within a resolution of about 2 km.
During January 2003, Odin was mainly devoted to aeronomy. This period was chosen to test the 3D-Fgat assimilation algorithm on the SMR data using the Cariolle chemistry scheme. The main difficulty came across was to adjust the background error statistics according to the observation error ones. Nevertheless, this step realized, results were not as encouraging as for MIPAS. Due to a lower observation density, the information bring by the Odin data have to be spread vertically by the assimilation procedure in order to improve the analysis quality. This vertical diffusion of the information is still not implemented in the assimilation suite.
Moreover, all the information available from SMR was not taken into account since the actual top level of Mocage vertical resolution is 5 hPa (near 35 km). Since a few time, a new version of Mocage is developed with an extension of the top level to 0.1 hPa (near 65 km). The assimilation suite is now able to use this new version but not significant results can be presented yet.

6.2.3 Simultaneous assimilation of MIPAS and SMR data (E. Renard, V.-H. Peuch, S. Massart)

A trainee work was proposed by the CNRM to assimilated together ozone profiles from both MIPAS and SMR measurements. This work has shown that one main hypothesis of assimilation, an observation bias

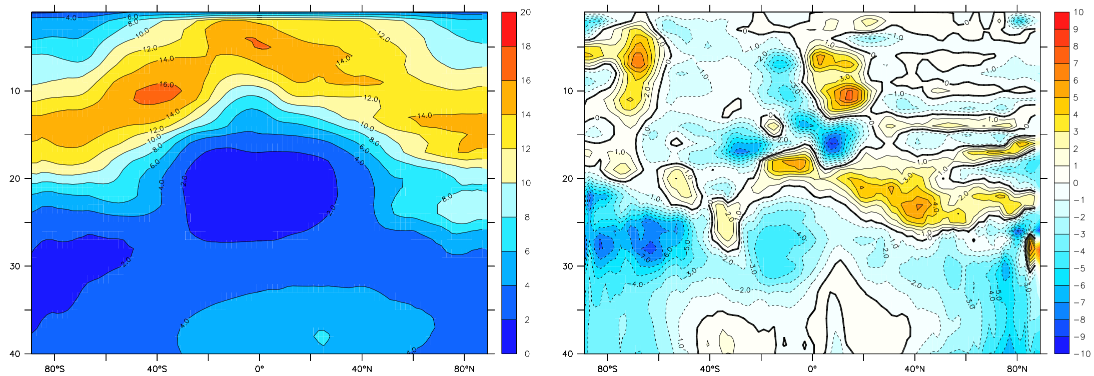

FIG. 6.3 – Zonal mean ozone in mPa averaged over July 2003 as a function of pressure levels for the 4D-Var analysis with the Cariolle schem (left) and difference between the 4D-Var and the 3D-Fgat analysis (right).

equal to zero, has to be respect in this context. The observations have first to be assimilated separately in order to estimate their respective bias through the comparison between analyses. Moreover, the observations covariance matrices have also to be well specified in order to respect the weight of each type of observation in the analysis process. Then, the simultaneous assimilation of the two varieties of observations, unbiased compared to TOMS, provides analyzed ozone fields closer to TOMS measurement than the fields from the separated analyses.

6.2.4 The ADOMOCA project (A. Piacentini, S. Massart, D. Cariolle, P. Ricaud, J.-L. Attie)

The aim of the ADOMOCA (Assimilation de DOnnées pour les MOdèles de Chimie Atmosphérique) project is to gather together the French atmospheric chemistry community working or wishing to work on the assimilation of tropospheric and stratospheric chemistry species. Due to the large number of existing tools (models, measurements, assimilation methods) in this field, the PALM software has appeared as the best way to couple the assimilation pieces together to build an assimilation algorithm. In the context of the ADOMOCA project, the structure of the MOCAGE-PALM algorithm has to become more modular in order to admit other chemistry transport models and to assimilate other kind of chemistry data not restricted to ozone and to profiles.

This new prototype is presently used to produce ozone analysis from MIPAS measurements with the new Mocage vertical resolution extended to 0.1 hPa. As with the 4D-Var, this system has still to be tested and validated using the available diagnostics, before producing interesting scientific results.

7 Data assimilation for nuclear plant modelling

Simulation of nuclear plant reactors plays a vital role for their security and operation. For that reason, EDF R&D and its partners develop complex neutronic models which are used in operational and allows to optimize refueling and to monitore the core of the reactors. Some incore and excore instrumentations are used routinely to have a better knowledge of the reactors state. However, few are used for improving simulations. The use of data assimilation techniques has now become systematic in fields such as weather or oceanography forecast to take advantage of the maximum amount of available information (simulations, measurements, ...) about a given physical system, in order to compute the best estimate of its state. The objective of the ADONIS project, created at EDF in 2003 in the framework of the 2010 challenges, is to study the feasability and potential contribution of such methods for the simulation of nuclear plant reactors. The "Data assimilation for nuclear plant modelling" project has been created in the Global Change and Climate Modelling team at the end of year 2003, on an EDF demand, to contribute to the ADONIS project by bringing the expertise developed at CERFACS about the study and implementation (PALM software) of data assimilation systems.

The main objective of this project is to demonstrate, in collaboration with the ADONIS team, the potential contribution of data assimilation methods on a set of neutronic applications. To realize this objective, it has been decided to develop several prototypes of data assimilation systems for applications of gradual complexity for which these techniques seems to be adapted. The use of the PALM software ([4]) plays an important role by facilitating the implementation and ensuring the evolutivity of these systems by coupling their elementary components. On the period 2004-2005, two systems have been implemented. The following sections will detail each one of these applications.

7.1 MANARA : a Modular Application for Neutronic Activity Reconstruction by Assimilation (S. Buis, S. Massart, G. Gacon, N. Aguir)

MANARA (Modular Application for Neutronic Activity Reconstruction by Assimilation) has been implemented to address the same problem as the EDF code CAMARET - that is to provide a fine estimate of the 3D power map given some located measures and the simulation computed by a model - but with using data assimilation techniques. The knowledge of this map is necessary in an operational context, in particular for hot spot localization and depletion correction. However, the methods currently used in CAMARET have several drawbacks. In particular, they are difficult to justify on a theoretical point of vue and they do not take into account measurement errors. In addition, CAMARET exclusively uses in-core measurement system. Data assimilation methodology addresses all these points, that's why the use of these techniques seems to be relevant in seach a context.

The problem solved by MANARA is the minimization of the classic incremental 3D-VAR cost function. It produces as an analysis a 3D power map using the one computed by the neutronic model COCCINELLE at a given time as a background, and the measurements provided by movable detectors at corresponding time. The model COCCINELLE is the official EDF neutronic code used in operational conditions. It computes a 3D nodal calculation for 2-groups diffusion, with feedback and depletion effects. COCCINELLE is used in MANARA as it is in CAMARET, that is to provide an a priori estimate of the sought power map. All the operators implied in the computation of the 3DVAR system - the COCCINELLE model, the observation operator, its adjoint, the inverse of the error covariance matrices, ... - have been implemented and tested as independent components. Then, these components have been assembled in PALM to build the full 3D-VAR system, as shown in Fig. 7.1. Several internal diagnostics have been successfully performed to check the validity of the system and of its components among which adjoint test and gradient test. The full application suite (3D-VAR and associated tests) is handled with PALM and under CVS. The development of this system is described in [GLO69]. This tool is a base to test several configurations of the assimilation system. In particular, the addition of new kind of observations (in-core or ex-core) is facilitated thanks to its modularity. Another version of the system, based on the direct resolution of the BLUE equations, has been recently included in the suite. It turns out to be faster and more precise in certain cases than the 3D-VAR version.

A first set of experiments have been computed with MANARA using a simple background-error covariance matrix B. In this case, B contained uniform variances on its diagonal and covariances decreasing exponentially with the distance between the considered points. 126 independent assimilation experiments have been computed using 42×38 observations extracted from the complete observation dataset while the other 16×38 have been kept for comparison. The same has been computed using CAMARET. The comparison between the CAMARET analysis-minus-observations and the MANARA analysis-minus-observations shows that MANARA already gives promising results (Fig. 7.2). Furthermore, it offers a natural framework to combine several kinds of observations and their error statistics which is not case in CAMARET.

The quality of the estimation resulting from a data assimilation system largely depends on the quality of the error covariance matrices modelling. In particular, the estimated 3D map computed in MANARA is not used as an initial condition for a new simulation but as the best-known estimation of the reactor state. As the observed reaction rates locations correspond to a restricted number of points of the COCCINELLE computation grid, a particular attention must be paid to the modelling of the background error covariances, because it determines the way the correction at observation points is spread on the rest of the computation grid. A study of the background-error correlations based on the analysis of the background-minus-observations, using the so-called observational method ([5]), has been performed. A preliminary study of the model biases had been necessary since model or observation biases can affect the results of this method as well as the result of the data assimilation system. An analysis of the discrepancy between the COCCINELLE simulations and the corresponding in-core observations shows several model biases with strong horizontal spatial structures ([GLO92]). A procedure has been implemented to automatically remove these first order biases from the background with a simple 2D modelisation of these structures. The analysis of the unbiased background-minus-observations with the observational method did not allow us to identify spatial correlation structures ([GLO92]). The heterogeneity of the in-core medium and the granularity of the mesh may explain that the background-error correlation between two points is not influenced at a first order by the distance between these points in our case. This study suggests that other factors, such as for example nature or depletion of the assemblies, have to be investigated for the influence on the background-error correlation.

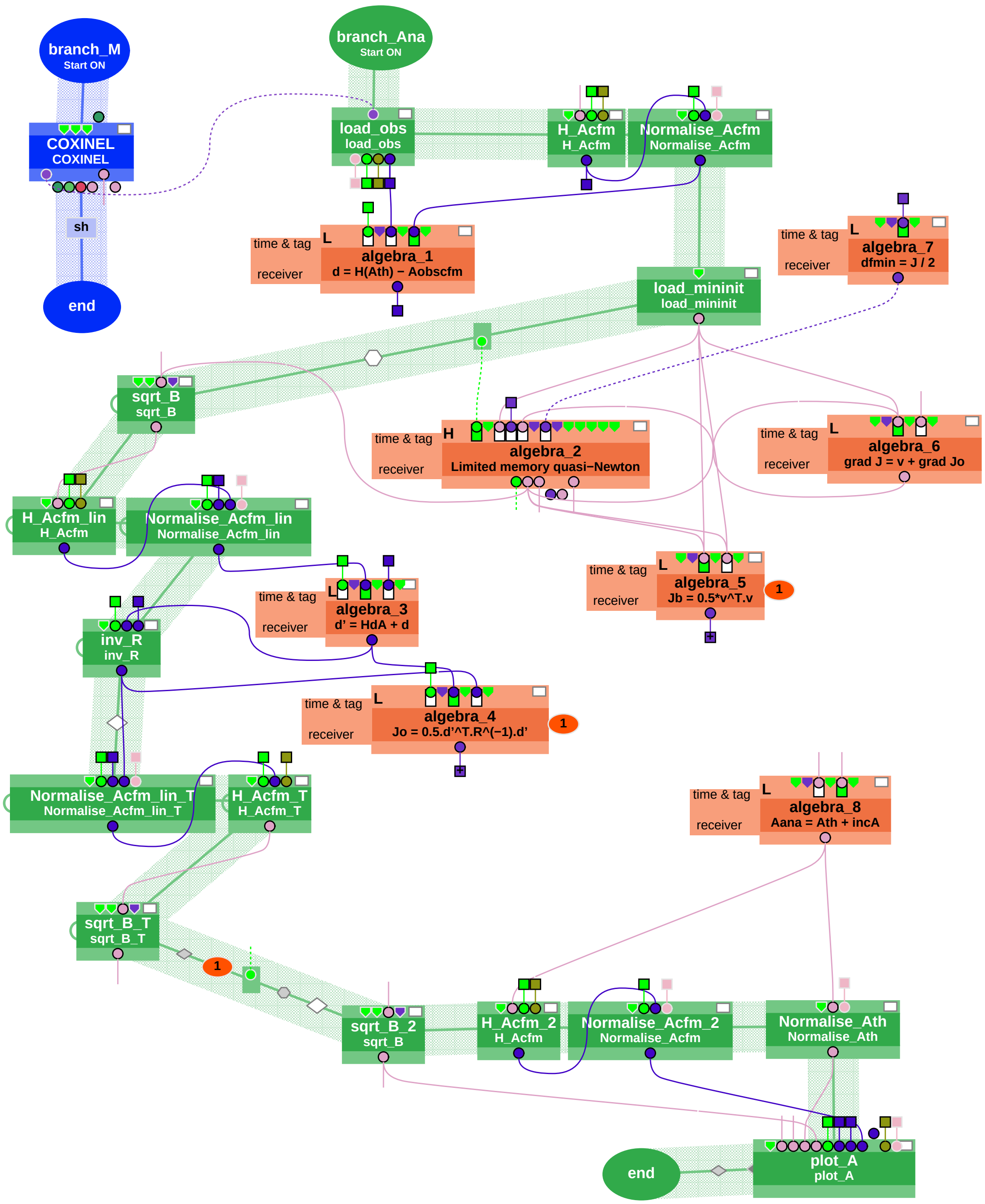

FIG. 7.1 – The MANARA 3D-VAR in PALM. Each color box represents a PALM unit, that is a computational component of the system. Color lines between PALM units represent data exchanges. Orange boxes are pre-defined units of the PALM algebra toolbox that compute algebra operations on the data exchanged by the user's units.

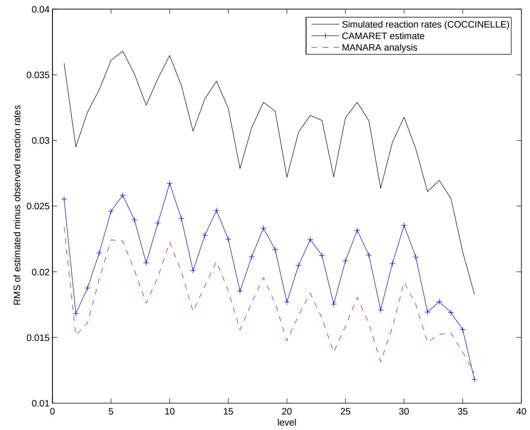

FIG. 7.2 – RMS of the discrepancy between estimated reaction rates and non-assimilated observations per level of the mesh. It can be seen that the estimate produced by MANARA fits the observation better than CAMARET on almost all the axial points.

7.2 KAFEINE : KAlman Filter Estimation In NEutronic (S. Massart, G. Gacon, S. Buis)

Given a set of initial conditions for a nuclear reactor, neutronic model simulation depends on few parameters that are the degrees of freedom of the model. The aim of these models is to simulate as accurately as possible the neutronic 3D field for any reactor. Thus, some few parameters have to be tuned once, using the available data. At each new release of the EDF R&D operational neutronic model, a calibration of its input parameters is performed. This calibration procedure tunes a given set of parameters in order to make the results of the model as close to in-core measures as possible, on a great number of experiments. Nowadays, five model coefficients are sequentially optimized and two more parameters are corrected by hand. This quite heavy procedure is not fully automated and thus limited to a restricted number of parameters. A system, called KAFEINE, has been developped under the PALM framework to test the potential contribution of data assimilation methods for this kind of application. These methods can contribute to automatically and simultaneously adjust a large number of parameters and/or to use a heterogeneous parameter adjustment map in code calibration procedures, instead of taking one single homogeneous correction value for each parameter. This issue should be of primary importance in the future since models, such as multi-group reflectors for instance, tend to become increasingly complex. Moreover, data assimilation techniques offer the possibility to take into account all different measurement systems existing in a Pressured Water Reactor core with their uncertainties as well as model uncertainties. Finally some useful information about the uncertainties of the estimated parameters can be provided by the system.

The KAFEINE calibration system is based on an extended Kalman filter method. It simultaneously adjusts several neutronic parameters of the model COCCINELLE to best-fit a series of in-core measurement campaigns. In this context, given a set of parameters, COCCINELLE outputs have to be compared to observations on several experiments. The observation operator of the system contains two distinct components that are the model itself and some classical conversions from model outputs to observations. This operator is linearized by finite difference ([6]). Contrary to classical use of the Kalman filter, no state propagation model is needed and it is replaced by the identity matrix in equations. The development phase of this system is now accomplished. A qualitative and quantitative comparison between KAFEINE and the procedure currently used at EDF will soonly be performed, with simplified covariance error matrices, to have a first guess of the interest of data assimilation method for neutronic parameters calibration.

[4] S. Buis, A. Piacentini, and D. Déclat, (2006), PALM : A Computational Framework for assembling High Performance Computing Applications, *Concurrency and Computation : Practice and Experience*, **18(2)**, 247–262.

[5] A. Hollingsworth and P. Lönnberg, (1986), The statistical structure of short-range forecast errors as determined from radiosonde data. Part I : The wind field, *Tellus*, **38A**, 111–136.

[6] S. Massart, (2005), Linéarisation du modèle COCCINELLE par différences finies., technical report, CERFACS. In preparation.

8 The PALM coupler

8.1 Support and Training for the PALM_RESEARCH product (T. Morel, S. Buis, A. Piacentini, N. Barriquand)

The PALM_RESEARCH sofware (Fortran 90 programming, SPMD - Single Program Multiple Data paradigm, MPI1 message passing library) has been delivered at the end of 2001. This product is used in the MERCATOR project. Its use is free for research purposes and is encouraged for the MERCATOR-related assimilation activities.

The PALM project is thoroughly presented on the web site : `http ://www.cerfacs.fr/~globc`.

The software is provided with an installation guide and a user guide. The user guide includes a tutorial to go progressively through all the features of the PALM prototype and of its graphical interface PrePALM.

A three day training session can be provided if necessary. Five sessions were organized in 2004 and 2005 for a total of fifty trained people.

The PALM team provides a constant user support for the PALM products. The mail address `palmhelp@cerfacs.fr` can be used by all registered users to contact the PALM team.

The PALM users' community is now spured to use the PALM_MP release instead of PALM_RESEARCH to take advantage of the new functionalities and the improvements on memory management. The change to this new release is transparent for the source developped by the users, due to an upward compatibility of the latest release of PALM.

8.2 Implementation of the final version (S. Buis, T. Morel, N. Barriquand)

The last two years main activity of the PALM team was the development of new functionalities on the MPMD release of the coupling software PALM called PALM_MP. This one is based on MPI2 which provides communications between independant processes. On the contrary of the MPI1 standard which is used on the SPMD release of PALM, the MPI2 standard, now available on most common platforms using native or public implementation such LAM, allows a better memory management and leads to an higher and clearer independence between sources which have to be coupled. In concrete terms, although some main parts of the previous PALM kernel as the management of the distributed objects have been re-used, PALM_MP Kernel was largely rewritten.

The main PALM_MP new features are the introduction of the sub-object concept which allows to pick up only a part of an object, the possibility for the users to use C/C++ languages as well as FORTRAN77 and 90 to develop their own PALM units, and a more flexible temporal management of objects. At the same time, tools for real-time supervision has been developped. The Algebra toolboox, included parallel operations and minimisers is now available on the PALM_MP software At present, the first tests on concrete assimilation data cases with PALM_MP are in progress.

8.3 Development of a PALM breadboard (S. Buis, T. Morel)

The development activity was accompanied by an extensive testing of the new code. With the aim of testing the flexibility, the performances and the portability of the PALM software and of its interface PrePALM, a bench case has been designed. It is based on a 2D shallow water nonlinear model and it makes use of its linear tangent and adjoint versions. The models have been developed and set into the PALM formalism. These models have been used to implement a 3D-Var and a 4D-Var assimilation scheme. Starting from these assimilation schemes, the bench case has been improved and it includes now twelve different cases implementing the 3D-Var, the 3D-FGAT, the 3D-PSAS, the 4D-Var, the incremental 4D-Var methods with different minimizers. This bench case is the base of the development of an advanced tutorial for the PALM applications in data assimilation.

8.4 PALM applications

Several applications of PALM are described in other sections :

- Data assimilation assimilation for oceanic modeling
- Data assimilation for nuclear plant modeling
- Data assimilation for atmospheric chemistry

The PALM coupler is also used in others applications at CERFACS on compututional fluid dynamic team to optimize the design of aero-engine. Others projects have choosen the PALM_MP software to couple parallel codes : CESBIO, IUSTI, SNECMA...

9 SMOS Mission

E. Anterrieu, B. Picard

9.1 Introduction

9.1.1 Introduction

The SMOS (Soil Moisture and Ocean Salinity) space mission is now undergoing phase C study in the frame of the Earth Explorer Program of the European Space Agency. During the last years, CERFACS has been involved in the regularization of the inverse problem which aims at retrieving the brightness temperature map of the observed scene from experimental interferometric data named complex visibilities.

9.1.2 Image reconstruction algorithm

Three regularizing methods have been examined and compared, all leading to the same results with regards to the propagation of random radiometric noise [GLO21]. Two of them, the Tikhonov and the minimum-norm approaches, depend on a numerical regularization parameter, while the third one, the band-limited approach, does not depend on such a numerical parameter. Moreover, with the latter approach the dimension of the system to be solved is reduced to the minimum number of unknowns (or degrees of freedom), the number of non-redundant frequencies in the experimental frequency coverage, while taking into account, in the least-square sense, all the available complex visibilities without averaging the potentially redundant ones.

9.1.3 Inverse problem

The inverse problem aims at inverting the discrete version of the integral relation between the radiometric brightness temperature map T and the complex visibilities V, i.e. solving the linear system :

$$\mathbf{G}T = V, \tag{9.1}$$

where $\mathbf{G}$ is the discrete linear operator from the object space E into the data space F describing the basic relation between T and V. Since the direct problem is stated via an integral equation, the inverse problem does not usually have a straightforward solution. Moreover, since the dimension of the object space E (here the n^2 pixels used to sample T) is often larger than the dimension of the data space F (the $\ell(\ell-1)/2$ samples of V), the linear system (1) is an underconstrained problem with multiple solutions for T. Consequently, the minimum of the least-square criterion

$$\min_{T \in E} \|V - \mathbf{G}T\|_F^2 \,, \tag{9.2}$$

which is also the solution of the normal equation $\mathbf{G}^*\mathbf{G}T = \mathbf{G}^*V$, is therefore not unique because the square matrix $\mathbf{G}^*\mathbf{G}$ is singular. Thus, according to the definition given by Hadamard, the inverse problem is ill-posed and has to be regularized in order to provide a unique and stable solution for T.

9.1.4 Band-limited regularization

Referring to a physical concept, namely the limited resolution of the instrument, a new approach has been proposed to ESA [GLO4]. According to this principle, the reconstructed brightness temperature map is the temperature distribution T_r which has its Fourier transform confined to the experimental frequency coverage H. This band-limited solution realizes the minimum of the constrained optimization problem

$$\left\{ \begin{array}{l} \min\limits_{T \in E} \|V - \mathbf{G}T\|_F^2 \\ (\mathbf{I} - \mathbf{P}_H)T = 0 \end{array} \right. \tag{9.3}$$

where $\mathbf{P}_H$ is the projector onto the subspace $\mathcal{E}$ (of E) of the H-band limited functions. The unique solution of (3) is given by :

$$T_r = \mathbf{U}^* \mathbf{Z} \mathbf{A}^+ V, \tag{9.4}$$

where $\mathbf{A}^+ = (\mathbf{A}^* \mathbf{A})^{-1} \mathbf{A}^*$ is the More-Penrose pseudo-inverse of the rectangular matrix $\mathbf{A} = \mathbf{G}\mathbf{U}^*\mathbf{Z}$, $\mathbf{U}$ is the Fourier transform operator and $\mathbf{Z}$ is the zero-padding operator beyond H.

9.1.5 Conclusion

The band-limited regularization approach developped at CERFACS has been proposed to ESA for a competition with other inversion methods developped by German and Spanish laboratories. After theoretical and numerical comparisons, ESA has decided to select the band-limited regularization approach for implementation in the SMOS Level 1 processor prototype.

10 CERFACS contribution to the MERCATOR project

This report, summarizing CERFACS' contributions to the MERCATOR project, appears also as such in the MERCATOR activity report prepared by the Groupement d'Intérêt Public (GIP) MERCATOR-OCEAN.

10.1 Introduction

The Mercator project develops several ocean circulation-modeling and assimilation systems to both serve the international Global Ocean Data Assimilation Experiment (GOAD) and the future French 'Centre d'Océanographie Opérationnelle'. Three main research axis have been selected. The 'Système d'Assimilation Mercator' (SAM) is an essential component of the different ocean prediction systems or prototype systems. The 'Prototype Atlantique et Méditerranée' (PAM) is designed to investigate very high resolution forecasting feasibility over a region that has already been widely studied. The 'Prototype Océan Global' (POG) addresses the global objective of *GODAE* and benefits from the previous PAM implementation.

10.2 The Assimilation System SAM (M. Drevillon, J.M. Lellouche,E. Rémy and B. Tranchant)

The Mercator project adopted a strategy for incremental improvement of data assimilation schemes, i.e., first starting with a well-known method (Optimal Interpolation) and progressively using of more advanced techniques such as SEEK or 4D-VAR [23]. That is why the main characteristic of the Mercator Assimilation Systems (SAM) is the use of the PALM software [36] which is a modular tool for coupling and running ocean configurations and various data assimilation schemes such as OI, SEEK, 3D-VAR or 4D-VAR [23]. Actually, it provides a general structure for a modular implementation of a data assimilation system. This section presents the suite of assimilation tools of increasing complexity.

10.2.1 SAM-1

The first System of Assimilation Mercator (SAM-1) is the reduced-order optimal interpolation scheme SOFA [15] which is able to incorporate both altimeter and *in situ* observations.

10.2.1.1 SAM-1-v1

This first version SAM-1-v1 developed in the Mercator project allows the assimilation of anomalies of the sea level (altimetry) and it is an univariate scheme. It is adapted to the constraints of the scientific computation multiprocessors for the configurations of great dimension like ORCA-025 (see 10.5) and relatively easy to implement.

There are two types of data used in the first system. The assimilated data are altimetric tracks from JASON, ERS-2 or ENVISAT and GFO and also a pseudo-data of Mean Sea Surface Height (MSSH) as a reference level for the Sea Surface Height (SSH) based on the work of [40]. Following [14], for Optimal Interpolation an approximate background error covariance matrix B^f is used, such as :

$$B^f = D^{f^{\frac{1}{2}}} C D^{f^{\frac{1}{2}}} \tag{10.1}$$

where D^f is a background error variances matrix and C a correlation matrix. In SAM-1-v1, a constant 7 cm background error variance has been chosen and the correlation structure for the background (C matrix) has the form of a spatio-temporal bell which varies in shape according to the geographical position. Observation errors are assumed to be decorrelated in space and time. The observation error variances are specified according to the knowledge of instrumental characteristics. So, a 3 cm error is used for JASON and a 4.5 cm error is used for ERS-2 or ENVISAT and GFO.

The model initialization is realized by converting the 2D SLA analysis increments into 3D increments of prognostic variables using an algorithm based on the lifting-lowering method [12]. Now, only two global prototypes use this system and run operationally : PSY2G1 (MiniPOG : ORCA2^o) and PSY3v1(POG :ORCA025^o), see section 10.5.

10.2.1.2 SAM-1-v2

A second version of SAM-1 has been developed [15], which allows to use multivariate modes on the vertical (1D EOFs). This approach was first explored by [16]. The background error covariance matrix is modeled as :

$$B^f = S^T Br^f S \tag{10.2}$$

The Br^f matrix contains the background error covariances in the reduced space and S^T are the eigenvectors of B^f with S the reduced space simplification operator. Br^f is block diagonal and organized in mode-based block where each one modeled using the OI parameterization 10.1 [15]. The *estimation* state vector is x=(ψ : barotropic stream-function, T : temperature, S : salinity), so vertical EOFs are trivariate in these variables. Compared to the previous system, this multivariate scheme assimilates both altimeter data from satellites, *in-situ* (T,S) data from the CORIOLIS database, but also weekly SST and SSS climatology. Since 2004, this multivariate scheme is used operationally for the MNATL (1/3^o) configuration, named PSY1v2 prototype. Since September of 2005 is also operationally used in the PAM (1/15^o) configuration (PSY2-V2), see section 10.4.

10.2.2 SAM-2

The incremental improvement of data assimilation schemes lead to upgrade the 3D background error modelisation from a sequential point of view. Indeed, some limitations due to the concept of separability (separation between horizontal and vertical correlations) led to develop a more advanced assimilation system. Therefore one needs to use advanced estimation techniques, adapted to the high resolution, using coherent multivariate covariances of error with dynamics.

SAM2 is the second release which can be considered as a Singular Extended Evolutive Kalman (SEEK) filter ([35] analysis method. The SEEK (Singular Evolutive Extended Kalman) filter algorithm ([35],[42]) is a Reduced Order Kalman Filter designed to assimilate altimeter, *in-situ* profile and high resolution surface temperature data.

As in the SAM1 scheme, SAM2 is a reduced order Kalman filter, but the main difference comes from the error sub-space. In SAM2, the background error covariance matrix is approximated by a singular low-rank matrix. Unlike the SAM1 scheme for which the inversion of the innovation covariances matrix is performed in the observational space, the inversion is done in the modal space for the SAM2 scheme. Indeed, the error statistics of SEEK filter is represented in a sub-space spanned by a small number of dominant error directions. From a computational point of view, and to minimize the computational requirements, the analysis kernel in SAM2 has been massively parallelized and integrated in a generic platform hosting the SAM-1 and SAM-2 kernel families ([GLO68]). This platform is driven by the PALM software [36] which makes the coupling between the model codes and the assimilation schemes more effective. In SAM-2, the background error covariance is represented by means of a set of 3D error modes (3D EOFs of model variability) in the control space. The control state vector includes the temperature, salinity ant barotropic height model variables. Nevertheless the correction modifies the whole model state with a geostrophic adjustment at each analysis step. Several experiments have been realized over the year 2003 with the North Atlantic configuration (1/3^o). In this hindcast experiment, we used seasonal 3D EOFs computed from a multivariate SEEK analysis (1993-1998) where only surface data (SST, SLA) were assimilated, see ([41]). To validate the method with independent in situ temperature, an assimilation skill is illustrated in Figure 10.1. It shows the vertical distribution of the misfit variance computed between non-assimilated temperature profiles and the climatology, the control run and the hindcast experiments with 21 and 71 modes. Only the assimilation with the larger amount of modes improves the temperature field at all depths, whereas a significant reduction of the error in the thermocline takes place for the two hindcast experiments. Our next main developments are focused on the calculation protocol of the EOFs basis. In addition, an adaptative scheme of the background variance error is being developed which will allow its better fit at each analysis step. The next important step is the implementation of SAM2 into POG (PSY3-v2). Now, it is also being implemented into the ORCA2^o configuration (PSY2Gv2).

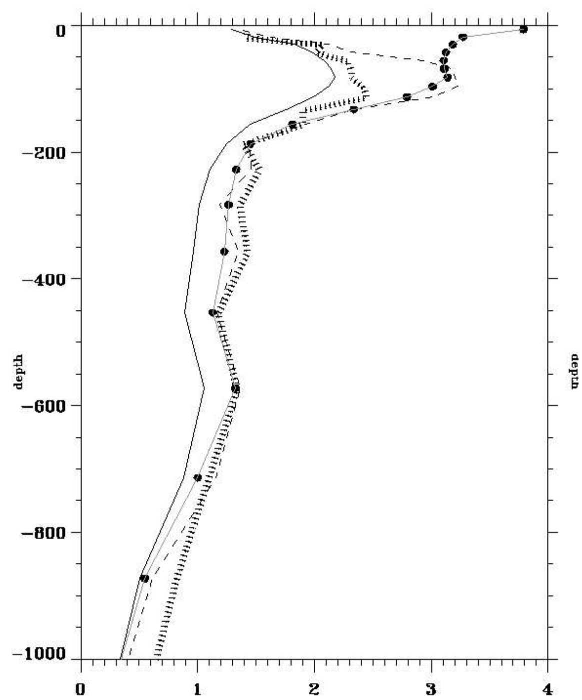

FIG. 10.1 – Variance of the temperature misfit (in C^2) between in situ data and : (i) the climatology (dots), (ii) the control run (dashed line) and (iii) the assimilation simulation with 71 modes (solid line) and 21 modes (dotted line) until 1000 meter depth during 2003 over the North Atlantic

10.2.3 SAM-3

The third one, SAM-3, is targeting more advanced approaches such as the 4D variational method and is still under construction in R&D mode. As for the temporal dimension of the assimilation problem, a major simplification is considered in the SAM-1 and SAM-2 schemes since the analysis is performed at regular times intervals which do not necessarily correspond to the measurement times. This was identified as one of the major limitations of operational NWP systems, impacting sometimes severely the forecast performances. The 4D-VAR variational formulation developed with a global ocean model by [46] takes a rigorous account of the temporal dimension and has the additional advantage of computing increments that are consistent with the linearized model dynamics. The four-dimensional variational formulation is based on the minimization of a cost function that measures the weighted squared difference between observations (including a background state) and the model counterpart. The given solution is the closest model trajectory to the observations and is dynamically consistent with the linearized model equations and the background state. At a given time, this solution is constrained by both past and future observations available in the assimilation window. The development of a third type of assimilation tool (noted SAM-3) has been initiated in MERCATOR which relies on the OPAVAR system. The technical and scientific features of the algorithm are under investigation to assimilate in situ and altimetric data simultaneously with the PSY3 global ocean configuration. The variational approach is particularly well suited to control of the dominant processes taking place in the tropical region where equatorial waves can propagate over several grid points during an assimilation window. As a first evaluation of the sensitivity of the variational system to the prescribed error statistics, different hindcast experiments have been performed using SAM-3 in a 3D-VAR setup, assimilating temperature and salinity profiles in the PSY3 configuration with different distributions of observation error variance on the vertical.

10.3 The high resolution ocean model (Romain Bourdallé-Badie, Yann Drillet)

10.3.1 Oceanographic developments

10.3.1.1 Local mesh refinement

The development of high resolution ocean models is strongly constrained by the computational cost. To simulate meso-scale phenomena in the ocean (10 to 100km) and take into account their influence on the global circulation, the horizontal resolution is a key of the main parameters. Two solutions are available : models with limited area or embedded model with increasing horizontal resolution. The AGRIF tool (Adaptive Grid Refinement In Fortran) allows this grid refinement, the large scale model benefits retroactively from the high resolution solution (coupling two-ways) [GLO78]. We have worked on this topic with Olivier Le Galloudec during his training period [34]. In a first time, a work on the stabilization of meso-scale activity during a simulation using an AGRIF zoom have been performed. We had also quantify the improvement due to the mesh refinement on the dynamics and on the physics in the Bay of Biscay. We have estimated that the stabilization of the high resolution is around 1 month and the creation of the meso-scale activity of the order of one week, which is quite long in the context of the Mercator prediction tools. In the second time, we have studied the influence of the interpolation parameters on the AGRIF simulation, the meso-scale representation and the numerical noise during the initialization. Especially during the spin up (stabilization) phase, we have tested several interpolations (linear, splines) for the initial conditions of the parent grids on the fine grid as well as for the forcing on the fine grid and the Two Way method. The main conclusion of this study are :

– the impact of a offline interpolation to decrease the initial noise
– the negligible improvement of the 2 way method in the context of 2 week simulations

Thus, we have been able to obtain a significant noise decreasing with the spline method. The two-way method on a short simulation (fourteen days) does not improve significantly the simulation.

10.3.1.2 Validate the monthly forecasts

The ensemble 1 month atmospheric forecast system developed by ECMWF is now available. During the training period of Xavier Le Vaillant, we have validate the use of this new atmospheric forcing data set in the Mercator System to improve the two week forecast and to validate the first 1 month ocean forecast [25]. The 1/3rd of degree North Atlantic system has been chosen to realize these experiments over the 2004 year. The new set of atmospheric forcing for this study is based on the ensemble mean of the ECMWF forecast with a daily frequency for a flux and a bulk formulations. The forecast scores based on RMS and correlation between ocean forecast and ocean best analysis show a good 7-days forecast(equivalent to the operational one), a small improvement for the 14-days forecast compared to the operational and a encouraging results with the 1-month forecast which is always better than the persistence. The Sea Surface Temperature forecast represented on Figure 10.2 show a really comparable result for the 7-day forecast. A noticeable improvement take place particularly in the south of the subtropical gyre, in the Sargasso Sea and in the North Atlantic current. The one-month forecast is quite good with a correlation between the best analysis of SST and the SST forecast larger than 0.90 excepted in the equatorial domain, in the North Brazil current and in the Gulf Stream. Compared to the persistence, the 1-month forecast presents a obvious benefit.

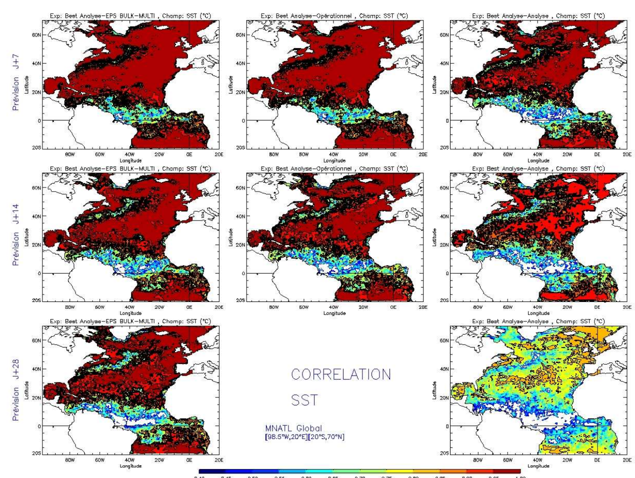

FIG. 10.2 – Temporal correlation between forecast and best analysis of SST in 2004. 1st line : 7-days forecast ; 2nd line : 14-days forecast ; 3rd line : 1 month forecast. 1st column : Best analysis compared to forecast forced by the ensemble mean atmospheric forcing ; 2nd column : Best analysis compared to Mercator operational forecast ; 3rd column : Best analysis compared to persistence.

10.3.1.3 Parameterization of the continental fresh water

During the first half of 2005, we have supervised Remi Vucher who worked on a review of the the continental fresh water apports in the ocean (runoffs) and their parametrization in the OPA model [38]. In a first time, the runoff input file for the ocean model has been improved in agreement with the work realized on the GPCP data base [13]. The aim of this study was to take into account the coastal runoff, which was ignored since today and to generate an automatic method to build the file. In a second time, a study of two parameterizations for the continental fresh water apports parameterization has been performed. Several sensitivity experiments have been led :

– Influence of the vertical mixing parameters on the river mouth
– On a numeric method including the “open boundaries” : in order to consider the runoff as a moving quantity of fresh water entering in the ocean, and not as an imposed quantity of fresh water falling on a limited area at the ocean surface (like the precipitation in the model).

The goal is to choose the better method for the runoff modeling in the future configurations used in Mercator-Océan.

10.3.1.4 Sub grid parameterization of the re-stratifi cation

The Gent and Mc Williams parameterization (GM90) [GLO77] is a subgridscale parameterization which allows the re-stratification of the water column during the summer when the model is not eddy-resolving. In the case of the Labrador Sea, re-stratification during the summer is due to the atmospherics fluxes but also to some warm eddies detaching from the North Atlantic current and from the Greenland current. These eddies are advected in the centre of the Labrador Sea where they diffuse and warm the upper layers. In the case of MNATL and PAM model is not sufficient to simulate this re-stratification. However, the simulation of such events can be reproduced with a good realism with the GM90 parameterization, which acts in the model like a diffusion operator. The aim being to have the best compromise between the current representations (intensity, turbulence) and the water mass (salinity, temperature, vertical stratification) in the PAM model, experiments with a regionalization of the GM90 parameterization in PAM model have been carried. The summer re-stratification is clearly better with GM90.

10.3.1.5 Vorticity conserving energy and enstrophy scheme

A new scheme for the computation of the vorticity term has been implemented in NEMO. The conservation of the energy and the enstrophy leads to an improvement of the solution as DRAKKAR project showed in the ORCA025 configuration. So, the implementation of this scheme have been done in all Mercator configurations and particularly in PAM model [GLO65]. Two simulations have been led, the first one without the vorticity scheme (PAM2-04) and the second one with (PAM2-05). The main conclusions are : With the new scheme we have observe no significant improvement in the Gulf Stream separation but an improvement in its penetration and in the representation of the Azores front. Now, this new scheme is use in all operational Mercator prototypes.

10.3.2 Oceanographic studies with PAM model

The North Atlantic and Mediterranean Mercator configuration PAM is a very high resolution (5 to 7 km) model based on the OPA-8.1 ocean general circulation model [30]. The PAM configuration benefited from the experience gained with the lower resolution (1/3^{o}) MNATL configuration which has been inherited from the CLIPPER project [10] aiming at simulating the Atlantic basin circulation. MNATL is used as a handy research and development tool and is part of the first Mercator operational system which is used for real time analysis and forecasts since January 17th 2001.

The PAM model configuration was designed in 1998, implemented and tuned in 1999 and 2000. Sensitivity tests have been conducted during the years 2000 and 2001 which are described in [18]. During 2002-2003, PAM model has been improved with the implementation of new parameterizations. Validation and quantification of the gain between several experiments were also performed, as well as scientific studies about meso-scale activities and the transport trough North Atlantic straits. At this time around 40 years of simulation with the PAM model have been realized, which represents 10000 h CPU on the Fujitsu VPP5000 and 50 Terabytes of output files.

The analysis and forecasting system PSY2-V2 (Prototype SYstem 2) uses the PAM model and the SAM-1-v2 system (see section 10.4).

10.3.2.1 The Meddies in the PAM model

The present generation of high-resolution ocean model offers a new way to investigate the characteristics and evolution of the ocean meso-scale. An analysis of the simulated Mediterranean eddies, the so called Meddies, has been performed [GLO12] and an article has been published in *Journal of Geophysical Research*. Hereafter the abstract is proposed :

The new generation of high resolution ocean model offers a new way to investigate the characteristics and the evolution of the ocean meso-scale. An analysis of the simulated Mediterranean eddies, the so called Meddies, is presented. The model used in this study is the Mercator North Atlantic [9^{o}N, 70^{o}N] and Mediterranean Sea Prototype (PAM), a high-resolution configuration (3.5-8 km horizontal grid) based on the OPA ocean general circulation model. The Meddies are coherent structures of warm and salt Mediterranean Water advected in the North-East Atlantic. A five-year experiment performed with PAM reproduced the main observed characteristics of the Meddies : thermohaline properties (11.8^{o}C, 36 PSU), sizes (radius between 25 and 110 km), thickness (between 500 and 1000 m), westward advection velocities (1.4 cm.s^{-1}), angular velocities (a period of 20 days), a good estimate of the number of Meddies in the north-east Atlantic (˜22) and their realistic geographical distribution (80% south of 40^{o}N). Moreover, and in agreement with a previous study based on an observation cruise, these modeled Meddies represent half of the westward salinity transport of MW.

10.3.2.2 Comparison with the *in_situ* profiles

A simulation over the last decade of the 21 century, without assimilation, has been led to estimate the ability of this model to simulate ocean over a large period. Specific areas have been established to study the model behaviors in different regions of the North Atlantic. Principal dynamical bias observed in the model are the disappearance of the cold coastal current along the America (not represented in the Levitus climatology), the separation of the Gulf Stream and the increase of salinity in the Labrador Sea. The spatial variability is smaller in the model, it is due to an homogenization problem of the water characteristics. It could be the result of a too important convection or a too big value of the diffusion coefficient. The upper ocean in the European coast is the area which has the best agreement with the *in_situ* profiles (cf fig 10.3). It could be due to several reasons :

- Better resolution of the model in this area.
- In this place currents are weaker and the representation of the gradients is easier. The diffusion operator works better.

10.3.3 Perspectives

A new strategy has been defined to develop future Mercator configurations. All of them should be based on ORCA grid (tripolar grid to avoid the singularity problem in the Arctic sea). With this strategy, the future configurations are homotetic each others. It permits to use quick in-line interpolation for the input file (forcing flux will be generate just at one resolution) and diagnostics implementation becomes general for all Mercator models. In this way, a new high resolution model of the North Atlantic is being developed. The domain covers North Atlantic (between 20^{o}S and 80^{o}N) and Mediterranean Sea and it coupled with an ice model. This is the first step for the next 1/12^o global Mercator configuration. A such model should be develop at the horizon 2008 and implies an important work on the size of the input and output files. 400 processors on an IBM SP4 (computer at the ECMWF, Reading, UK) and 300 Gigabytes of memory are needed.

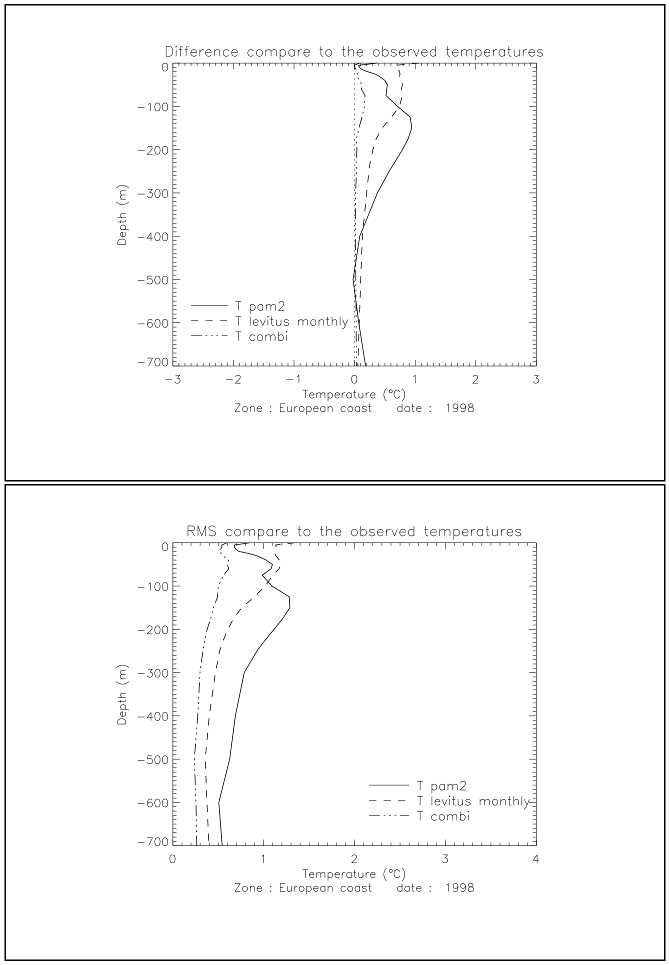

FIG. 10.3 – Vertical profiles over Europe area for the temperature : mean difference (up) ; RMS (bottom). PAM minus observation in solid line, Levitus climatology minus observations in dashed line, a combination of observations and Levitus minus observations (dashed dots line).

The future configurations will be developed with a refined vertical grid near the surface. The vertical resolution will be less than 1m at the surface. This is a requirement condition to take into account correctly the diurnal cycle. This new vertical discretization will implied a study of the vertical physic in the code. Several new parameterizations of the vertical mixing will be tested like KPP mixing scheme [24], impact of the surface mixing due to the wave, to the tide.

10.4 The second operational Prototype System PSY2v2(Jean-Michel Lellouche)

During these two years, a new assimilation system based on the Reduced-Order Optimal Interpolation algorithm using 1D vertical multivariate EOFs has been implemented in the Mercator North Atlantic and Mediterranean High Resolution model. This new multivariate prototype is called PSY2v2. The ocean model is based on OPA-8.1 [30], a general circulation model developed at LODYC (IPSL Paris), and is designed to simulate the Atlantic and Mediterranean oceans with a very high horizontal resolution (5 to 7 km).

The assimilation system is based on the Reduced-Order Optimal Interpolation algorithm and uses 1D vertical multivariate EOFs to extract statistically-coherent information from the observations (Benkiran et al., 2005). The PSY2v2 prototype assimilates, in a fully multivariate way, conjointly altimeter data (JASON1,ENVISAT and GFO), Reynolds SST and temperature and salinity vertical profiles provided by the CORIOLIS centre. The previous high resolution prototype PSY2v1 assimilates only the Sea Level Anomaly (SLA) from satellites measurements along tracks with a univariate mode. The 2D increments of SLA are then converted into 3D increments of U, V, S, T and TKE using an algorithm based on the "lifting-lowering" method (Cooper and Haines, 1996).

10.4.1 The new assimilation method

The assimilation method used by PSY2v2 is based on SAM1v2 (see section 10.2.1.2) and works as follows :
- The differences between SLA, T and S observations and model forecast are computed at appropriate time and data locations for a full week model integration.
- These misfits are projected in a 2D reduced space using a fully multivariate Optimal Interpolation (OI) :
  - The estimation state vector is composed by the vertical profiles of temperature and salinity and the barotropic stream function.
  - EOFs of the estimation state vector are computed once at each point of the model grid from hindcast simulations.
  - The OI gain is computed for each of the EOFs independently (EOFs orthogonality) for a given number of dominant EOFs (order reduction up to 20 modes).
- The model state is updated by the sum of the contribution of each selected EOF to the gain multiplied by the innovation vector.
- The baroclinic velocity increments, which are not in the estimation state vector, are computed assuming geostrophy.
- A new model state analysis is updated using the innovation vector computed above.
- Starting from this new ocean state, the model runs for the next week of prediction, using the atmospheric forcing fields provided by the ECMWF.

10.4.2 PSY2v2 Results

Some results obtained with the multivariate multi-data prototype PSY2v2 are presented hereafter. The real time has been caught up by January 1th 2003 from the climatology Medatlas2 in the Mediterranean and Reynaud in the Atlantic until now.

10.4.2.1 Assimilation diagnostics

The figure 10.4 (left) concerns the number of temperature profiles entered into the system versus time and depth. This number becomes particularly important in the second half of the year (about 500 profiles). The figure 10.4 (middle) shows the variations of the mean value of the misfits (differences between the observation and model forecast), which is weak during the whole year. The RMS value of the misfit is plotted on the figure 10.4(right) and proves to be close to zero, with a maximum at the thermocline depth.

Satellite altimetry are used to constrain weekly the geostrophic currents, here in 2004. The data number exhibits the data availability in real-time. The misfits (i.e., correction to apply to the model) reach 8cm, and represents 75% of the data variability (Figure 10.5).

10.4.2.2 Impact of T/S vertical profi les assimilation on water masses representation

We compare here the water masses in PSY2v1 and PSY2v2 systems.

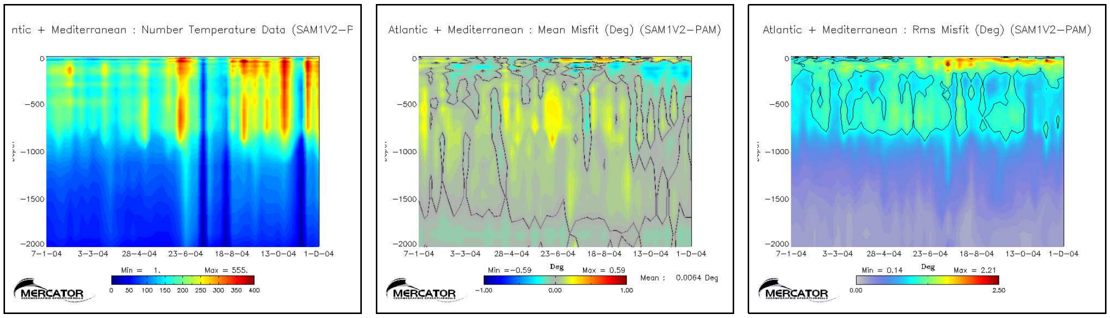

FIG. 10.4 – Assimilation diagnostics with respect to the vertical temperature profiles over the year 2004 : Number of temperature data (left), Mean misfit between observations and model forecast (middle) and RMS of the misfit (right).

– A WOCE zonal salinity section at 26°N (figure 10.6) shows the Subtropical Underwater (STUW), with salinity characteristics ranging from 36.6 PSU to 36.9 PSU, centered at 200m depth in the western Atlantic basin from 80°W to 50°W. The same salinity section in PSY2v1 does not display the STUW salinity characteristics, whereas PSY2v2 does (figure 10.6). Hence we show that assimilation of salinity vertical profiles in PSY2v2 allows to better represent the STUW salinity characteristics, although STUW are less salty in PSY2v2 than in the WOCE observations. This might be due to a lack of salinity vertical profiles to be assimilated in this region, or to an annual variation of the STUW salinity characteristics between the time of the WOCE cruises (1992) and the time when we look at PSY2v2 (2003).
– One of the main problems with univariate prototypes is the representation of Mediterranean waters, mainly its vertical position near 1000m. The figure 10.7 shows the salinity at 1000m for April 2004 from PSY2v1 and PSY2v2 simulations. For PSY2v1, the Mediterranean Water Outflow (MOW) is maintained by the relaxation bellow 500m to Reynaud climatology in the Gulf of Cadiz, that is not the case anymore for PSY2v2. We can see on the figure 10.7 salty water which corresponds to the characteristics of Mediterranean waters (salinity close to 36.5 PSU), with meddies formation and better propagation in the PSY2v2 case,showing impact of T/S vertical profiles assimilation.

10.4.2.3 The Mixed Layer Depth in the POMME area

In this paragraph, we give an overview of the physical and biological processes taking place in the POMME area (16°W-22°W and 38°N-45°N). We will then look whether those processes are well represented in the two MERCATOR systems. The POMME project investigates the processes of subduction and mode water formation at the meso-scale, as well as the coupling between the subduction dynamical processes and the Carbon cycle biological processes [32]. The region selected (Black square on figure 10.8) presents subduction of the 11-12°C North-East Atlantic Mode Water. The POMME area is, according to the climatology [8], a transition zone between deep late winter Mixed Layers (ML) in the North and shallower winter ML in the South. The POMME1 cruise during the winter 2001 (February-March 2001) with meridional sections at 20°W and 15.2°W shows ML with depth ranging from 20m to 250m (Reverdin G., personal communication) with ML deeper in the northern than in the southern POMME area. The deep northern part is associated with a rather biologically productive area, when the south one is more oligotrophic [27]. Moreover, as subduction and the spring bloom both occurs at the end of the winter, it is important to understand the timing of these two processes : subduction drives the bio-geochemical characteristics of the water masses before they are incorporated into the main thermocline [27]. The PSY2v1 and PSY2v2 (figure 10.8), in average over the winter 2004 (Jan-Feb-Mar) shows Mixed Layer Depth (MLD) deeper in the northern than in the southern POMME area, in agreement with Reverdin (personal

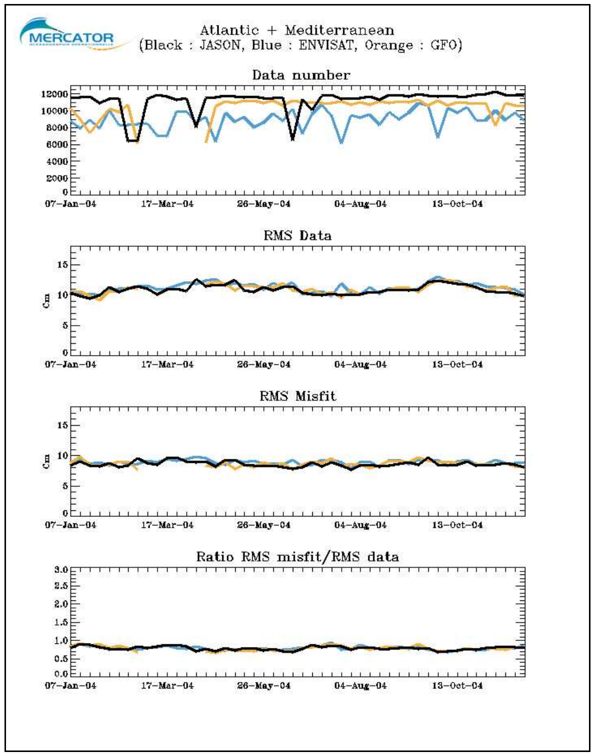

FIG. 10.5 – Assimilation diagnostics with respect to the SLA for the three satellites JASON1, ENVISAT and GFO. From top to bottom : Data number, RMS data, RMS misfit and ratio (RMS misfit / RMS data).

communication) and the Boyer-Montegut et al. (2004) climatology. In the high resolution CLIPPER simulation [44], the MLD seasonal cycle is well represented, with nevertheless overestimated amplitude by up to 100m in March [28]. An hovmuller diagram (figure 10.9) shows that the seasonal cycle phase is also well represented in PSY2v1 and PSY2v2, with amplitudes ranging from 40m in the South to a maximum of 180m in the northern part for PSY2v1, and 20m in the South along with maximum values of 260m in the northern part for PSY2v2. Following Reverdin (personal communication), PSY2v2 MLD agrees better with observations. Figure 10.9 suggests that the PSY2v2 system display more MLD fine scale structures of importance for the biological activity, than the PSY2v1 system. Although the two systems have the same horizontal and vertical resolution, this suggests that assimilation of temperature and salinity vertical profiles in the PSY2v2 system enhances the development of MLD fine scale structures.

10.4.2.4 Sea Surface Temperature and generation of the loop current eddies in the Gulf of Mexico

Sea surface temperature (SST) in the PSY2v2 system is compared to independent observations (i.e. not assimilated) (figure 10.11) at 4 buoys locations (figure 10.10) for the period June 15th 2004 to October 19th 2004. The PSY2v2 SST temporal variability agrees very well with observations, although the model shows a 0.5°C to 1°C bias with observations, maybe because the model SST is a 3m depth temperature, whereas the observed SST is a 0.6m depth temperature. The generation and evolution of the loop current eddies in the Gulf of Mexico is represented in a very realistic way by the PSY2v2 system. Indeed, a comparison of the PSY2v2 SLA with Chlorophyll-A concentration (independent data, i.e. not assimilated) in the Gulf of Mexico, during a cycle of 6 weeks from July to September 2004, shows a very good agreement between the

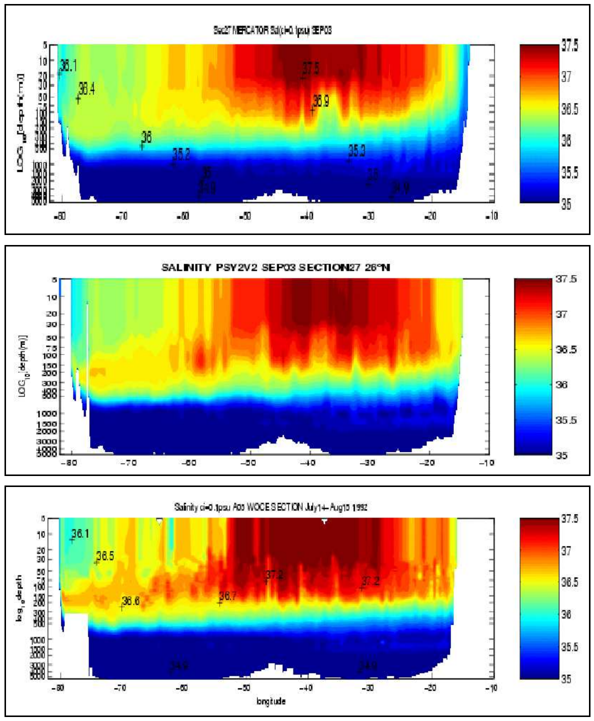

FIG. 10.6 – Zonal salinity (psu) section across latitude 26°N in the North Atlantic as a function of longitude and log10(depth) : PSY2v1 in September 2003 (top panel), PSY2v2 in September 2003 (middle panel), WOCE A05 synoptic section Jul-Aug 1992 (lower panel).

model and the observations (figure 10.12). The loop current eddy is characterized by very low chlorophyll-A concentration. From week1 to week6 (from top to bottom, figure 10.12), we can follow the generation, the detachment and then the westward translation of the eddy, which happen in the model in phase with observations. Such eddies are generated by the instability of the Yucatan current, which is realistically represented in the PSY2v2 system (not shown). The Yucatan current maximum velocity is 130cm/s at the end of summer 2003, in agreement with observations from [9]. Two deep counter-currents on the Yucatan and Cuban side observed by [9] are also present in the PSY2v2 system. In the western part of the Gulf of Mexico, we notice several patches with a very low chlorophyll-A concentration (figure 10.12, left column), associated with small scale eddies in the MERCATOR2 sea level anomaly (figure 10.12, right column). Those structures are coming from a former loop current eddy which disintegrated into smaller scale eddies when colliding with the Mexican continental plateau.

10.4.3 Perspectives

We described the new Mercator fully multivariate high resolution prototype. This new prototype has a very good statistical comportment and allows, among other things, to better represent water masses, like for example, the Mediterranean Water Outflow, with a very advanced description of the meso-scale patterns. A more comprehensive validation of PSY2v2 prototype is in progress and we plan to provide on the Web, analysis and forecasts in a operational mode from the beginning of October 2005.

Next step will concern reanalysis with PSY2v2 over the last decade period.

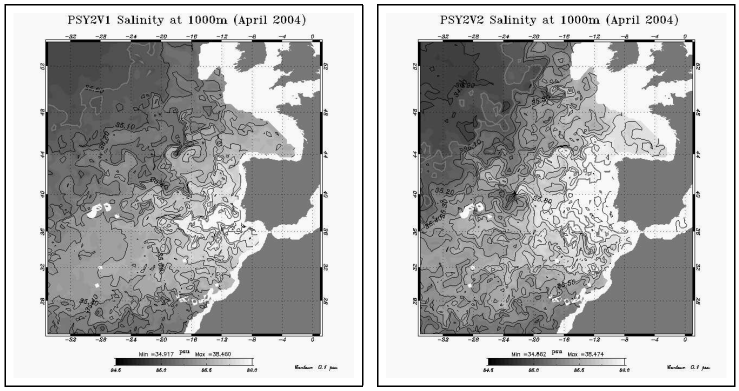

FIG. 10.7 – Salinity at 1000m in April 2004 for PSY2v1 (left) and PSY2v2 (right) simulations.

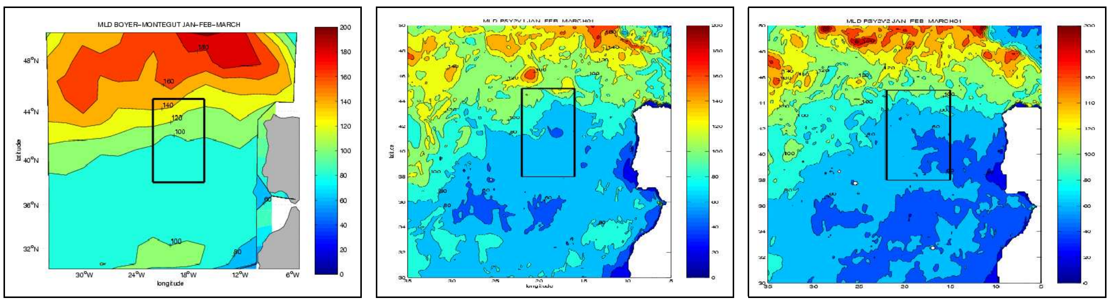

FIG. 10.8 – Winter Mixed Layer Depth (meters) in the Boyer-Montegut 2004 climatology (left), in PSY2v1 system winter 2004 (middle), in the PSY2v2 system winter 2004 (right).

10.5 The global configuration models (C. Derval, L. Fleury, G. Garric, M. Laborie and E. Rémy)

The ORCA025 team is in charge of developing a global ocean model configuration at medium resolution. This component is actually part of the global ocean forecasting system of MERCATOR PSY3v1 launched in october 2005. The set-up of the configuration began in 2001 and was focused on the horizontal and vertical resolution taking into account the future computer capacities. The numerical model is the ocean general circulation model OPA elaborated in LODYC (Paris). The horizontal grid is an ORCA type grid, with two poles on land in the Northern Hemisphere to avoid singularities at the north geographic Pole. The ORCA025 configuration, with a free-surface formulation, corresponds to a 1/4deg resolution, e.g. with 1042x1021 horizontal grid points. The use of the NetCDF format for input and output was chosen for easy-handling purpose. Until now, the development was mainly focused on the OPA8.2 version with a diagnostic sea ice model only. The recent development of the NEMO configuration (OPA9) initiated by the DRAKKAR Project allowed us to implement and to adapt for our purposes all the updates implicitly included in the NEMO configuration.

In the two next sections we present briefly firstly the work done on the first version of ORCA025 with the diagnostic-only sea ice (OPA8.2) and, in the second section, the preparation of the coupled ocean ice model configuration (NEMO ; OPA9), ORCA025-LIM, the target configuration, a specific analysis of the

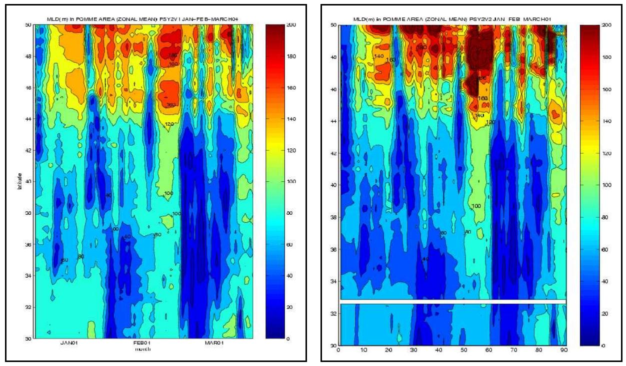

FIG. 10.9 – Hovmuller diagram (time as a function of latitude) of the Winter 2004 (JFM) Mixed Layer Depth (meters) in PSY2v1 (left) and in PSY2v2 (right).

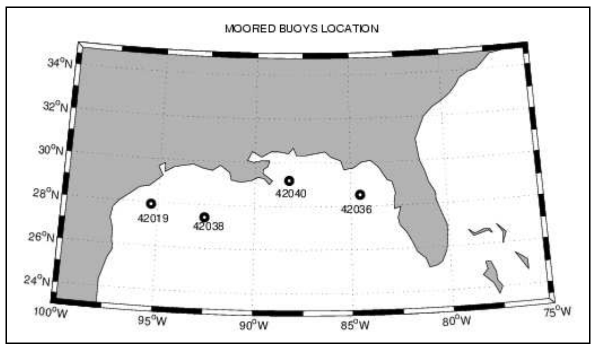

FIG. 10.10 – Location of the four moored buoys (with buoy numbers) in the Gulf of Mexico.

ORCA025-LIM at high latitudes and the description of various experiments performed with the ORCA2-LIM configuration.

10.5.1 The ORCA confi gurations

10.5.1.1 The 3-year climatological simulation : POG-04

A 3-year climatological simulation, POG-04, driven by the ERA15 climatological forcing fields, but with the evaporation flux scaled by 0.6 to equilibrate the freshwater budget, have been performed ([GLO75]). The main circulation features, as the gyres, are well- represented, but the usual problems in z-coordinates eddy- permitting configuration are also present like the wrong position of the Gulf Stream. A first analysis of the experiment was done per ocean basin, compared to Levitus salinity and temperature fields used to initialize the simulation. Due to the resolution, strong and narrow western boundary currents are present, mass transports through major straits and between oceans basins are coherent with the observations. At the equator a cold bias is observed, especially in the the Atlantic and Pacific eastern basin, this being probably due the forcing fields. The amplitude of the undercurrent is comparable to the observed ones. The variability of the Indian Ocean due to the monsoon is well represented. The spatial resolution permits the explicit representation of some eddy activity, for example in the Aghulas region.

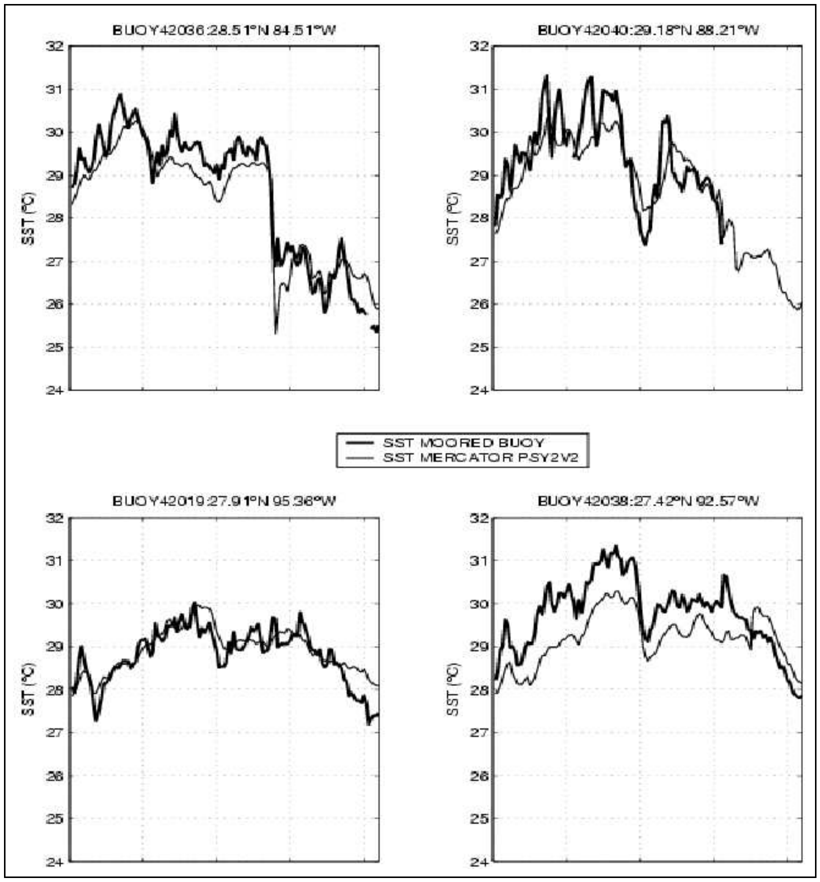

FIG. 10.11 – Moored buoys Sea Surface Temperature (°C) (at 0.6m depth) (Bold black curve) in the Gulf of Mexico from June 15 to October 19 2004. Light black curve shows the PSY2v2 three meters depth temperature (°C) at the closest location and for the same time period.

10.5.1.2 The Interannual experiment "POG05B"

The experiment has been performed on the ECMWF's IBM calculator during March 2005 with the CVS-basis OPA8.2 Mercator model configuration ([GLO76]). As a reminder, here are the main physical attributes which have been retained in the configuration : free surface, diagnostic sea ice model, non linear bottom friction, free slip lateral boundary conditions, turbulent closure scheme (TKE) for vertical mixing with viscosity/diffusivity coefficient enhancements in case of static instability (convection), horizontal biharmonic viscosity for momentum, laplacian lateral isopycnal diffusion on tracers, a monthly relaxation towards Levitus temperature and salinity is applied in the Gibraltar and Bal el Mandeb straits. A daily correction of the surface mass budget (EmP) is arbitrarily imposed to zero in order to avoid any mass drift. In collaboration with the DRAKKAR project, a new algorithm for the total vorticity term in the momentum advection has been implemented. This scheme conserves both total energy for general flow and, as the former scheme, the potential enstrophy for flow with no mass flux divergence. The interannual (1993-2001) daily atmospheric forcing is issued from the ERA40 reanalysis ; a damping term (40 W/m2) towards the weekly Reynolds SST is applied to the heat surface budget.

Compared to the POG04 experiment, the mean eddy kinetic energy in the western boundary currents is more realistic, with a better representation of the downstream flow, due to the use of the new vorticity scheme. This behaviour is particularly marked in the Agulhas Current. However, the global upper layers (0-1000m) remain cooler and less salty than the Levitus climatology. The interannual atmospheric forcing allowed us to evaluate the interannual variability simulated in POG05B. The figure 10.13 represents the temperature adjustement under the 1997-1998 ENSO event in the eastern part of the Pacific. This ENSO is, among others properties, characterised by a Kelvin wave initiated by a westerly wind bursts in March 1997. Compared to the TAO data, POG05B reproduces correctly the intensity (150m) of the thermocline deepening and the occurence of the Kelvin wave (summer 1997) and of the main ENSO signal (end 1997). Similarly, the shallowing of the mixed layer in spring 1998 (Nina event) is well reproduced by POG05B. The realistic representation of these events are particularly encouraging for further use of the 1/4deg global configurations.

10.5.2 The ORCA-LIM configurations

10.5.2.1 The ORCA025-LIM configuration

The setup of the ORCA025-LIM in the OPA8.2 version has been achieved in 2004 ([GLO80]). Briefly, the ORCA025-LIM configuration (OPA8.2) is similar to the ORCA025 configuration used to perform the POG04 experiment ; the ORCA model is coupled to the full thermodynamic-dynamic sea ice model LIM (Louvain Ice Model) developped by T. Fichefet and his team at the "Institut d'Astronomie et de Géophysique G. Lemaître" at the University of Louvain La Neuve (Belgium) ; the atmospheric forcing is in "bulk" formulae mode, i.e. heat and momentum fluxes are re-calculated by the model with the appropriate surface model conditions. An adaptation of the ORCA025-LIM with the NEMO configuration (OPA9), initially developped by the DRAKKAR Project, have also been recently achieved for Mercator purposes. With a substantial optimisation by a complete re-writting of the code (Fortran 90), this new configuration includes different improvments as the partial steps, a new vertical grid with refined surface layers (1m) and a new coastal and rivers runoffs package. An interannual experiment has also been performed with the same interannual forcing as the POG05B experiment. The Analysis are under process.
In the meantime, sea ice related activities has been initiated through identification of available datasets (essentially as a first step these data were from the National Snow and Ice Data Center) to evaluate future ORCA-LIM configurations (see [GLO81] for more details). More recently, a close collaboration with the CERSAT allowed us to identify satellite products (sea ice concentration and sea ice drift) which are supposed to be used in a near future for validations and operationnal purposes (see [GLO82] for more details). A sea ice intercomparison project involving sea ice operationnal systems has also initiated to define common standard sea ice diagnostics. This collaboration have ended in definition of "metrics" Class1 in the MERSEA Project classification and proposal for the followings Class 2 and 3.

10.5.2.2 The Antarctica zoom interannual experiment

Conjointly with the global 1/4deg resolution, we developed a 1/4deg configuration constrained to the (30řS-80řS) domain. This development with the OPA8.2 version allowed us to progress in the set up of the global configuration and, in the same time, to study the feasibility of the 1/4deg horizontal resolution to reproduce the life cycle of the Antarctica polynias. Considering their significative impacts on climate in general (see [31] for example), various studies have recently put these well-known meso-scale phenomena under new considerations. We performed an interannual experiment with this *zoom Antarctica* configuration forced by daily ECMWF analysis and seasonal surface salinity restoring. The large-scale sea ice extent simulated by this configuration is close to observations ([11]) during winter but is largely underestimated during summer, especially along the East Antarctica coastline where sea ice is nearly absent. These shortcomings raised the importance of the surface atmospheric forcing as the same model forced by climatological atmospheric datasets simulated sea ice extent closer to observations ([43]). We have selected 6 coastal areas known to be favourable of polynias formation : Terra Nova Bay, Mertz Glacier, Adélie, Shackleton ice-shelf, Prydz Bay and Enderby. Characterised by a relative decrease of the sea ice concentration in timeseries, our modelled polynias are well correlated with observed polynias in Shackleton ice-shelf, Prydz Bay and Enderby. Highly correlated with the occurrence of the katabatic winds in the ECMWF analysis, the polynias are badly represented in the Terra Nova Bay, Mertz Glacier and Adélie. The correlation between the katabatic winds and the sea ice concentration reaches 0.63 in Prydz Bay during winter 1995. The increase of these correlations with a positive lag (wind in advance) of few days (1 day in general) highlights the relative inertia of sea ice under the dynamical forcing.

A more detailed analysis of a particular events in the Prydz Bay between the 26th april and 14th august 1994 revealed the formation of polynias are associated with periods of strong winds (above 10 $\mathrm{m.s^{-1}}$) during 10-20 days (Figure 10.14). A close link is also present between the wind and the sea ice drift. We can also note that the surface air temperature is highly correlated with the winds : the air advected by the katabatic flow is warmed adiabatically and, subsequently, the surface air atmosphere increased along the shore under katabatic winds regime. As the sea ice formation is closely linked to surface heat losses and, then, to the temperature gradient between the surface and the atmosphere, the increase of the surface air temperature counteracts the ice formation. The oceanic heat flux, prognostic quantity in the model, is also highly correlated with the winds (not shown) via the vertical mixing in the upper oceanic layers. Although the transport of the warm air prevents the formation of ice in the polynia, the vertical mixing induced by the winds upwells the heat needed to self-sustain the polynia and the sea ice formation. The analysis of this event highlighted the complex feedbacks in the polynias life cycle and, furthermore, the key role played by the sea ice in high latitudes. This study has also shown the feasibility of the 1/4deg horizontal resolution coupled ocean/sea ice model to represent the processes inside the polynias, given a more adapted surface atmospheric forcing. Part of this work has been published in the Mercator Newsletter ([GLO14]).

10.5.2.3 The surface mass budget with the ORCA2-LIM configurations

In the framework of studying the surface atmospheric forcing applied to the future global prototype, we performed an experiment with the ORCA2-LIM configuration and forced by the interannual ECMWF analysis dataset over the 1993-2004 period. The simulated global mean of the sea surface height (SSH) exhibits a very large positive interannual trend (280 $\mathrm{mm.year^{-1}}$) which reveals an unrealistic accumulation of mass in oceans. The surface mass excess is undoubtedly issued from the large overestimation of the ECMWF rainfall compared to the GPCPv2 dataset ([22]). Although no significant trend has been found in the GPCPv2 dataset and, in general, in precipitation measurements [33], the ECMWF rainfall exhibits unrealistic trends during this decadal period. The ECMWF reanalysis ERA-40 project shows also an overestimation but, with the use of the same system (model + assimilation scheme) during the experiment, the excess remains constant (close to $+1\mathrm{mm.day^{-1}}$ compared to GPCP dataset). This overestimation is essentially found in the tropical bands for both ECMWF datasets. However, medium-and-large-scales bias features are also observed in various areas : the large underestimation found in Southern mid-latitudes is in fact a result of a less well marked circumpolar trough in the ECMWF model ; systematic overestimation (resp. underestimation) are found upstream (resp. downstream) orography (the Andes cordillera, the Antarctic Peninsula, Greenland) ; underestimation is also found at the end of the Atlantic storm tracks in the Norwegian Sea. In order to correct this large positive SSH trend, we have tempted to correct this systematic bias present in the ECMWF rainfall dataset by applying the concept of the method described in [45]. Briefly, they assume four assumptions : 1) *The ECMWF precipitation field should conform to the observed precipitation field* (the GPCPv2 dataset for our purpose) ; 2) *The water budget, precipitation minus evaporation* (calculated by the ORCA-LIM model in our case), *has to be zero in a global sense for the concerned period* ; 3) *The evaporation field is treated as error-free* ; 4) *The temporal variability is not affected to first order.* The minimisation procedure involves a single coefficient, α, calculated as the solution of the following system :

$$\overline{\mathrm{P}}_{\mathrm{C}} = \overline{\mathrm{P}} - \alpha(\overline{\mathrm{P}} - \overline{\mathrm{P}}_{\mathrm{OBS}}) \text{ with } \overline{\mathrm{P}}_{\mathrm{C}} + \overline{\mathrm{R}} - \overline{\mathrm{E}} = 0 \tag{10.3}$$

this can be reduced to the simple equation :

$$\alpha = \frac{(\overline{\mathrm{P}}_{\mathrm{C}} + \overline{\mathrm{R}} - \overline{\mathrm{E}})}{\overline{\mathrm{P}} - \overline{\mathrm{P}}_{\mathrm{obs}})} \tag{10.4}$$

where P is the ECMWF (either analysis or reanalysis) precipitation (and $\overline{\mathrm{P}}$ its mean), $\mathrm{P}_{\mathrm{obs}}$ is the GPCP climatological precipitation (and $\overline{\mathrm{P}}_{\mathrm{obs}}$ its mean). $\overline{\mathrm{P}}_{\mathrm{C}}$ is the mean corrected precipitation, $\overline{\mathrm{E}}$ is the mean evaporation and $\overline{\mathrm{R}}$ is the mean river runoff set to 0.31 mm.day-1 (elaborated from different references not listed here) in our experiments. All these quantities have been evaluated on oceanic values only. We have adopted a different method from the [45] paper : the correction is applied on the global ocean and not only on the tropical band ; the correction is applied locally (each grid point) and not latitudinal dependent ; we use a monthly GPCP dataset sampling. As our different sensitivity experiments are all performed after the implementation of the 4DVAR assimilation scheme in the ECMWF forecast system, in 1998, we have applied the correction on two time series : 1993-1997 and 1998-2004. However, the interannual variability of the precipitations profile of the mass surface budget in the experiment shows large difference before and after 1998.

The evaporation issued from the previous experiment has been used to evaluate the alpha coefficient and the ECMWF analysis corrected precipitation. A similar experiment is then performed with this corrected precipitation field. With different mean values of the evaporation flux at different periods, the Figure 8 and the Table 2 show a nearly closed surface mass budget during 1998-2004 : the more alpha is close to 1.0, the more the corrected precipitation is close to observed value and the more the evaporation flux issued from the experiment allows to close the mass budget. Although the equilibrated budget during the period 1993-1997 is due to the cancellation of gained and loss of mass (Figure 9), the nearly closed budget during 1998-2004 exhibits a realistic trend. Moreover, the trend of the SSH during 1998-2004 is in the order of magnitude of the estimated thermosteric sea level rise (1.6 $\pm$ 0.3 mm/year for 1993-2003) [47] or the total observed sea-level rise (2.5 $\pm$ 0.4 mm/year for 1993-2003) [29] The magnitude of the mass damping is also divided by more than two between the first experiment and the corrected experiment on the 1998-2004 period. The stabilisation of the damping term after the year 2000 under a value of 10-3*mm.day-1 is particularly encouraging We can also note that the damping term is no longer concentrated in the tropical band but is spread all over the global ocean with peaks in the mid-(Northern Atlantic) and high-(Arctic Ocean) latitudes (not shown).

We applied the same method of correction on the ECMWF ERA-40 reanalysis precipitations, performed with the ORCA2-LIM configuration forced by interannual ERA-40 ECMWF dataset on the 1993-2001 periods. An experiment performed in the same conditions but uses the corrected precipitation on the 1993-2001 periods. With a mean value of 1.0, the alpha coefficient reveals an appropriate evaporation flux to close the surface mass budget. Once again, the interannual variability of SSH exhibits a realistic trend (4mm/year). The magnitude of the mass damping is also significantly reduced. However, this relaxation is not stabilised after ten years of experiment ; this behaviour is still under investigations.

This work has allowed us to close the surface mass budget in hindcast and reanalysis configurations for the recent ECMWF analysis and reanalysis datasets (refer to [GLO83] for more details). This method should be applied to the spin up to real time for the PSY3v2 prototype as long as the GPCP datasets are available. These precipitation datasets, delayed to present time, are not available in real time. However, we used the monthly mean fields which are not designed to be used in forecast mode. A method to use the GPCP datasets low frequency (monthly) variability in forecast mode is under investigations. Daily GPCP datasets will be also used in the method to check the input of higher variability in the previous results. This method is also linked to the runoffs estimation used in the model. Further developments should implement any new runoffs releases.

10.6 The first global 1/4^o operational Prototype System PSY3(M. Drevillon)

10.6.1 Main PSY3v1 developments in years 2004-2005

PSY3 aims at delivering weekly global oceanic forecasts, allowing meso-scale processes in the ocean. In order to build the first PSY3 prototypes, data assimilation methods of growing complexity will be implemented in the POG configuration at 1/4^o, starting with SAM1v1 (10.2.1.1),assimilating only satellite altimetry measurements.
The so-called **PSY3v1** development began in 2004, by merging the sources from POG-05 (ORCA 1/4^o) (see 10.5 and the PSY2G1 system (ORCA 2^o SAM1V1), which was done by E. Remy and N. Ferry. Mid 2004, M. Drévillon began to test a first version of the system (the size of the executable is more than 60 Go), running experiments of one cycle of one week on a local opteron processors cluster (Baltic).
These tests were constrained by the progressive tuning of the machine by the Mercator system team, which consisted in several changes of Fortran compiler, addition of processors, and the tests of a proper batch submission system. The code was thus tested on several machines at the same time : Baltic at Mercator, kami (Fujitsu VPP 5000) at Météo-France, and hpca (IBM cluster) at ECMWF.
After this series of tests, giving satisfactory results on Baltic by the end of 2004, the model sources were upgraded to POG05b, in order to use the enstrophy conserving scheme. The mean dynamic topography used by SAM1 is thus derived from the POG05b inter-annual experiment. The SAM1v1 sources were included and adapted to the SAM1/SAM2 platform.
A number of modifications have also been made in SAM1v1 : The vertical interpolation scheme of the lifting/lowering method has been upgraded to a cubic spline (instead of linear spline) by N. Ferry.
The canvas was initially designed to be monotonic, as the data was located on this intermediate grid via a dichotomy scheme. The analysis, done on the canvas grid, were then interpolated on the model initial ORCA grid (which is not monotonic). This method proved to generate a lot of errors in the case of the ORCA025 grid, and the canvas was finally taken identical to the ORCA grid, and the scheme to locate the data on the grid was changed, based on PSY2 developments.
The arrival of 18 new bi-processor nodes on Baltic in march 2005 allowed to run a 20 processors version. Moreover, this configuration is designed to run operationally either on Baltic or on Kami.
The first global oceanic forecast with PSY3v1 is made in autumn 2005, and the system runs operationally by the end of 2005.

10.6.2 Preliminary results with 2003 boundary conditions

Preliminary experiments, using January 2003 atmospheric forcings and satellite measurements, were performed in order to test the system, and compare it with the other Mercator systems. In Fig 10.15, two analyzed sea level anomalies are one month apart (from an experiment starting January 2003, the 8th). After only four cycles of assimilation with assimilated SLA over a 7-day window, the meso-scale activity is clearly enhanced, mostly in the Gulf stream and Kuroshio regions, and in the circumpolar Current for the southern Hemisphere.

[7] M. Benkiran, E. Greiner, and E. Dombrowsky, (2005), Multivariate and multidata assimilation in the Mercator project, *submitted to Journal of Marine System*.

[8] C. Boyer-Montegut, G. Madec, A. Fisher, A. Lazar, and D. Ludicone, (2004), Mixed layer depth over the global ocean : An examination of profi le data and a profi le-based climatology, *J. Geophys. Res.*, **109**.

[9] J. Candela, S. Tanahara, M. Crepon, and B. Barnier, (2003), Yucatan channel fbw : observations versus CLIPPER ATL6 and MERCATOR PAM models, *J. Geophys. Res.*, **108(C12)**, 3385.

[10] P. CLIPPER, (2000), Modélisation à haute résolution de la circulation dans l'océan Atlantique forcée et couplée océan-atmosphère, *Rapport Scientifi que et Technique 1998*, **CLIPPER-R3-2000**.

[11] J. Comiso, (2002), *Bootstrap sea ice concentrations for Nimbus-7 SMMR and DMSP SSM/I*, Boulder, CO, USA : National Snow and Ice Data Center. Digital Media.

[12] M. Cooper and K. Haines, (1996), Data assimilation with water property conservation, *J. Geophys. Res.*, **101**, 1059–1077.

[13] Dai and Trenberth, (2003), New estimates of continental discharges and ocean freshwater transport, *AMS Symposium on Observing and Understanding the Variability of Weather and Climate, Long Beach*.

[14] R. Daley, (1991), Atmospheric Data Analysis, *Cambridge University Press, England*, 457 pp.

[15] P. De Mey and M. Benkiran, (1991), A multivariate reduced-order optimal interpolation method and its application to the Mediterranean basin-scale circulation, *Ocean Forecasting : Conceptual basis and applications,N. Pinardi Ed., Springer-Verlag*, 281–303.

[16] P. De Mey and A. Robinson, (1987), Assimilation of altimeter Eddy Fields in a Limited-Area Quasi-Geostrophic Model, *J. Phys. Oceanogr.*, **17**, 2280–2293.

[17] C. "Derval, (2003), "Paramétrisation de la viscosité dans la bande équatoriale pour la confi guration ORCA025, Oct. 2003", *Rapport Technique CERFACS*.

[18] Y. Drillet, R. Bourdallé-Badie, and S. L, (2002), Tests de sensibilité dans le modèle haute résolution Mercator, *Annales Math. Blaise Pascal*, **9**, 283–298.

[19] L. Fleury", (2003), "Dossier de défi nition de l'outil ORCA025, édition 02, avril 2003", *Document MERCATOR*.

[20] H. Goosse and T. Fichefet, (1999), Importance of ice-ocean interactions for the global ocean circulation : a model study, *Jour.Geo.Res.*, **104**, 23,337–23,355.

[21] H. Goosse, J.-M. Campin, E. Deleersnijder, T. Fichefet, P.-P. Mathieu, M. A. Morales Maqueda, and B. Tartinville, (2001), Description of the CLIO model version 3.0.

[22] G. J. Huffman, P. Arkin, A. Chang, R. Ferraro, A. Gruber, J. E. Janowiak, J. Joyce, A. McNab, B. Rudolf, U. Schneider, and P. Xie, (1997), The Global Precipitation Climatology Project (GPCP) Combined Precipitation Data Set, *Bull. Amer. Met. Soc.*, **78**, 5–20.

[23] K. Ide, P. Courtier, P. Ghil, and A. Lorenc, (1997), Unifi ed Notation for Data Assimilation : Operational, Sequential and Variational, *J. Meteorol. Soc. Japan (Special issue)*, **75-1B**, 181–189.

[24] W. Large, (1998), Modeling and parameterization ocean planetary boundary layers, *E.P. Chassignet and J. Verron (Eds), Ocean Modeling and Parameterization, Kluwer Academic Publishers*, 81–120.

[25] X. Le Vaillant, (2005), Impact du forçage atmosphérique sur un modèle opérationnel de prévision océanique : Rálisation de prévision à un mois.

[26] S. Levitus, (1982), Climatological Atlas of the World Ocean, *NOAA Professional Paper 13*.

[27] M. Levy, M. Gavart, L. Memery, G. Caniaux, and A. Paci, (2005b), A 4D-mesoscale map of the spring bloom in the northeast Atlantic (POMME experiment) : results of a prognostic model, *J. Geophys. Res.*, **110**.

[28] M. Levy, Y. Lehahn, J. Andre, L. Memery, H. Loisel, and E. Heifetz, (2005a), Production regimes in the NorthEast Atlantic : a study based on Seawifs chlorophyll and OGCM mixed layer depth, *submitted*.

[29] A. Lombard, A. Cazenave, P. Le-Traon, and M. Ishii, (2005), Contribution of thermal expansion to present-day sea-level change revisited, *Global Planet. Change*, **47**, 1–16.

[30] G. Madec, P. Delecluse, M. Imbard, and C. Levy, (1998), OPA8.1 : Ocean general circulation model reference manual, *Notes du pole de modélistaion, Institut Pierre-Simon Laplace (IPSL)*.

[31] S. Marsland, N. Bindoff, G. Williams, and W. Budd, (2004), Modelling water mass formation in the Mertz Glacier Polynia and Adélie Depression, East Antarctica, *J. Geophys. Res.*, **109, C11003**, doi :10.1029/2004JC002441.

[32] G. Memery L., G. Reverdin and J. Paillet, (2005), The POMME Program (Programme Ocean Multidisciplinaire Meso Echelle). Subduction, thermocline ventilation, and biogeochemical tracer distribution in the North-East Atlantic Ocean : Impact of mesoscale dynamics, *submitted to EOS*.

[33] M. New, M. Todd, M. Hulme, and P. Jones, (2001), Precipitation measurements and trends in the twentieth century, *Int. J. Climatol.*, **21**, 1899–1922.

[34] L. G. O., (2004), Méthode de raffi nement de maillage dans le cadre de la modélisation océanique.

[35] D. Pham, J. Verron, and M. Roubaud, (1998), A Singular Evolutive Extended Kalman Filter for data assimilation in oceanography, *J. Marine Syst.*, **16(3-4)**, 323–340.

[36] A. Piacentini, S. Buis, D. Declat, and the PALM group, (2003), PALM : A computational Framework for assembling high performance computing applications, *Concurrency and Computat.*, **00**, 1–7.

[37] "POG-Team", (2003), "Dossier de definition de l'outil ORCA025, edition 03, oct. 2003", *Document MERCATOR*.

[38] V. R., (2005), Les runoffs dans le modèle numérique d'océan OPA.

[39] E. "Remy, (2003), "Construction de la bathymétrie pour la configuration modèle ORCA025, Mai 2003", *Rapport Technique CERFACS*.

[40] M. H. Rio and F. Hernandez, (2002), Estimation d'une topographie dynamique moyenne sur l'Atlantique Nord et Tropical, *Rapport nř CLS/DOS/NT/02.515*, pp. 48.

[41] C. Testut, P. Brasseur, J. Brankart, and J. Verron, (2003), Assimilation of sea surface temperature and altimetric observations during 1992-1993 into an eddy-permitting primitive equation model of the North Atlantic Ocean, *J. Mar. Syst.*, **40-41**, 291–316.

[42] C.-E. Testut, (2000), *Assimilation de données satellitales avec un filtre de Kalman de rang réduit dans un modèle aux Equations Primitives de l'océan Atlantique*, PhD thesis, Université Joseph Fourier (Grenoble I).

[43] R. Timmermann, H. Goosse, G. Madec, T. Fichefet, C. Ethe, and V. Duliere, (2004), On the representation of high latitude processes in the ORCA-LIM global coupled sea ice-ocean model, *Ocean Modelling*, **6**, 175–201.

[44] A. Treguier, O. Boebel, B. Barnier, and G. Madec, (2003), Agulhas eddy fluxes in a 1/6 ř Atlantic model, *Deep Sea res. II*, **50**, 251–280.

[45] A. Troccoli and P. Kallberg, (2004), Precipitation correction in the ERA-40 reanalysis, Tech. Rep. 13, ERA-40 Project Report Series.

[46] A. Weaver, J. Vialard, and L. Anderson, (2003), Three- and Four-Dimensional Variational Assimilation with a General Circulation Model of the Tropical Pacific Ocean ;, Part I : Formulation, Internal Diagnostics, and Consistency Checks, *Mon. Wea. Rev.*, **131**, 1360–1378.

[47] J. Willis, D. Roemmich, and B. Cornuelle, (2004), Interannual variability in upper-ocean heat content, temperature and thermosteric expansion on global scales, *J. Geophys. Res. - Oceans*, **109-C12036**, doi :10.1029/2003JC002260.

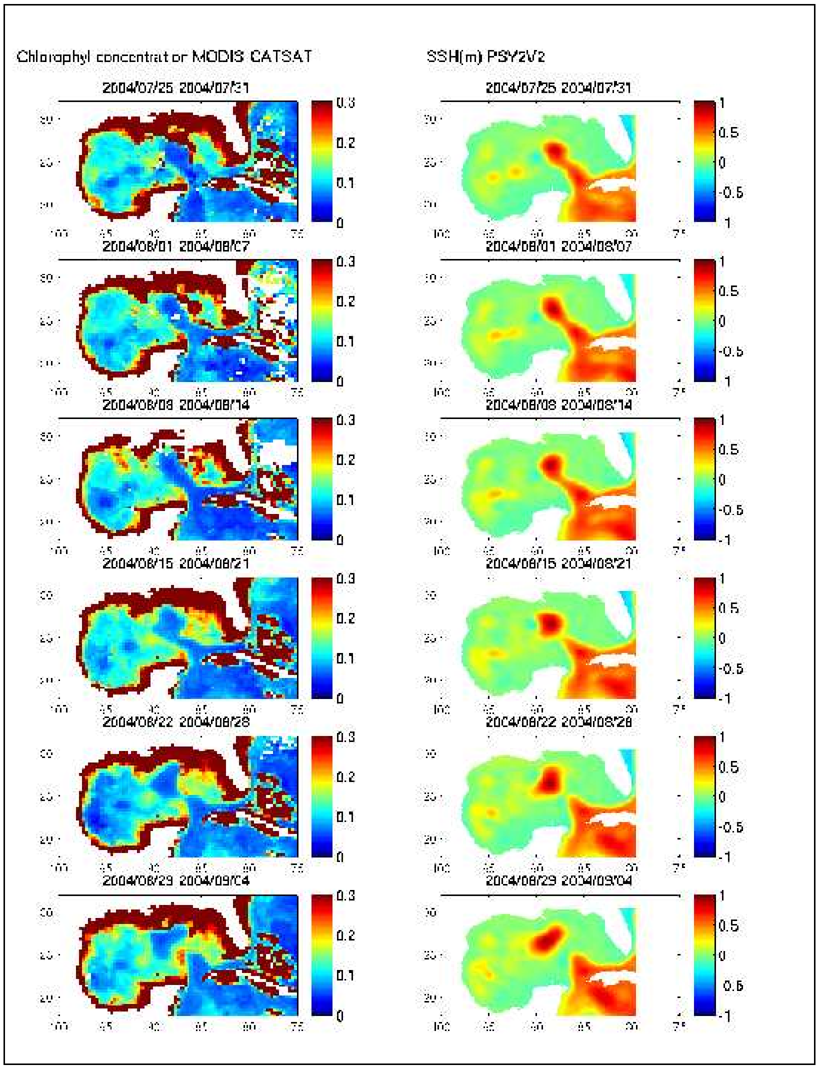

FIG. 10.12 – Weekly mean Chlorophyll-A concentration from MODIS-CATSAT (left column) and weekly mean Sea Level anomaly (meters) from PSY2v2 (right column) during 6 weeks in a raw. The first week (top panels) is from July 25th to 31th 2004. The last week (lower panels) is from August 29th to September 4th 2004.

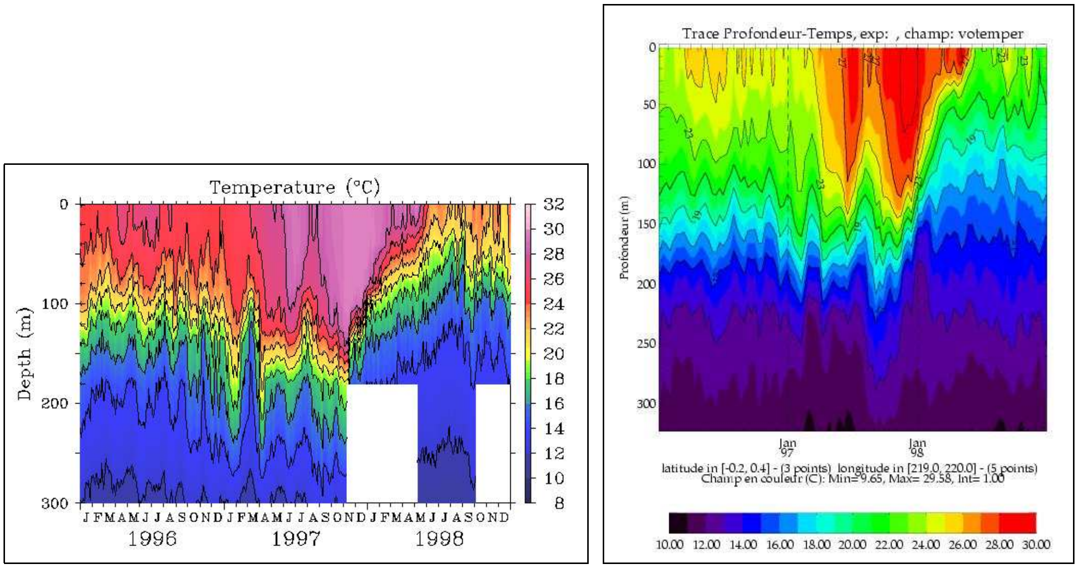

FIG. 10.13 – Timeseries (1996-1998) of the temperature with depth at the Equator and 220řE longitude from : the POG05B experiment(right) and the TAO datasets (left).

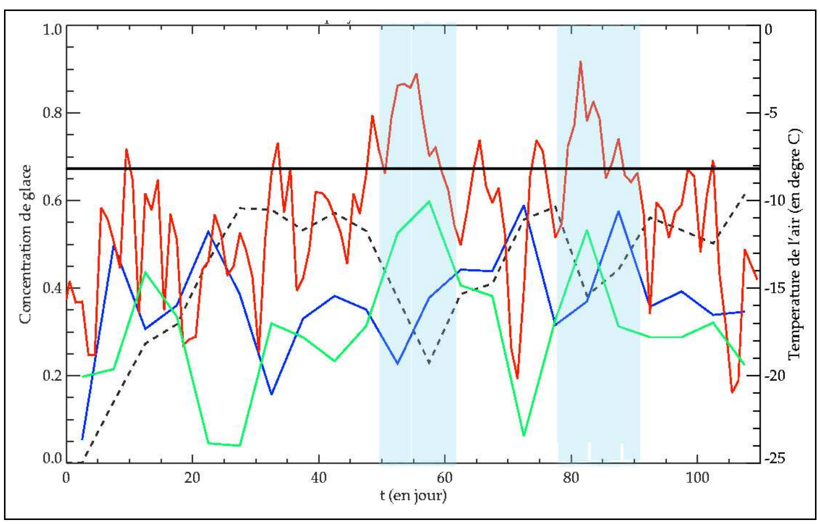

FIG. 10.14 – Time series of sea ice concentration (black dotted line), katabatic winds magnitude (red), sea ice production (blue) and surface air temperature (green) in the Prydz Bay area between the 26th april and 14th august 1994. The black heavy line is the 10 $\mathrm{m.s^{-1}}$ threshold for the wind ; the shaded blue areas in the figure represent the polynias occurrence in the experiment.

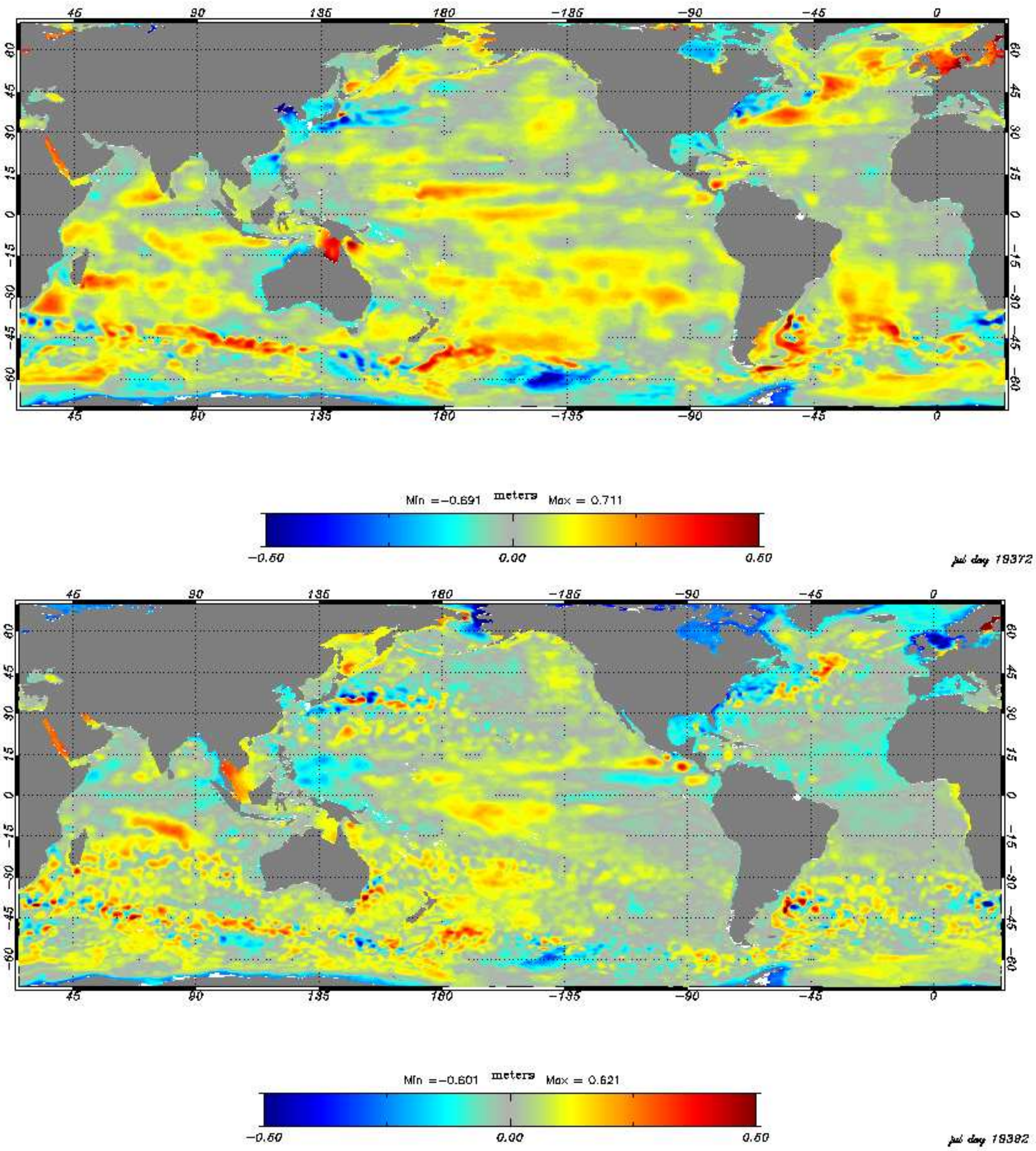

FIG. 10.15 – PSY3v1 analyzed sea level anomalies (m) : (top) First SLA analysis (2003 January), (bottom) after 4 cycles of SLA assimilation (February 2003) (one month January climatological forcing spin-up)

11 Publications

11.1 Journal Publications

[GLO1] M. Alexander, J. Yin, G. Branstator, A. Capotondi, C. Cassou, R. Cullather, Y.-O. Kwon, J. Norris, J. Scott, and I. Wainer, (2005), Extratropical atmosphere-ocean variability in CCSM3, *J. Climate*, In Press.

[GLO2] J.-C. André, M. Dequé, P. Rogel, and S. Planton, (2004), La vague de chaleur de l'été 2003 et sa prévision saisonnière, *C.R. Geoscience*, **336**, 491–503.

[GLO3] E. Anterrieu, S. Gratton, and B. Picard, (2004), Problème inverse en télédétection spatiale par imagerie à synthèse d'ouverture, *Revue Traitement du Signal*, **21(1)**, 1–15.

[GLO4] E. Anterrieu, (2004), A resolving matrix approach for Synthetic Aperture Imaging Radiometers., *IEEE Trans. on Geosci. And Remote Sens.*, **42(8)**, 1649–1656.

[GLO5] S. Buis, A. Piacentini, and D. Déclat, (2006), PALM : A Computational framework for assembling high performance computing applications, *Concurrency Computat. : Pract. Exper.*, **18(2)**, 247–262.

[GLO6] C. Cassou, C. Deser, L. Terray, J. W. Hurrell, and M. Drévillon, (2004), Summer Sea Surface Temparature Conditions in the North Atlantic and their Impact upon the atmospheric circulation in early Winter, *J. Climate*, **17**, 3349–3363.

[GLO7] C. Cassou, L. Terray, and A. S. Phillips, (2005), Tropical Atlantic influence on European Heatwaves, *J. Climate*, **18**, 2805–2811.

[GLO8] C. Cassou, L. Terray, J. W. Hurrell, and C. Deser, (2004), North Atlantic Winter Climate Regimes : Spatial Asymmetry, *J. Climate*, **17 No3**, 1055–1068.

[GLO9] C. Cassou, (2004), Du changement climatique aux régimes de temps : L'Oscillation Nord Atlantique, *La météorologie*, **45**, 21–32.

[GLO10] C. Cibot, E. Maisonnave, L. Terray, and B. Dewitte, (2005), Mechanisms of tropical Pacific interannual-to-decadal variability in the ARPEGE/ORCA global coupled model, *Clim. Dyn.*, **24**, 823–842.

[GLO11] M. Collins, M. Botzet, A. Carril, H. Drange, A. Jouzeau, M. Latif, S. Masina, O. H. Otteraa, H. Pohlmann, A. Sorteberg, R. Sutton, and L. Terray, (2005), Interannual to Decadal Climate Predictability : A Multi-Perfect-Model-Ensemble, *J.Climate*, in press.

[GLO12] Y. Drillet, R. Bourdallé-Badi, L. Siefridt, and C. Le Provost, (2005), The Meddies in the Mercator North Atlantic and Mediterranean Sea eddy resolving model, *J. of Geophysical Research*, In Press.

[GLO13] E. Frankignoul C., Kestenare, M. Botzet, A. F. Carril, H. Drange, A. Pardaens, L. Terray, and R. Sutton, (2004), An intercomparison between the surface heat flux feedback in five coupled models, *Clim. Dyn.*, **22**, 373–388.

[GLO14] G. Garric and P. Charpentier, (2005), Sea Ice : new component of the Mercator Project, *Mercator Newsletter*, **16**.

[GLO15] E. Guilyardi, S. Gualdi, J. Slingo, A. Navarra, P. Delecluse, J. Cole, M. G., M. Roberts, M. Latif, and L. Terray, (2004), Representing El Nino in Coupled Ocean-Atmosphere GCMs : The Dominant Role of the Atmospheric Component, *J. of Climate*, **17**, 4623–462.

[GLO16] A. Lazar, F. Vintzileos, A. Doblas-Reyes, P. Rogel, and P. Delecluse., (2005), Seasonal forecast of tropical climate with coupled ocean-atmosphere GCMs : On the respective role of the atmosphere and the ocean model components in the drifting mean climate, *Tellus*, **57A**, 387–397.

[GLO17] S. Massart, D. Cariolle, and V.-H. Peuch, (2005), Vers une meilleure représentation de la distribution et de la variabilité de l'ozone atmosphèrique par l'assimilation des données satellitaires, *C.R. Acad. Sci.*, **337-15**, 1305–1310.

[GLO18] S. Massart, D. Cariolle, and P. V.-H., (2005), Vers une meilleure représentation de la distribution et de la variabilité de l'ozone atmosphérique par l'assimilation des données satellitaires, *C. R. Geosciences*, in press.

[GLO19] A. M. Moore, J. Zavala-Garay, Y. Tang, R. Kleeman, A. T. Weaver, J. Vialard, K. Sahami, D. L. T. Anderson, and Fisher, (2006), On the low-dimensionality of ENSO as evidenced by the optimal forcing patterns of coupled models, *J. Climat*, **to appear**.

[GLO20] T. N. Palmer, A. Alessandri, U. Andersen, P. Cantelaube, M. Davey, P. Delécluse, E. Déqué, M. Diez, F. J. Doblas-Reyes, H. Feddersen, R. Graham, S. Gualdi, R. Guérémy J.-F., Hagedorn, M. Hoshen, N. Keenlyside, M. Latif, A. Lazar, E. Maisonnave, V. Marletto, A. P. Morse, B. Orfi la, P. Rogel, and M. C. Terres, J.-M. andT homson, (2004), Development of a European Multi-Model Ensemble System for Seasonal to Inter-Annual Prediction (DEMETER), *Bull. Amer. Meteorol. Soc.*, **85**, 853–872.

[GLO21] B. Picard and E. Anterrieu, (2005), Comparizon of regularized inversion methods in synthetic aperture imaging radiometry, *IEEE Transactions on Geoscience and Remote Sensing*, **43(2)**, 218–224.

[GLO22] S. Ricci, A. T. Weaver, J. Vialard, and P. Rogel, (2005), Incorporating state-dependent temperature-salinity constraints in the background-error covariance of variational ocean data assimilation., *Mon. Wea. Rev.*, **133,**, 317–338.

[GLO23] M. J. Rodwell, C. Drévillon, M. Frankignoul, J. W. Hurrell, H. Pohlmann, M. Stendel, and R. T. Sutton, (2004), North Atlantic forcing of climate and its uncertainty from a multi-model experiment, *Q. J. Roy. Meteorol. Soc*, **130**, 2013–2032.

[GLO24] P. Rogel, A. T. Weaver, N. Daget, S. Ricci, and E. Machu, (2005), Ensembles of global ocean analyses for seasonal climate prediction : impact of temperature assimilation, *Tellus*, **57A**, 375–386.

[GLO25]

[GLO26] Y. Tang, R. Kleeman, A. M. Moore, J. Vialard, and A. T. Weaver, (2004), An offline, numerically effi cient initialization scheme in an oceanic general circulation model for El Nino-Southern Oscillation prediction, *J. Geophys. Res.*, **109 (C5)**.

[GLO27] L. Terray, M. E. Demory, M. Déqué, G. De Coetlogon, and E. Maisonnave, (2004), Simulation of late twenty-fi rst century changes in wintertime atmospheric circulation over Europe due to anthropogenic causes, *J. Climate*, **17**, 4630–4635.

[GLO28] Y. M. Tourre, C. Cibot, L. Terray, W. B. White, and B. Dewitte, (2005), Quasi-decadal and inter-decadal climate fluctuations in the Pacifi c Ocean from a CGCM, *Geophys. Res. Lett.*, **32**.

[GLO29] S. Valcke, E. Guilyardi, and C. Larsson, (2006), PRISM and ENES : A European approach to Earth system modelling., *Concurrency Computat. :Pract. Exper.*, **18(2)**, 231–245.

[GLO30] P. A. Vidard, A. Piacentini, and F.-X. Le Dimet, (2004), Variational data analysis with control of the forecast bias, *Tellus*, **56A**, 177–188.

[GLO31] F. Vossepoel, A. T. Weaver, J. Vialard, and P. Delecluse, (2004), Adjustment of near-equatorial wind stress with four-dimensional variational data assimilation in a model of the Pacifi c Ocean, *Mon. Wea. Rev.*, **132**, 2070–2083.

11.2 PhD and HdR Thesis

[GLO32] E. Anterrieu, (2005), Problèmes inverses en traitement des images : régularisation et mise en oeuvre, habilitation à diriger des recherches, université paul sabatier.

[GLO33] C. Cibot, (2004), Variabilité décennale dans le Pacifi que tropical et modulation basse fréquence de l'activité ENSO, thèse de doctorat de l'ups.

[GLO34] S. Ricci, (2004), Assimilation variationelle océanique : modélisation multivariée de la matrice de covariance d'erreur d'ébauche, thèse de doctorat de l'inpt.

11.3 Conference Proceedings and Book Chapters

[GLO35] E. Anterrieu and P. Waldteufel, (2005), A regularized approach for processing full-polarimetric data in synthetic aperture imaging radiometry, In *Proc. 31st International Symposium on Remote Sensing of Environment*, (ISRSE'05) Saint-Petersburg (Russia).

[GLO36] E. Anterrieu, B. Picard, and A. Tanner, (2004), On the regularization of inverse problems in imaging radiometry by aperture synthesis, Proc. 8th Specialist Meeting on Microwave Radiometry and Remote Sensing Applications Rome (Italy), 64 pp.

[GLO37] E. Anterrieu, B. Picard, M. Martin-Neira, P. Waldteufel, M. Suess, J.-L. Vergely, Y. Kerr, and S. Roques, (2004), A strip adaptive processing approach for the SMOS space mission, International Geoscience And Remote Sensing Symposium (IGARSS'04) Anchorage (Alaska), 922–1925.

[GLO38] S. Buis, S. Massart, P. Erhard, and G. Gacon, (2005), Use of data assimilation techniques in neutronics : benefi ts and fi rst results, International Topical Meeting on Mathematics and Computation, Supercomputing, Reactor Physics and Nuclear and Biological Applications, Avignon, France., 12–15 september 2005.

[GLO39] K. Béranger, M. Crépon, Y. Drillet, R. Bourdallé-Badie, and L. Izart, (2005), Convection in the Mediterranean Sea :impact of the spatial resolution of the ECMWF atmospheric forcing, AGU, Vienne., April 200.

[GLO40] C. Cassou, (2004), coupled to a mixed layer ocean model : Model physics and climate, CCSM Annual workshop, Santa Fe, invited paper.

[GLO41] C. Cassou, (2004), North Atlantic winter climate regimes : spatial asymmetry, stationarity with time and ocean forcing, EGU, Nice.

[GLO42] C. Cassou, (2005), Tropical Atlantic forcing and predictability of extreme warm events in Europe., EGU, Vienne.

[GLO43] D. Declat, R. Redler, H. Ritzdorf, S. Valcke, and R. Vogelsang, (2004), The PRISM coupler and I/O System, The 1st Internationnal Kyosei Workshop, Honolulu,Hawaii, USA, February 25–27.

[GLO44] Y. Drillet, R. Bourdallé-Badie, and N. Daget, (2004), Last decade simulation with the Mercator North Atlantic Prototype, EGS - AGU - EUG Joint Assembly, Nice, France, April.

[GLO45] O. Le Galloude, R. Bourdallé-Badie, D. Y., and G. Madec, (2005), Strategy for the development of the futur mercator ocean prototype, EGU, Vienne., April 2005.

[GLO46] J. M. Lellouche, E. Greiner, Y. Drillet, and R. Bourdallé-Badie, (2004), Near-real-time Assimilation of Satellite Data in the North Atlantic and Mediterranean High Resolution Model, EGS - AGU - EGU Joint Assembly, Nice, France, April.

[GLO47] S. Massart, D. Cariolle, V.-H. Peuch, H. Manzoni, L. Elamraoui, and E. Renard, (2005), Intercomparison of satellite ozone measurements using CTM data assimilation system, EGS-AGU-EUG Joint Assembly, Vienne, 24–29 April 2005.

[GLO48] S. Massart, V. H. Peuch, D. Cariolle, S. Pradier, H. Manzoni, and L. Elamraoui, (2005), Assimilation of ozone satellite measurements and its impact on both numerical weather and "chemical weather", 4th WMO Symposium on Data Assimilation, Prague, April 2005.

[GLO49] S. Massart, (2004), Impact des données satellites d'ozone sur la validation du modèle de chimie-transport MOCAGE, Atelier de modélisation de l'atmosphère AMA2004, CNRM, Météo France.

[GLO50] S. Massart, (2004), Improving global chemical simulations with variational assimilation of GOME data, Air Pollution XII, WIT press, 507–515.

[GLO51] S. Massart, (2005), In *Optimisation des déformations différées du béton par fi ltre de Kalman*, XVIIeme Congres Francais de Mecanique, Troyes, France, 29 August –2 September 2005.

[GLO52] (200).

[GLO53] J.-P. Pérez, avec la collaboration de, and E. ăAnterrieu, (2004), Optique : fondements et applications (7ème Edition), In *Editeur DUNOD (Paris)*, Collection MASSON SCIENCES, 698 pages.

[GLO54] ă. Picard, ă. Reul, ă. Waldteufel, and ă. Anterrieu, (2004), Impact of solar radiation on sea surface salinity remote sensing by spaceborne Synthetic Aperture Imaging Radiometers, In *Proc. International Geoscience And Remote Sensing Symposium (IGARSS'04) Anchorage (Alaska)*, Vol.ă3 pp.ă1926–1929.

[GLO55] C. Testut, B. Tranchant, F. Birol, N. Ferry, and P. Brasseur, (2005), SAM2 : The Second Generation of MERCATOR Assimilation System, EGU Joint Assembly, Vienne, 24–29 April 2005.

[GLO56] C. Testut, B. Tranchant, P. Brasseur, and P. De Mey, (2004), Recent developments of the Mercator Assimilation System (SAM) : towards the Seek filter, 1st General Assembly Nice, France., 25 – 30 April.

[GLO57] B. Tranchant, C.-E. Testut, N. Ferry, and P. Brasseur, (2005), SAM2 : The Second Generation of MERCATOR Assimilation System, 4th EuroGOOS Conference, Brest, France, 6–9 June, 2005.

[GLO58] B. Tranchant, C.-E. Testut, B. P., and P. De Mey, (2004), Recent Developments of the Mercator Assimilation System (SAM) : Towards the Seek Filter, The 2004 Joint Assembly (CGU, AGU, SEG, EEGS), Montréal, Canada.

[GLO59] S. Valcke, A. Caubel, D. Déclat, M.-A. Foujols, J. Latour, R. Redler, H. Ritzdorf, and T. Schoenemeyer, (2005), The PRISM couplers : OASIS3 and OASIS4, EGU, Vienne.

[GLO60] S. Valcke, D. Declat, R. Redler, H. Ritzdorf, T. Schoenemeyer, and R. Vogelsang, (2004), The PRISM Coupling and I/O System, VECPAR'04 6th international meeting for high performance computing for computational science, Valencia, 6 pp.

[GLO61] S. Valcke, P. Pellerin, M. Valin, D. Bouhemhem, M. Faucher, S. Desjardins, and H. Ritchie, (2005), The Europeo-Canadian unified coupler OASIS3-GOSSIP2 and first coupled applications using the atmospheric model GEM., Canadian Meteorological and Oceanographic Society 39th Annual Congress, Vancouver (B.C), Canada.

11.4 Technical Reports

[GLO62] V. Benoit, (2005), Prévision saisonnière sur l'Afrique de l'Ouest à partir des produits DEMETER, Technical Report TR/CMGC/05/50, CERFACS. Available on Global Change web.

[GLO63] J. Boe, L. Terray, F. Habets, and E. Martin, (2005), A simple statistical-dynamical downscaling scheme based on weather types and conditional resampling, *J. Geophys. Res.*, Submitted.

[GLO64] J. Boe, (2004), Intensité du cycle hydrologique dans le climat perturbé par l'augmentation des gaz à effet de serre d'origine anthropique, Technical Report WN/CMGC/04/65, CERFACS. Available on Global Change web.

[GLO65] R. Bourdallé-Badie and Y. Drillet, (2004), Definition of PAM2 model, Rapport Mercator April 2004, CERFACS.

[GLO66] R. Bourdallé-Badie and Y. Drillet, (2005), PAM2 vorticity scheme, Rapport Mercator février 2005, CERFACS.

[GLO67] R. Bourdallé-Badie, Drillet, E. Greiner, J. Lellouche, and N. Y. Verbrugge, (2004), Saut Qualitatif dans le modèle Atlantique Nord et Méditerranée haute résolution (PSY2V1), Lettre Trimestrielle MERCATOR 12, CERFACS.

[GLO68] P. Brasseur, P. Bahurel, L. Bertino, J. Brankart, N. Ferry, S. Losa, E. Remy, J. Schroter, S. Skachko, and C.-E. Testut, (2005), Data assimilation in operational ocean forecasting systems : The MERCATOR and MERSEA developments, *Q. .J.Roy. Meteorol. Soc.*, **submitted**.

[GLO69] S. Buis and S. Massart, (2004), Implémentation d'une maquette PALM de système d'assimilation d'activités neutroniques avec le modèle COCCINELLE, Technical Report TR/CMGC/04/67, CERFACS.

[GLO70] S. Buis, A. Piacentini, and D. Déclat, (2005), PALM : A Computational Framework for assembling High Performance Computing Applications, *Concurrency and computation : practice and experience*, In Press.

[GLO71] C. Caminade, L. Terray, and E. Maisonnave, (2005), West African Monsoon System response to greenhouse gas and sulfate aerosols forcing under two emissions scenarios., *Clim. Dyn.*,, In press.

[GLO72] N. Daget, (2005), Etude préliminaire sur la palmérisation de OPAVAR, Technical Report TR/CMGC/05/18, CERFACS.

[GLO73] D. Déclat, (2004), Interface between the transformer and the PSMILe in the OASIS4 coupler, Technical Report TR/CMGC/04/09, CERFACS. Available on Global Change web.

[GLO74] E. Denoux, C. Cassou, and S. Valcke, (2005), Les modèles de circulation générale, *Les dossiers de l'ingénierie éducative*, **53**, 43–45.

[GLO75] E. Derval, C.and Durand, E. Fleury, and E. Remy, (2004), Dossier de définition de l'outil ORCA025-V3, Tech. Rep. MOO-ST-425-98-MER, Projet Mercator, France.

[GLO76] E. Derval, C.and Durand, G. Garric, and E. Remy, (2005), Dossier d'experimentation ORCA-R025 POG05B, Tech. Rep. MOO-ED-425-327-MER, Projet Mercator, France.

[GLO77] Y. Drillet and R. Bourdallé-Badie, (2004), Régionalisation of the Gent and McWilliams parameterization, Rapport Mercator janvier 2004, CERFACS.

[GLO78] Y. Drillet, R. Bourdallé-Badie, and O. Le Galloudec, (2004), Utilisation de AGRIF dans la configuration MNATL/BABY, Rapport Mercator octobre 2004, CERFACS.

[GLO79] Y. Drillet, R. Bourdallé-Badie, C. Le Provost, and G. Madec, (2004), Results and validation of the last decade simulation performed with the 1/15° mercator prototype, Colloque en l'honneur et la mémoire de Christian Le Provost, Toulouse, France. January 2004, CERFACS.

[GLO80] C. Garric, G.and Derval, E. Durand, and E. Remy, (2004), Dossier de définition de l'outil ORCA025-LIM, Tech. Rep. MOO-ST-425-274-MER, Projet Mercator, France.

[GLO81] G. Garric, (2004), Rapport d'activites sur la glace de mer, Tech. Rep. MOO-DS-421-281-MER, Projet Mercator, France.

[GLO82] G. Garric, (2005), Sea ice report activity (2) - CERSAT satellite data and model diagnostics, Tech. Rep. MOO-DS-421-xxx-MER, Projet Mercator, France.

[GLO83] G. Garric, (2005), Surface atmospheric forcing (1) - The global surface mass budget, Tech. Rep. MOO-RC-425-xxx-MER, Projet Mercator, France.

[GLO84] D. Hodson, R. Sutton, H. Pohlmann, M. Rodwell, M. Stendel, and L. Terray, (2005), Influence of the oceans on North Atlantic climate variability : a comparison of results from 4 atmospheric GCMs, *Clim. Dyn.*, Submitted.

[GLO85] O. Le Galloudec, R. Bourdallé-Badie, and Y. Drillet, (2004), Raffinement de maillage dans le cadre des prévisions, Lettre Trimestrielle MERCATOR 15, CERFACS.

[GLO86] E. Maisonnave, (2004), Arpege PC : Note technique relative au portage, Technical Report TR/CMGC/04/99, CERFACS. available on Global Change web.

[GLO87] E. Maisonnave, (2004), Arpege PC : Puisque la modélisation du climat entre dans une nouvelle ère, Technical Report WN/CMGC/04/100, CERFACS. available on Global Change web.

[GLO88] E. Maisonnave, (2005), SAFO : Guide Utilisateur, Technical Report TR/CMGC/05/16, CERFACS. Available on Global Change web.

[GLO89] S. Massart, D. Cariolle, and V.-H. Puech, (2004), Vers une meilleure représentation de la distribution et de la variabilité de l'ozone atmosphérique par l'assimilation des données satellitaires, Technical Report TR/CMGC/04/107, CERFACS. available on Global Change web.

[GLO90] T. Morel, S. Buis, and N. Barriquand, (2004), Utilisation du coupleur dynamique PALM-MP 2.1.0, Technical Report TR/CMGC/04/112, CERFACS. available on Global Change web.

[GLO91] T. Morel, S. Buis, N. Barriquand, D. Déclat, and S. Massart, (2004), Utilisation du coupleur Dynamique PALM-MP 2.0.0, Technical Report TR/CMGC/04/30, CERFACS. Available on Global Change web.

[GLO92] A. Naila, (2005), Estimation des statistiques d'erreur du modèle de neutronique COCCINELLE pour son utilisation dans le cadre de méthodes d'assimilation de données., Technical Report TR/CMGC/05/61, CERFACS. Available on Global Change web.

[GLO93] A. Pélissier, (2004), Évolution des événements météorologiques extrêmes en France sur la période 1950-1999, Technical Report TR/CMGC/04/70, CERFACS. available on Global Change web.

[GLO94] E. Rapaport, (2004), Développement de l'interpolation vectorielle dans le coupleur OASIS, Technical Report TR/CMGC/04/69, CERFACS. available on Global Change web.

[GLO95] E. SanchezGomez and L. Terray, (2005), Large-scale atmospheric dynamics and local intense precipitation episodes, *Geophys. Res. Lett*, **in press**.

[GLO96] E. SanchezGomez, G. de Coëtlogon, L. Terray, and A. Joly, (2005), Estimating the risk of climate extreme events in a future climate change scenario, *Climate Dynamics*, **submitted**.

[GLO97] C. Ubelman, (2005), Etude de la variabilité du niveau de la mer à l'aide de réanalyses globales de le circulation océanique, Technical Report TR/CMGC/05/49, CERFACS. Available on Global Change web.

[GLO98] S. Valcke, A. Caubel, R. Vogelsang, and D. Déclat, (2004), OASIS3 Ocean Atmosphere Sea Ice Soil User's Guide (oasis3-prism-2-2), Technical Report TR/CMGC/04/48, CERFACS. Available on Global Change web.

[GLO99] S. Valcke, A. Caubel, R. Vogelsang, and D. Déclat, (2004), OASIS3 User Guide (oasis3-prism-2-4), Technical Report WN/CMGC/04/143, CERFACS. Available on Global Change web.

[GLO100] S. Valcke, A. Caubel, R. Vogelsang, and D. Déclat, (2004), OASIS3 User's Guide (oasis3-prism-2-3), Technical Report TR/CMGC/04/68, CERFACS. available on Global Change web.

[GLO101] S. Valcke, R. Redler, R. Vogelsang, D. Déclat, H. Ritzdorf, and T. Schoenemeyer, (2004), OASIS4 User Guide, Technical Report WN/CMGC/04/144, CERFACS. Available on Global Change web.

[GLO102] S. Valcke, (2004), Minutes of the WP3a meeting (DeBilt, January 13, 2004), Technical Report WN/CMGC/04/14, CERFACS. Available on Global Change web.

[GLO103] S. Valcke, (2004), PRogramme for Integrated earth System Modelling, Technical Report WN/CMGC/04/62, CERFACS. Available on Global Change web.

[GLO104] S. Valcke, (2005), COUPLING MEC with IML ocean model through OASIS3-GOSSIP2, Technical Report TR/CMGC/05/111, CERFACS. Available on Global Change web.

[GLO105] S. Valcke, (2005), COUPLING MEC with IML ocean model through OASIS3-GOSSIP2, Technical Report TR/CMGC/05/111, CERFACS. Available on Global Change web.

[GLO106] A. T. Weaver, C. Deltel, E. Machu, and S. Ricci, (2005), A multivariate balance operator for variational ocean data assimilation, *Q. J. Roy. Meteor. Soc.*, **submitted**.

5

Environmental Impact of Aviation

1 Introduction

Daniel Cariolle

The aircraft emissions have an impact on atmospheric chemistry and on the radiative balance of the atmosphere. For example, contrails formed by condensation of water vapor onto exhaust aerosols and soot particles trigger the formation of cirrus clouds. Emissions of nitrogen oxides perturb the natural chemical cycles and lead to ozone production or destruction depending on local air mass composition and insolation. These ozone perturbations along with the emissions of CO2, water vapour and ice particles formation, soot particles, sulphuric aerosols from the burning kerosene give an additional contribution to the green house forcing. The most recent evaluations of those effects show the existence of an amplification factor of about 3 for green house potential factor from aircraft emission : a molecule of CO2 emitted from a jet airplane is a factor of 3 more efficient for green house forcing than a similar molecule emitted at ground level.

Given the exponential increase of the air traffic it is anticipated that the aircraft emissions will double by year 2020 compared to present. The air traffic would then be a major player of the climate change. There is no doubt that in future negotiation processes for the limitation of green house gas emissions aviation sources will be a central issue. It is therefore important that the regulations that could be imposed on aviation be based on well-sound scientific studies.
As this thematic was recognised as an important issue for the CERFACS shareholders and for the ministry of transportation (which has the administrative supervision of Météo-France), it was decided in 2003 to settle a new project Òaviation and environmentÓ within the CERFACS and CNRM teams.

The main objective of the project is to better quantify the chemical and radiative atmospheric impacts of aviation at the various scales from the aircraft near field to the global atmosphere. An integrated evaluation of the different steps that involves the emission transformations must be performed, from the gaseous and particulate species generation in the combustion chambers, their chemical and microphysical transformations in the aircraft near field, their vertical and horizontal dilution in the far wake along the contrail path, up to the formation of corridors by the fleets and their transport by the general circulation of the atmosphere. At each of those steps the chemical and radiative atmospheric perturbations must be assessed.

During this last 2 year period emphasis has been placed on the model developments. At small and mesoscale the numerical models NTMIX and Méso-NH have been developed in the area of transport schemes for chemical species and microphysic associated to the formation of ice particles. Preliminary results are expected by the end of the year on the coupling of NTMIX and meso-NH, that would allow contrail simulations from the near-field to the atmospheric mesoscale.

On global scale a linearized approach to the atmospheric chemistry has been developed and validated, and has been introduced in the latest version the the CNRM ARPEGE/Climat global model. On the same line an equivalent approach has been developed for a radiative scheme that allows a rapid evaluation of the impact of possible ozone change on the stratospheric temperatures. Validation of the radiative scheme has been performed using the IFS global model of the ECMWF and sensitivity experiments have been obtained with the 2D Chemical Transport Model MOCAGE. The next steps will concentrate on the extension of the ozone linear scheme to account for the injection of NOx, H2O and CO from air traffic, and assessment of their chemical and radiative perturbations.

We have establish numerous cooperations within the present project. First with the CNRM for the use of Méso-NH and ARPEGE/Climat and MOCAGE models, and second at the european level within the QUANTIFY project coordinated by the DLR where CERFACS is responsible of the activity II "Dilution and Processing".

The next sections details the results obtained within the period covered by this report.

2 Small-scale simulations of aircraft emissions

2.1 Development of NTMIX model for contrail formation and aircraft emissions (R. Paoli)

A two-phase flow model based on a mixed Eulerian/Lagrangian approach was developed in NTMIX solver to simulate the formation and evolution of a contrail in an aircraft wake. Large-eddy simulations were used for the carrier gaseous phase, while a Lagrangian particle tracking method was used for the dispersed phase, consisting of ice crystals and exhauts soot particles. A microphysical model for vapour condensation was also integrated, so that the proposed method provides a detailed monitoring of the evolution and growth of each crystal and cluster of crystals in the wake. The analysis, initiated in 2003 at Stanford, focused on the interaction between a trailing vortex and an exhaust jet loaded with soot particles and water vapour, and was finalized in two journal articles by Paoli *et al.* [PAE1] and Paoli and Garnier [PAE2]. This work has been recently extended by Cariolle *et al.* [PAE4] including a measured aircraft wake as the background flow-field, instead of an analytical vortex model, see Fig. 2.1. The thermodynamic conditions for contrail formation were identified by tracking the spatial distribution of supersaturation S_{ice} around particles as shown in the snapshot of Fig. 2.1. This is a key variable since the growth rate of each particle depends on the local supersaturation, $\dot{r}_p \sim S_p$, which in turn depends on the local temperature. Therefore, due to the exhaust cooling in the plume, water vapor condenses over soot particles and forms ice crystals whose sizes grow until thermodynamic equilibrium between the two phases is reached. The evolution of the mean crystal radius r_{avg} in Fig. 2.2 shows that it attains an asymptotic value around $1\,\mu m$ which is in the range of observations reported in the literature.
In the framework of our long-term collaboration with Univ. of Strasbourg, a module developed by Prof. MirabelâĂŹs group which provides a unified treatment of aerosols, soot and ice particles has been recently installed on CERFACS machines. The final goal is to develop an integrated tool to predict the chemical and

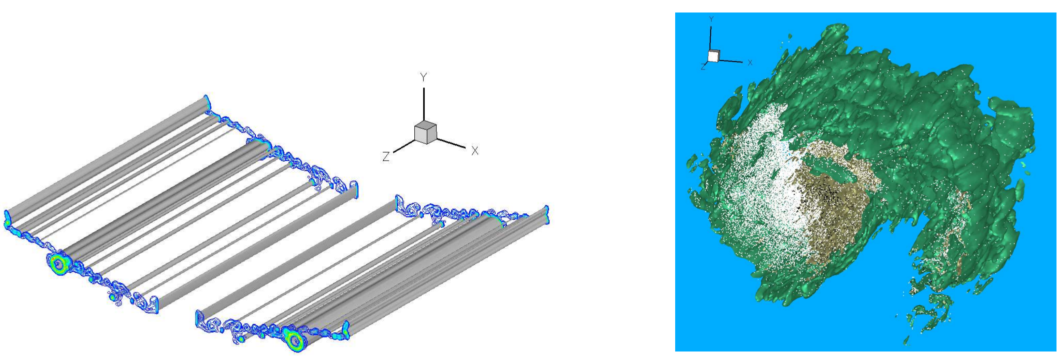

FIG. 2.1 – Contrail formation in a measured aircraft wake. Left, initial vorticity distribution. Right, iso-surface of ice supersaturation S_{ice} at $t = 8\,sec$: green, $S_{ice=0} = 0$; yellow, $S_{ice} = 10\%$; soot particles and ice crystals are represented by black and white dots, respectively.

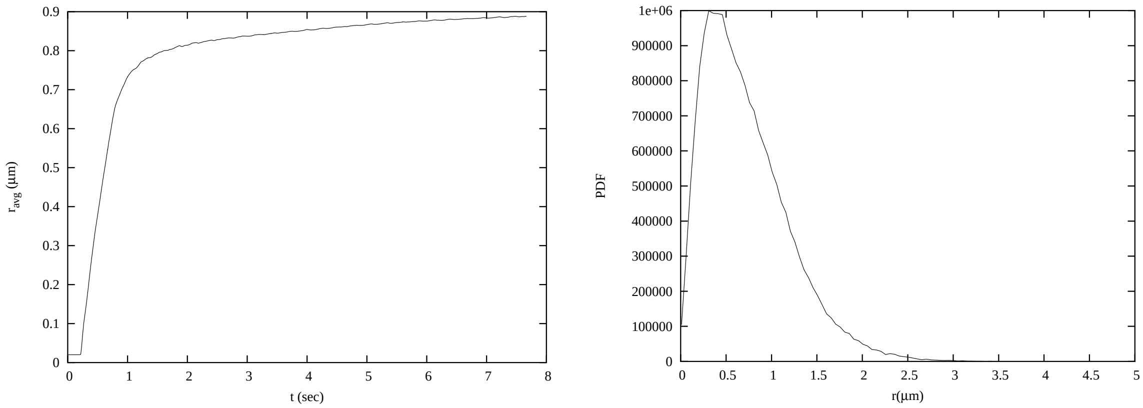

FIG. 2.2 – Ice crystal radius evolution. Left, temporal evolution of the mean radius r_{avg}. Right : crystal size spectrum at $t = 8\,sec$.

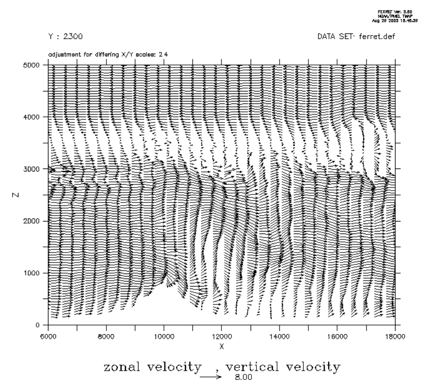

FIG. 2.3 – Velocity vector plot in 3D shear under a single bell mountain simulated with Méso-NH code.

microphysical transformations of exhausts in the wake. An âĂIJoff-lineâĂİ coupling was obtained by using the particle-trajectory solutions computed by NTMIX as input parameters for the box model. The feasibility of an âĂIJon lineâĂİ integration into a cfd code represents a challenging scientific and technical task, and is still an ongoing action.

2.2 Simulation at mesoscale : setting-up Méso-NH and coupling with NTMIX (R. Paugam , R. Paoli)

The object of this topic is to extend the simulations described above to cover the far-field wake (5 to 10 km from the aircraft), and the following dispersion region (10 to 100 km from the aircraft) using the Météo-France meteorological code Méso-NH. A significant effort has been made to understand the complex structure of Méso-NH and the development of post processing tools using widespread and portable output format, such as NetCDF. Some preliminary academic cases were also run for the sake of validation. An example is the 3D shear flow over a single bell mountain reported in Fig. 2.3. The figure shows that orographic forcing produces gravity wave propagating right- and upward. A strategy to properly initialize these simulations in Méso-NH to cover the mesoscale 100 km domain is now investigated, as well as

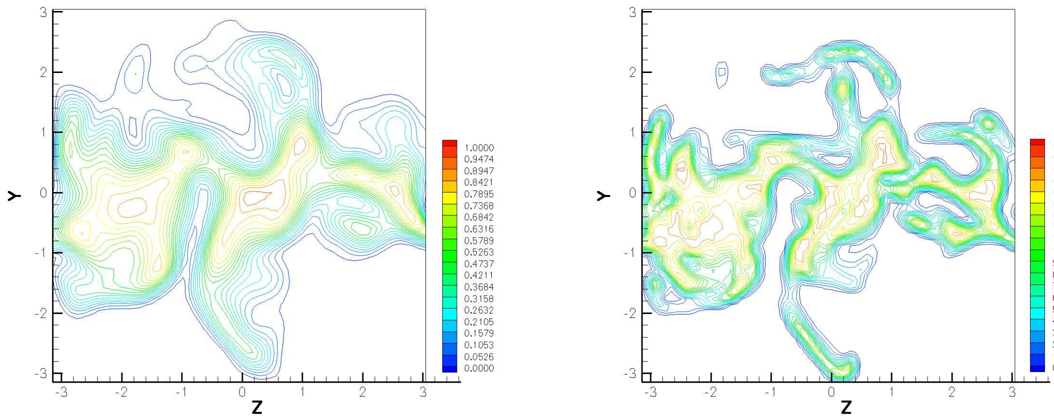

FIG. 2.4 – Snapshot of particle-laden slab advected in isotropic and homogeneous turbulence. Left : scalar field in a Semi-Lagrangian simulation. Right : (reconstructed) number density field in a fully Lagrangian simulation (initially 100 particles per cell).

the possible use of a nested version of Méso-NH. Emphasis is put on the contrail-to-cirrus transition that occurs after the vortex breakdown, due to the combined action of wind shear and stratification, with the wake and atmospheric turbulence. The overall approach of these mesoscale simulations will be validated using existing (in situ and satellite) observations.

2.3 Numerical algorithms : Semi-Lagrangian (R. Paoli and the cfd/combustion team)

A significant part of the team activity has been dedicated to the development of an efficient numerical algorithm to transport the dispersed phase in two-phase flow simulations (aerosols and ice crystals in the present case). To that end, a Semi-Lagrangian scheme advection has been implemented in NTMIX for its good computational efficiency in long-lasting simulations, as already experienced in the atmospheric sciences community. These kind of methods can also be designed to supply local diffusion around propagating fronts of non-diffusive scalars. In particular, a Conservative Quasi-Monotone Semi-Lagrangian scheme (CQMSL) has been implemented that switches from high-order Hermite to low-order Lagrange interpolation in the vicinity of strong gradients. Conservation is further guaranteed via a-posteriori mass recovering. A preliminary test was run, consisting in a Direct Numerical Simulation of a particle-laden slab advected in isotropic and homogeneous turbulence. The scalar field shown in Fig. 2.4 compares reasonably with the number density field reconstructed from a fully Lagrangian-particle simulation. Next steps will be to include the dispersed phase velocity in the numerical method, as well as the advection of particle size distributions.

3 Large scale ozone distribution and radiative response

3.1 Linearization of the atmospheric chemistry (D. Cariolle, H. Teyssèdre)

A linearized ozone scheme is used in the ARPEGE/Climat model. It has been developed by Cariolle and Déqué (1986) in order to study the interactions between the ozone distribution and the climate evolution. It is computationally efficient and can be used for first rapid assessment of impacts without the need to use more sophisticated chemical transport models such as MOCAGE, which is much more resource demanding.

The ozone scheme needed to be updated, the major objectives were first to remove as much as possible the bias of the parameterization and second to better take into account the effects of the heterogeneous chemistry. In particular attention has been paid to the systematic under evaluation of the ozone content at the equator in the lower stratosphere that has been pointed out with the original parameterization. To this end the photochemical 2D MOBIDIC model that generates the coefficients of the parameterization has been upgraded after detailed analysis of the relative effects of transport and chemistry and comparisons with various climatological datasets (Cariolle [PAE6]).
The following improvements have been introduced :
- careful analysis of the computation methods to obtain the meridional residual circulation from ARPEGE/climat
- removal in the chemical computations of the cold bias found in the ARPEGE forcing in the middle and high stratosphere
- analysis of the influence of horizontal and vertical diffusion
- evaluation of the computations method used for the photolysis rates
- introduction of a new formulation for the ozone destruction due to heterogeneous chemistry based on the local total ozone chlorine
- upgrade the chemistry according to the JPL-2003-25 recommendations
- tune the vertical diffusion coefficient above the equatorial tropopause to be in better agreement with distributions of CH_4 and N_2O measured by HALOE
- increase the wash out rates in the boundary layer to improved the tropospheric ozone content (less NOx)

After having introduced several improvements in those areas the MOBIDIC model produces a significantly improved O_3 simulation. This derived new version v2 of the parameterization has been extensively tested using the MOCAGE CTM and the ARPEGE and IFS models. As an example, figure 3.1 shows the comparison between the TOMS data and the MOCAGE ozone field for a 4 year simulation using the v2.1 scheme. As can be seen the model reproduces quite well the ozone variability at the equator, the spring maxima at the NH high latitudes and the ozone destruction in the SH near the pole in Septembre-Octobre.
In order to use the linearized scheme for emission scenarios from aircraft it must be further developed to include the influence on ozone chemical production and destruction rates of the perturbations due to NOy species (mainly $NO + NO_2$ and HNO_3), CO and H_2O. To this end the MOBIDIC model will be used and comparison with the MOCAGE model will be performed using emissions and/or distributions of perturbed

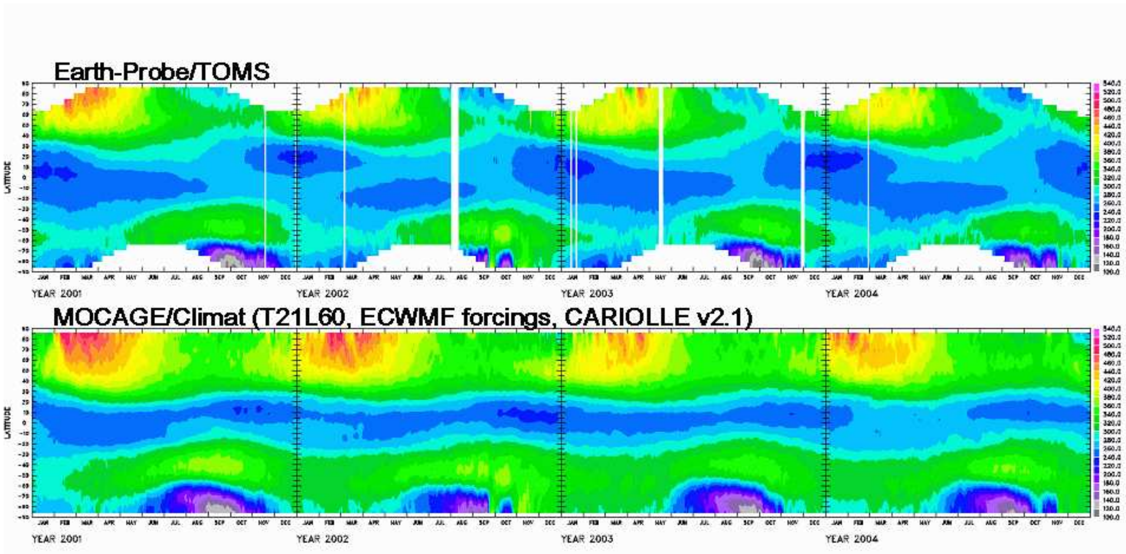

FIG. 3.1 – Total ozone distributions given by the MOCAGE simulations at T21 using the v2.1 scheme and forced by ECMWF operational analyses, and TOMS data.

species from the FP5 SCENIC project. This task is undertaken by D. Cariolle in collaboration with the CAIAC team (H. Teyssèdre) of the CNRM.

3.2 A linear approach to the atmospheric radiative transfer (D. Cariolle, J.-J. Morcrette)

A linearized model of the atmospheric radiative transfer has been derived from the detailed radiative model used at the ECMWF within the IFS operational model.
A column version of the radiative operational code has been used to derive the sensibility matrix of the radiative tendencies to temperature [DQ/DT] and ozone [DQ/DO$_3$]. These matrix are the jacobians of the radiative code as a function of temperature and ozone. They have been calculated by applying local perturbations to a 1D vertical temperature profile representative of the equatorial latitude for equinox (see table I). For the computation of [DQ/DT] a perturbation of +/- 5 K has been applied at each level, the radiative code integrated and the tendencies calculated. Similarly, for the computation of [DQ/DO$_3$] an O_3 perturbation of +/- 20 % has been applied at each level. The matrix [DQ/DO$_3$] is in fact the sum of 2 matrices, one for the longwave and one for the shortwave radiations.
The linear radiation model simply works as following. Given a vertical profile that deviates from ΔT and ΔO_3 from the referenced profile it is then possible to evaluate the perturbation of the heating rate ΔQ using the matrix product :

$$\Delta Q = [DQ/DT] \otimes \Delta T + [DQ/DO_3] \otimes \Delta O_3 \tag{3.1}$$

This model has been tested using uniform temperature and ozone perturbations (with some tests of mixed O_3 and T changes) over the vertical (as large as 20 K and 50% ozone) and heating rates were found to deviate less than a few percent relative to full radiative calculations. This mean that for a large range of temperature and O_3 changes the response of the radiative model is approximately linear, provided that in the calculation of partial derivatives care is taken to allow for the radiation exchange between layers.

The importance of the exchange between layers is illustrated by calculating the vertical dependence of the radiative damping time. The radiative damping time is defined here as the time necessary to damp a specific temperature perturbation. It is obtained directly from the linear model by integrating equation (1) with $\Delta O_3 = 0$, and $\Delta T = 1$ K, the result ΔQ gives the damping time $\tau = \Delta Q^{-1}$ at each level. If the temperature perturbation is applied to one level only, one obtains the time necessary to damp the temperature anomaly having the depth of the corresponding layer. In that case the ΔQ term is equal to the diagonal term of the matrix [DQ/DT]. In case of a temperature perturbation with effect on the whole vertical, one obtains the so-called Newtonian damping time, the time to damp the local temperature anomaly taking account of the influence of the changes in the radiative fluxes coming from all levels above and below the level in consideration.

Figure 3.2 shows the vertical distributions of τ when the temperature perturbation affects one layer, 3 layers centered at a given level, 5 layers, 7 layers and so on... If the radiation exchange between layers was unimportant the vertical distributions of τ should be very close from one another.

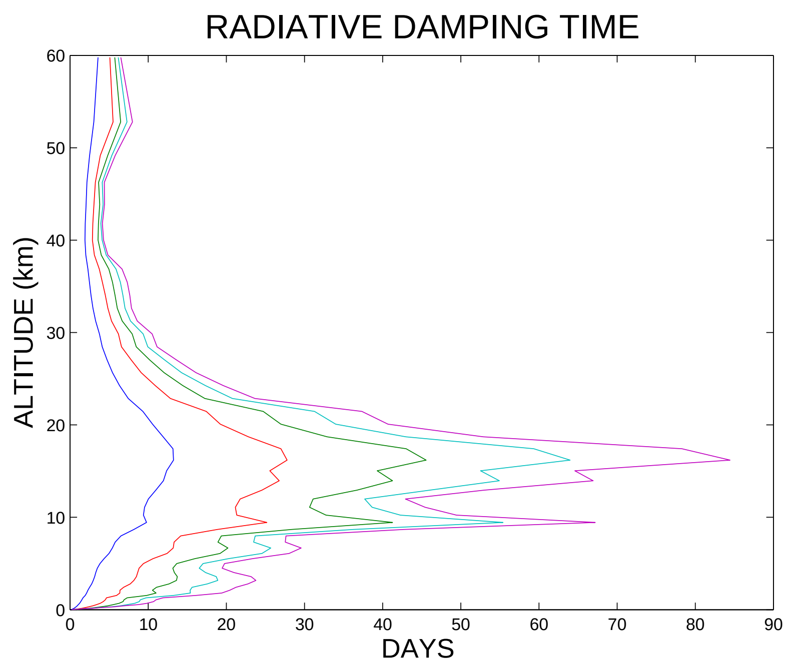

FIG. 3.2 – Radiative damping time as a function of the depth of the temperature perturbation. The dark blue curve corresponds to perturbation of one model layer, red for 3 layers, green for 5 layers, light blue for 7 layers and purple for 9 levels.

This is the case in the upper stratosphere above 30 km where the different evaluations of τ show a good convergence as the depth of the temperature perturbation increases. In that altitude range the matrix $[DQ/DT]$ is diagonally dominant and it makes sense to consider the Newtonian damping time as the time representative to damp any temperature perturbation. In contrast below 25 km, in the lower stratosphere, the damping time increases with the depth of the temperature perturbation with no sign of convergence. For example more than 60 days are needed to relax the temperature to the reference profile for an anomaly spanning from 20 hPa to 100 hPa, a value consistent with the time taken by the IFS model to respond to the ozone perturbation described above. As discussed by many authors, in the lower stratosphere the equilibrium temperatures are very sensitive to the convergence of the infrared radiation fluxes. What we have shown is that it can be accounted for within a linear framework, and that perturbations that affect the lower stratosphere can take several months to displace the model equilibrium state.

The response of the linear radiation model to ozone change was found to be very consistent with the sensitivity of the ECMWF general circulation model (Cariolle [PAE5] ; Cariolle and Morcrette [PAE3]). In particular, the lower stratospheric temperatures of the linear model and of the GCM respond similarly to changes in the vertical ozone gradient in the upper troposphere-lower stratosphere. We can conclude that the GCM sensitivity to ozone is mostly a linear response via changes in the solar and long wave radiation absorption, combined with the very long radiative damping times that prevail in the lower stratosphere. On time-scales of several months, heat transport, chemistry-temperature interactions, possible re-adjustments in the water vapor and cloud distributions, and dynamical feed-backs do not play an important role in the GCM response. The present linearized approach to radiative transfer can therefore constitute a valuable mean to obtain at low computational cost a first guess of the stratospheric temperature response of coupled GCM-Chemical Transport Models to ozone distribution changes.

This linearized code will be used within the MOBIDIC model and used to evaluate the upper atmosphere temperature evolution due to aircraft induced ozone change. This task is undertaken by D. Cariolle in collaboration with the J.J. Morcrette from ECMWF, DLR and the University of Reading within the QUANTIFY project.

4 Publications

4.1 Journal Publications

[PAE1] Paoli, R., Hélie, and Poinsot, T. (2004), Contrail formation in aircraft wakes, *J. Fluid Mech*, 504, 361-373.

[PAE2] Paoli, R. anf Garnier, F. (2005), Interaction of exhaust jets and aircraft wake vortices : small-scale dynamics and potential microphysical-chemical transformations wakes, *Comptes Rendus Phys.*, in press.

[PAE3] Cariolle, D. and J.-J. Morcrette (2005), A linearized approach to the radiative budget of the stratosphere : influence of the ozone distribution,*Geophys. Res. Lett.*, submitted.

4.2 Technical reports

[PAE4] Cariolle D., R. Paoli and B. Cuenot (2004), COS midterm.

[PAE5] Cariolle, D. (2005), Stratospheric temperature sensitivity to the ozone distribution. Internal report, May 2005.

[PAE6] Cariolle, D. and H. Teyssèdre (2005), Development of a revised O3 parameterization for use in general circulation models, transport models and assimilation studies. Internal report, May 2005.

6

ENScube Group

1 Introduction

Pierre-Henri Cros

For these two years, the N'S^3 group has focused its activity on the development of an expertise in the domain of heating, ventilation and air conditioning (HVAC) systems and on the improvement of the N'S^3 solution.

The HVAC activity has introduced the CFD simulation toward the responsible of the ventilation system of professional building or plant.

First used in addition of a campaign of measures it is now asked, thanks to the obtained results, to study the ventilation system of building on project.

The version of the N'S^3 solution achieved in 2004 has been tested in 2005 by Airbus and Turbomeca in order to define improvements to be done to make it use on regular basis by them.

The version achieved in 2005 has been installed at Turbomeca site in Bordes on a renting basis and is used for their daily work with CERFACS.

The results obtained with the Airbus test group allows N'S^3 group to submit its use in the framework of the Virtual Testing Airbus project. The challenge will be to contribute to a better collaboration between Computation and tests.

2 Heating, Ventilation and Air Conditioning Flow Modelling

In the field of airflow modelling, the group has carried out CFD simulations in the domain of heating, ventilation and air conditioning (HVAC) systems. This activity had been initiated in the framework of the FP5 European project ASICA which allowed acquiring expertises in the field.
The objectives of this activity are to model and simulate airflows in buildings, the use of reliable, efficient and flexible predictive CFD software's, and the supply of support to traditional design and experimental methods for the management of comfort conditions in buildings and HVAC systems.

2.1 Industrial ventilation simulation in a large workshop(G. Jonville, C. Garrigue, consultant T. Schönfeld)

In the frame of the first phase of this project, numerical airflow simulations of the industrial ventilation in a very large aircraft workshop have been performed during 2004 and 2005. The main objectives were to study the relevance of industrial ventilation flow modelling by means of CFD modelling and to define the reliable domain of airflow predictions.
Depending on the industrial configuration, several cases of the ventilation system have been modelled. Further, different geometric representations of the material environment in the workshop have been considered.
The air inlet vents were positioned either on the ceiling, either on some walls. The air outlet vents were positioned on the floor.
Realistic inlet, outlet and wall boundary conditions have been defined based on measured data from measurement campaigns on site. Some measured values of air velocity and temperature inside the workshop were also available. Structured and unstructured computational grids with up to 2M hexahedral cells and 3.5M tetrahedral cells (Fig. 2.1) were generated by means of advanced CFD grid generation tools.

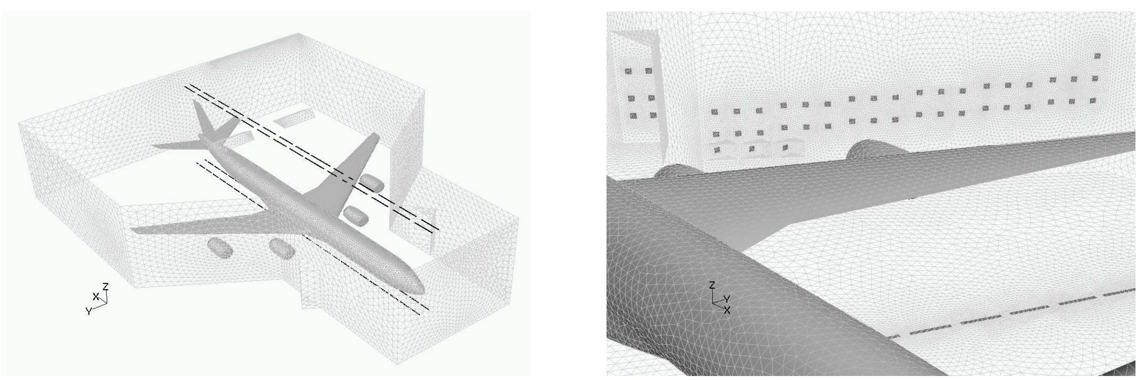

FIG. 2.1 – Unstructured tetrahedral meshes generated around generic aircraft placed in industrial workshop.

Physical and numerical models have been implemented for setting up the airflow simulation runs : steady Navier-Stokes equations for modelling the transport of momentum, k- model for modelling turbulence and energy equation for temperature. The computations have been performed with a bi-processor computer of 4Gb main memory capacity. The run times range between 18 and 34 CPU hours for one computation case.

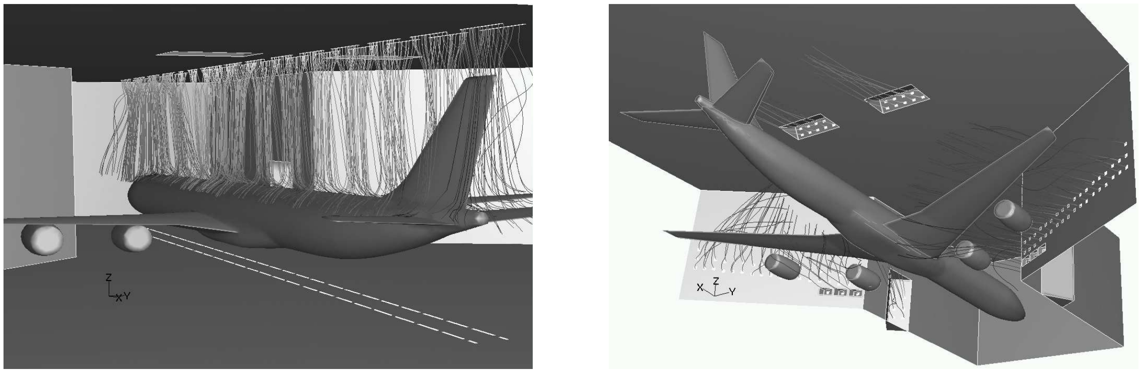

FIG. 2.2 – Path lines illustrating flow field in workshop for different configuration.

The numerical approach to the airflow investigation showed that advanced CFD software, pre and post-processors with a significant level of complexity and flexibility have sufficient potential to predict the global airflow in large industrial buildings with a good accuracy at reasonable cost. Some correlations between simulation results and observations on site have been underlined.
The simulations allowed visualising and understanding of the physical phenomena, to provide velocity direction and intensity, temperature distribution and particles path (Fig. 2.2).
The first phase of this project proved that the numerical airflow simulation in buildings is a reasonable support to the traditional design and experimental methods. The approach is very informative in practical design and a promising essential tool for the management of large industrial workshops and HVAC systems.

2.2 Airfbw simulations in an enclosure polluted by particles (G. Jonville)

A study has been realised concerning the numerical simulation of internal airflow in a ventilated enclosure polluted by particles. The enclosure represents an industrial room. The aim was to optimise the ventilation system according to the efficiency of extracting particles.
For the CFD simulations the enclosure was modelled as a 3D parallelepiped box. The air inlet was positioned on the ceiling and the air outlet on the floor with identical mass flow rates. Several configurations have been considered depending on the size of the inlet and outlet surfaces.
Structured computational grids with 850,000 hexahedral cells have been generated by means of an advanced CFD grid generation tool. For setting up the airflow simulation runs, steady Navier-Stokes equations in conjunction with a k- turbulence model have been used. The transport of particles has been computed with a discrete phase model. Particles of 20 diameter and 1600 Kg/m3 were uniformly injected in the enclosure at an initial time and were tracked according to the resident time (Fig. 2.3).

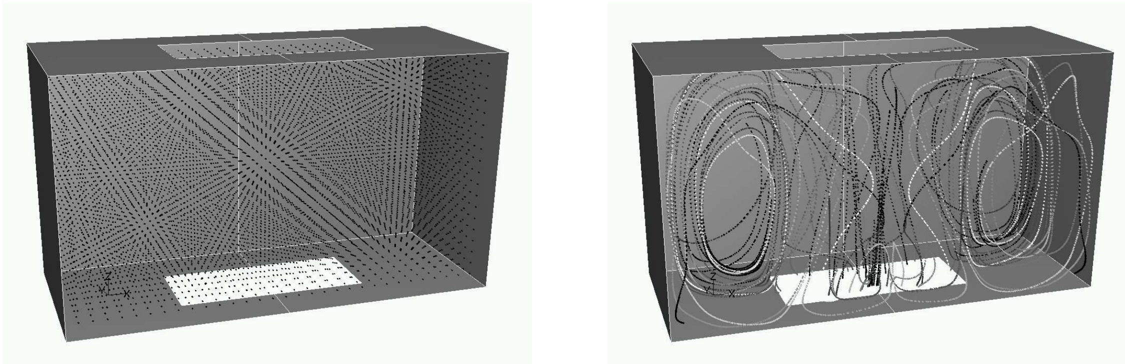

FIG. 2.3 – Initial particles injection (left) and paths of some particles colored by resident time (right) in small inlet surface configuration.

The results allowed comparing the extraction time of particles between each configuration and to choose the best solution in terms of extraction efficiency and implementing facility. This solution was implemented at the end of 2005 and the air quality in the industrial room was indeed improved.

2.3 Air conditioning system simulation in a glass-fronted cabinet exposed to solar radiation (G. Jonville)

A study has been conducted concerning the internal airflow simulation in a building to verify and validate the air conditioning system operation and the air temperature distribution.
The building under construction is destined to receive fragile objects and to welcome the public. Objects will be exposed at different levels in a large and rounded glass-fronted cabinet of 9m height.
The cabinet is divided by vertical girders to glass cases with a ventilation system installed in each one to control the temperature. Cooling air is injected from floor and extracted in the upper part.
One glass case has been chosen for the simulation in the situation of which the thermal flux on the external glass was maximum.
Adapted physical models have been used for setting up the airflow simulation runs : steady Navier-Stokes equations for modelling the transport of momentum, k- model for modelling turbulence, energy equation for temperature, gravity, convection and radiation models.
The glass case geometry has been modelled and a structured computational grid with 750,000 hexahedral cells has been generated by means of an advanced CFD grid generation tool.
The results show thermal stratification in the glass case (Fig. 2.4), with a global average temperature of 31řC. The average temperatures computed on four different levels from the temperature fields (Fig. 2.4), allow identifying excessively high temperature in the upper part. These results proved before installing the system, the necessity to modify the global device in order to obtain the certification for exposing objects.

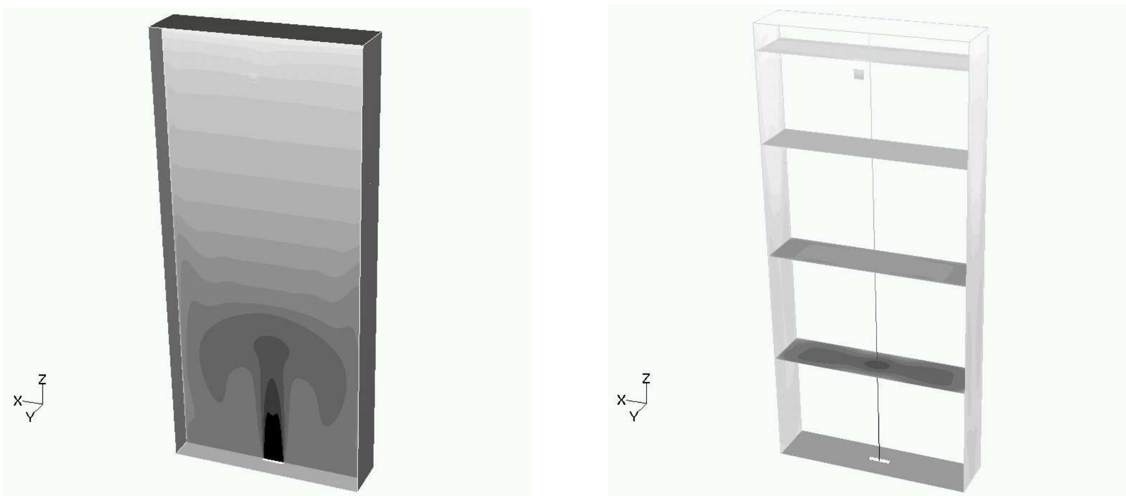

FIG. 2.4 – Distribution of air temperature in central plane showing thermal stratification (left) and temperature field in horizontal planes (right).

3 Development of collaborative working solutions

S. Milhac

3.1 Presentation of the N'S^3 solution

The N'S^3 solution is a Computer Supported Collaborative Working (CSCW) tool designed to ease the co-operation between remote partners in the context of numerical simulations projects. It is designed to replace a real meeting room in a distributed working environment.

The N'S^3 solution allows the user to exploit all the classical WEB conferencing tools as the audio/video system, the sharing applications, the whiteboard and the chat, but also to co-visualize and co-manipulate 3-dimensional data with his partners. The N'S^3 solution is designed to be of very intuitive use : most of the functionalities can be activated with simple mouse clicks. A particular effort was also made to develop a clear ergonomic interface. The strategy is to use three monitors. Each has a specific role. The central screen contains the tools for controlling the conference. On the left screen, the usual office applications can be shared for interactive and collaborative editing. The right screen is devoted to the 3D co-visualization.

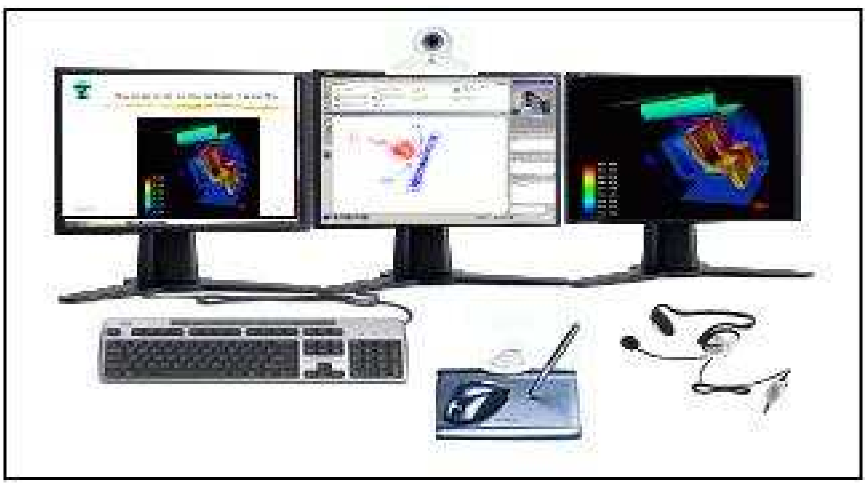

FIG. 3.1 – N'S^3 solution, a clear ergonomic interface.

Since 2004, different functionalities have been added to enrich the solution :

Functions	Version 2004	Version 2005
Audio, video, white board, chat, application sharing	X	X
Desktop sharing		X
File sharing		X
Progress bar		X
One mouse, one keyboard		X
Viewer 3D for CAD and CAE Data	X	X
CAE 3D data base sharing	X	X
Change scalar variables of the 3D visualization	X	X
Change vector variables of the 3D visualization		X

In addition, the N'S^3 solution proposes the following specificities :
– Launch the presentation of the numerical simulation results directly out a PowerPoint document :

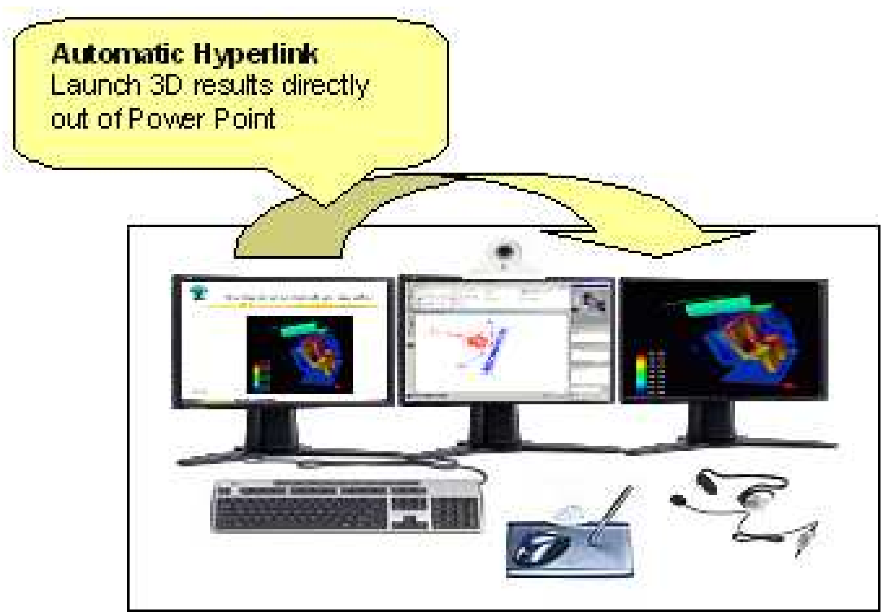

FIG. 3.2 – N'S^3 hyperlink.

– Cut and paste a snapshot of the 3D data onto the whiteboard and add comments ;
– Save the whiteboard content as a basis for the minutes.

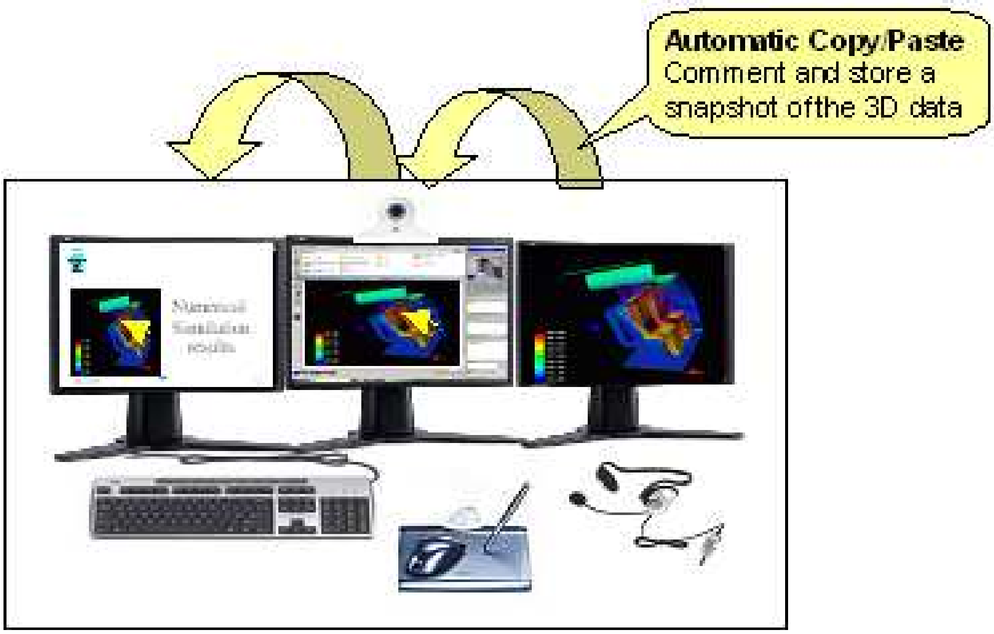

FIG. 3.3 – N'S^3 snapshot.

3.2 N'S^3 group's strategy

The N'S^3 group's strategy is :
- Integrate efficient and easy to use COTS[1] or develop his own specific applications,
- Propose an intuitive GUI managing all the applications and facilitating the use of the N'S^3 solution.

3.2.1 COTS of the N'S^3 solution

COTS are used to support Web conferencing functions. The IBM solution is used for audio/video when the Windows solution has been selected to support whiteboard, chat, application sharing and file transfer. Desktop sharing is possible via the VNC application.

To get an intuitive GUI which is the key point of the N'S^3 solution, the COTS have been customized thanks Java and C++ developments to propose only the useful functions and have them accessible via simple clicks.

[1]Component On The Shelf

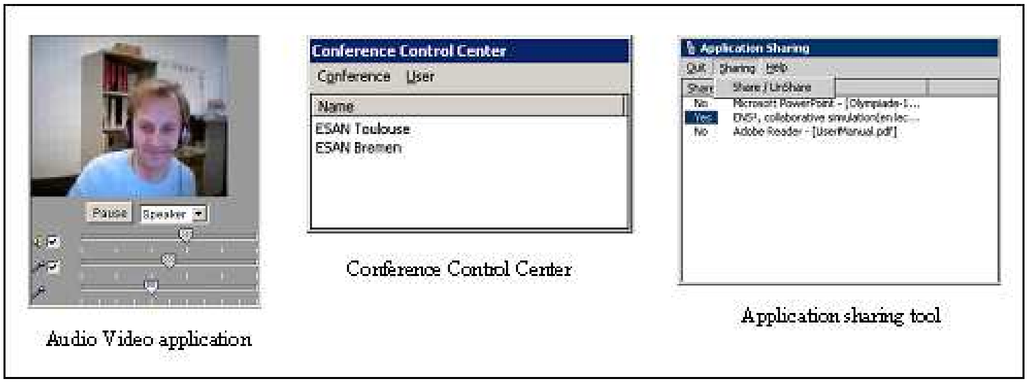

FIG. 3.4 – COTS of the N'S^3 solution.

3.2.2 N'S^3 developments

For the 3D data, the N'S^3 group has developed a universal viewer called NS3D. It is collaborative visualization software allowing co-editing and co-manipulating numerical simulation 3D data without having the source application on both sides. NS3D, written in C++ and based on OpenInventor, has various input interfaces. At the moment Radioss, Nastran, LS-Dyna and Ensight are fully supported and many others are basically developed (Abaqus, Ansys, Fluent, Tecplot,) The data coming from different source applications are mapped to a common N'S^3 format. The viewer functions like zooming, rotating, clipping and animation are proposed. In addition the user can show colored surfaces, cutting surfaces, isosurfaces and tracelines. To make it easy to use, NS3D offers a set of functions which are defined by the user and the complexity of the visualisation task is then reduced to a couple of parameters.

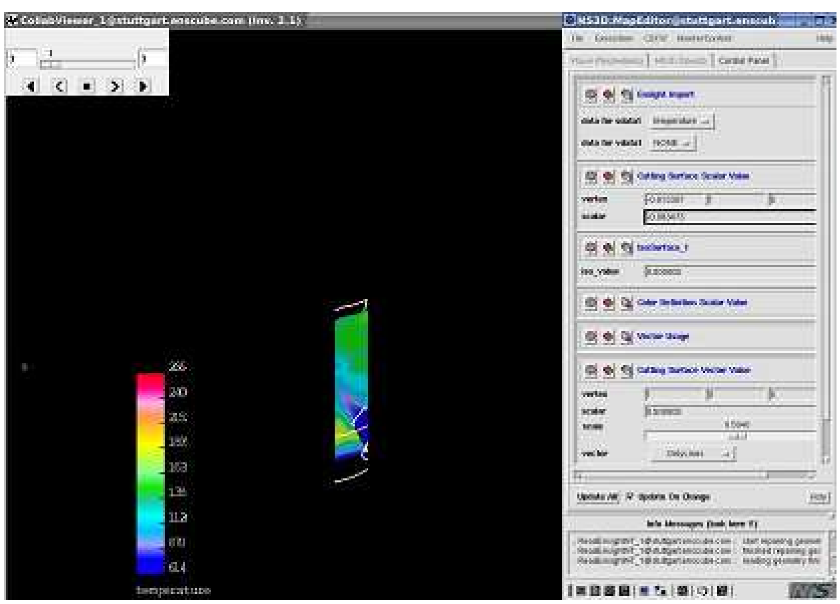

FIG. 3.5 – NS3D.

3.2.3 Intuitive GUI

To get an intuitive GUI, the N'S^3 group has implemented the N'S^3 layer made of scripts and Java applets.

The rule of the N'S^3 layer is to take in charge transparently the hardware settings and the communication between all the applications. The objective is to facilitate and minimize the actions of the user to implement a virtual meeting. The N'S^3 layer helps on four aspects :

- **Hardware settings** : From the starting process, the settings of each PC and their gateway are transparently taken in charge. To increase the commodity of the N'S^3 solution, the N'S^3 layer shares one mouse and one keyboard for both computers. The USB hard drive is automatically mounted when data are required.
- **Ergonomic interface** : The N'S^3 layer manages the size and position of each frame on the three screens. A toolbar on the central screen proposes shortcuts to the most used functionalities.
- **Applications communication** : The different collaborative tools, COTS or NS3D, are automatically started when needed and all functionalities are reachable from simple buttons. Moreover, the N'S^3 layer assures the N'S^3 hyperlink and snapshot functionalities.
- **User information** : In addition a progress bar and alert messages keep the user informed about the status of his actions.

As shown in the figure, the N'S^3 layer is not a simple tool but association of different kinds of tools and technologies :

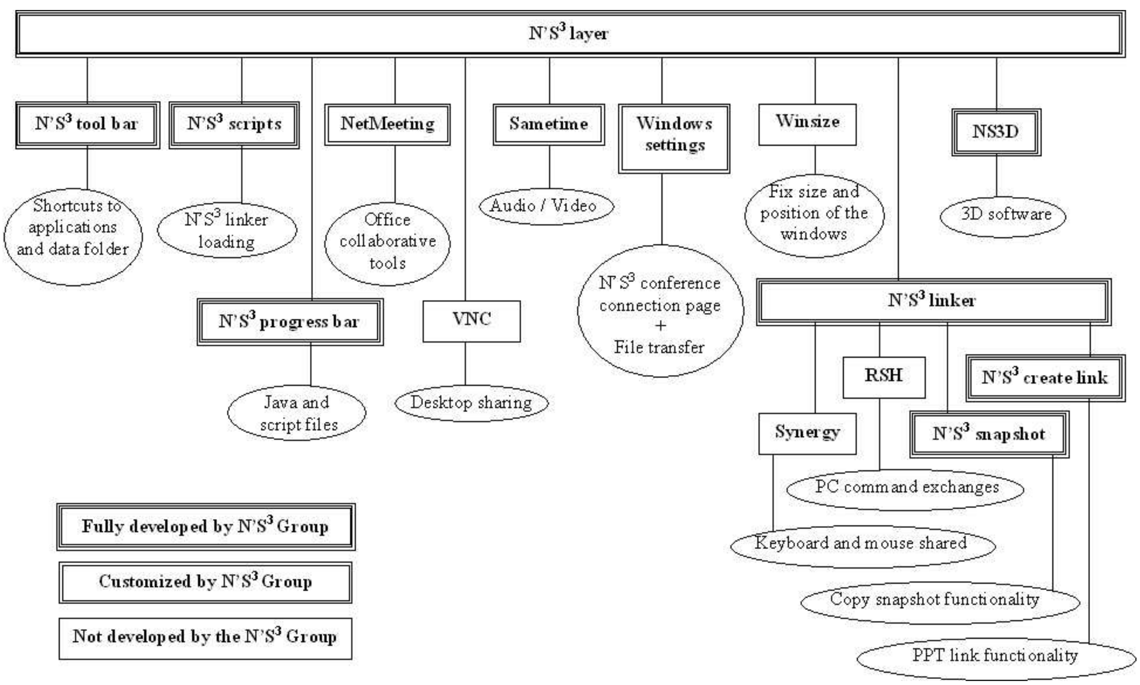

FIG. 3.6 – N'S^3 layer.

3.3 N'S^3 solution compared to others

The N'S^3 solution is unique by providing within a videoconferencing tool a viewer 3D for CAD and CAE data allowing real-time co-visualization and co-manipulation with transient data.

Functions	WebEx	Workspace 3D	N'S^3 solution
Audio - video	X	X	X
White Board	X	X	X
Chat	X	X	X
Application sharing	X		X
Desktop sharing	X	X	X
Recording	X	X	
File sharing	X	X	X
Viewer 3D for CAD Data		X	X
Viewer 3D for CAE Data			X
CAE 3D data base sharing			X
Change variables of the 3D visualization			X
Copy on white board of 3D data base views			X
Launch 3D data base from ppt document			X

FIG. 3.7 – N'S^3 comparative

7

Computer Support Group

1 Introduction

Nicolas Monnier

1.1 Key responsibilities

Key responsibilities of CERFACS’ "Computer Support Group" are :

– To define CERFACS’ Computer and Network architectures and perspectives for their upgrade and evolution ;
– To provide, integrate and maintain all necessary and selected CERFACS’ hardware and software solutions ;
– To address CERFACS teams’ needs with integrated solutions and services ;
– To assist researchers, providing them technical and application expertise including assistance with programming and optimisation ;
– To spread all necessary practical information advising CERFACS’ users in their main areas of interest.

This support activity is the responsability of a five people team.

1.2 General strategy

General strategy is :

– Listening to the users’ needs, federating them to benefit from scaling factors ;
– With the help of HPCN suppliers, allow CERFACS’ researchers to work in an up-to-date software and hardware HPCN environment (Storage capacities, Computing power, Post-processing and Networking) ;
– Ensure developments portability through the access to a wide range of architectures ;
– Establish partnership for accessibility to high-end configurations.

2 Architecture and Actions.

Isabelle d'Ast, Gerard Dejean, Fabrice Fleury, Patrick Laporte

2.1 CERFACS' computing resources (As of Dec 05).

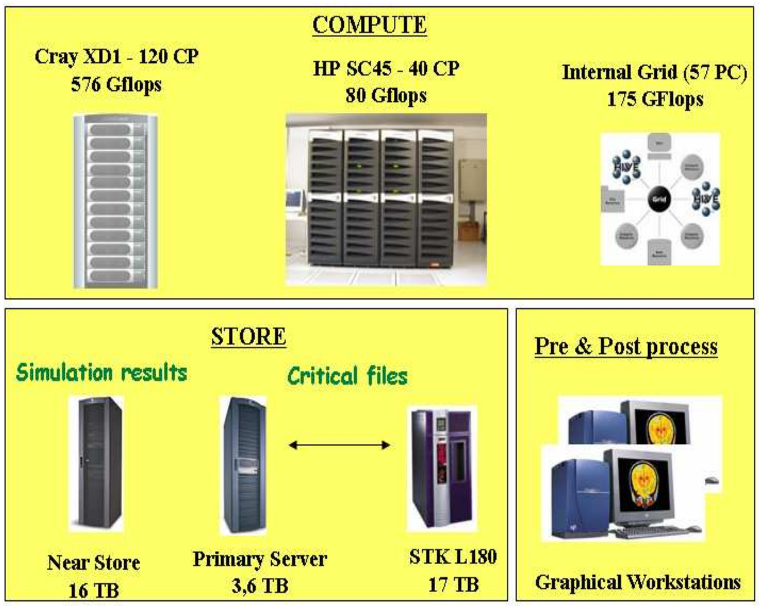

During the period CERFACS' computer resources have seen two main improvements :

– Computing power : 6 times faster with a Cray XD1 installation. The new computer, installed in june 2005, offers a peak performance of 576 Gflops with 120 AMD Opteron processors interconnected on a Cray high speed and low latency network, 240 GB of memory and 3 TB of disk.
– Storage : 9 times more capacity on two new fileservers. The first one (Network appliance FAS 960 with 3.6 TB of fiber channel disks) is dedicated to high bandwidth access to critical files, the second one (Network appliance R200 with 16 TB os SATA disks) is dedicated to the storage of large simulations results.

2.2 Software environment and Support.

CERFACS' software environment covers three domains :

– Scientific development tools : CERFACS' users need a whole array of tools which allow them to create, test, debug and exploit their computational simulations. In this frame, one looks for availability of a wide range of scientific tools (compilers, profilers, debuggers, scientifical libraries, and parallelization tools) and their associated documentation. The availability of several Operating Systems associated with their scientifical development environment guarantes portability of developments on a wide range of Unix machines ;

– Job and data management tools : giving users a complete set of tools is not enough. One has to provide a job management environment on the central computers, including batch queues, rules of usage and accounting means to optimise global throughput of CERFACS' computers (LSF and PBS batch systems are currently in use). On the other hand, the "Computer Support Group" provides data backup / restore (Time Navigator) ;
– Dedicated applications servers : in addition to development and management tools, several dedicated application servers are essential to complete a high-level software environment. These application servers are either an extension of computing facilities (Visualization servers, Data A Management Server, MatLab servers) or an integral part of CERFACS' infrastructure (Web servers, Mail server, printer server, NIS, ...).

2.3 AVBP and elsA standard production on Cray XD1 and HP Alphaserver

Our Cray configuration (116 computing processors) allows researchers to use 16 processors / 32 GB memory for their day-to-day standards simulations. The server supports up to seven simultaneous standards simulations, it is near two times more than on our Alphaserver which supports only four standard simulations, each of them using 8 processors / 16 GB memory.

The performance ratio (elapse time for a standard simulation on AlphaServer / elapse time for a standard simulation on XD1) is 1.25 for elsA and 2.05 for AVBP : a xd1 standard simulation is two times larger on Cray than on AlphaServer and the restitution time is two times faster for AVBP and 1,25 faster for elsA on the new server.

2.4 AVBP and elsA performance results on GigaEthernet and Infiniband

To prepare our last tender of offering (new computing solution) we measure AVBP and elsA scaling performance on clusters with low latency interconnect and clusters with GigaEthernet interconnect. Measurements have been done on the same computer in dedicated mode, we only switch from one network to the other.

Number of processors	1	4	8	16	32
AVBP elapse time on GB	1369	409	213	135	99
AVBP elapse time on IB	1373	350	177	92	48

Number of processors	1	4	8	16
elsA elapse time on GB	2100	833	709	490
elsA elapse time on IB	2086	653	398	271

With 16 processors interconnected with Infiniband network we got AVBP results two times faster than on the same 32 processors interconnected with GigaEthernet network, elsA is even more demanding : the same simulation ran faster on 8 processors interconnected on Infiniband than on 16 processors interconnected with GigaEthernet.